

DYNAMIC MODELING AND ANALYSIS OF 6X6 SKID STEERED
MILITARY VEHICLE WITH ARTICULATED DOUBLE-ACTING
HYDRO-PNEUMATIC SUSPENSION SYSTEM

A THESIS SUBMITTED TO
THE GRADUATE SCHOOL OF NATURAL AND APPLIED SCIENCES
OF
MIDDLE EAST TECHNICAL UNIVERSITY

BY

DERİN TÜREDİ

IN PARTIAL FULFILLMENT OF THE REQUIREMENTS
FOR
THE DEGREE OF MASTER OF SCIENCE
IN
MECHANICAL ENGINEERING

DECEMBER 2022

Approval of the thesis:

**DYNAMIC MODELING AND ANALYSIS OF 6X6 SKID STEERED
MILITARY VEHICLE WITH ARTICULATED DOUBLE-ACTING
HYDRO-PNEUMATIC SUSPENSION SYSTEM**

submitted by **DERİN TÜREDİ** in partial fulfillment of the requirements for the degree of **Master of Science in Mechanical Engineering, Middle East Technical University** by,

Prof. Dr. Halil Kalıpçılar
Dean, Graduate School of **Natural and Applied Sciences** _____

Prof. Dr. M. A. Sahir Arıkan
Head of the Department, **Mechanical Engineering** _____

Prof. Dr. Erhan İlhan Konukseven
Supervisor, **Mechanical Engineering, METU** _____

Examining Committee Members:

Prof. Dr. Yiğit Yazıcıoğlu
Mechanical Engineering, METU _____

Prof. Dr. Erhan İlhan Konukseven
Mechanical Engineering, METU _____

Assoc. Prof. Dr. Ender Yıldırım
Mechanical Engineering, METU _____

Assist. Prof. Dr. Gökhan Özgen
Mechanical Engineering, METU _____

Assist. Prof. Dr. Selçuk Himmetoğlu
Mechanical Engineering, Hacettepe University _____

Date: 12.12.2022

I hereby declare that all information in this document has been obtained and presented in accordance with academic rules and ethical conduct. I also declare that, as required by these rules and conduct, I have fully cited and referenced all material and results that are not original to this work.

Name Last name : Derin Türedi

Signature :

ABSTRACT

DYNAMIC MODELING AND ANALYSIS OF 6X6 SKID STEERED MILITARY VEHICLE WITH ARTICULATED DOUBLE-ACTING HYDRO-PNEUMATIC SUSPENSION SYSTEM

Türedi, Derin

Master of Science, Mechanical Engineering
Supervisor: Prof. Dr. Erhan İlhan Konukseven

December 2022, 239 pages

Vehicle simulation is an essential step for the evaluation of control algorithms on vehicles. In this respect, there are various approaches in the literature such as quarter car, half car and full car. Most of these studies have been conducted for specific use cases, for instance examining only vertical behavior of the vehicle by ignoring its longitudinal and lateral dynamics. In addition to the conventional methods, there are simulation environments which analyze the characteristic of the vehicle dynamics. However, these simulations are restricted to traditional vehicles such as passenger cars and trucks. For more complex multi axle and robot-like vehicles, models that are created based on conventional Newtonian mechanics still play an important role for the analysis of the vehicle behavior.

Main objective of this study is to develop a full car model for a tactical wheel 6x6 skid steered military vehicle with an articulated hydro-pneumatic suspension system on MATLAB/Simulink environment, in order to analyze vehicle behavior on different road conditions and traction inputs. In addition to the created model, to be

able verify its accuracy, MSC. ADAMS software is used to simulate the same vehicle. Unlike the conventional vehicle structure, skid steering mechanism, robotic articulated suspension mechanism, hydro-pneumatic suspension system, and multi-axle load distribution subjects are considered as the fundamental differences. In order to make coherent simulation comparisons, flat road, sinusoidal bump, road with constant irregularities, and ramp with constant slope are considered on the model as road profiles. Also, to analyze the performance of the suspension system, different road profiles are supplied to the counter tires simultaneously. Furthermore, different torque inputs are fed to the system to observe the lateral dynamics of the vehicle.

Keywords: Dynamic Modeling, Vehicle Dynamics, Skid Steering, Hydro-Pneumatic Suspension

ÖZ

KOL BAĞLANTILI ÇİFT EKİLİ HİDRO-PNÖMATİK SÜSPANSİYON SİSTEMİNE SAHİP 6X6 NOKTA DÖNÜŞLÜ ASKERİ KARA TAŞITININ MODELLENMESİ VE ANALİZ EDİLMESİ

Türedi, Derin
Yüksek Lisans, Makina Mühendisliği
Tez Yöneticisi: Prof. Dr. Erhan İlhan Konukseven

Aralık 2022, 239 sayfa

Geliştirilen kontrol algoritmalarının test edilebilmesi adına araç simülasyonları oldukça önemli bir yere sahiptir. Bu anlamda litetürde çeyrek, yarım ve bütün araç modelleri olmak üzere farklı yaklaşımlar bulunmaktadır. Düşey eksenini incelemek için boylamsal ve yanal dinamiğin yok sayılması gibi yapılan çalışmaların birçoğu spesifik kullanım amaçları için oluşturulmuştur. Geleneksel methodların yanı sıra, simülasyon ortamları da araç dinamik karakteristiğini incelemek adına kullanılmaktadır. Ancak kullanılan simülasyon platformları genellikle yolcu araçları ve kamyonet tarzı araçlar için sınırlıdır. Daha kompleks yapıya sahip çok akslı ve robot şeklinde değerlendirilen araçlar için, davranış analizlerinde kullanmak adına, Newton mekaniği dayanarak oluşturulan modeller hala oldukça önemli bir rol oynamaktadır.

Bu çalışmanın temel amacı, kontrol algoritmaları geliştirebilmek ve farklı yol profilleri için araç davranışlarını inceleyebilmek adına, taktik tekerlekli 6x6 noktasal dönüşlü, kol mekanizmalı hidro-pnömatik süspansiyon sistemine sahip askeri kara aracının MATLAB/Simulink ortamında modellenmesi üzerinedir. Oluşturulan modele ek olarak, sonuçların doğruluğunu incelemek adına, MSC. ADAMS programı kullanılarak aynı aracın benzer bir simülasyonu oluşturulmuştur.

Geleneksel araç yapılarından farklı olarak, noktasal dönüş, robotik süspansiyon kolu, hidro-pnömatik süspansiyon sistemi ve çok akslı araçlarda yük dağılımı konuları esas farklar olarak ele alınmıştır. Tutarlı kıyaslamalar yapabilmek adına, düz yol, sinus tümseği, sürekli düzensiz yol ve sabit eğimli rampa profilleri yol girdisi olarak ele alınmıştır. Süspansiyon sisteminin performansını incelemek adına, karşılıklı tekerlere eş zamanlı olarak farklı yol profil girdileri beslenmiştir. Ayrıca, aracın yanal dinamiğini incelemek adına, tekerlekler üzerinde farklı tork girdileri değerlendirilmiştir.

Anahtar Kelimeler: Dinamik Modelleme, Araç Dinamiği, Diferansiyal Dönüş, Hidro-Pnömatik Süspansiyon

To my mother and father

ACKNOWLEDGEMENTS

I wish to express my deepest gratitude to my supervisor Prof. Dr. Erhan İlhan Konukseven for his guidance, advice, criticism, encouragements, and insight throughout the research.

I also offer my sincere thanks to Hidroan Ankara Hidrolik Mak. San. for the support in the development of this project and contributions to this study. Furthermore, I would like to especially thank my colleague dear Kaan Berke Ulusoy for his highly appreciated help and support. I would like to thank the committee members as well, for their much valuable advice and criticism.

Last but not least, I would like to express my gratitude for the support and encouragement of my dear family and dear Pınar Cemre Yazıcı.

TABLE OF CONTENTS

ABSTRACT.....	v
ÖZ.....	vii
ACKNOWLEDGEMENTS.....	x
TABLE OF CONTENTS.....	xi
LIST OF TABLES.....	xiii
LIST OF FIGURES.....	xvi
LIST OF ABBREVIATIONS.....	xxii
LIST OF SYMBOLS.....	xxiii
CHAPTERS	
1 INTRODUCTION.....	1
1.1 Problem Definition.....	1
1.2 Thesis Outline.....	2
2 LITERATURE REVIEW.....	5
3 DYNAMIC MODEL.....	9
3.1 Kinematic Relations.....	13
3.2 Road Profile.....	21
3.3 Wheel Dynamics.....	23
3.4 Tire Model.....	24
3.5 Load Distribution.....	27
3.6 Suspension System.....	31
3.7 Arm Dynamic Model.....	38
3.8 Vehicle Body Model.....	44

3.1	Resistances to Motion.....	47
3.1.1	Longitudinal Resisting Forces	48
3.1.2	Resisting Turning Moment	49
3.2	Skid Steering Model.....	50
4	ADAMS MODEL	55
4.1	Modelling of the Bodies	56
4.2	Modelling of the Tires and the Suspension System	57
4.3	Inputs and ADAMS/Control.....	61
4.4	Road Generation.....	62
5	SIMULATION RESULTS AND COMPARISON	65
5.1	Case 1 – Flat Road Acceleration	65
5.2	Case 2 – Road with a Single Bump	76
5.3	Case 3 – Road with Irregularities	98
5.4	Case 4 – Road with a Gradient Angle of 15°	117
5.5	Case 5 – Steering with Different Torque Inputs.....	138
5.6	Case 6 – Skid Steering Around Body Center of Gravity.....	157
6	CONCLUSIONS AND FUTURE WORK.....	175
7	REFERENCES	177
8	APPENDIX	181

LIST OF TABLES

TABLES

Table 3-1. List of the Vehicle Parameters	10
Table 3-2. List of the Suspension Parameters.....	33
Table 4-1. Initial preload of the suspensions	60
Table 5-1. Comparison of Translational Velocity Data Produced between Models for Case 1	69
Table 5-2. Comparison of Translational Acceleration Data Produced between Models for Case 1	72
Table 5-3. Comparison of Data of Arm Angles Produced between Models for the First Case	75
Table 5-4. Comparison of Translational Velocity Data Produced between Models for Case 2	80
Table 5-5. Comparison of Translational Displacement Data Produced between Models for Case 2	82
Table 5-6. Comparison of Translational Acceleration Data Produced between Models for Case 2	83
Table 5-7. Comparison of Angular Position Data Produced between Models for Case 2.....	86
Table 5-8. Comparison of Angular Velocity Data Produced between Models for Case 2.....	88
Table 5-9. Comparison of Angular Acceleration Data Produced between Models for Case 2	91
Table 5-10. Comparison of Arm Angle Data Produced between Models for Case 2	93
Table 5-11. Comparison of Longitudinal Tire Force Data Produced between Models for Case 2	98

Table 5-12. Comparison of Longitudinal Motion Results Between Models for Case 3	100
Table 5-13. Comparison of Vertical Motion of the Body for Case 3	105
Table 5-14. Comparison of Pitch Motion of the Body for Case 3	109
Table 5-15. Comparison of Arm Angles for Case 3	113
Table 5-16. Comparison of Translational Motion Along the Longitudinal Axis between Models for Case 5	120
Table 5-17. Comparison of Translational Motion Along the Lateral Axis between Models for Case 5	122
Table 5-18. Comparison of Translational Motion Along the Vertical Axis between Models for Case 4	124
Table 5-19. Comparison of Rotational Motion Along the Roll Axis between Models for Case 4	127
Table 5-20. Comparison of Rotational Motion Along the Pitch Axis between Models for Case 4	129
Table 5-21. Comparison of Rotational Motion Along the Yaw Axis between Models for Case 4	131
Table 5-22. Comparison of Arm Angles between Models for Case 4	133
Table 5-23. Comparison of Load Distribution between Models for Case 4	135
Table 5-24. Comparison of Longitudinal Tire Forces for Case 4	138
Table 5-25. Comparison of Longitudinal Motion Between Models for Case 5	141
Table 5-26. Comparison of Lateral Motion Between Models for Case 5	143
Table 5-27. Comparison of Roll Motion Between Models for Case 5	145
Table 5-28. Comparison of Pitch Motion Between Models for Case 5	147
Table 5-29. Comparison of Yaw Motion Between Models for Case 5	149
Table 5-30. Comparison of Arm Angles Between Models for Case 5	151
Table 5-31. Comparison of Longitudinal Tire Forces Between Models for Case 5	153
Table 5-32. Comparison of Lateral Tire Forces Between Models for Case 5	154
Table 5-33. Comparison of Roll Motion Between Models for Case 6	165

Table 5-34. Comparison of Yaw Motion Between Models for Case 6	167
Table 5-35. Comparison of Arm Angles Between Models for Case 6	168
Table 5-36. Comparison of Suspension Torques Between Models For Case 6....	173

LIST OF FIGURES

FIGURES

Figure 3-1. (a) 6x6 test vehicle. (b) CAD design of the test vehicle. (c) CAD design of arm rod, suspension and wheel. (d) Assembled arm rod, suspension, and tire of the test vehicle.	12
Figure 3-2. Free body diagrams depicting the forces and reactions in each body ..	13
Figure 3-3. Figure depicting the left arm body connection points and the position vectors from the center of gravity of the vehicle body to the connection points	14
Figure 3-4. Velocity components of the arm and body connection, arm center of gravity, and tire center of gravity	16
Figure 3-5. (a) Road with a gradient of 15° (b) Bumps used in Aberdeen Proving Grounds	22
Figure 3-6. FBD showing wheel dynamics	23
Figure 3-7. Load distribution of the vehicle	27
Figure 3-8. Schematic and CAD drawing of double acting hydro-pneumatic suspension system	32
Figure 3-9. Suspension stiffness for different arm angles	37
Figure 3-10. Damper for different suspension velocities	37
Figure 3-11. Free body diagram of the arm and tire assembly in the xz-plane	39
Figure 3-12. Free body diagrams of the arm and tire assembly in yz- and xy-planes	40
Figure 3-13. Free body diagram of the body from left view	44
Figure 3-14. Free body diagram of the body top view	45
Figure 3-15. Free body diagram of the body from front view with left and right arm reaction forces grouped together	45
Figure 3-16. FBD showing resistances to motion	47
Figure 3-17. Resisting Turning Moment [12]	50
Figure 3-18 Vehicle in Turn with Radius R	53
Figure 4-1. Assembled vehicle in ADAMS	57

Figure 4-2. Front Spring Torque vs Angular Deformation.....	59
Figure 4-3. Middle Spring Torque vs Angular Deformation.....	59
Figure 4-4. Rear Spring Torque vs Angular Deformation.....	59
Figure 4-5. Plot of damping torque with respect to angular velocity as derived from the data implemented on ADAMS.....	60
Figure 4-6. Block diagram as created with ADAMS/Control and Simulink.....	62
Figure 4-7. Figure showing the user interface for road builder in ADAMS.....	63
Figure 5-1. Plots of Longitudinal Velocity of the Body for Case 1.....	66
Figure 5-2. Plots Lateral Velocity of the Body for Case 1.....	67
Figure 5-3. Plots of Vertical Velocity of the Body for Case 1.....	68
Figure 5-4. Plots of Longitudinal Acceleration of the Body for Case 1.....	69
Figure 5-5. Plots of Lateral Acceleration of the Body for Case 1.....	70
Figure 5-6. Plots of Vertical Acceleration of the Body for Case 1.....	71
Figure 5-7. Plots of Longitudinal Displacement of Body for Case 1.....	72
Figure 5-8. ADAMS Longitudinal Tire Forces for Case 1.....	73
Figure 5-9. Simulink Longitudinal Tire Forces for Case 1.....	73
Figure 5-10. ADAMS Arm Angles for Case 1.....	74
Figure 5-11. Simulink Arm Angles for Case 1.....	75
Figure 5-12. Initial position of the vehicle on the road with single bump in ADAMS.....	76
Figure 5-13. Plots of Longitudinal Velocity of Body for Case 2.....	77
Figure 5-14. Plots of Lateral Velocity of Body for Case 2.....	78
Figure 5-15. Plots of Vertical Velocity of the Body for Case 2.....	79
Figure 5-16. Plots of Longitudinal Displacement of the Body for Case 2.....	80
Figure 5-17. Plots of Vertical Displacement of the Body for Case 2.....	81
Figure 5-18. Plots of Vertical Acceleration of the Body for Case 2.....	83
Figure 5-19. Plots of Roll Angle of the Body for Case 2.....	84
Figure 5-20. Plots of Pitch Angle of the Body for Case 2.....	85
Figure 5-21. Plots of Yaw Angle of the Body for Case 2.....	86
Figure 5-22. Plots of Roll Angular Velocity of the Body for Case 2.....	87

Figure 5-23. Plots of Pitch Angular Velocity of the Body for Case 2.....	87
Figure 5-24. Plots of Yaw Angular Velocity of the Body for Case 2	88
Figure 5-25. Plots of Roll Angular Acceleration of the Body for Case 2	89
Figure 5-26. Plots of Pitch Angular Acceleration of the Body for Case 2	90
Figure 5-27. Plots of Yaw Angular Acceleration of the Body for Case 2.....	91
Figure 5-28. ADAMS Arm Angles for Case 2.....	92
Figure 5-29. Simulink Arm Angles for Case 2.....	92
Figure 5-30. ADAMS Load Distribution for Case 2	94
Figure 5-31. Simulink Load Distribution for Case 2.....	94
Figure 5-32. ADAMS Suspension Torques for Case 2	95
Figure 5-33. Simulink Suspension Torques for Case 2.....	96
Figure 5-34. ADAMS Longitudinal Tire Forces for Case 2	97
Figure 5-35. Simulink Longitudinal Tire Forces for Case 2	97
Figure 5-36. Initial Position of the vehicle on the road with gradient in ADAMS .	98
Figure 5-37. Plots of Longitudinal Displacement of Body for Case 3	99
Figure 5-38. Plots of Longitudinal Velocity of Body for Case 3	99
Figure 5-39. Plots of Longitudinal Acceleration of Body for Case 3	100
Figure 5-40. Plots of Lateral Displacement of the Body for Case 3	101
Figure 5-41. Plots of Lateral Velocity of the Body for Case 3.....	101
Figure 5-42. Plots of Lateral Acceleration of the Body for Case 3	102
Figure 5-43. Plots of Vertical Displacement of the Body for Case 3	103
Figure 5-44. Plots of Vertical Velocity of the Body for Case 3	103
Figure 5-45. Plots of Vertical Acceleration of the Body for Case 3	104
Figure 5-46. Plots of Roll Angle of the Body for Case 3	105
Figure 5-47. Plots of Roll Angular Velocity of the Body for Case 3.....	106
Figure 5-48. Plots of Roll Angular Acceleration of the Body for Case 3	106
Figure 5-49. Plots of Pitch Angle of the Body for Case 3.....	107
Figure 5-50. Plots of Pitch Angular Velocity of the Body for Case 3.....	108
Figure 5-51. Plots of Pitch Angular Acceleration of the Body for Case 3	108
Figure 5-52. Plots of Yaw Angle of the Body for Case 3	110

Figure 5-53. Plots of Yaw Angular Velocity of the Body for Case 3	110
Figure 5-54. Plots of Yaw Angular Acceleration of the Body for Case 3	111
Figure 5-55. ADAMS Arm Angles for Case 3	112
Figure 5-56. Simulink Arm Angles for Case 3	112
Figure 5-57. ADAMS Suspension Torques for Case 3	114
Figure 5-58. Simulink Suspension Torques for Case 3	114
Figure 5-59. ADAMS Longitudinal Tire Forces for Case 3	115
Figure 5-60. Simulink Longitudinal Tire Forces for Case 3	115
Figure 5-61. ADAMS Load Distribution for Case 3	116
Figure 5-62. Simulink Load Distribution for Case 3	116
Figure 5-63. Ramp Road Profile in ADAMS	117
Figure 5-64. Plots of Longitudinal Displacement of the Body for Case 4	118
Figure 5-65. Plots of Longitudinal Velocity of the Body for Case 4	118
Figure 5-66. Plots of Longitudinal Acceleration of the Body for Case 4	119
Figure 5-67. Plots of Lateral Displacement of the Body for Case 4	120
Figure 5-68. Plots of Lateral Velocity of the Body for Case 4	121
Figure 5-69. Plots of Lateral Acceleration of the Body for Case 4	121
Figure 5-70. Plots of Vertical Displacement of the Body for Case 4	122
Figure 5-71. Plots of Vertical Velocity of the Body for Case 4	123
Figure 5-72. Plots of Vertical Acceleration of the Body for Case 4	123
Figure 5-73. Plots of Roll Angle of the Body for Case 4	125
Figure 5-74. Plots of Roll Angular Velocity of the Body for Case 4	125
Figure 5-75. Plots of Roll Angular Acceleration of the Body for Case 4	126
Figure 5-76. Plots of Pitch Angle of the Body for Case 4	127
Figure 5-77. Plots of Pitch Angular Velocity of the Body for Case 4	128
Figure 5-78. Plots of Pitch Angular Acceleration of the Body for Case 4	128
Figure 5-79. Plots of Yaw Angle of the Body for Case 4	129
Figure 5-80. Plots of Yaw Angular Velocity of the Body for Case 4	130
Figure 5-81. Plots of Yaw Angular Acceleration of the Body for Case 4	130
Figure 5-82. ADAMS Arm Angles for Case 4	131

Figure 5-83. Simulink Arm Angles for Case 4.....	132
Figure 5-84. ADAMS Load Distribution for Case 4.....	133
Figure 5-85. Simulink Load Distribution for Case 4.....	134
Figure 5-86. ADAMS Suspension Torques for Case 4.....	135
Figure 5-87. Simulink Suspension Torques for Case 4.....	136
Figure 5-88. ADAMS Longitudinal Tire Forces for Case 4.....	136
Figure 5-89. Simulink Longitudinal Tire Forces for Case 4.....	137
Figure 5-90. Plots of Longitudinal Displacement of the Body for Case 5.....	139
Figure 5-91. Plots of Longitudinal Velocity of the Body for Case 5.....	139
Figure 5-92. Plots of Longitudinal Acceleration of the Body for Case 5.....	140
Figure 5-93. Plots of Lateral Displacement of the Body for Case 5.....	141
Figure 5-94. Plots of Lateral Velocity of the Body for Case 5.....	142
Figure 5-95. Plots of Lateral Acceleration of the Body for Case 5.....	142
Figure 5-96. Plots of Roll Angle of the Body for Case 5.....	143
Figure 5-97. Plots of Roll Angular Velocity of the Body for Case 5.....	144
Figure 5-98. Plots of Roll Angular Acceleration of the Body for Case 5.....	144
Figure 5-99. Plots of Pitch Angle of the Body for Case 5.....	145
Figure 5-100. Plots of Pitch Angular Velocity of the Body for Case 5.....	146
Figure 5-101. Plots of Pitch Angular Acceleration of the Body for Case 5.....	146
Figure 5-102. Plots of Yaw Angle of the Body for Case 5.....	147
Figure 5-103. Plots of Yaw Angular Velocity of the Body for Case 5.....	148
Figure 5-104. Plots of Yaw Angular Acceleration of the Body for Case 5.....	148
Figure 5-105. ADAMS Arm Angles for Case 5.....	150
Figure 5-106. Simulink Arm Angles for Case 5.....	150
Figure 5-107. ADAMS Longitudinal Tire Forces for Case 5.....	152
Figure 5-108. Simulink Longitudinal Tire Forces for Case 5.....	152
Figure 5-109. ADAMS Lateral Tire Forces for Case 5.....	153
Figure 5-110. Simulink Lateral Tire Forces for Case 5.....	154
Figure 5-111. ADAMS Load Distribution for Case 5.....	155
Figure 5-112. Simulink Load Distribution for Case 5.....	155

Figure 5-113. ADAMS Suspension Torques for Case 5.....	156
Figure 5-114. Simulink Suspension Torques for Case 5	156
Figure 5-115. Plots of Longitudinal Displacement of the Body for Case 6.....	157
Figure 5-116. Plots of Longitudinal Velocity of the Body for Case 6.....	158
Figure 5-117. Plots of Longitudinal Acceleration of the Body for Case 6	158
Figure 5-118. Plots of Lateral Displacement of the Body for Case 6.....	159
Figure 5-119. Plots of Lateral Velocity of the Body for Case 6	160
Figure 5-120. Plots of Lateral Acceleration of the Body for Case 6	160
Figure 5-121. Plots of Vertical Displacement of the Body for Case 6	161
Figure 5-122. Plots of Vertical Velocity of the Body for Case 6.....	162
Figure 5-123. Plots of Vertical Acceleration of the Body for Case 6.....	162
Figure 5-124. Plots of Roll Angle of the Body for Case 6	163
Figure 5-125. Plots of Roll Angular Velocity of the Body for Case 6	164
Figure 5-126. Plots of Roll Angular Acceleration of the Body for Case 6.....	164
Figure 5-127. Plots of Yaw Angle of the Body for Case 6.....	165
Figure 5-128. Plots of Yaw Angular Velocity of the Body for Case 6.....	166
Figure 5-129. Plots of Yaw Angular Acceleration of the Body for Case 6	166
Figure 5-130. ADAMS Arm Angles for Case 6	167
Figure 5-131. Simulink Arm Angles for Case 6	168
Figure 5-132. ADAMS Longitudinal Tire Forces for Case 6.....	169
Figure 5-133. Simulink Longitudinal Tire Forces for Case 6.....	169
Figure 5-134. ADAMS Lateral Tire Forces for Case 6	170
Figure 5-135. Simulink Lateral Tire Forces for Case 6	170
Figure 5-136. ADAMS Load Distribution Forces for Case 6.....	171
Figure 5-137. Simulink Load Distribution Forces for Case 6	171
Figure 5-138. ADAMS Suspension Torques for Case 6.....	172
Figure 5-139. Simulink Suspension Torques for Case 6	172

LIST OF ABBREVIATIONS

DoF: Degree(s)-of-freedom

CAD: Computer Aided Design

ADAMS: Automatic Dynamic Analysis of Mechanical Systems

HPS: Hydro-Pneumatic Suspension

APG: Aberdeen Proving Grounds

MSE: Mean Squared Error

FBD: Free Body Diagram

LIST OF SYMBOLS

SYMBOLS

A_f : Frontal area of the vehicle

A_{fp} : Floating piston area

A_p : Main piston area

A_{pr} : Remaining area between piston and rod

A_r : Piston rod area

A_{v1} : Area of the first orifice

A_{v2} : Area of the second orifice

a_x : Longitudinal acceleration of the vehicle with respect to the ground

a_y : Lateral acceleration of the vehicle with respect to the ground

a_z : Vertical acceleration of the vehicle with respect to the ground

$\bar{\alpha}_{armi}$: Angular acceleration vector of the i^{th} arm with respect to the ground in the body fixed reference frame

$\alpha_{w,i}$: Slip angle of the wheel

C_d : Drag coefficient

C_l : Tire longitudinal stiffness

C_s : Tire lateral stiffness

$DCM_{b,e}$: Direction cosine matrix between the inertial frame and the body frame

F_a : Air resistance

F_r : Rolling resistance

f_r : Rolling resistance friction coefficient

F_{tx} : Traction force produced in the tire

F_{ty} : Lateral force produced in the tire

F_{tz} : Normal force applied to the tire

F_{sx} : Reaction force in the joint between the body and arm along the body x-axis

F_{sy} : Reaction force in the joint between the body and arm along the body y-axis

F_{sz} : Reaction force in the joint between the body and arm along the body z-axis

F_{st} : Gradient resistance

F_{spring} : Spring force produced in the suspension

F_{damper} : Damping force produced in the suspension

g : Gravitational acceleration

h_{cg} : Height of the center of gravity of the vehicle with respect to the ground

$h_{cg,arm}$: Vertical distance between the center of gravity of the vehicle body and arm connection points in the body fixed reference frame

\check{I}_a : Inertia tensor of the arm

$I_{arm,x}$: Inertia of the arm along the x-axis in the body fixed reference frame

$I_{arm,y}$: Inertia of the arm along the y-axis in the body fixed reference frame

$I_{arm,z}$: Inertia of the arm along the z-axis in the body fixed reference frame

$I_{s,x}$: Inertia of the sprung mass along the x-axis in the body fixed reference frame

$I_{s,y}$: Inertia of the sprung mass along the y-axis in the body fixed reference frame

$I_{s,z}$: Inertia of the sprung mass along the z-axis in the body fixed reference frame

I_w : Inertia of the tire along the spin axis in the tire body frame

κ : Polytopic gas constant

k_{susp} : Stiffness constant of the suspension

k_{tire} : Spring stiffness of the i^{th} tire

L_{arm} : Length of the arm rods

l_i : Longitudinal distance between the center of gravity of the vehicle body and arm connection point in the body fixed reference frame

L_f : Distance between the arm front arm connection points and body center of gravity

L_m : Distance between the arm middle arm connection points and body center of gravity

L_r : Distance between the arm rear arm connection points and body center of gravity

L_{susp} : Distance between the arm and body connection and the arm and suspension connection

m_{arm} : Mass of the arm rods

M_{fp} : Mass of the floating pistons

m_{sprung} : Sprung mass

M_r : Resisting turning moment

M_{sx} : Reaction moment generated in the arm and body connection point along the x-axis

M_{sy} : Reaction moment generated in the arm and body connection point along the y-axis

M_{sz} : Reaction moment generated in the arm and body connection point along the z-axis

m_v : Total mass of the vehicle

m_w : Mass of the wheel

M_{tz} : Self aligning moment produced in the tire

μ_0 : Static tire/road friction coefficient

p : Angular velocity of the center of gravity of the vehicle body with respect to the ground along the longitudinal axis of the body fixed reference frame

\dot{p} : Angular acceleration of the center of gravity of the vehicle body with respect to the ground along the longitudinal axis of the body fixed reference frame

P_{atm} : Atmospheric pressure

P_{30i}, P_{40i} : Initial accumulator pressures

ϕ : Euler roll angle of the vehicle body

q : Angular velocity of the center of gravity of the vehicle body with respect to the ground along the lateral axis of the body fixed reference frame

\dot{q} : Angular acceleration of the center of gravity of the vehicle body with respect to the ground along the lateral axis of the body fixed reference frame

r : Angular velocity of the center of gravity of the vehicle body with respect to the ground along the vertical axis of the body fixed reference frame

\dot{r} : Angular acceleration of the center of gravity of the vehicle body with respect to the ground along the vertical axis of the body fixed reference frame

\bar{r}_{arm_i} : Relative position vector of the center of gravity of the i^{th} arm from arm body connection point in the body fixed reference frame

$\dot{\vec{r}}_{arm_i}$: Translational velocity vector of the center of gravity of the i^{th} arm with respect to the ground in the body fixed reference frame

$\ddot{\vec{r}}_{arm_i}$: Translational acceleration vector of the center of gravity of the i^{th} arm with respect to the ground in the body fixed reference frame

ρ_h : Density of the hydraulic fluid

\vec{r}_{o,a_i} : Position vector of the i^{th} arm and body connection point in body fixed reference frame

$\dot{\vec{r}}_{o,a_i}$: Velocity vector of the i^{th} arm and body connection point with respect to the ground in body fixed reference frame

$\ddot{\vec{r}}_{o,a_i}$: Acceleration vector of the i^{th} arm and body connection point with respect to the ground in body fixed reference frame

$\dot{r}_{o,a_i,x}$: Velocity of the i^{th} arm and body connection point with respect to the ground along the longitudinal axis of the body fixed reference frame

$\dot{r}_{o,a_i,y}$: Velocity of the i^{th} arm and body connection point with respect to the ground along the lateral axis of the body fixed reference frame

$\dot{r}_{o,a_i,z}$: Velocity of the i^{th} arm and body connection point with respect to the ground along the vertical axis of the body fixed reference frame

$\ddot{r}_{o,a_i,x}$: Acceleration of the i^{th} arm and body connection point with respect to the ground along the longitudinal axis of the body fixed reference frame

$\ddot{r}_{o,a_i,y}$: Acceleration of the i^{th} arm and body connection point with respect to the ground along the lateral axis of the body fixed reference frame

$\ddot{r}_{o,a_i,z}$: Acceleration of the i^{th} arm and body connection point with respect to the ground along the vertical axis of the body fixed reference frame

r_w : Dynamic rolling radius of the wheel

\bar{r}_{w_i} : Position vector of the center of gravity of the i^{th} wheel from arm body connection point in the body fixed reference frame

$\dot{\bar{r}}_{w_i}$: Translational velocity vector of the center of gravity of the i^{th} wheel with respect to the ground in the body fixed reference frame

$\ddot{\bar{r}}_{w_i}$: Translational acceleration vector of the center of gravity of the i^{th} wheel with respect to the ground in the body fixed reference frame

$\hat{R}(\phi)$: Rotation matrix derived from the roll angle

$\hat{R}(\theta)$: Rotation matrix derived from the pitch angle

$\hat{R}(\psi)$: Rotation matrix derived from the yaw angle

$\hat{R}(\theta_{arm})$: Rotation matrix derived from the arm angle

S_{x_i} : Longitudinal slip ratio of the tire

t_w : Track width

T_w : Torque applied to the wheel

T_{susp} : Total torque produced in the suspension

$\theta_{arm,i}$: Angle of the i^{th} arm around its rotation axis

θ : Euler pitch angle of the vehicle body

θ_g : Road gradient

V_{30i}, V_{40i} : Initial volume of the gas inside the accumulator

\bar{V}_b : Velocity vector of the center of gravity of the vehicle body with respect to the ground in body fixed reference frame

V_x : Velocity of the center of gravity of the vehicle body with respect to the ground along the longitudinal axis of the body fixed reference frame

V_y : Velocity of the center of gravity of the vehicle body with respect to the ground along the lateral axis of the body fixed reference frame

V_z : Velocity of the center of gravity of the vehicle body with respect to the ground along the vertical axis of the body fixed reference frame

$V_{t,xi}$: Longitudinal velocity of the tire

$V_{t,yi}$: Lateral velocity of the tire

$\bar{\omega}_b$: Angular velocity vector of the center of gravity of the vehicle body with respect to the ground in body fixed reference frame

$\bar{\omega}_{armi}$: Angular velocity vector of the i^{th} arm with respect to the ground in the body fixed reference frame

$\bar{\omega}_{armi/b}$: Relative angular velocity vector between the i^{th} arm and the vehicle body

ω_w : Angular velocity of the wheel along the spin axis

$\dot{\omega}_w$: Angular acceleration of the wheel along the spin axis

x_i : Relative distance of the i^{th} arm and body connection point to the center of gravity of the vehicle body along the longitudinal axis of the body fixed reference frame

y_i : Relative position of the i^{th} arm and body connection point to the center of gravity of the vehicle body along the lateral axis of the body fixed reference frame

ψ : Euler yaw angle of the vehicle body

z_r : Elevation of the road profile at the tire ground contact point

z_w : Elevation of the tire center

Δz : Displacement of the piston

z_i : Relative position of the i^{th} arm and body connection point to the center of gravity of the vehicle body along the vertical axis of the body fixed reference frame

CHAPTER 1

INTRODUCTION

1.1 Problem Definition

Development of ground vehicles has been a subject of great interest for engineers for a long time. Especially, passenger cars, which appeal to a wide range of community, are considered to be the main field of study. In order to examine the vehicle behavior by means of handling, road holding, ride comfort, and its performance under the effects of innovative control strategies the field of vehicle dynamics are still in progress. Because the traditional structure of conventional vehicles is preserved over the years, modeling of such vehicles is mostly straight-forward and shared in the literature. Due to this fact, instead of spending too much time on modeling of such a complex system, using the simulation environments such as ADAMS, CarMaker, LGSVL, and CarSim, would be more efficient and realistic on behavior analysis of four-wheel passenger cars. However, the structure of the heavy terrain vehicles varies depending on the task it must accomplish. In this respect, number of axles, traction type, suspension system and its mechanism, and steering system can be modified. Hence, it is necessary to develop unique dynamic models for the simulation of these robot-like systems. It is important to mention that the degree of freedom of these systems depend on the application that it will be used. In the literature, most of these studies are restricted with a few degrees of freedom to reduce the complexity only considering the subject that is investigated.

In the literature, for the heavy military vehicles, there are two types of traction mechanisms are shared. These are classified as tracked and wheeled vehicles. For handling and stability studies, these traction mechanisms are analyzed together with their steering systems, considering only the longitudinal, lateral, and yaw motion of these vehicles.

To be able to analyze the characteristics of the suspension systems and capabilities of their mechanisms, only the vertical motion, pitch angle and roll angle are taken into account, in the previous studies. That is because, ignoring the lateral, longitudinal and yaw motion would eliminate the undesired complexity in the model.

In this study, in order to examine the vehicle behavior with respect to various traction inputs and road conditions, an 18 DoF model is developed considering every motion in space for 6x6 skid steered terrain vehicle with articulated double-acting hydro-pneumatic suspension system by using MATLAB/Simulink. To estimate the accuracy of the dynamic vehicle model, results are compared with a multi body dynamic simulation of the same vehicle created on ADAMS software.

1.2 Thesis Outline

In this thesis, the first chapter contains the problem statement regarding the dynamic modeling of heavy-duty vehicles, together with the content structure.

Subsequently, the literature survey is presented for the modeling of steering mechanism, tire and wheel dynamics, load distribution, articulated suspension mechanism, hydro-pneumatic suspension system and sprung mass.

Utilizing the information obtained from the literature review, the equations to be used in the model are modified for the 6x6 vehicle starting from the kinematic relations to resistance forces acting on the vehicle itself. The implementation of these equations into MATLAB/Simulink environment is also indicated in the same chapter.

In order to verify the results of the simulation, same vehicle is modeled as multi body dynamic simulation on ADAMS software for which the model generation of each rigid body and road profile is presented in the next step.

In the fifth chapter, the simulation configurations are shared together with the simulation results explaining every outcome. Also, comparison of the results

obtained from MATLAB/Simulink and ADAMS and discussions on these assessments are presented as well.

In the last chapter, conclusion remarks of the presented study and the future works are stated.

CHAPTER 2

LITERATURE REVIEW

In this section, previous studies related to dynamic modeling of multi-axle heavy terrain vehicles are presented. The literature research of this study comprise of skid steering mechanism, tire and wheel dynamics, load distribution, articulated suspension mechanisms, hydro-pneumatic suspension systems, and the motion of the sprung mass.

Heavy terrain vehicles are examined in two groups in the sense of their traction mechanism as tracked and wheeled vehicles. Even though it has been proved that, the tracked vehicles perform better mobility for off-road applications, in the case of load distribution adjustment and high obstacle crossing scenarios wheeled vehicles has superiorities especially the ones which have articulated suspension mechanisms. [1- 6].

In the literature, different steering mechanisms are utilized for ground vehicles to change the vehicle heading by providing yawing moment. The most common approach for steering is so called front wheel steering [7]. Due to its compact structure and low turning resistance, it is the most convenient steering mechanism for on-road vehicles. In addition to front wheel steering, to generate yawing moment, all wheel steering is also considered for ground vehicles to increase mobility while performing rapid maneuvers [8].

This study is conducted with a 6x6 terrain vehicle containing a skid steering mechanism which is another favored approach in particular for heavy military

vehicles. That is mainly because of its durability under high load applications and severe impact conditions on unmaintained natural roads. Furthermore, because the skid steering mechanism does not require additional components other than the tire itself, it is highly convenient for space constrained vehicles [9]. From another point of view, in case of an all wheel drive vehicle the turning can be achieved with any of two tandem tires while others lose their road contact. However, due to excessive lateral forces exerted on the tires that are away from the projection of the center of gyration on the sagittal (longitudinal) plane, the power requirement is quite a lot on skid steered vehicles [10 - 12].

In order to evaluate the forces and moments on the tires, both analytical and empirical models are studied in the literature [13]. Since there are lots of parameters that affect the characteristic of the tires, in the recent studies the empirical models are preferred over the others, because they reflect the reality pretty accurately. However, most of these studies are conducted for passenger car tires for which the parameters to model the dynamic characteristics of the tires are available in the literature [14 - 16].

On the other hand for the tires that are suitable for rough terrain applications, using the empirical models are very challenging due to lack of parameter information. To be able to use empirical models, one can either prefer to use the parameters from the multibody dynamics simulation platform ADAMS which has very close tire examples or another costly way to obtain these parameters is to cooperate with the companies that examine the tire dynamics like CALSPAN. To decrease the complexity of the model while keeping it as realistic as possible, an analytical model that is called as Dugoff Tire Model is used in this work. The longitudinal and cornering stiffness values of the occupied tire are obtained from the literature [7] [11]. However, to obtain similar results from both MATLAB/Simulink and ADAMS, the Magic Formula is also used in the Simulink model.

Since individual traction and braking forces on tires depend on load distribution for both analytical and empirical models, it is necessary to calculate the load transfer

between the axles. The calculation of the load transfer for the vehicles with two axles is presented in the literature as a straight forward procedure which considers two force and moment equations [17]. However, for the multi-axle vehicles the elevation difference between the consecutive axles should be taken into account as well [8] [11, 18]. In contrast to the axle structure, the 6x6 vehicle discussed in this study contains individual tire connections. That is why, it is essential to consider the load transfer between left and right tires [19].

Suspension mechanisms are utilized to absorb the road shock, preserve the road holding and provide ride comfortability. Suspension systems differ according to their components and controllability [20]. In general, these systems comprise of spring and damper elements. In this study a hydro-pneumatic suspension system, that is first invented by Citroen, is preferred to develop further control algorithms for height adjustment and configurable damping characteristics. Even though the components to be used in a hydro-pneumatic suspension system can differ, they are mainly composed of a hydraulic piston, at least one hydraulic accumulator to generate spring effect and an orifice to provide damping characteristics [21 - 23]. Depending on the configuration, the hydro-pneumatic suspension systems can be used for various applications. Even though double-acting hydro-pneumatic suspensions are more complex than single-acting systems, to achieve fast response for both compression and decompression scenarios, a double-acting hydro-pneumatic suspension structure is discussed in this study [24 - 25].

It is crucial to analyze the behavior of the vehicle under the effects of applied forces and moments. Hence, the sprung mass models are used to obtain the acceleration, velocity and the position of the bodyfixed frame with respect to ground frame. For the specialized studies which are conducted to observe the motion only in one sense, one can reduce the degree of freedom of the sprung mass model by ignoring the other motion equations. Nevertheless, to observe the vehicle movement for the given inputs in any direction, a full vehicle model is evaluated in this work [16][19].

CHAPTER 3

DYNAMIC MODEL

Dynamic models are constructed to study the behaviour, obtain realistic results and develop controllers for the system. Models can range from being simplistic to being very complex, depending on the applications they are going to be used. If a model is going to be utilized to develop controllers, having a simple yet accurate model can suffice. However, in order to simulate the model as close as possible to its real life counterpart, a complex model can yield more accurate results. In both situations, the model should contain as many degrees of freedom as needed to observe the behaviour in the scope of study.

In the case of vehicle dynamics, the models are commonly constructed to examine the performance, handling or ride comfort of the vehicle. If the ride of the vehicle is to be studied; longitudinal, lateral and yaw motion can be neglected in the model and only bounce, pitch and roll motions can be included. On the other hand, if only handling is in the scope of research, the vertical motion of the vehicle and the road irregularities can be assumed to be non-existent.

In this thesis, the motion of a 6x6 skid steering vehicle is studied and validated. As such, a model having 18 degrees-of-freedom is constructed on MATLAB Simulink environment. In order to validate the results, a second model is constructed in the ADAMS software. Assumptions are made for a more robust solution and ease of calculations. However, the model is complex enough to reflect the real life behaviour of the vehicle. The model is non-linear and time invariant. The sprung mass of the vehicle is modeled as a rigid body and its motion in three translational degrees-of-freedom; longitudinal, lateral and vertical, and three rotational degrees-of-freedom; roll, pitch and yaw are examined. The list of parameters used in the model are presented in table 3-1.

Table 3-1. List of the Vehicle Parameters

Symbol of the Parameters	Values	Explanation
m_v	10000 [kg]	Total mass of the vehicle
m_s	7600 [kg]	Sprung mass
$I_{s,x}$	8728 [kg. m ²]	Inertia of the sprung mass along the longitudinal axis of the body fixed frame
$I_{s,y}$	21866 [kg. m ²]	Inertia of the sprung mass along the lateral axis of the body fixed frame
$I_{s,z}$	26413 [kg. m ²]	Inertia of the sprung mass along the vertical axis of the body fixed frame
m_a	130 [kg]	Mass of the arm rods
$I_{a,x}$	10.23 [kg. m ²]	Inertia of the arm rod along its principal x-axis
$I_{a,y}$	11.18 [kg. m ²]	Inertia of the arm rod along its principal y-axis
$I_{a,z}$	1.22 [kg. m ²]	Inertia of the arm rod along its principal z-axis
m_w	270 [kg]	Mass of the tires
I_w	42.44 [kg. m ²]	Inertia of the tire along the rotating axis of the wheel carrier frame
R_w	0.65 [m]	Dynamic radius of the tires
l_{arm}	0.8 [m]	Length of the arm rods
l_{susp}	0.316 [m]	Distance between the suspension connections and arm connections on arm rods
t_w	2.44 [m]	Track width of the vehicle

Table 3-1. List of the Vehicle Parameters (Continued)

Symbol of the Parameters	Values	Explanation
l_f	1.34 [m]	Longitudinal distance between the connection points of the front arms and the center of gravity of the body
l_m	0.9156 [m]	Longitudinal distance between the connection points of the middle arms and the center of gravity of the body
l_r	-0.96 [m]	Longitudinal distance between the connection points of the rear arms and the center of gravity of the body
$h_{cg,arm}$	0.2023 [m]	Vertical distance between the connection points of the arms and the center of gravity of the body
$k_{t,s}$	1e + 06 [N/m]	Tire stiffness

The vehicle is inspected by using a body fixed reference frame. The differential equations of motions are written in order to observe the motion of the vehicle with respect to the ground. The x-axis points towards the front end of the vehicle, the y-axis points towards the driver side in a conventional vehicle and the z-axis points upwards. The roll, pitch and yaw angles abide by the right hand law along the x-,y- and z-axes, respectively.

The body of the vehicle is connected to six arms with rigid connections and individual suspension systems. The suspension systems are modelled as double acting hydro-pneumatic suspensions. Each of the arms are able to rotate around their rigid connections to the sprung mass, which give additional six degrees-of-freedom to the system. The rotational dynamics of each of the wheels also introduce six degrees-of-freedom resulting in a total of 18 degrees-of-freedom. Furthermore, tire dynamics and load distribution of the vehicle are also included in the model. The details of each of the mentioned systems are explained in the following chapters.

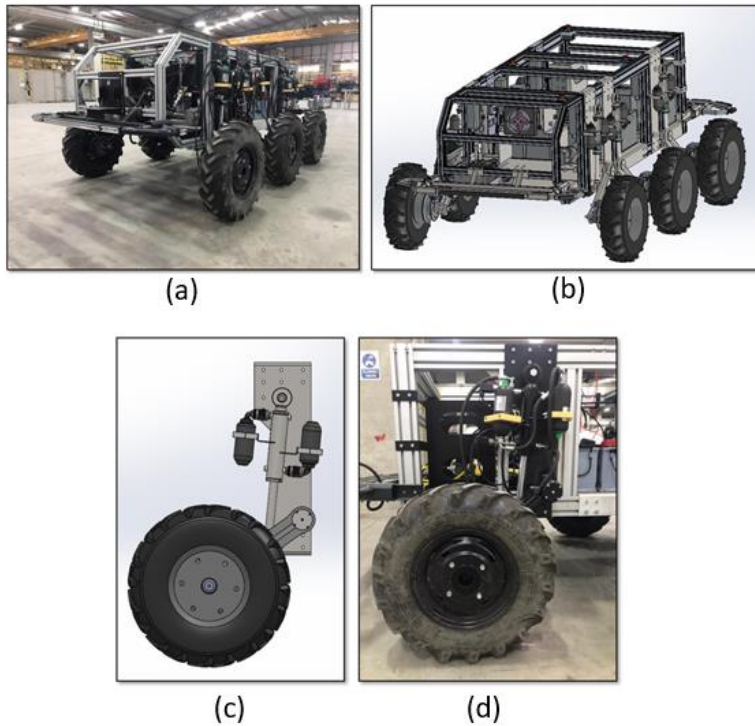


Figure 3-1. (a) 6x6 test vehicle. (b) CAD design of the test vehicle. (c) CAD design of arm rod, suspension and wheel. (d) Assembled arm rod, suspension, and tire of the test vehicle.

The wheels and arms are numbered for ease of referencing from left to right and front to back. In other words, front-left arm is called arm 1, front-right arm is arm 2, middle-left arm is arm 3 and so on.

Each of the parts are constructed as a separate subsystem in Simulink. However, as the resultant motions and forces interact with and are dependent on each other, each of the subsystems work together in order to yield valid results. The inputs to the system are the road profile and the torques applied to the tires. The vehicle in this study uses skid steering. As such, for steering, different torques are applied to left and right wheels.

Eighth order Dormand-Prince fixed solver is used in Simulink with a step size of 0.001. The figures of the Simulink model are supplied in the appendices.

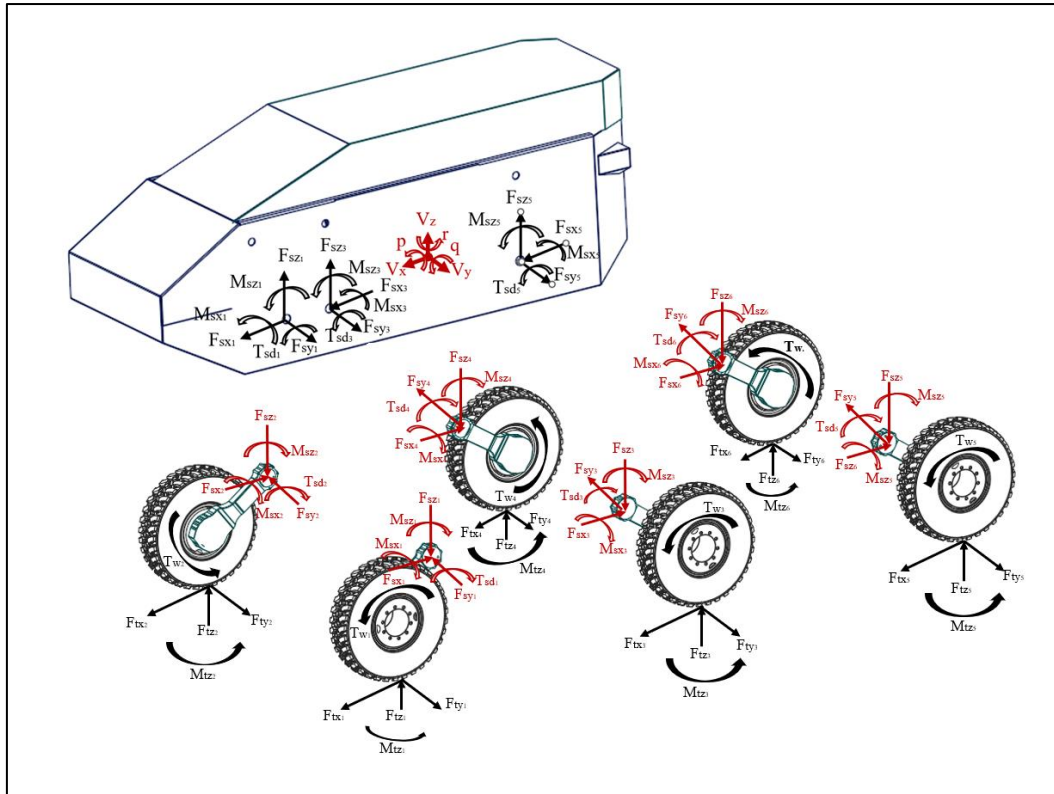


Figure 3-2. Free body diagrams depicting the forces and reactions in each body

3.1 Kinematic Relations

Equations of motion are written in order to derive the motion of the bodies in the system with respect to the ground. For the sprung mass, the result of these equations yield translational and rotational accelerations directly. However, for the tires and arms, the equations of motion yield the reaction forces in the joints if the motion is constrained. These reaction forces are then transferred to the vehicle body subsystem. In doing so, the effects of the forces generated in the tires can be seen in the sprung mass while considering the effect of other bodies in the system.

As the motion of the arms are also desired to be examined and the equations of motion for the tires and arms use the accelerations and the velocities of the corresponding components, these variables have to be derived using kinematic relations between bodies. Since the motion of the sprung mass is known at each time

step, the motion of the remaining bodies can be found using the constraint equations imposed by the rigid connections and equations of motion where necessary.

The system is initially considered to be at equilibrium with the given initial conditions. The kinematic relations are computed at separate subsystems. The motions of each component are calculated in these subsystems using initial conditions at the start and the body or arm states as the simulation progresses. Firstly, consider the figure 3-3 where the vehicle body is shown together with the arm connections.

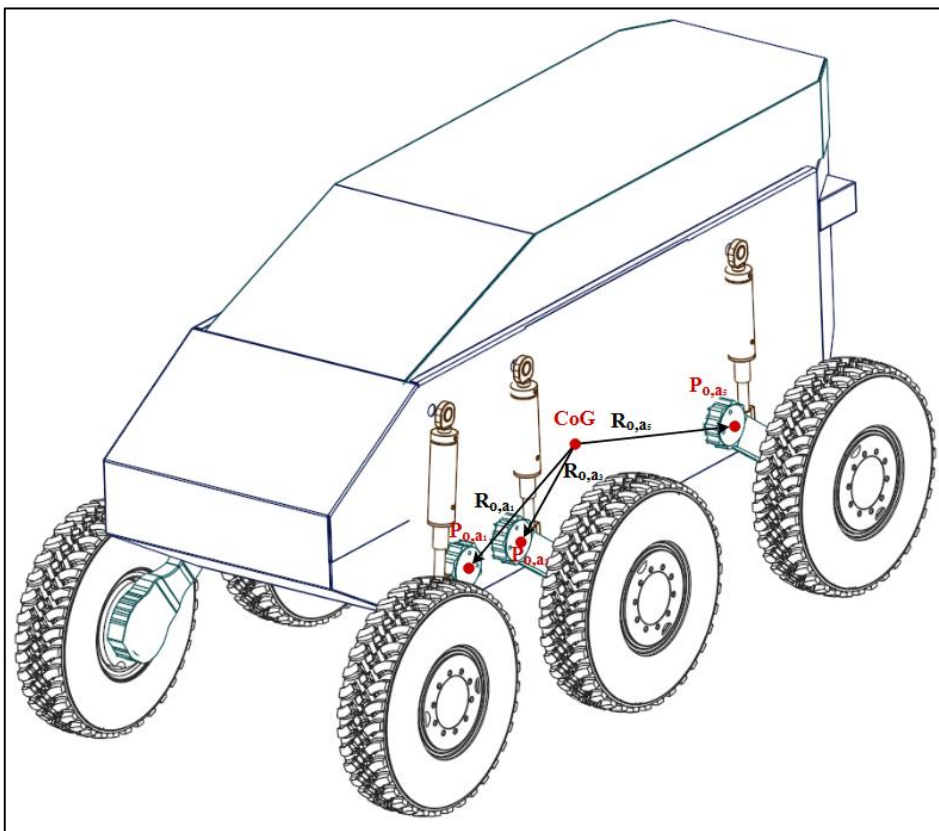


Figure 3-3. Figure depicting the left arm body connection points and the position vectors from the center of gravity of the vehicle body to the connection points

Consider the points labelled as P_{o,a_i} which is located at the connection between the vehicle body and i^{th} arm rod. The subscript “ i ” denotes the arm or tire number. As explained in the beginning of this chapter, arms and tires are numbered from left to right and front to back. In other words, front left arm is denoted with subscript “1”,

front right arm is denoted with subscript “2”, middle left arm is denoted with subscript “3” and so on. The connection points have the same numbering system. The position vector from the center of gravity of the vehicle to the points where the arm and body connections are denoted as \bar{r}_{o,a_i} . If the instantaneous velocities of the origin of the body fixed reference frame are V_x, V_y and V_z along the longitudinal, lateral and vertical axes and the angular velocities along these axes are p, q and r , by noting that the connection point has no velocity with respect to the body-fixed reference frame due to the rigid body assumption, the velocity of the point P_{o,a_i} with respect to the ground in body fixed reference frame can be written as the following:

$$\dot{\bar{r}}_{o,a_i} = \bar{V}_b + \bar{\omega}_b \times \bar{r}_{o,a_i} \quad (3.1)$$

In equation (3.1) \bar{V}_b denotes the translational velocity vector of the body in the body fixed reference frame, $\bar{\omega}_b$ denotes the angular velocity vector of the body, \bar{r}_{o,a_i} denotes the relative position vector of the i^{th} arm and body connection point with respect to the origin of the body-fixed reference frame.

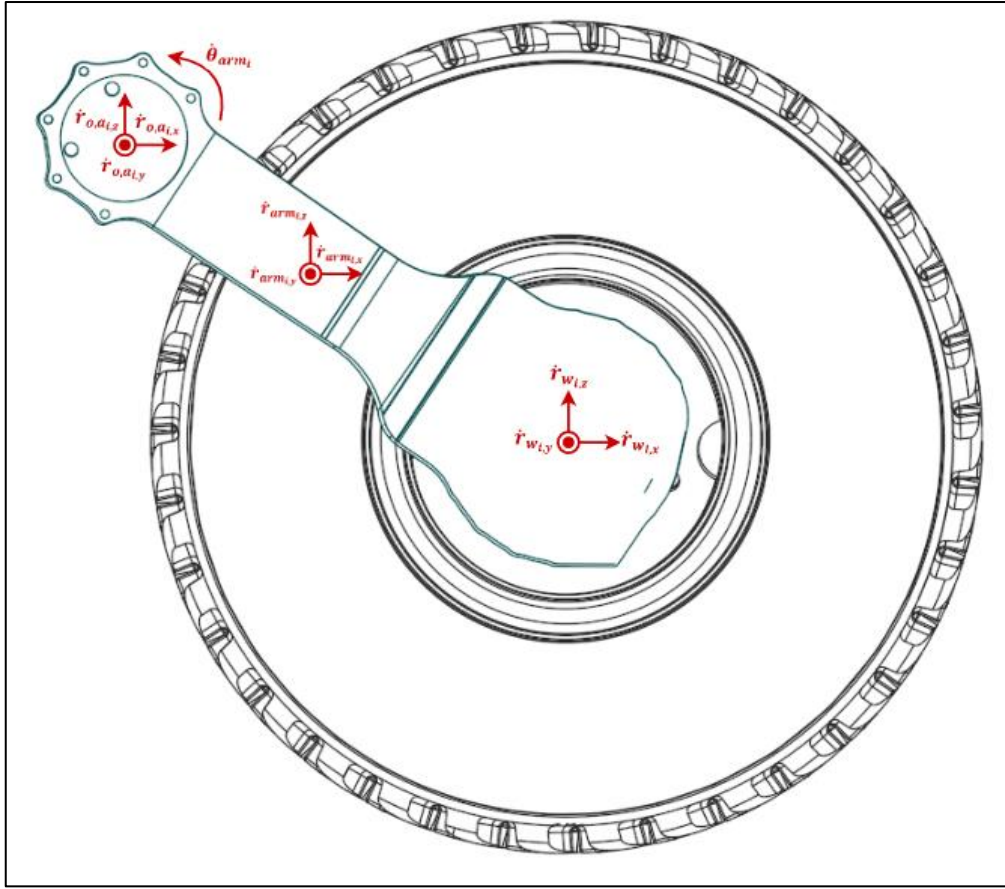


Figure 3-4. Velocity components of the arm and body connection, arm center of gravity, and tire center of gravity

If the equation is expanded and velocities are written along the x, y and z-axes, they can be seen as:

$$\dot{r}_{o,a_{i,x}} = V_x + qz_i - ry_i \quad (3.2)$$

$$\dot{r}_{o,a_{i,y}} = V_y + rx_i - pz_i \quad (3.3)$$

$$\dot{r}_{o,a_{i,z}} = V_z + py_i - qx_i \quad (3.4)$$

In equations (3.2) to (3.4), the terms $\dot{r}_{o,a_{i,x}}$, $\dot{r}_{o,a_{i,y}}$, and $\dot{r}_{o,a_{i,z}}$ denote the velocities of the i^{th} arm and body connection points along the longitudinal, lateral, and vertical axes of the body frame, respectively. Similarly, x_i , y_i , and z_i denote the distance

along the three axes between the connection points and the origin of the body reference frame which is coincident with the center of gravity of the body. Similarly, the accelerations of the point in consideration can be written as the following in the vector-matrix form:

$$\ddot{\vec{r}}_{o,a_i} = \dot{\vec{V}}_b + \bar{\alpha}_b \times \vec{r}_{o,a_i} + \bar{\omega}_b \times (\bar{\omega}_b \times \vec{r}_{o,a_i}) \quad (3.5)$$

In equation (3.5), $\bar{\alpha}_b$ denotes the angular acceleration of the vehicle body. If the equation is expanded, the equations for accelerations of the connection points along the three body axes can be written as shown in equations (3.6) to (3.8).

$$\begin{aligned} \ddot{r}_{o,a_i,x} = & (\dot{V}_x + qV_z - rV_y) + (\dot{q}z_i - \dot{r}y_i) \\ & + (-[r^2 + q^2]x_i + pqy_i + prz_i) \end{aligned} \quad (3.6)$$

$$\begin{aligned} \ddot{r}_{o,a_i,y} = & (\dot{V}_y + rV_x - pV_z) + (\dot{r}x_i - \dot{p}z_i) \\ & + (pqx_i - [p^2 + r^2]y_i + qrz_i) \end{aligned} \quad (3.7)$$

$$\begin{aligned} \ddot{r}_{o,a_i,z} = & (\dot{V}_z + pV_y - qV_x) + (\dot{p}y_i - \dot{q}x_i) \\ & + (prx_i + qry_i - [p^2 + q^2]z_i) \end{aligned} \quad (3.8)$$

Equations from (3.1) to (3.8) denote the velocities and accelerations of the point where the connection between body and i^{th} arm is located. Similar to dynamic equations of motions which will be derived in the following chapters, these equations are coupled and non-linear. As the components such as the suspensions and tires already exhibit a non-linear behaviour, these equations pose a challenge for convergence to a solution while the system is being solved simultaneously. However, the solutions are obtained using numerical methods already integrated in MATLAB/Simulink software.

Due to lateral lengths of arms and tire connections being small, the distance between body center and arm/body connections, arm centers and tire centers are treated as equal for the sake of simplicity of operations.

Although the motions of these points are not in direct interest, they are necessary to obtain in order to derive the motions of the center of masses of arms and tires as well as the suspension connection points.

Indeed, in order to write the kinematic equations of the arms and wheels, the velocities and accelerations of their respective points of connection to the body will be considered. The velocity of the center of gravity of the i^{th} arm and wheel can be written as:

$$\dot{\bar{r}}_{arm_i} = \dot{\bar{r}}_{o,a_i} + \bar{\omega}_{arm_i} \times \bar{r}_{arm_i} \quad (3.9)$$

$$\dot{\bar{r}}_{w_i} = \dot{\bar{r}}_{o,a_i} + \bar{\omega}_{arm_i} \times \bar{r}_{w_i} \quad (3.10)$$

In equations (3.9) and (3.10) \bar{r}_{arm_i} and \bar{r}_{w_i} denote the position vector of the center of gravity of arm and wheel with respect to its arm/body connection and noting that the arms are connected to the body with revolute joints, $\bar{\omega}_{arm_i}$ can be defined as:

$$\bar{\omega}_{arm_i} = \bar{\omega}_b + \bar{\omega}_{arm_i/b} \quad (3.11)$$

$$\bar{\omega}_{arm_i} = \begin{bmatrix} \omega_{arm_i,x} \\ \omega_{arm_i,y} \\ \omega_{arm_i,z} \end{bmatrix} = \begin{bmatrix} p \\ q \\ r \end{bmatrix} + \begin{bmatrix} 0 \\ \dot{\theta}_{arm_i} \\ 0 \end{bmatrix} = \begin{bmatrix} p \\ q + \dot{\theta}_{arm_i} \\ r \end{bmatrix} \quad (3.12)$$

In a similar fashion, the accelerations of the arm and wheel's center of gravity is given below:

$$\ddot{\bar{r}}_{arm_i} = \ddot{\bar{r}}_{o,a_i} + \bar{\alpha}_{arm_i} \times \bar{r}_{arm_i} + \bar{\omega}_b \times (\bar{\omega}_b \times \bar{r}_{arm_i}) \quad (3.13)$$

$$\ddot{\bar{r}}_{w_i} = \ddot{\bar{r}}_{o,a_i} + \bar{\alpha}_{arm_i} \times \bar{r}_{w_i} + \bar{\omega}_b \times (\bar{\omega}_b \times \bar{r}_{w_i}) \quad (3.14)$$

Again, in equations (3.13) and (3.14) $\bar{\alpha}_{arm_i}$ denotes the angular acceleration the i^{th} arm and it can be found as:

$$\bar{\alpha}_{arm_i} = \bar{\alpha} + \bar{\alpha}_{arm_i/b} + \bar{\omega} \times \bar{\omega}_{arm_i/b} \quad (3.15)$$

$$\begin{aligned} \bar{\alpha}_{arm_i} &= \begin{bmatrix} \bar{\alpha}_{arm_i,x} \\ \bar{\alpha}_{arm_i,y} \\ \bar{\alpha}_{arm_i,z} \end{bmatrix} = \begin{bmatrix} \dot{p} \\ \dot{q} \\ \dot{r} \end{bmatrix} + \begin{bmatrix} 0 \\ \ddot{\theta}_{arm_i} \\ 0 \end{bmatrix} + \begin{bmatrix} p \\ q \\ r \end{bmatrix} \times \begin{bmatrix} 0 \\ \dot{\theta}_{arm_i} \\ 0 \end{bmatrix} \\ &= \begin{bmatrix} \dot{p} - r\dot{\theta}_{arm_i} \\ \dot{q} + \ddot{\theta}_{arm_i} \\ \dot{r} + p\dot{\theta}_{arm_i} \end{bmatrix} \end{aligned} \quad (3.16)$$

Thus, the velocities and accelerations of the arm and wheel center of gravities are obtained which are to be used in dynamical equations of motion. It should be noted that the accelerations and velocities derived in this chapter thus far are resolved in the vehicle body fixed reference frame although the derivatives are taken with respect to the ground. However, the wheel dynamics equations and the tire models have to be solved in the inertial reference frame as the tire – ground contact is the main interest. Hence, a reference transformation is necessary before writing the forementioned equations.

In addition, the motion of the vehicle with respect to the inertial reference frame is also desired. The transformation is done by forming a direction cosine matrix using Euler angles. In order to derive the Euler angles from body angles, a mapping between the Euler angle rates and body angular velocity has to be formed. Using the yaw-pitch-roll sequence, the transformation between the Euler angle rates and body angle rates can be written as;

$$\begin{aligned}
\begin{bmatrix} p \\ q \\ r \end{bmatrix} &= \begin{bmatrix} \dot{\phi} \\ 0 \\ 0 \end{bmatrix} + \begin{bmatrix} 1 & 0 & 0 \\ 0 & \cos(\phi) & \sin(\phi) \\ 0 & -\sin(\phi) & \cos(\phi) \end{bmatrix} \begin{bmatrix} 0 \\ \dot{\theta} \\ 0 \end{bmatrix} \\
&+ \begin{bmatrix} 1 & 0 & 0 \\ 0 & \cos(\phi) & \sin(\phi) \\ 0 & -\sin(\phi) & \cos(\phi) \end{bmatrix} \begin{bmatrix} \cos(\theta) & 0 & -\sin(\theta) \\ 0 & 1 & 0 \\ \sin(\theta) & 0 & \cos(\theta) \end{bmatrix} \begin{bmatrix} 0 \\ 0 \\ \dot{\psi} \end{bmatrix} \quad (3.17) \\
&= J^{-1} \begin{bmatrix} \dot{\phi} \\ \dot{\theta} \\ \dot{\psi} \end{bmatrix}
\end{aligned}$$

$$\begin{bmatrix} \dot{\phi} \\ \dot{\theta} \\ \dot{\psi} \end{bmatrix} = \begin{bmatrix} 1 & \sin(\phi) \tan(\theta) & \cos(\phi) \tan(\theta) \\ 0 & \cos(\phi) & -\sin(\phi) \\ 0 & \frac{\sin(\phi)}{\cos(\theta)} & \frac{\cos(\phi)}{\cos(\theta)} \end{bmatrix} \begin{bmatrix} p \\ q \\ r \end{bmatrix} = J \begin{bmatrix} p \\ q \\ r \end{bmatrix} \quad (3.18)$$

By integrating the equation (3.18), the Euler angles can be obtained at each time step.

Then, the rotation matrices can be formed using Euler angles.

$$\begin{aligned}
\hat{R}(\phi) &= \begin{bmatrix} 1 & 0 & 0 \\ 0 & \cos(\phi) & \sin(\phi) \\ 0 & -\sin(\phi) & \cos(\phi) \end{bmatrix} \\
\hat{R}(\theta) &= \begin{bmatrix} \cos(\theta) & 0 & -\sin(\theta) \\ 0 & 1 & 0 \\ \sin(\theta) & 0 & \cos(\theta) \end{bmatrix} \quad (3.19) \\
\hat{R}(\psi) &= \begin{bmatrix} \cos(\psi) & \sin(\psi) & 0 \\ -\sin(\psi) & \cos(\psi) & 0 \\ 0 & 0 & 1 \end{bmatrix}
\end{aligned}$$

Finally, the direction cosine matrix between the inertial reference frame and the body fixed reference frame.

$$DCM_{b,e} = \hat{R}(\phi)\hat{R}(\theta)\hat{R}(\psi) \quad (3.20)$$

3.2 Road Profile

The vehicle in the scope of this study is mainly going to be operated in off-road conditions. In order to observe the dynamic response characteristics of the vehicles, full scale field tests are conducted. However, as the computer based simulations can reflect real life behavior of the models accurately, they offer the opportunity to show the response of the vehicle without having to run field tests. Indeed, the main objective of the prepared simulations in this research is to observe and study the vehicle's behaviour before testing it in real life. As such, the conditions imposed on the model should reflect the real life ones as accurately as possible.

To this end, road profile, which is one of the inputs of the system, is modeled based on the environment the vehicle is expected to face. However, in order to properly test the system, standardized versions of the road profiles are used. Aberdeen Proving Grounds (APG) have test courses for heavy off-road vehicles similar to the one investigated in this study. Using the data of the APG's test course, several road profiles are constructed. These road profiles include a flat road, a bump, a constant sine wave, and a ramp [28][29]. These road profiles can be supplied to the left and right tires individually, meaning that it is possible to supply left and right tires with different road profiles to examine the roll behaviour. The positions of the tires are known at each time step as a result of the calculations in the kinematic relations section. Knowing the positions of the wheels, it is possible to obtain the elevations of the road profile corresponding for each tire. The same road profile will be effecting each tire with a time difference depending on the velocity of the vehicle. If the vehicle is accelerating, the same bump will be traversed faster by the rear tires compared to front tires and their effects on the vehicle can differ.

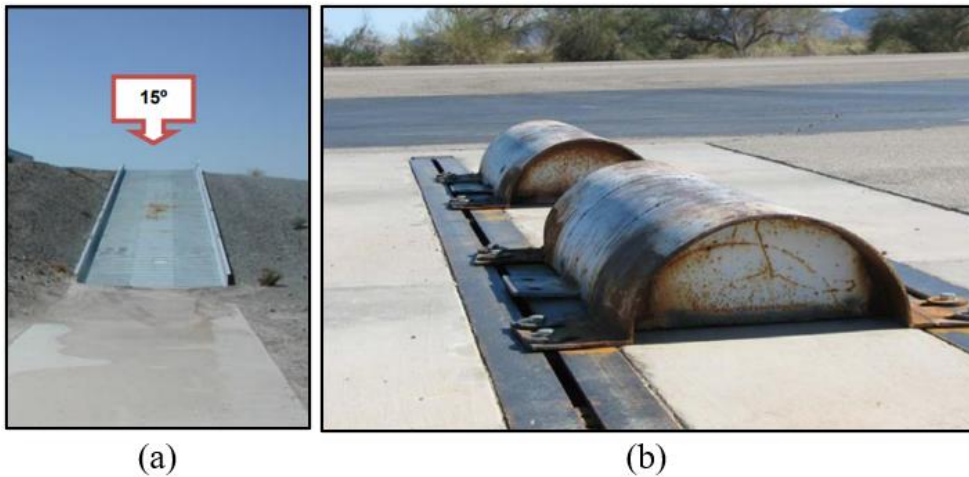


Figure 3-5. (a) Road with a gradient of 15° (b) Bumps used in Aberdeen Proving Grounds

It should be noted that mainly the vertical response of the vehicle is in the focus during these tests. Although this is true in this case as well, the traction capabilities of the tires are also in consideration of this study. The load distribution algorithm which works together with the tire module calculates the vertical load acting on the tires. Due to this change, the traction forces of the tires also differ. As each of the wheels are actuated independently, a control algorithm can be created in order to get desired traction forces on each of the tires by considering vehicle's orientation, accelerations and the road profile the vehicle is traversing which might have gradient or bank angles.

3.3 Wheel Dynamics

One of the inputs to the system is the road profile as explained in the previous section. The second input is the torques transmitted to the wheels.

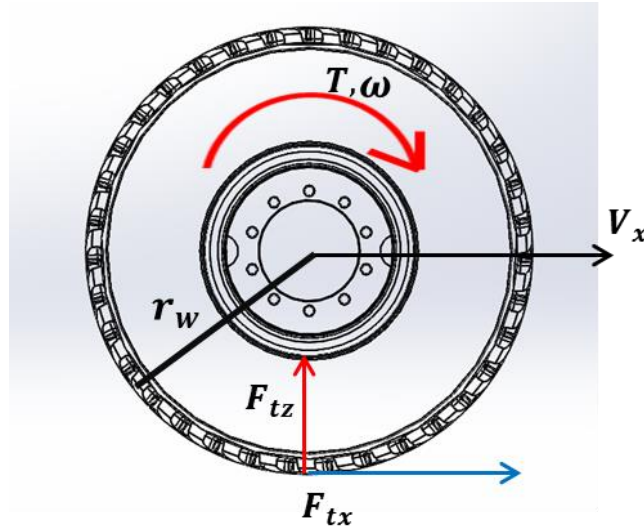


Figure 3-6. FBD showing wheel dynamics

The torque applied to the wheels results in a rotational acceleration which is dependent on the inertia of the wheels. Then, as the wheels rotate, longitudinal and lateral forces are developed in the tire contact patch. The longitudinal force creates a moment at the tire center which acts against the rotational direction of the wheels and the applied torque. As such, the torque inputs to the wheels are governed by the equation;

$$T_w - F_{tx}r_w = I_w\dot{\omega}_w \quad (3.21)$$

By solving the differential equation (3.21) for ω_w and feeding the result to the tire subsystem, F_{tx} is obtained which is the traction force that drives the vehicle and acts against the rotation of the wheels. The traction force is then fed back to the equation and the rotational speed of the wheels are calculated accordingly. It should be noted that equation (3.21) is written in the inertial reference frame as the tire-ground contact is of importance.

3.4 Tire Model

Tires can be considered as one the most complex component in vehicle dynamics. Extensive research have been conducted in the past decades to better understand tire characteristics and their use in vehicle dynamic models. Many models have been proposed and the researches still continue to develop new models which yield better results.

The proposed models differ in complexity, accuracy, and capability. Both analytical and experimental models are used in variety of operations. Experimental models generally yield more accurate results, but it is expensive and time consuming to generate enough data in order to use them. Analytical models which yield qualitatively valid results to carry out vehicle dynamic simulations can be considered rather than experimental models for the sake of simplicity [13].

In this study, to observe more realistic results in case of combined slip scenarios, Pacejka's Magic Formula is preferred. The required tire parameters are extracted from ADAMS software for the tire 315/80 R 22.5 that is used for heavy terrain applications. The constructed tire model provides longitudinal and lateral forces as well as self-alignment moment for both pure and combined slip cases [15] [30].

Both analytical and empirical models take into consideration of slip angle, vertical load and slip ratio. The slip ratio can be obtained using the following expressions:

$$S_{xi} = \left\{ \begin{array}{l} \frac{r_w \omega_{w,i} - V_{t,xi}}{r_w \omega_{w,i}} \text{ if } r_w \omega_{w,i} - V_{t,xi} \geq 0 \text{ (traction)} \\ \frac{V_{t,xi} - r_w \omega_{w,i}}{V_{t,xi}} \text{ if } r_w \omega_{w,i} - V_{t,xi} < 0 \text{ (braking)} \end{array} \right\} \quad (3.22)$$

The expression for slip angle for a conventional vehicle can be written as:

$$\alpha_{w,i} = \arctan\left(\frac{V_{t,yi} - \dot{\psi}_{w,i}l_i}{V_{t,xi} \mp \dot{\psi}_{w,i}\frac{t_w}{2}}\right) - \delta_{w,i} \quad (3.23)$$

However, noting that the vehicle is being modeled in 6 degree-of-freedom, instead of writing the equation (3.22) just by using the motions in the xy-plane, the roll and pitch angles of the vehicle are also taken into consideration. Furthermore, the kinematic relations used in this model also use the arms' rotational velocities to calculate the tires' velocities in the wheel plane. So, the velocity in the slip ratio expression in equation (3.23) and the slip angle equation (3.24) are written using the results given by equation (3.10).

$$\alpha_i = \arctan\left(\frac{V_{tyi}}{V_{txi}}\right) \quad (3.24)$$

It should also be noted that for skid steered vehicles, there are no steering angles. As such, δ_i is also dropped from equation.

The formulation for the Pacejka's Magic Formula can be found below [30]. Although existing Simulink blocks are used for Magic Formula tire models, the main formulation is still shared. Magic Formula uses test data to curve fit the desired tire behavior in empirical equations. The main governing equation is as follows;

$$Y = S_y + D \sin\{C \arctan[B(X - S_x)(1 - E) + E \arctan(B(X - S_x))]\} \quad (3.25)$$

In equation (3.23), the desired tire variable is denoted with Y which can be traction force, lateral force, etc. The constants B, C, D, E, S_x , and S_y take different values depending on the tire parameters and road conditions as well as the which response quantity is of interest in the governing Magic Formula equation. Variable X also depend on which response quantity is being examined. For example, longitudinal slip value can be used in the place of X if the equation is being solved for traction force or if the lateral tire force is of interest, it can take the value of lateral slip angle.

For cases where the tire data cannot be obtained, Dugoff model provides an analytical solution for calculation of tire forces. Although Magic Formula provides more realistic results, Dugoff model still yields acceptable results. However, as comparison between Simulink and ADAMS is in the objective of this study, Magic Formula tire models are used in Simulink. However, the formulation for the Dugoff tire model is also shared below.

$$V_{s,i} = V_{t,xi} \sqrt{S_{x,i}^2 + \tan^2(\alpha_{w,i})} \quad (3.26)$$

In equation (3.26) $V_{t,xi}$ denotes the longitudinal velocity of the vehicle and $S_{x,i}$ and $\tan(\alpha_{w,i})$ are obtained from equations (3.22) and (3.24) respectively.

$$\mu = \mu_0(1 - A_s V_s) \quad (3.27)$$

Here, μ_0 stands for the static tire/road friction coefficient.

$$z = \frac{\mu F_{tz}(1 - S_x)}{2\sqrt{(C_l S_x)^2 + (C_s \tan(\alpha))^2}} \quad (3.28)$$

In equation (3.28), F_{tz} is obtained from load distribution algorithm for each of the tires. Furthermore, C_l and C_s are longitudinal and cornering stiffness values for the tires.

$$f(z) = \begin{cases} z(2 - z) & \text{for } z < 1 \\ 1 & \text{for } z \geq 1 \end{cases} \quad (3.29)$$

Then, the longitudinal and lateral forces produced by the tires are given as:

$$F_{tx} = \frac{C_l S_x f(z)}{1 - S_x} \quad (3.30)$$

$$F_{ty} = \frac{C_s \tan(\alpha) f(z)}{1 - S_x} \quad (3.31)$$

3.5 Load Distribution

During motion the translational and rotational acceleration together with the orientation of the vehicle body effects how the loads are distributed to each of the tires. Although the system is treated as at static equilibrium initially when writing the dynamic equations of motions, the load distribution is critical for the generation of forces in the tire system. As the terrain vehicle transverses will be rough and uneven for the most part, the forces generated in the tires will play an important part in the vehicle's performance and behavior. As such, the effect of the load distribution on the tires are included in this study by considering the vehicle's orientation and motion together with the road profile.

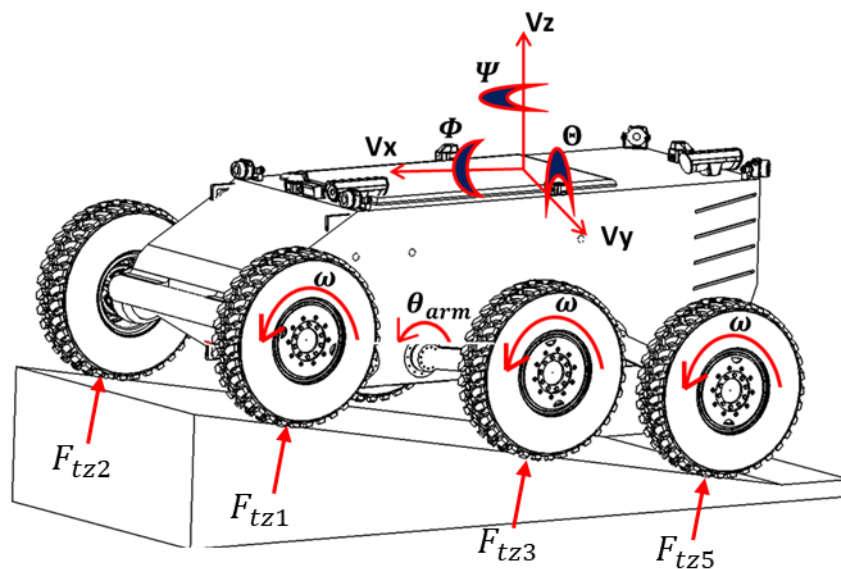


Figure 3-7. Load distribution of the vehicle

Firstly, in order to distribute the load to each of the tires, the lateral weight transfer is considered. The left and right side of the wheels are considered to be carrying the load exerted by the vehicle under any existing roll angle or lateral acceleration which can be produced during steering maneuvers. While considering the lateral weight transfer, all the tires in left and right side of the vehicle are assumed to be carrying the total weight. If the vertical forces exerted by the ground to the left tire set is F_{tzL}

and for the right tire sets F_{tzR} , the vertical forces acting on the tires need to satisfy the force and moment equations given below:

$$m_v g \left(\frac{t_w}{2} \cos(\phi) - h_{cg} \sin(\phi) \right) - F_{tzL} t_w a_y = 0 \quad (3.32)$$

$$m_v g \left(\frac{t_w}{2} \cos(\phi) + h_{cg} \sin(\phi) \right) - F_{tzR} t_w a_y = 0 \quad (3.33)$$

Here; m_v stands for the total mass of the vehicle, g denotes the gravitational acceleration, roll angle is shown by ϕ , and t_w is the track width.

Note that during cornering events, weight will be distributed to left or right tires depending on the direction of motion. The effect of the lateral acceleration can be added to the constructed equations as seen below:

$$\frac{m_v g \left(\frac{t_w}{2} \cos(\phi) - h_{cg} \sin(\phi) \right)}{t_w} + a_y h_{cg} t_w = F_{tzL} \quad (3.34)$$

$$\frac{m_v g \left(\frac{t_w}{2} \cos(\phi) + h_{cg} \sin(\phi) \right)}{t_w} - a_y h_{cg} t_w = F_{tzR} \quad (3.35)$$

Having distributed the load to the left and right tire sets, the longitudinal load distribution has to be considered to find each individual vertical force acting on the tires.

Firstly, consider a conventional vehicle with two axles and four wheels, two equations are sufficient in order to determine the weights carried by each of the axles. These equations are the force equation along the z-axis and the moment equation along the y-axis. For a vehicle at rest, they can be written as;

$$\sum F_{tzi} - m_v g \cos(\theta) = 0 \quad (3.36)$$

$$\sum x_i F_{tzi} + \sum z_i F_{txi} = 0 \quad (3.37)$$

Here, the term θ stands for the pitch angle. It should also be noted that the longitudinal and vertical distances of each tire to the vehicle's center of gravity, x_i and z_i , are calculated as explained in the kinematic relations section. Another adjustment to be made comes from the fact that dynamic solutions to the equations are sought at each time step. As such, effects of the accelerations should also be added to the equations. Since the loads are distributed to the left and right tires, the loads acting on each tire sets F_{tzj} , where $j = L, R$ depending on the tire sets considered. Then, by adding the acceleration terms, the equations become;

$$\sum F_{tzi} = \frac{F_{tzj}}{g} (\ddot{V}_z + \dot{V}_y \dot{\phi} - \dot{V}_x \dot{\theta} + g \cos(\theta)) \quad (3.38)$$

$$\sum x_i F_{tzi} = -(I_y \ddot{\theta} + [I_x - I_z] \dot{\phi} \dot{\psi}) - \sum z_i F_{txi} \quad (3.39)$$

As mentioned before, these two equations suffice for a vehicle with two axles or four tires. However, in order to distribute the load to three axles, or three tires in a tire set as in this case, an additional equation is required. For vehicle with n-axles, by ignoring the tires' compliance, the rigid vehicle must have;

$$\frac{z_i - z_1}{x_i - x_n} = \frac{z_n - z_1}{x_n - x_1}, \quad i = 2, 3, \dots, n - 1 \quad (3.40)$$

Assuming that suspensions carry the vehicle loads and transfer these loads to the tires directly the vertical load on the tires can be written as;

$$F_{tzi} = k_{susp,i} z_i \quad (3.41)$$

And equation (3.40) becomes;

$$\frac{F_{tzi}/k_{susp,i} - F_{tz1}/k_{susp,1}}{x_i - x_1} = \frac{F_{tzn}/k_{susp,n} - F_{tz1}/k_{susp,1}}{x_n - x_1} \quad (3.42)$$

Expanding the equation for a 3-axle vehicle;

$$F_{tz1}[k_{susp,2}k_{susp,3}(x_2 - x_3)] + F_{tz2}[k_{susp,1}k_{susp,3}(x_3 - x_1)] + F_{tz3}[k_{susp,1}k_{susp,2}(x_1 - x_2)] = 0 \quad (3.43)$$

Then for the tires in the left and right, the constructed equations can be written in matrix form to find the loads in the front, middle and rear tires.

$$[A]\{F_{tzi}\} = [B] \quad (3.44)$$

$$\begin{bmatrix} 1 & 1 & 1 \\ x_1 & x_2 & x_3 \\ k_2k_3(x_2 - x_3) & k_1k_3(x_3 - x_1) & k_1k_2(x_1 - x_2) \end{bmatrix} \begin{Bmatrix} F_{tz1} \\ F_{tz2} \\ F_{tz3} \end{Bmatrix} = \begin{bmatrix} \frac{F_{tzj}}{g} (\dot{V}_z + \dot{V}_y\phi - \dot{V}_x\theta + g\cos(\theta)) \\ -(I_y\ddot{\theta} + [I_x - I_z]\dot{\phi}\psi) - \sum z_i F_{txi} \\ 0 \end{bmatrix} \quad (3.45)$$

Then, premultiplying each side with $[A]^{-1}$, front, middle, and rear tire loads denoted as F_{tz1} , F_{tz2} , and F_{tz3} can be found.

$$\begin{Bmatrix} F_{tz1} \\ F_{tz2} \\ F_{tz3} \end{Bmatrix} = [A]^{-1}[B] \quad (3.46)$$

Thus, the loads acting on each tire are found. The found tire loads are sent to the tire module so that the traction and lateral forces generated change according to the weight distribution and yield more realistic results.

3.6 Suspension System

Suspension systems connect wheels to the vehicle body. Their task is to temporarily store and dissipate energy induced by the irregularities on the road, such as bumps. How much the suspension system achieves this task is vital to riding performance. Fulfilling all requirements of the ride performance with a suspension design having fixed parameters is a complex task since performance metrics such as ride comfort and traction require parameters to be set in contradicting manner. These contradictions pose a significant challenge for engineers and scientists.

Passive suspension systems are most common because of their simplicity and low cost [32]. Passive suspension systems have fixed parameters and optimization studies have to be performed to balance ride comfort and performance and the vehicle. For military vehicles and trucks which are operated in varying road and loading conditions, the passive suspensions' limitations become much more visible. Semi-active and active suspensions are developed to overcome these problems. Semi-active suspensions have the ability to adjust stiffness and damping of the system during operation while active suspensions can additionally introduce or remove energy from the system using an actuator. Semi-active and active suspension systems are generally more complex and expensive compared to their passive counterparts.

Hydro-pneumatic suspensions are developed in this regard. They offer the simplicity of passive systems while also being able to meet the requirements of varying ride conditions. Hydro-pneumatic suspension systems consist of a hydraulic cylinder, accumulator, and orifice in their simplest form. The hydraulic cylinder is connected to the wheel. Oil in the cylinder flows to the accumulator when the road displaces the wheel, and the oil removed from the cylinder compresses the gas in the accumulator. The energy is temporarily stored in the compressed gas; hence the effect of spring is achieved. The oil displaced to the accumulator flows back to the cylinder via an orifice while the wheel returns to its' neutral position, dissipating the energy stored in the gas [33] [34].

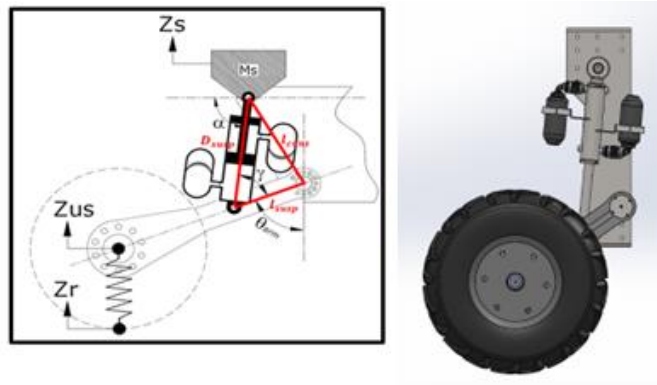


Figure 3-8. Schematic and CAD drawing of double acting hydro-pneumatic suspension system

The force needed to compress a gas rises with increasing pressure [21]. This inherently non-linear behavior of gases provides a significant advantage to hydro-pneumatic suspension systems. Compressing gas gets harder with increasing wheel displacement or vehicle load; hence spring gets stiffer. Parameters of the semi-active hydro-pneumatic suspension system are adjusted spontaneously without the need for an external controller [35].

Vehicles with a hydro-pneumatic suspension system are generally built with a hydraulic reservoir and pump to adjust pressure. Drive height can be adjusted using this hydraulic system without any additional investment. It is also possible to add or remove energy by changing the volume of oil in the chamber, so active control of the system is also possible.

In this study, double-acting configuration of the hydro-pneumatic suspension is used. In this respect the values used during the modeling of the suspension system, for which the structure can be seen in the Figure 3-3, are presented in Table 3-2. The suspension system is modeled as the connection between the vehicle and suspension arm to increase allowable wheel displacement.

Table 3-2. List of the Suspension Parameters

Symbol of the Parameters	Values
A_{fp}	0.003 [m ²]
A_{pis}	0.015 [m ²]
A_{pr}	0.0108 [m ²]
A_r	0.0042 [m ²]
A_{v1}, A_{v2}	$2 \cdot 10^{-5}$ [m ²]
C_d	0.8
k	1.4
M_{fp}	1 [kg]
P_{40}	25bar
P_{atm}	1bar
ρ_{oil}	800 [kg/m ³]
V_{30}	0.0045 [m ³]
V_{40}	0.001[m ³]

The main objective of the double-acting hydro-pneumatic suspension system in this system is to introduce spring and damper characteristics to the system and control rotational movement of arms. Through arms, the vertical motion of the body as well as its rotation along pitch and roll axes are also affected. In modeling of the double-acting hydro-pneumatic suspension system the static case is considered first.

$$F_i = \left[\frac{(P_{30,i} - P_{atm})A_{fp} + M_{fp}g}{A_{fp}} \right] A_p \quad (3.47)$$

$$- \left[\frac{(P_{40,i} - P_{atm})A_{fp} - M_{fp}g}{A_{fp}} \right] A_{pr}$$

In the equation (3.47), F_i denotes the force necessary to maintain the static equilibrium condition. In this case, the static equilibrium condition is that the arms

remain stationary considering their rotation along y-axis. So, it can be written as the forces acting on wheels and arms which produce moment about the rotational axis at static conditions.

$$F_i L_{susp} = F_{tzi} L_{arm} \sin(\theta_{armi}) - m_w L_{arm} \sin(\theta_{armi}) - m_{arm} \frac{L_{arm}}{2} \sin(\theta_{armi}) \quad (3.48)$$

As the necessary condition here is to hold arms stationary, a moment equation is written. By simply dividing both sides of the equation by L_{susp} which is the distance between the location of the connection point between arms and suspensions, and the location of the connection point between arms and the body.

In the design of hydro-pneumatic suspensions with double cylinders, the initial gas pressure in one of the cylinders, P_{40} , is set by the user considering the stiffness characteristics. A more pressurized cylinder shows stiffer behaviour. The initial gas pressure in the second cylinder, P_{30} , however, is determined from equation (3.47). Indeed, knowing P_{30} and F_i the equation can be solved and P_{40} is determined. In Simulink, necessary calculations are done in their respective blocks for each suspension system.

The spring force which gives the stiffness characteristic for the suspension system is given by equation (3.49).

$$F_{spring,i} = \left[\left(\frac{P_{30,i} V_{30,i}^k}{[V_{30,i} + A_p (\Delta Z_i)]^k} - P_{atm} \right) + \frac{M_{fp} g}{A_{fp}} \right] A_p - \left[\left(\frac{P_{40,i} V_{40,i}^k}{[V_{40,i} - A_{pr} (\Delta Z_i)]^k} - P_{atm} \right) - \frac{M_{fp} g}{A_{fp}} \right] A_{pr} \quad (3.49)$$

Note that at zero deflection, equation (3.49) reduces to equation (3.47). The stiffness of the suspensions can be found by taking derivative of the force equation with respect to deflection;

$$k_{susp,i} = -\frac{dF_{spring,i}}{d(\Delta z_i)} = \frac{P_{30,i}V_{30,i}^\kappa A_p^2 \kappa}{[V_{30,i} + A_p \Delta z_i]^{\kappa+1}} + \frac{P_{40,i}V_{40,i}^\kappa A_{pr}^2 \kappa}{[V_{40,i} - A_{pr} \Delta z_i]^{\kappa+1}} \quad (3.50)$$

Similarly, at static equilibrium the stiffness equation reduces to;

$$k_{susp,i} = \frac{P_{30,i}A_p^2 \kappa}{V_{30,i}} + \frac{P_{40,i}A_{pr}^2 \kappa}{V_{40,i}} \quad (3.51)$$

The deflection in the equations above stand for the deflection of the main piston in the suspension system. Its value is obtained by using kinematic relations between body and the arm which takes the motion of the body and the rotation of the arms into consideration.

$$\Delta z_i = h_{susp,b} + h_{arm,cg} + L_{susp} \cos(\theta_{arm,i}) - z_{susp,initial} \quad (3.52)$$

In equation (3.52), $h_{susp,b}$ stands for the vertical distance between the suspension/body connection and the center of gravity of the body. Similarly, $h_{arm,cg}$ denotes the vertical distance between the arm/body connections and the body's center of gravity. L_{susp} is the length of the arm rods from their body connection points to the suspension connection points. By adding the first three terms the lengths of the suspensions are obtained and when subtracted from their initial lengths, the deflection is found.

Then, the damping force produced by the suspension system can be written as;

$$F_{damper,i} = A_p \left[\frac{A_p(\Delta \dot{z}_i)}{C_d A_{v2}} \right]^2 \frac{\rho}{2} \text{sign}(\Delta \dot{z}_i) + A_{pr} \left[\frac{A_{pr}(\Delta \dot{z}_i)}{C_d A_{v1}} \right]^2 \frac{\rho}{2} \text{sign}(\Delta \dot{z}_i) \quad (3.53)$$

The spring and damper forces produced by the suspension systems are transferred to the moment equations of the respective arms they are connected to as moments.

$$T_{sd,i} = (F_{spring,i} + F_{damper,i})L_{susp} \quad (3.54)$$

The behavior of the double-acting hydro-pneumatic suspension system depend on the pre-load gas pressures. As explained earlier, initial pressure in one of the gas chambers is chosen by the user while the other one is derived from equation (3.47). The moment equation (3.54) shows that the initial gas pressure in the second gas chamber is affected by the initial load acting on the tires and the orientation of the arm. Considering the initial configuration and the load acting on the front tires, the suspension stiffness for different arm angles is given in figure 3-9.

Similarly, the damping force characteristic for the suspension system can be found in figure 3-10.

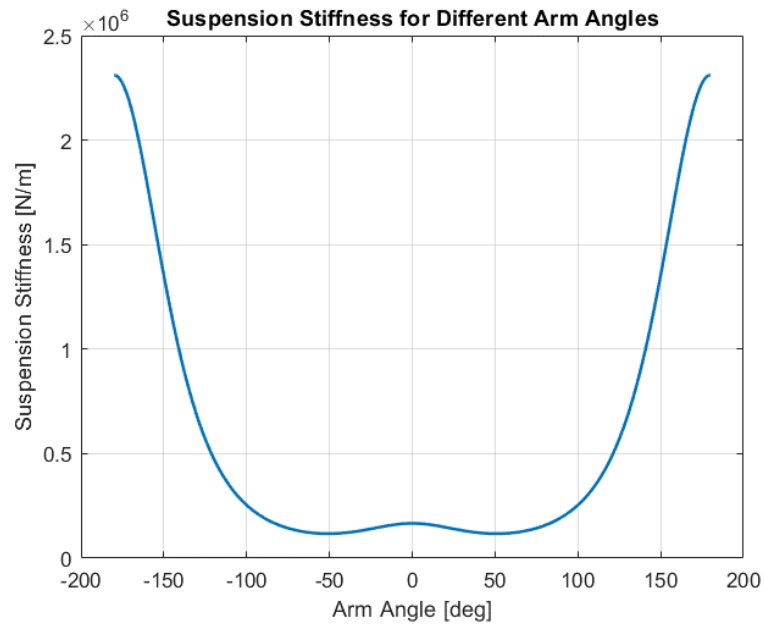


Figure 3-9. Suspension stiffness for different arm angles

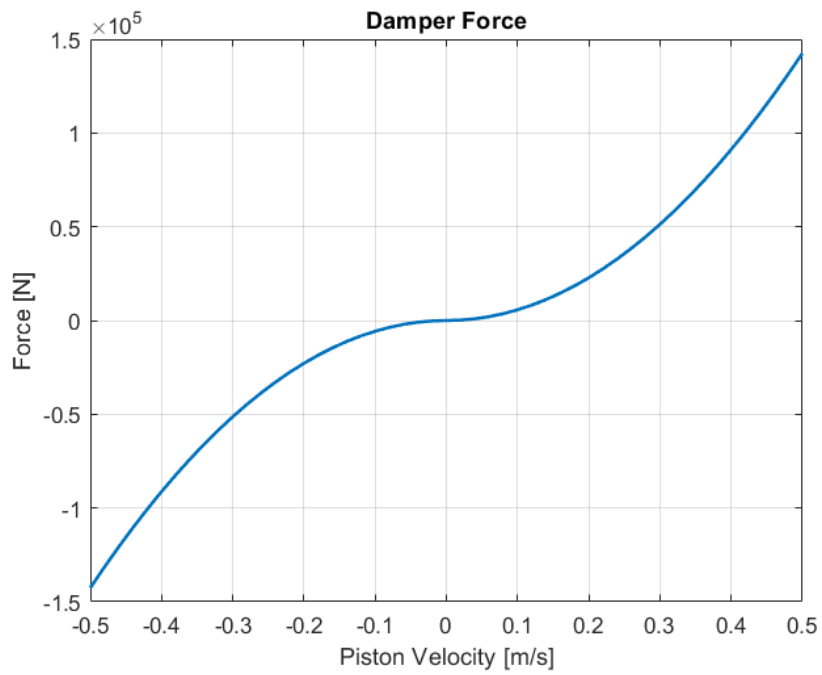


Figure 3-10. Damper for different suspension velocities

3.7 Arm Dynamic Model

The vehicle in the scope of this research is mainly going to be utilized in off road applications. The vehicle is expected to perform variety of tasks. The objectives can be carrying a payload in a specific orientation such as being parallel to the ground or traversing the bumps in the road can be too high for the vehicle to pass with its original ride height. Due to these requirements, the vehicle is designed with arm rods instead of conventional axles. The arm rods act as a supportive element which links the wheels and the suspension system to the sprung mass.

Each of the arms are connected to the sprung mass with a rigid connection in addition to the connection of the suspension. The arms can rotate along the lateral axis which allow the body of the vehicle to change its orientation and its ride height either for a smoother ride or increasing traction of the tires. The motion of the arms are examined using Newtonian mechanics. Newton – Euler equations are utilized to examine the reaction forces and accelerations in six degree of freedoms using six equations. A free body diagram of the arm-tire assembly is given in figure 3.9. The equations of motion are written in the body fixed reference frame denoted with the subscript “b” in the figure. The inertia values of the arm and tire are located at the origin of their respective frames which are denoted with subscripts “a” and “w”. As the equations are written in the body frame “b”, the inertias are firstly transported to the origin of the frame which is coincident with the axis of rotation of the arm. Parallel axis theorem is utilized to find the inertia values at this location. Then, the inertia values are resolved in the body frame by transforming the inertia tensor so that the effect of changes in the arm angles can be reflected into the equations.

$$\tilde{I}_a^{(b)} = \hat{R}(\theta_{arm})' \tilde{I}_a^{(a)} \hat{R}(\theta_{arm}) \quad (3.55)$$

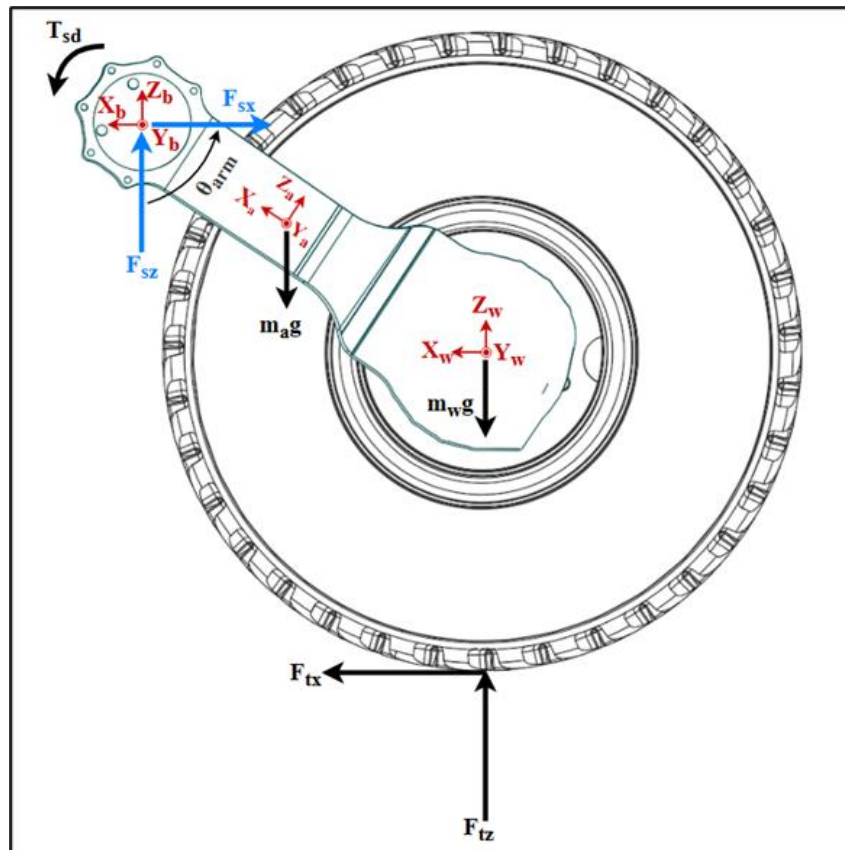


Figure 3-11. Free body diagram of the arm and tire assembly in the xz-plane

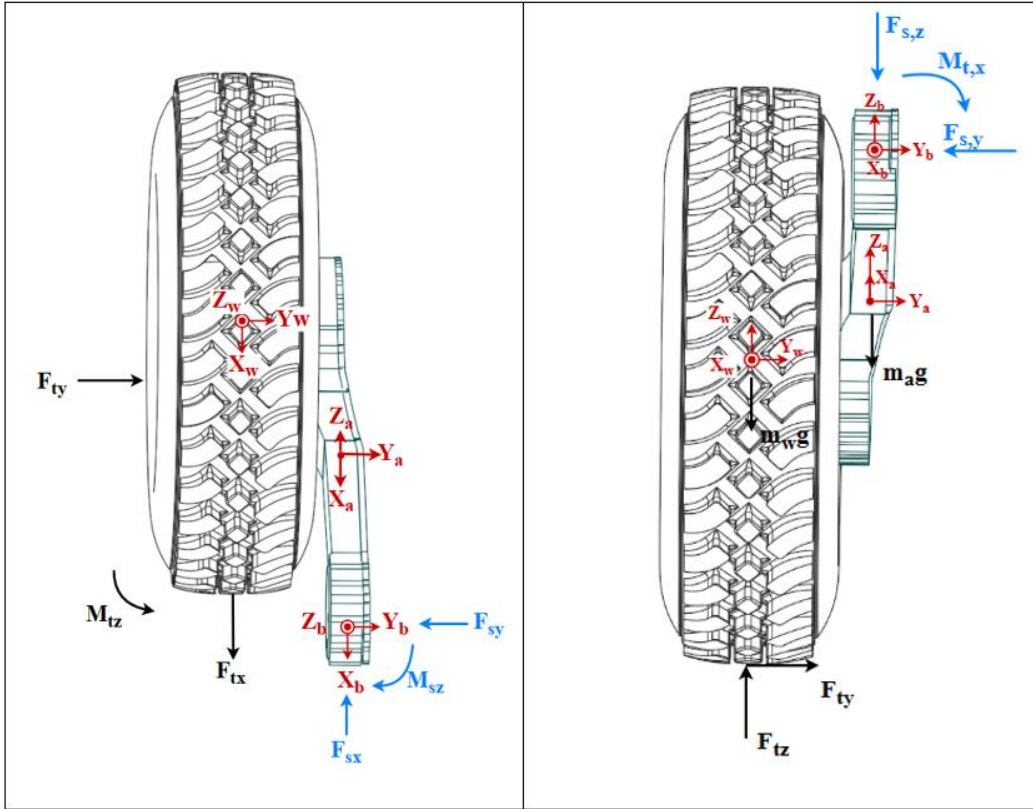


Figure 3-12. Free body diagrams of the arm and tire assembly in yz- and xy-planes

$$\sum F_x \rightarrow F_{txi} - F_{sxi} = m_{arm}\ddot{x}_{arm} + m_w\ddot{x}_w \quad (3.56)$$

$$\sum F_y \rightarrow F_{tyi} - F_{szi} = m_{arm}\ddot{y}_{arm} + m_w\ddot{y}_w \quad (3.57)$$

$$\begin{aligned} \sum F_z \rightarrow k_{tire}(z_r - z_w) - F_{szi} - m_a g - m_w g \\ = m_{arm}\ddot{z}_{arm} + m_w\ddot{z}_w \end{aligned} \quad (3.58)$$

$$\begin{aligned}
\sum M_x &\rightarrow F_{tyi}(l_{arm} \cos(\theta_{arm,i}) + r_w) - M_{sxi} & (3.59) \\
&= I_{arm,x} \alpha_{arm,xi} + (I_{arm,z} - I_{arm,y}) \omega_{arm,yi} \omega_{arm,zi} \\
&+ \left(m_w \ddot{y}_{wi} + \frac{m_{arm}}{2} \ddot{y}_{armi} \right) l_{arm} \cos(\theta_{arm,i})
\end{aligned}$$

$$\begin{aligned}
\sum M_y &\rightarrow l_{arm} \sin(\theta_{arm,i}) k_{tire} (z_r - z_w) & (3.60) \\
&- (l_{arm} \cos(\theta_{arm,i}) + r_w) F_{txi} - T_{susp,i} \\
&- m_a g l_{arm} \sin(\theta_{arm,i}) / 2 - m_w g l_{arm} \sin(\theta_{arm,i}) \\
&= I_{arm,y} \alpha_{arm,yi} + (I_{arm,x} - I_{arm,z}) \omega_{arm,xi} \omega_{arm,zi} \\
&- \left(m_w \ddot{x}_{wi} + \frac{m_{arm}}{2} \ddot{x}_{armi,i} \right) l_{arm} \cos(\theta_{arm,i}) \\
&+ \left(m_w \ddot{z}_{wi} + \frac{m}{2} \ddot{z}_{armi,i} \right) l_{arm} \sin(\theta_{arm,i})
\end{aligned}$$

$$\begin{aligned}
\sum M_z &\rightarrow -F_{tyi} l_{arm} \sin(\theta_{arm,i}) - M_{szi} & (3.61) \\
&= I_{arm,z} \alpha_{arm,zi} + (I_{arm,y} - I_{arm,x}) \omega_{arm,x} \omega_{arm,y} \\
&- \left(m_w \ddot{y}_w + \frac{m_{arm}}{2} \ddot{y}_{arm} \right) l_{arm} \sin(\theta_{arm,i})
\end{aligned}$$

Here it should be noted again that the lateral lengths of the arms are assumed to be zero due to being too small to contribute into the equations of motion. As such, several terms are omitted from the moment equations for ease of calculations. In addition, the accelerations of the arms are calculated using feedback from the vehicle body states. By using Coriolis transport theorem their accelerations and velocities with respect to the inertial frame are found using the body's accelerations and velocities together with their position vectors as explained in the kinematic relations section.

The equations of motion use the forces coming from the tires along with the road input coming from the road profile which is treated as a vertical force as a result of tires' compliance. Accelerations of the moving parts which are arms and wheels are also included in the equations. Using these six equations the reaction forces and moments, F_{sxi} , F_{syi} , F_{szi} , M_{sxi} and M_{szi} are calculated for each of the arms. However, the moment equation along the lateral axis, $\sum M_y$ is used in order to examine the change of the arm angles. As the rigid connections between arms and the body act as a rotary joint, the arms are able to rotate along the y-axis. More details are given in the kinematic analysis chapter. Furthermore, the arms are considered to be "closed" if they are oriented perpendicular to the ground. As such, the values of the arm angles are negative if they are opened towards front end of the vehicle, hence the signs in the moment equations which are products of the vector-matrix equations. This is in tandem with the reference frame although the initial angle is not.

As it is needed to observe the rotation of the arms, the moment equation along the y-axis has to be expanded due to the fact that the rotational acceleration of the arm is included in $\alpha_{arm,y}$ as it can be seen from equation (3.16).

$$\begin{aligned}
\sum M_{tyi} = & \left(I_{arm,y} + m_w l_{arm}^2 + m_{arm} \frac{l_{arm}^2}{4} \right) \ddot{\theta}_{armi} & (3.62) \\
& + \left(I_{arm,y} + m_w l_{arm}^2 + m_{arm} \frac{l_{arm}^2}{4} \right) \ddot{\theta} \\
& + \left(I_{arm,x} - I_{arm,z} \right. \\
& + [\cos^2(\theta_{armi}) - \sin^2(\theta_{armi})] \left[m_w l_{arm}^2 \right. \\
& \left. \left. + m_{arm} \frac{l_{arm}^2}{4} \right] \right) \phi \psi \\
& + \left(m_w + \frac{m_{arm}}{2} \right) l_{arm} (\ddot{z}_{o,i} \sin(\theta_{armi}) \\
& - \ddot{x}_{o,i} \cos(\theta_{armi})) \\
& + \left(m_w l_{arm}^2 \cos(\theta_{armi}) \sin(\theta_{armi}) \right. \\
& \left. + m_{arm} \frac{l_{arm}^2}{4} \cos(\theta_{armi}) \sin(\theta_{armi}) \right) \phi^2 \\
& - \left(m_w l_{arm}^2 \cos(\theta_{armi}) \sin(\theta_{armi}) \right. \\
& \left. + m_{arm} \frac{l_{arm}^2}{4} \cos(\theta_{armi}) \sin(\theta_{armi}) \right) \psi^2
\end{aligned}$$

In equation (3.62), $\sum M_{tyi}$ stands for the moment along the y-axis generated from the tire forces which can be found in the left hand side of equation (3.60). By leaving $\ddot{\theta}_{armi}$ alone and solving the equation, one can obtain the rotational acceleration of the arms around their connection points. Subsequently, integrating the rotational acceleration of the arms their velocities and angles can be found. These outputs are sent to the suspension and kinematical relations subsystems as inputs.

3.8 Vehicle Body Model

Vehicle body is modelled as having 6 degrees-of-freedom and its motion is examined using Newton-Euler equations. The inputs to the system are the reaction forces and moments of the arm equations together with the suspension forces. Using the six Newton-Euler equations, translational and rotational motion of the body along its principal axes are derived. The equations are written in the body fixed reference frame. The force equations are used to calculate the translational acceleration of the body along the longitudinal, lateral and vertical axes with respect to ground. Subtracting the Coriolis term from acceleration and using integration allows the calculation of the velocity of the body with respect to ground along the forementioned axes. In a similar fashion, the moment equations are used to find the rotational accelerations and velocities with respect to ground in the three principal axes. Since the body fixed reference frame uses the principal axes of the body, the inertia tensor only has diagonal elements. Free body diagrams from different views are shown in figures 3-10 and the equations of motion are given afterwards.

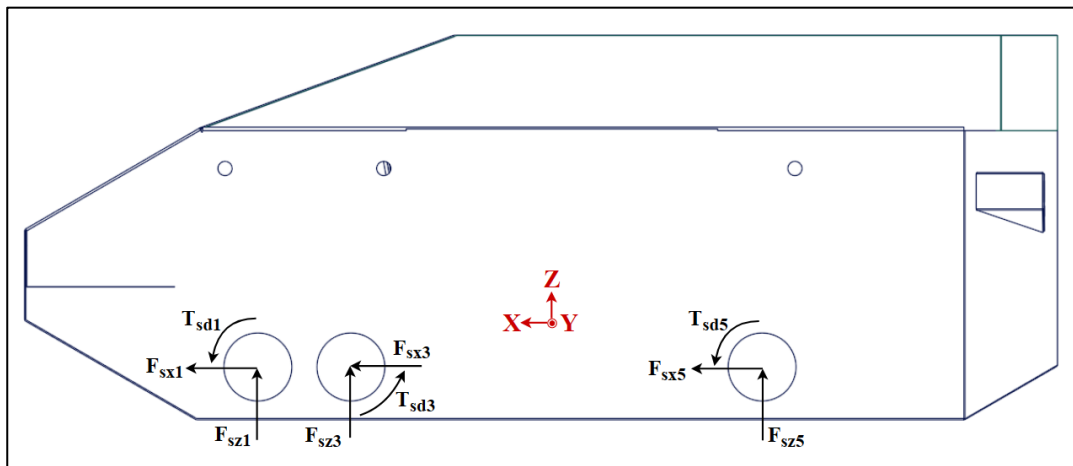


Figure 3-13. Free body diagram of the body from left view

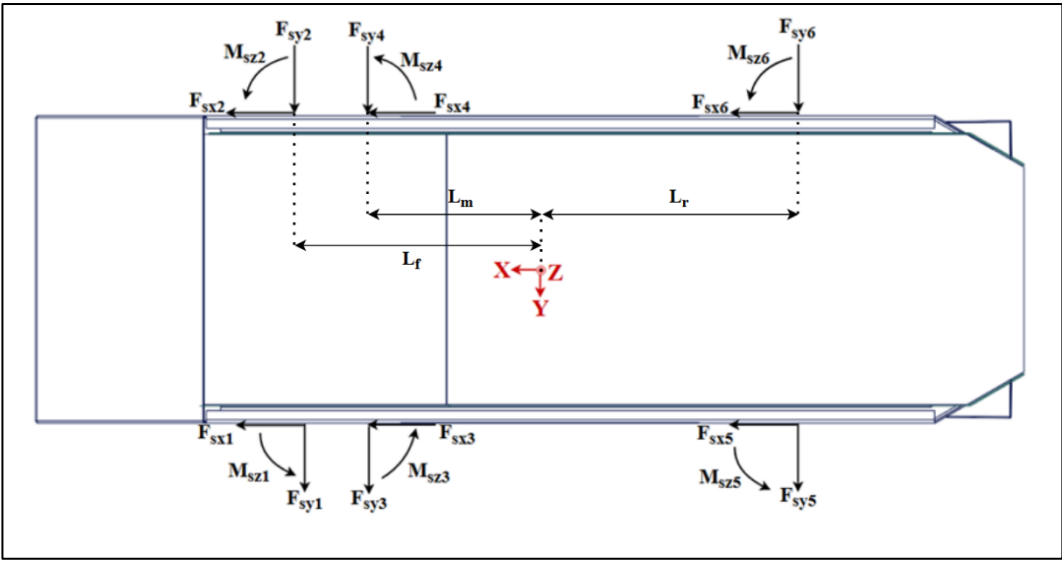


Figure 3-14. Free body diagram of the body top view

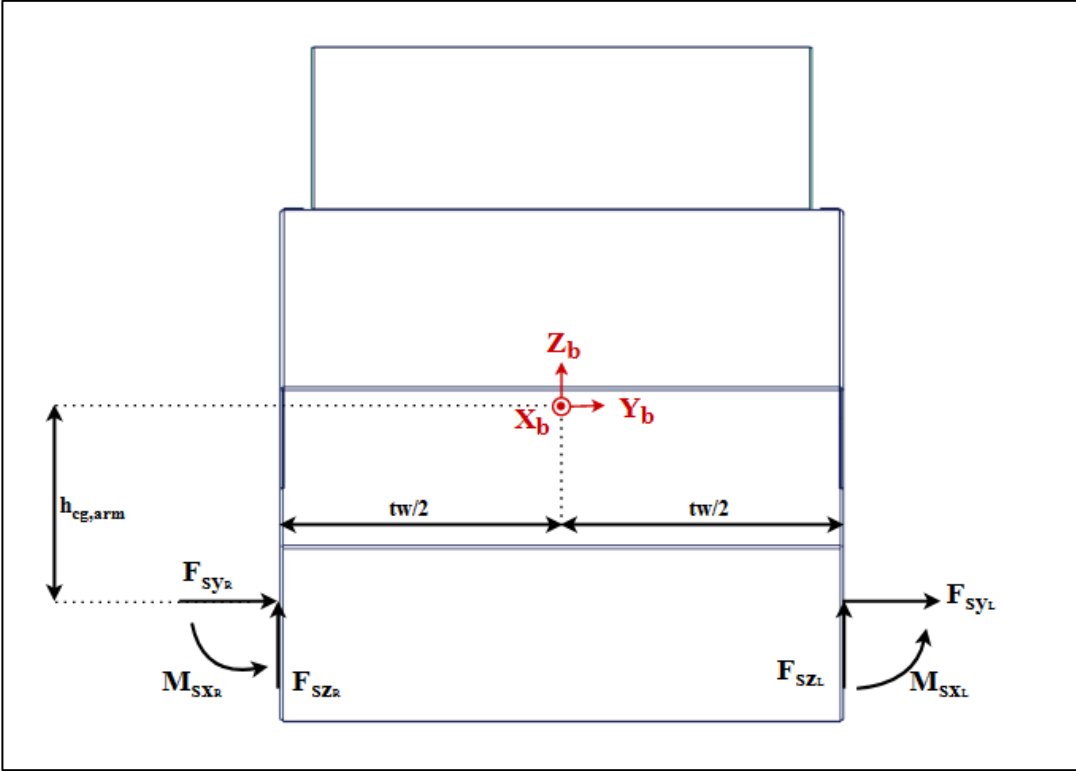


Figure 3-15. Free body diagram of the body from front view with left and right arm reaction forces grouped together

The six equations of motion can be written as follows:

$$\sum F_x \rightarrow \sum_{i=1}^6 F_{sxi} = m_{sprung}(\dot{V}_x + qV_z - rVy) \quad (3.63)$$

$$\sum F_y \rightarrow \sum_{i=1}^6 F_{syi} = m_{sprung}(\dot{V}_y + rV_x - pV_z) \quad (3.64)$$

$$\sum F_z \rightarrow \sum_{i=1}^6 F_{szi} = m_{sprung}(\dot{V}_z + pVy - qV_x) \quad (3.65)$$

$$\begin{aligned} \sum M_x &\rightarrow \sum_{i=1}^6 M_{sxi} + \sum_{i=1}^6 F_{szi} \frac{tw}{2} (-1)^{i+1} + \sum_{i=1}^6 F_{syi} h_{ca} \\ &= I_x \dot{p} + (I_z - I_y)qr \end{aligned} \quad (3.66)$$

$$\begin{aligned} \sum M_y &\rightarrow \sum_{i=1}^6 T_{sd,i} - \sum_{i=1}^6 F_{szi} l_i - \sum_{i=1}^6 F_{sxi} h_{cg,arm} \\ &= I_y \dot{q} + (I_x - I_z)pr \end{aligned} \quad (3.67)$$

$$\begin{aligned} \sum M_z &\rightarrow \sum_{i=1}^6 M_{szi} + \sum_{i=1}^6 F_{sxi} \frac{tw}{2} (-1)^i + \sum_{i=1}^6 F_{syi} l_i \\ &= I_z \dot{r} + (I_y - I_x)pq \end{aligned} \quad (3.68)$$

As the dynamic motion of the vehicle is in interest, the vehicle is treated as it is at equilibrium initially and so the weight is not included in the vertical force equation. Furthermore, the differential equations of motion are written with respect to ground using the body fixed reference frame. Using the reaction forces and moments coming

from arm and suspension models, the resultant motions of the vehicle body are obtained. The non-linear and coupled equations of motion are solved using numerical methods and integration. These outputs of the body system are then fed back to the tire, arm, suspension, and kinematic relations systems.

3.1 Resistances to Motion

In the literature, for the vehicles with steering mechanism, only the longitudinal resistances which are mainly rolling resistance, drive line resistance, air drag resistance, gradient resistance, and inertial resistance are considered. Because the scope of this study does not include the driveline configuration of the considered 6x6 vehicle, the driveline resistance is assumed to be zero. Figure 3-12 shows the resistive forces acting on the vehicle [17]. In addition to these forces, the skid steered vehicles also experience high amount of resisting turning moment, especially in case of turning with respect to its own center of rotation. In this work, both the longitudinal forces and yaw moments are taken into account to model the vehicle characteristics as realistic as possible.

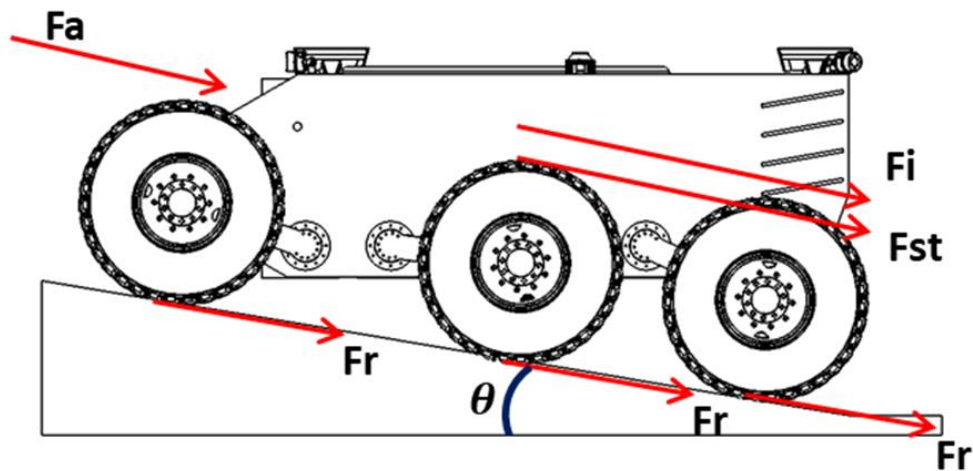


Figure 3-16. FBD showing resistances to motion

3.1.1 Longitudinal Resisting Forces

3.1.1.1 Rolling Resistance

As the Magic Formula tire model is used in this study, the rolling resistance is calculated by the tire model itself. However,

The rolling resistance is observed due to the deformation of the tire surface which contacts with the road, based on many different reasons such as irregularities on the road surface, vehicle speed, and tire inflation pressure. However, instead of considering all the terms one by one, it is assumed in the literature that the rolling resistance has linear relation with the tire load with a coefficient that approximates the effects of all above explained factors. These coefficients are presented in the literature depending on the road condition. In this study, average concrete and unmaintained natural road coefficients are supplied to the simulation [17]. In equation (3.69), the total rolling resistance force is shared. To be able to find the individual forces, one can use the instantaneous load distribution.

$$F_r = m_v g f_r \quad (3.69)$$

3.1.1.2 Air Resistance

The air drag force experienced on the vehicles depends on, unitless drag coefficient, C_d , that is obtained from coast-down tests and shared in the literature based on the shape and structure of the vehicles, longitudinal cross-sectional area of the vehicle, A_f , air density, ρ_{air} , and vehicle relative velocity with respect to wind speed, V_r . As it is shared in equation (3.70), the drag force is proportional to square of relative speed. That is why, in a constant wind speed case, as the vehicle accelerates the observed drag force increases parabolically.

$$F_a = \rho_{air} C_d A_f V_r^2 \quad (3.70)$$

3.1.1.3 Gradient Resistance

In case of climbing up on a hill, the component of the weight that is parallel to the road surface causes a gradient resistance in the longitudinal direction. In order to calculate the resistance force, the slope of the road, α , should be taken into account as in equation (3.71).

$$F_{st} = m_v g \sin \theta_g \quad (3.71)$$

3.1.1.4 Inertial Resistance

The total angular inertia of the vehicle components have a resistance effect during acceleration and braking. The angular inertia is observed due to the rotation of the driveline components. However, as it is explained at the very beginning of the resistance to motion section, the driveline configuration is out of scope of this study.

3.1.2 Resisting Turning Moment

Resisting turning moment gets excessive values for skid steered vehicles due to lateral friction forces exerted on tires, in particular vehicles with higher wheelbase. In this study, for the sake of completeness of the yawing motion the following resisting moment (M_r) for the 6x6 vehicle is considered. To preserve the simplicity, the distances from front and rear tires to the center of rotation, assumed to be equal [12]. For the lateral friction coefficient (μ_t) stated in equation (3.72), an average parameter is obtained from the literature for wheeled ground vehicles.

$$M_r = \frac{\mu_t W}{2} \left(\frac{2}{3} l + \frac{l_c}{6} \right) \quad (3.72)$$

However, as Magic Formula tire model is used in Simulink, the tire ground interaction is calculated inside the model and the turning resistance is reflected to the lateral tire force during steering motions.

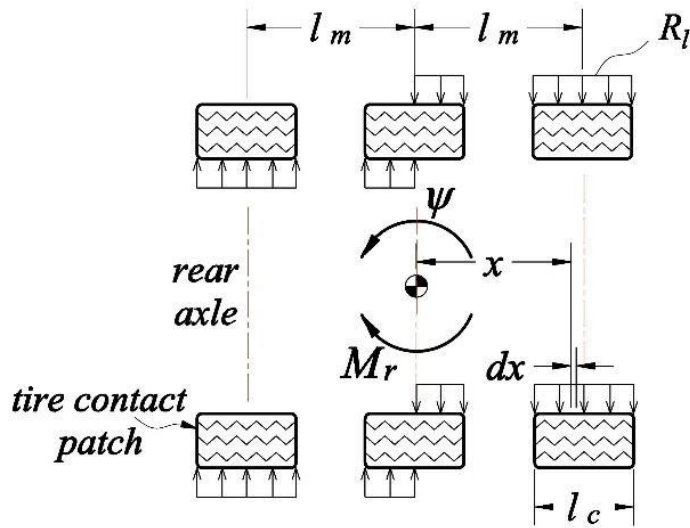


Figure 3-17. Resisting Turning Moment [12]

3.2 Skid Steering Model

Contrary to the conventional vehicles, the off-road vehicle studied in this work uses skid steering for maneuvers. As such, a skid steering model is constructed so that the torque inputs to the vehicle can be given for specific maneuvers.

Firstly, consider the case when the vehicle is moving in a straight line without any yaw motion. A general equation can be written for moving the vehicle with a desired acceleration as given in equation (3.73). Assuming the load is distributed evenly between facing tires, the forces exerted on the tires along the x-axis should be equal to each other to avoid any yaw moment component and perform straight movement.

$$\sum F_x = m_v a_x \quad (3.73)$$

The traction forces generated in the tires causes the vehicle to accelerate while the resistances to motion try to stop the motion so the equation can be expanded to the following form as explained in the previous sub-section.

$$\sum_{i=1}^6 F_{txi} - F_r - F_{st} - F_a = m_v a_x \quad (3.74)$$

Considering the zero slip case, the relation between the torque input and the generated traction force is given in the following equation.

$$T_{wi} = r_w F_{txi} \quad (3.75)$$

Thus, the equation (3.74) can be written in the form;

$$\sum_{i=1}^6 T_{wi}/r_w - F_r - F_{st} - F_a = m_v a_x \quad (3.76)$$

The longitudinal forces generated on the tires depend on the torque inputs. Although they are also effected by the vertical forces acting on the tires, which are found by the load distribution model, for this case same torque inputs can be supplied without considering the vertical forces as we assumed that the load is evenly distributed. So, in a pure longitudinal motion same torque inputs can be supplied depending on the desired acceleration of the vehicle.

In conventional vehicles a steering angle is given to the driving wheels to turn but for skid steering vehicles, the turning maneuvers are achieved by supplying different torques to the right and left tires depending on the direction of the desired motion. Again, a general equation can be written for the yaw motion of the vehicle.

$$\sum M_z = I_z \ddot{\psi} \quad (3.77)$$

For the desired rotational acceleration along the z-axis, the desired moment are obtained by the difference between the longitudinal and lateral tire forces. It is important to express that the lateral forces exerted on the tires are the resistances

for the yaw motion while the longitudinal forces provide the desired yaw acceleration.

$$\sum_{i=1}^6 F_{txi} \left(\frac{tw}{2}\right) (-1)^{i+1} + \sum_{i=1}^6 F_{tyi} x_i - M_r = I_z \ddot{\psi} \quad (3.78)$$

Since the z-axis is along the opposite direction to the ground, positive yaw angle denotes counter-clockwise rotation of the vehicle. In order to turn counter-clockwise, the forces generated in the right tires should be greater than those of in the left tires. Again, writing the equation in terms of the torque inputs;

$$\sum_{i=1}^6 \frac{T_{wi}}{r_w} \left(\frac{tw}{2}\right) (-1)^{i+1} + \sum_{i=1}^6 F_{tyi} x_i - M_r = I_z \ddot{\psi} \quad (3.79)$$

Torque distribution procedure requires a robust control algorithm, and the scope of this thesis is to focus only on dynamic modeling and simulation, in this respect, a simpler skid steering methodology is considered in this study [11]. According to the desired turning radius, the skid steering modeling can be interpreted as in Figure 3-18. In the equation (3.80), T_{exi} and T_{ini} represent individual external and internal torques respectively.

$$\sum_{i=1}^3 \frac{T_{exi}}{r_w} \left(R + \left(\frac{tw}{2}\right)\right) + \sum_{j=1}^3 \frac{T_{inj}}{r_w} \left(R - \left(\frac{tw}{2}\right)\right) + \sum_{i=1}^6 F_{tyi} x_i = I_z \ddot{\psi} \quad (3.80)$$

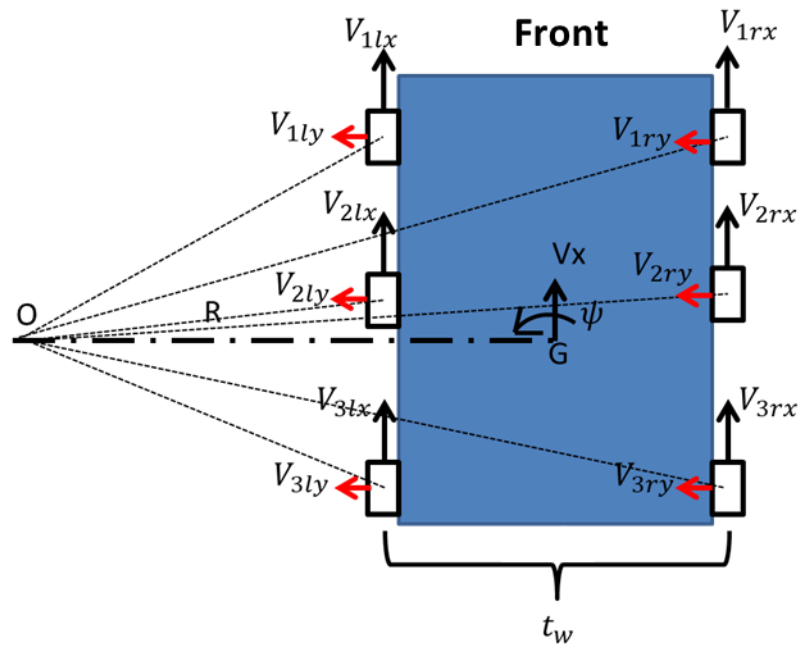


Figure 3-18 Vehicle in Turn with Radius R

CHAPTER 4

ADAMS MODEL

After the construction of the Simulink model another model is necessary in order to verify the results. As the Simulink model relies on mathematical formulation created by the user, it is important to verify the results against a more credible source. Furthermore, verification is also important to justify the assumptions made in the model. The assumptions used to simplify the model must not result in drastic changes in the result. Comparing the results also gives insight on what can be changed in the constructed models.

Real life testing of the model would give the most realistic results if the inputs and outputs can be measured accurately. Although the vehicle investigated in this thesis is being produced, it is not ready for real life testing scenarios due to time and financial constraints. As such, a multi-body dynamics modelling software is necessary to verify the results. ADAMS software allows simulation of mechanical systems and has the advantages of being able to allow modeling of accurate tire models together with tire and ground interaction, the interaction of joints between bodies and ease of accessibility.

ADAMS includes several modules which can be utilized based on the requirements and the scope of the model. Due to the fact that the powertrain is not in the scope of this study and the vehicle does not have a sophisticated steering system ADAMS/View is utilized. Indeed, the vehicle can be considered more as a mobile robot. ADAMS/View allows the usage of tire models and creates the tire-ground interface through working with its ADAMS/Tire module. Custom suspension systems can also be modeled and its interaction with other bodies can be designed. ADAMS/Controller also allows exporting the plant based on the variables chosen

for inputs and outputs and more complex inputs can be supplied to the system using softwares including MATLAB/Simulink.

4.1 Modelling of the Bodies

The bodies in the system consist of the sprung mass, six arms and six tires. The first stage of modeling in adams is to define the overall geometry and creating the necessary coordinates which will be used to insert parts, connections and forces. Starting with the body or the sprung mass, the necessary coordinates are created. These coordinates include the edges of the body in order to better define the geometry, the connection points and the location of the forces to be applied.

Having picked out the necessary coordinates for the topology of the system, the bodies are then inserted according to the points specified. Then the connection between the bodies are created for the assembly. The arms are connected to the body with rotary joints to allow the rotation of the arms around the body's lateral axis. Similarly, tires are connected to the arms with rotary joints so that they can be actuated with torque or rotational velocity inputs. The finalized system can be seen in the following figure.

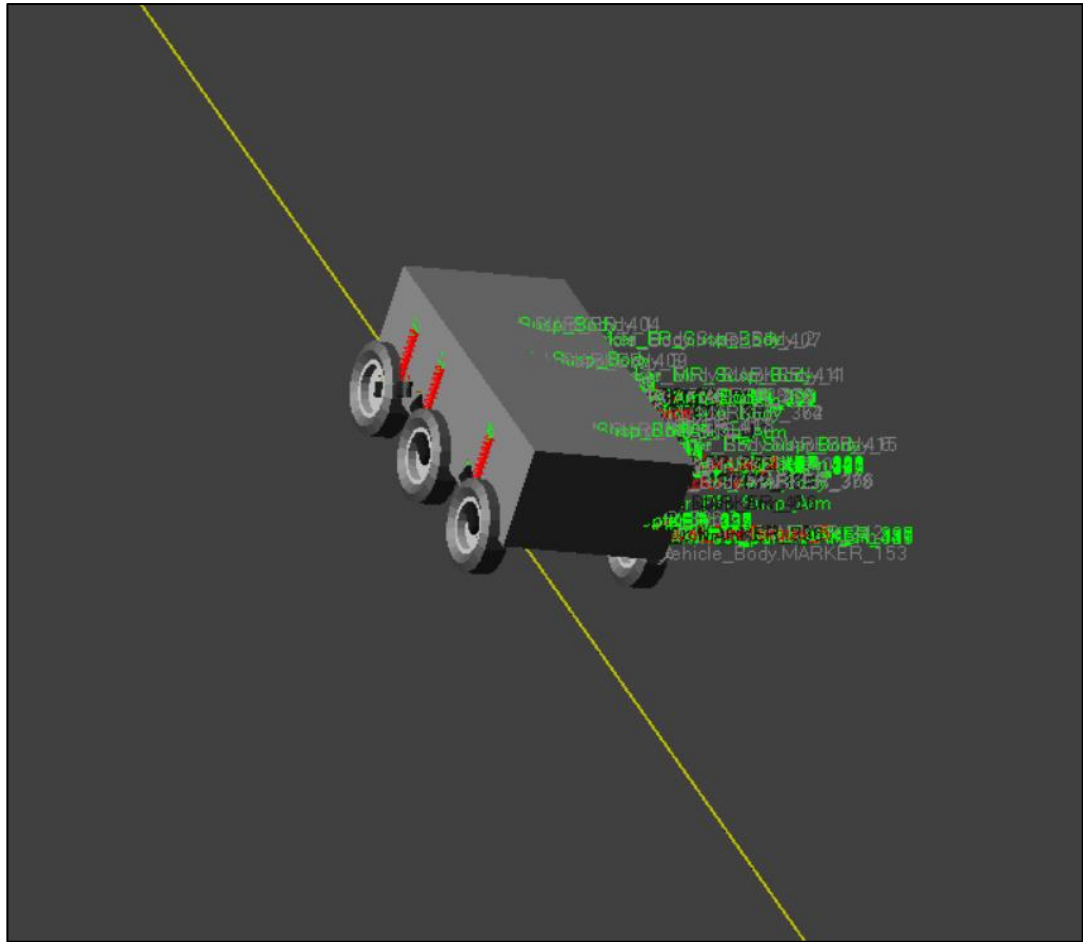


Figure 4-1. Assembled vehicle in ADAMS

4.2 Modelling of the Tires and the Suspension System

While modelling the tires the tires' center locations are determined first similar to the previous section in order to align it with the other bodies in the system. The mass and inertia values of the tires are chosen the same as the MATLAB data. For the tire characteristics, ADAMS allows the usage of its ADAMS/Tire library which contains tire properties such as radius, width, vertical stiffness, inflation pressure and the parameters required for Pacejka's Magic Formula. As ADAMS uses Magic Formula while solving for tire forces, it requires extensive test data in order to determine the necessary parameters. Due to the fact that getting these parameters for a specific tire is expensive and time consuming, a similar tire from the library is chosen. Certain

values such as the vertical stiffness and the tire radius are changed according to the existing tire data.

The vehicle uses double-acting hydro-pneumatic suspension system as explained in the dynamic modeling chapter. ADAMS does not allow the modeling of gases or liquids which are the main forcing elements in the hydro-pneumatic suspension systems. However, spring-damper connection elements can be created and given a forcing function which depend on deformation and velocity of the spring length and damper velocity respectively. The function is determined from a tabular data where the independent variable can be deformation or velocity depending on the element it is going to be used and the data for dependent variable is force or torque.

The required data is gathered from MATLAB. Model created for the double-acting hydro-pneumatic suspension system is run on its own, without being connected to the other components in the complete vehicle model. Firstly, angular velocity of the arms which is one of the inputs is taken as zero and the angle of the arms is increased from 60 degrees to 120 degrees and then gradually lowered to -120 degrees using two ramp inputs with different initialization times. It is necessary to start at 60 degrees which is the initial position of the arms because the preload force and the initial pressure which directly effects the spring force of the model are dependent on the initial arm angle and the initial load on the tires. The change of the suspension stiffness for different arm angles can be seen in the following figure. Note that the front, middle and rear stiffness values are different because of the difference in initial pressures as explained.

Thus, three different datasets are obtained for front, middle and rear torsional springs that are implemented on the ADAMS model. These datasets represent the torque that suspensions will produce depending on the deformation the springs face. The plots showing the torques versus angular deformation can be seen in the following figures for the front, middle and rear torsional springs. The figures are obtained from ADAMS postprocessor by plotting the tabular data.

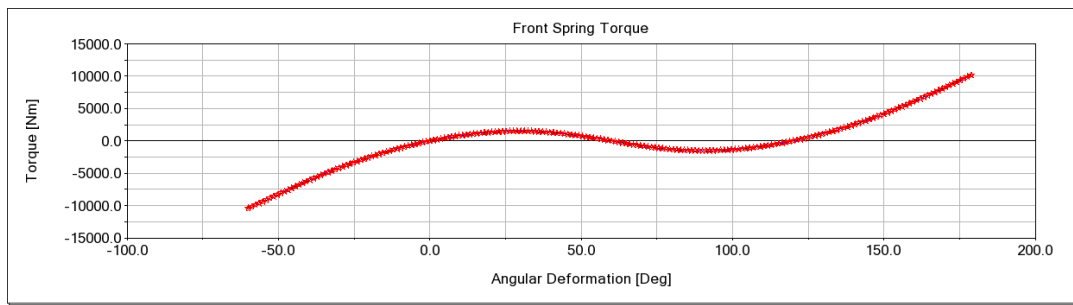


Figure 4-2. Front Spring Torque vs Angular Deformation

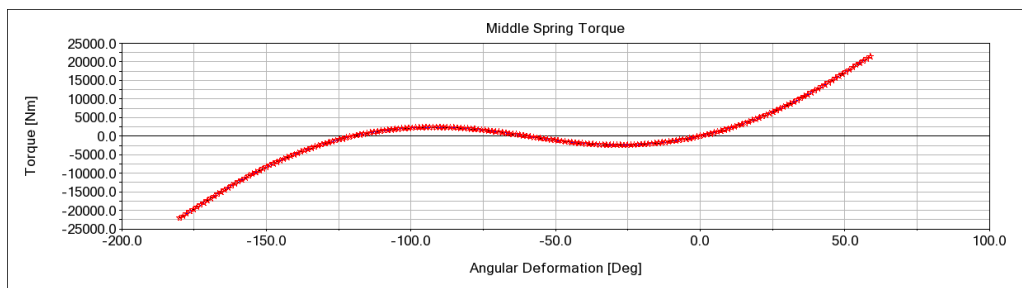


Figure 4-3. Middle Spring Torque vs Angular Deformation

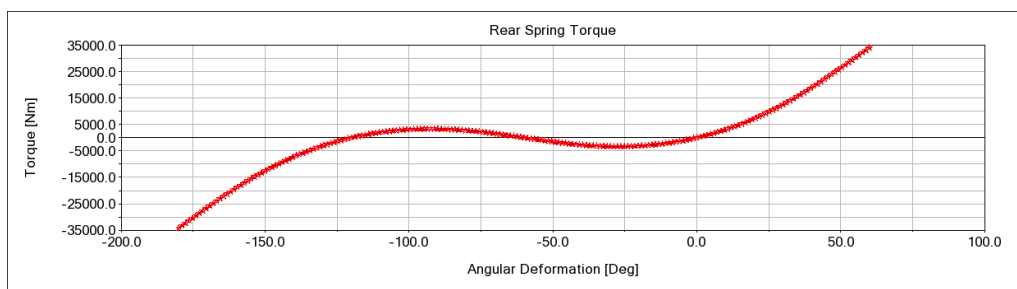


Figure 4-4. Rear Spring Torque vs Angular Deformation

As expected, the rear springs produce the highest torque, and the front springs produce the smallest. This is because the rear tires carry most of the weight, followed by the middle tires. The initial pressure in the second gas chamber is found from the moment equation about the y-axis as explained in the suspension model section of the dynamic modeling chapter. The preload values for the front, middle and the rear suspensions are also given in the table 4-1.

Table 4-1. Initial preload of the suspensions

	Front Spring	Middle Spring	Rear Spring
Initial Torque	3870 [Nm]	-11248 [Nm]	-18876 [Nm]

Note that the signs are dependent on the direction of the torques applied. The counter-clockwise direction along the vehicle’s positive y-axis denotes positive torque values.

In a similar fashion, the damper torque data are derived from the suspension model created in Simulink. However, for determination of the damping torques the angle is taken as constant and only velocity is changed. From equation (3.53) it can be seen that from state variables, the damping force of the suspension system is dependent only on the relative velocity. Contrary to the spring force, initial gas pressure does not change the characteristics of the damping force. As a result, the damping behavior is the same behaviour for front, middle and rear systems. The plot of the damping force with respect to angular velocity can be seen in figure 4-5.

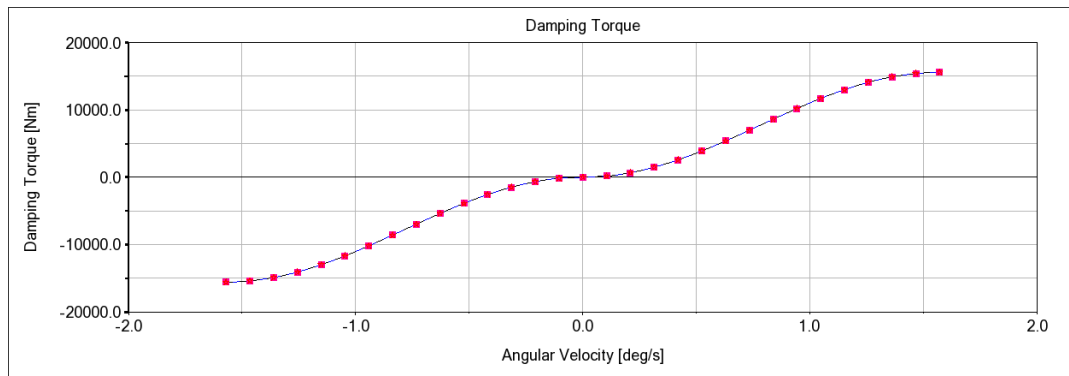


Figure 4-5. Plot of damping torque with respect to angular velocity as derived from the data implemented on ADAMS

With the implementation of the suspensions for which the locations was set in the first stage, the full assembly of the system is created.

4.3 Inputs and ADAMS/Control

After the construction of the system, the inputs can be appointed. ADAMS allows variety of inputs including motions, forces, and torques for the system. As the vehicle will be actuated using independent motors for each wheel, torques are chosen to give the vehicle motion. They are applied at the tire centers along the y-axis of the vehicle.

The magnitudes of the torques can be entered on the ADAMS/View interface for open loop simulation of the system. If a closed loop simulation is desired, predefined functions existing the ADAMS can be used. However, a better way to simulate the model is through the usage of ADAMS/Control. ADAMS/Control allows the user to export the plant of the model created to Easy5, MatLab or FMU softwares. However, in order to be able to export the plant, inputs and outputs have to be defined first. This is done through the creation of 'System Elements'. System elements can be either inputs or outputs depending on how they are defined. While creating the inputs their values are assigned as null. Regarding the model in the scope of this study, six control torque system elements are created which will be used as inputs. By referencing these system elements as the values of the torque forcing elements created in the ADAMS/View software. This allows the Control application to overwrite the null value at each step of the simulation and forcing elements created then get the magnitude values from the new values at each step. For the outputs, the predefined functions in ADAMS are used to determine the system elements.

After the inputs and outputs are chosen according to the objective of the closed loop system, the plant is exported and can be used in MATLAB/Simulink softwares. In figure 4-6. a closed loop system can be seen where the six inputs to the plant are the control torques created and the outputs are the longitudinal and yaw velocity of the vehicle. The system is designed simply for maintaining a constant speed.

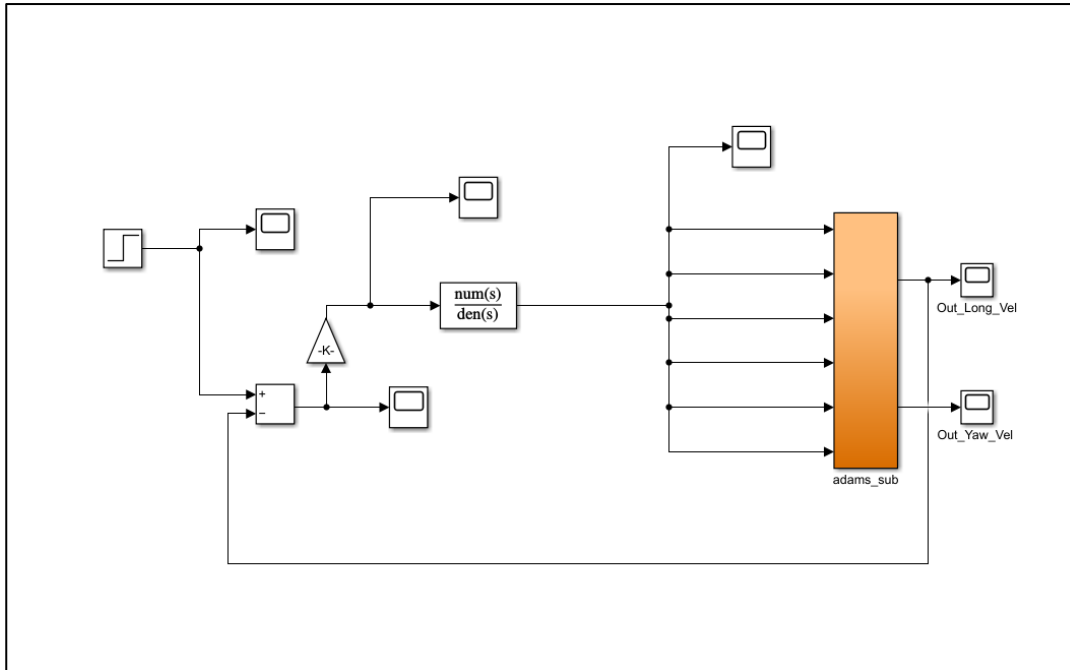


Figure 4-6. Block diagram as created with ADAMS/Control and Simulink

For different applications different inputs and outputs can be chosen and simulations can be run. The outputs are generated in Simulink using ADAMS and the simulation can be viewed in both softwares.

4.4 Road Generation

In order to be able to verify the results against the Simulink model, same road inputs have to be supplied for ADAMS as well. Using the road builder model of ADAMS/Car, custom roads can be generated to test the models. The road builder uses nodes to create roads. The coordinates for each node are entered along with the road width, bank angle, friction coefficients for the right and left side of the roads can be entered for each node as well as globally for the entire road. Furthermore, obstacles can be added to the road which can be modeled as bumps, ramps, curbs, potholes, etc.

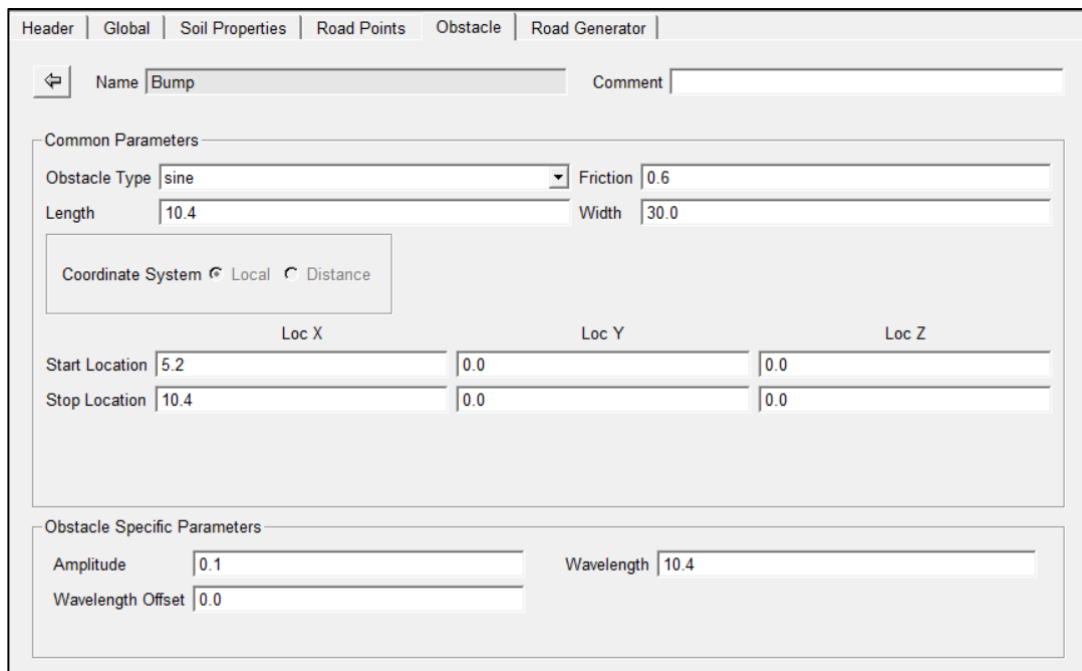


Figure 4-7. Figure showing the user interface for road builder in ADAMS

The road profiles generated in the Simulink model are also constructed in ADAMS using the road builder so that the models can be compared using same inputs.

CHAPTER 5

SIMULATION RESULTS AND COMPARISON

In this chapter, results of the simulations made in Simulink and ADAMS environments are compared and discussed. The models are supplied with the same torque inputs to the tires and road profiles so that the behaviors of the vehicle model constructed in both environments be compared for the same scenarios. The parameters for both models are set the same as well.

The results to be compared are selected according to the critical behaviors that want to be observed. For observing the performance of the vehicle longitudinal velocity, longitudinal acceleration of the sprung mass and longitudinal forces produced in the tires are observed. Lateral velocity, lateral acceleration, yaw rate, yaw angle of the sprung mass and lateral tire forces are also chosen as outputs to observe and compare the steering and maneuverability of the vehicle. Lastly, for the ride performance vertical acceleration, vertical velocity, pitch velocity, pitch angle, roll velocity and roll angle of the sprung mass, load distribution as vertical forces acting on the tires, arm angles and suspension forces are the results to be shown.

5.1 Case 1 – Flat Road Acceleration

For the first case, a flat road profile is selected. The vehicle's performance and stability under acceleration are the phenomena desired to be seen in this case. The torques to the wheels are supplied after 1 seconds in constant magnitude of 1500 Nm for each wheel.

Firstly, the longitudinal velocity is considered since for this case the performance of the vehicle is the focus.

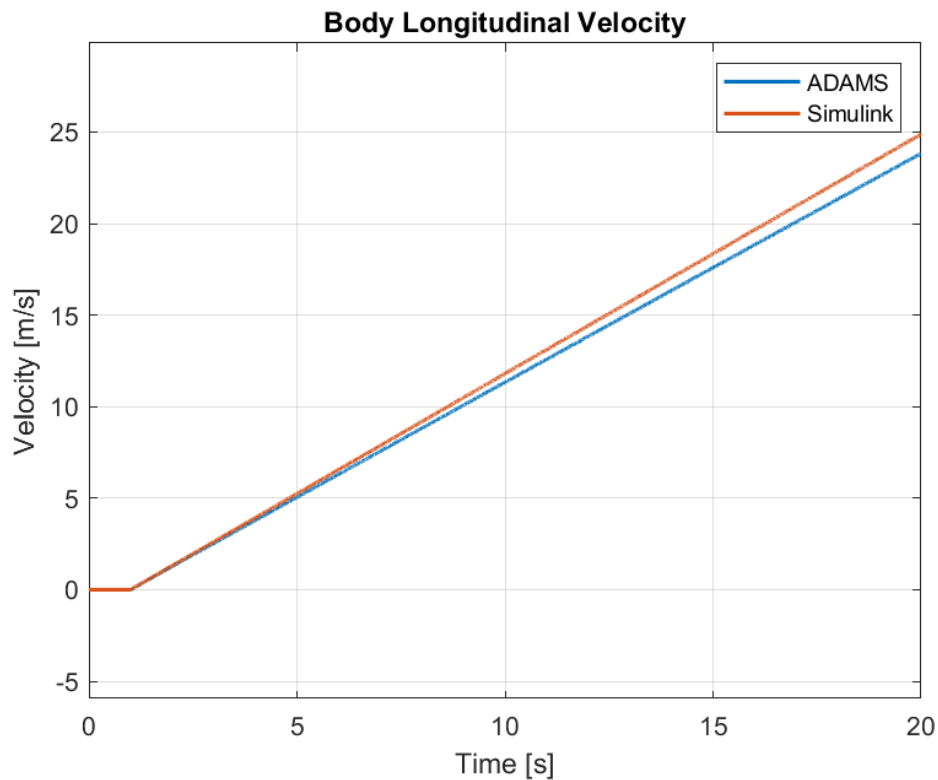


Figure 5-1. Plots of Longitudinal Velocity of the Body for Case 1

In figure 5-1, the velocity of the sprung mass in the longitudinal direction is shown for both ADAMS and Simulink simulations. As mentioned before a constant torque of 1500 Nm is supplied to each wheel after 1 second and the velocity of the vehicle reaches 23.800 m/s and 24.882 m/s in ADAMS and Simulink respectively. Mean squared error between the simulations is 0.334 and the mean values are 11.351 m/s and 11.832 m/s.

The velocities along the lateral and vertical directions are shared in the following figures. As expected, they are close to zero, however a small oscillation can be seen in the vertical direction as a result of the traction induced pitch motion.

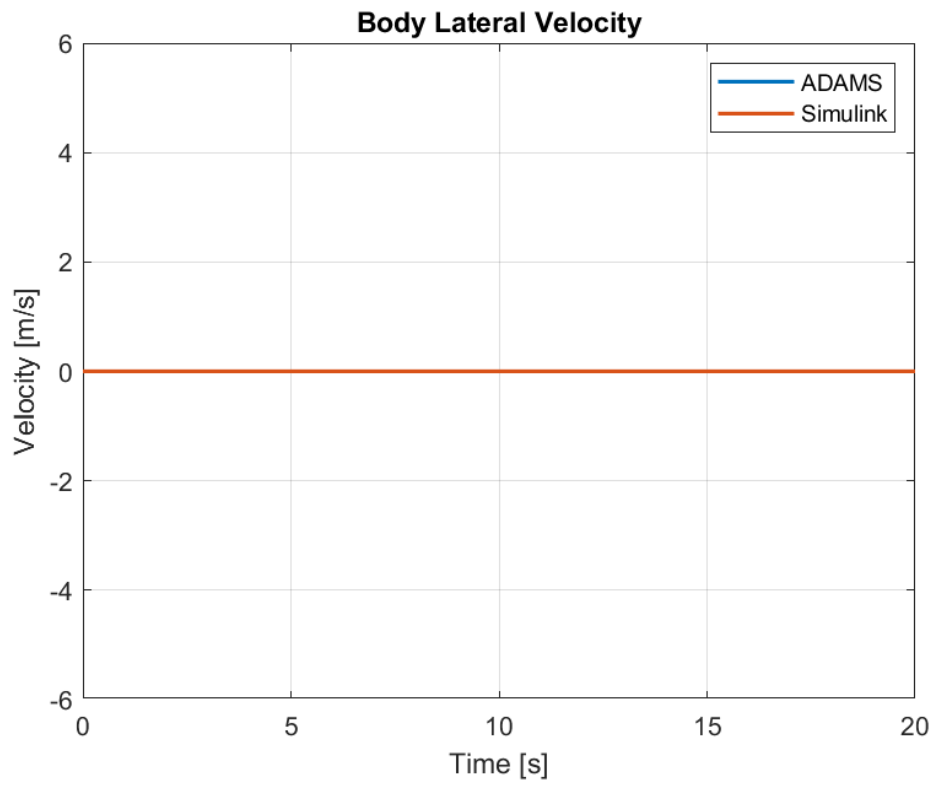


Figure 5-2. Plots Lateral Velocity of the Body for Case 1

As the same inputs are applied to the left and right tires, lateral velocity is almost zero as expected. The maximum values lateral velocity takes are in the powers of -14 and -12 for ADAMS and Simulink, respectively.

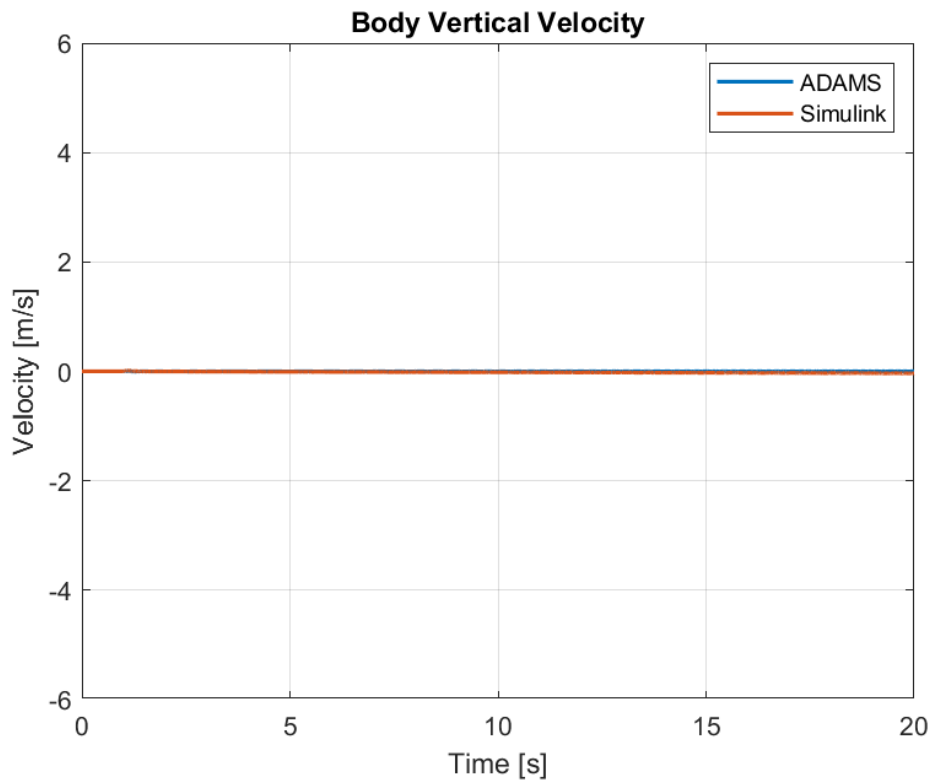


Figure 5-3. Plots of Vertical Velocity of the Body for Case 1

Although a flat road profile is supplied to the vehicle for this case, the traction forces which start when $t=1$ induce a pitch motion in the vehicle and as a result, the center of gravity of the vehicle moves along the vertical direction. However, the maximum values the vertical velocity takes are very low in both simulations, 0.0067 m/s for ADAMS and 0.0143 m/s for Simulink.

Table 5-1. Comparison of Translational Velocity Data Produced between Models for Case 1

Parameter	MSE	ADAMS Max	Simulink Max	ADAMS Mean	Simulink Mean
Long. Vel.	0.334	23.832	24.882	11.351	11.832
Lat. Vel.	1.67E-23	1.43E-14	7.28E-12	-2.03E-15	-3.36E-12
Vert. Vel.	0.000372	0.00668	0.0143	2.49E-05	0.0161

Similarly, the acceleration of the vehicle along the longitudinal, lateral and vertical directions can be seen in the figures below.

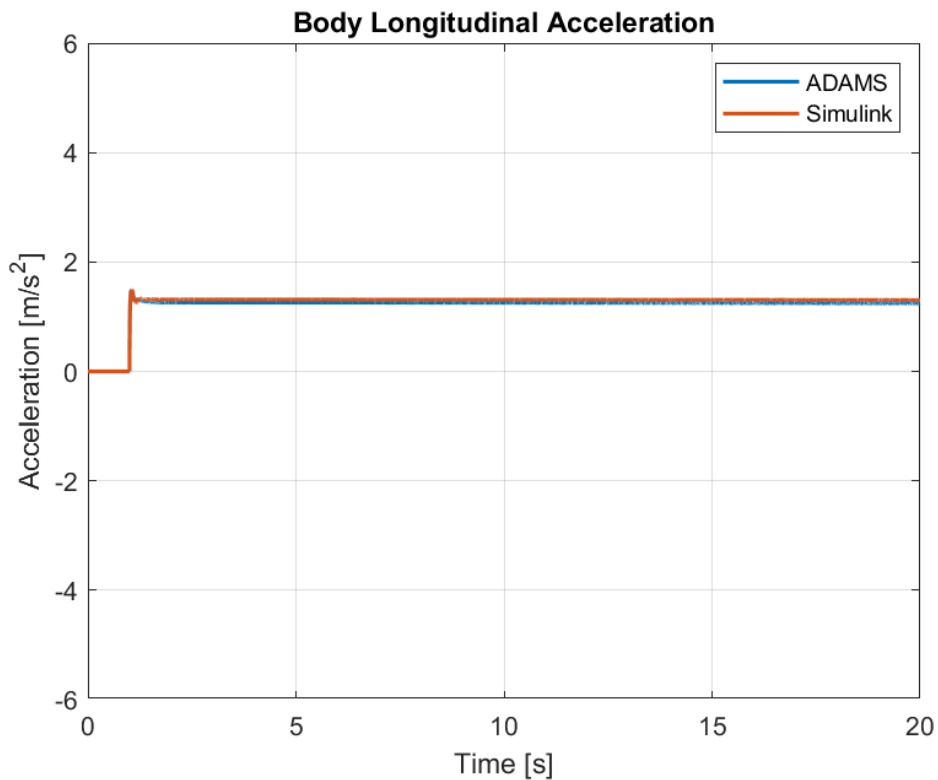


Figure 5-4. Plots of Longitudinal Acceleration of the Body for Case 1

As constant torque is supplied to the tires, almost a constant traction force is generated at each tire. The plot of the longitudinal acceleration show implies that this is the case as well. However, there is a slow decrease in the acceleration while the velocity increases which is a result of the resistance to the motion. The air resistance

and the rolling resistance take increasing values if the velocity increases and as a result, the resultant acceleration decreases over time.

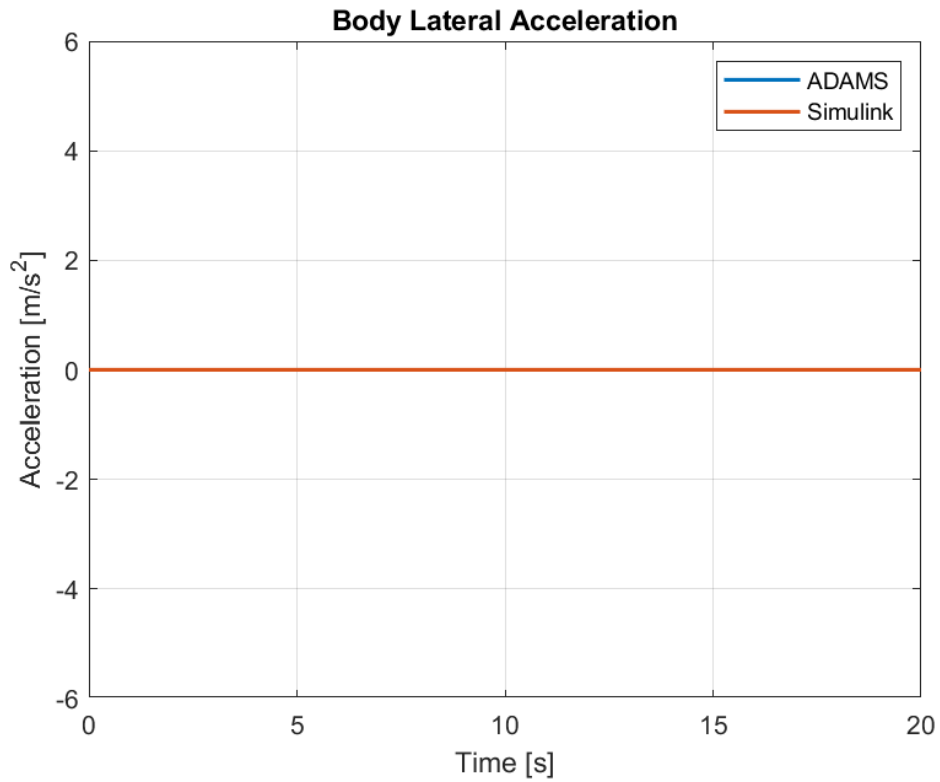


Figure 5-5. Plots of Lateral Acceleration of the Body for Case 1

As the same inputs are applied to the left and right tires, lateral acceleration is zero as expected.

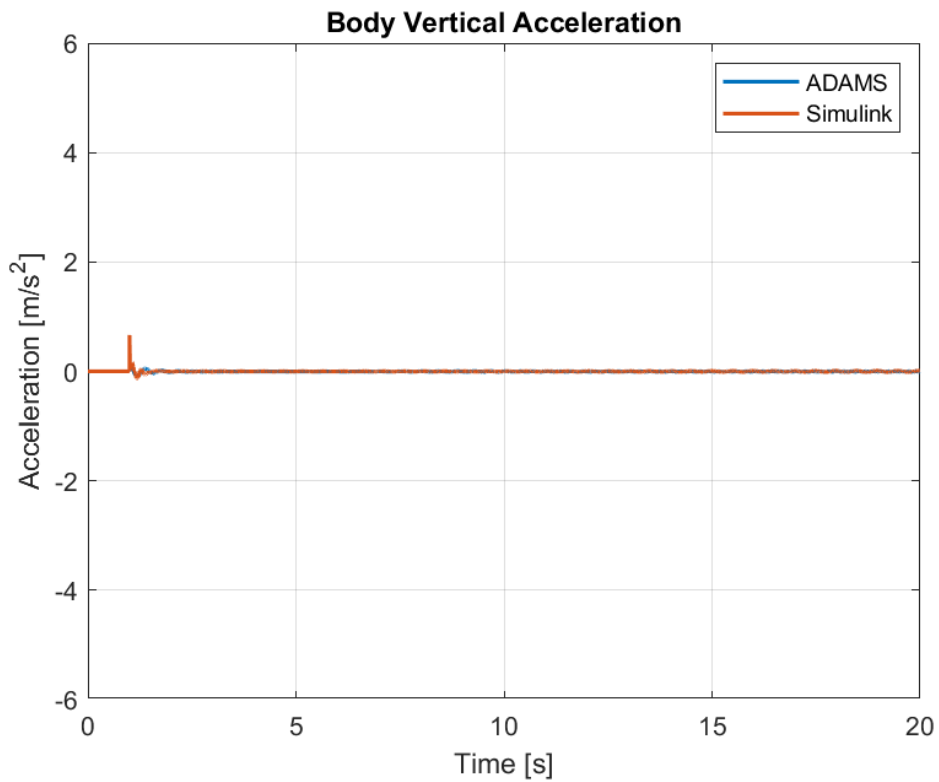


Figure 5-6. Plots of Vertical Acceleration of the Body for Case 1

For vertical acceleration, the peak occurs when the torques are supplied to the wheels. The Simulink model generates more acceleration in this case, but the result is damped quickly.

For translational accelerations along the three axes mean square error, maximum and mean values for both simulations are tabulated below.

Table 5-2. Comparison of Translational Acceleration Data Produced between Models for Case 1

Parameter	MSE	ADAMS Max	Simulink Max	ADAMS Mean	Simulink Mean
Long. Acc.	0.00304	1.49	1.50	1.19	1.24
Lat. Acc.	4.3E-21	1.7E-12	4.2E-9	2.7E-15	2.41E-13
Vert. Acc.	1.8E-21	0.149	0.665	-2.11E-3	2.42E-05

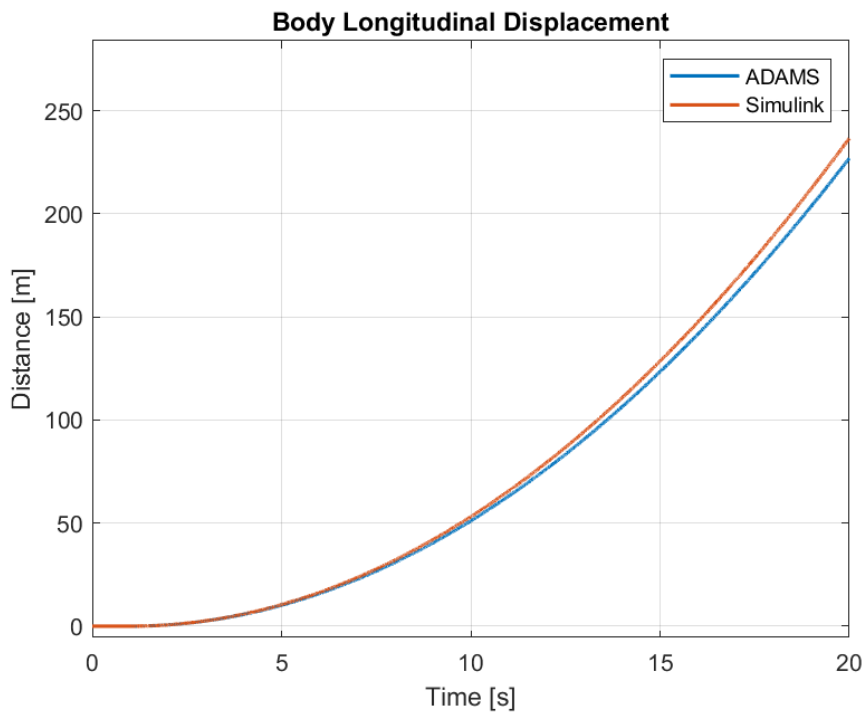


Figure 5-7. Plots of Longitudinal Displacement of Body for Case 1

At the end of 20 seconds of simulation, the vehicle covers 227.031 meters in ADAMS and 236.650 meters in Simulink, along the longitudinal direction. The main difference here is caused by the differences of the tire models between ADAMS and Simulink. Although both software employ Magic Formula, there are differences in the formulation and the constants employed. It can be observed that the tire models in Simulink generate more traction force, hence the cause of error.

For the constant torque input the generated forces in the tires are shown in the following figures for both software.

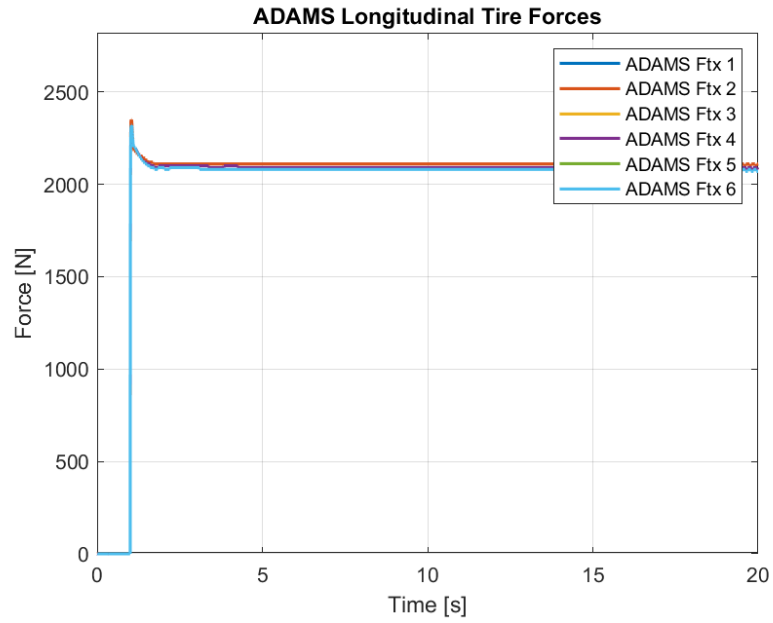


Figure 5-8. ADAMS Longitudinal Tire Forces for Case 1

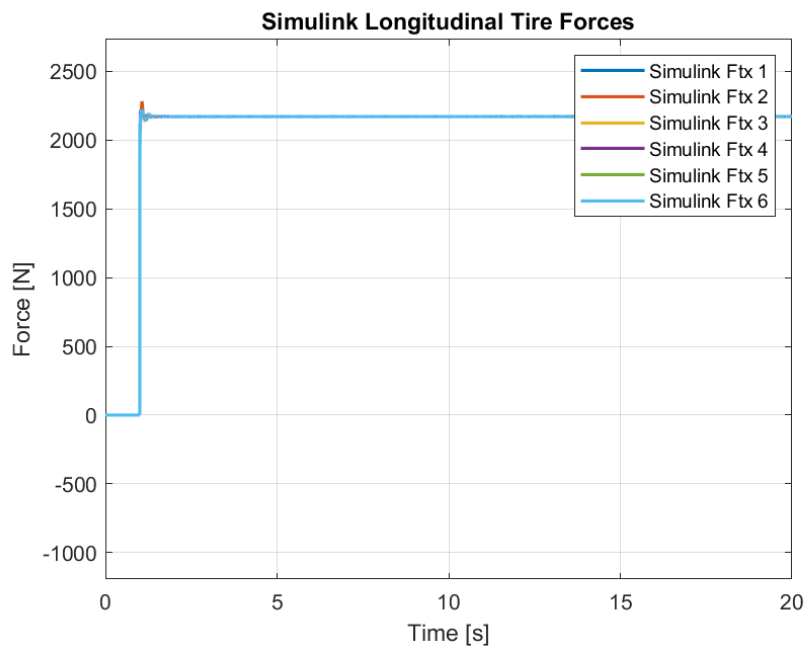


Figure 5-9. Simulink Longitudinal Tire Forces for Case 1

As it can be seen from the plots, the effect of the load distribution on the traction force is more apparent in ADAMS compared to Simulink.

Similarly, the change of the arm angles along the simulation can be seen in the figures below.

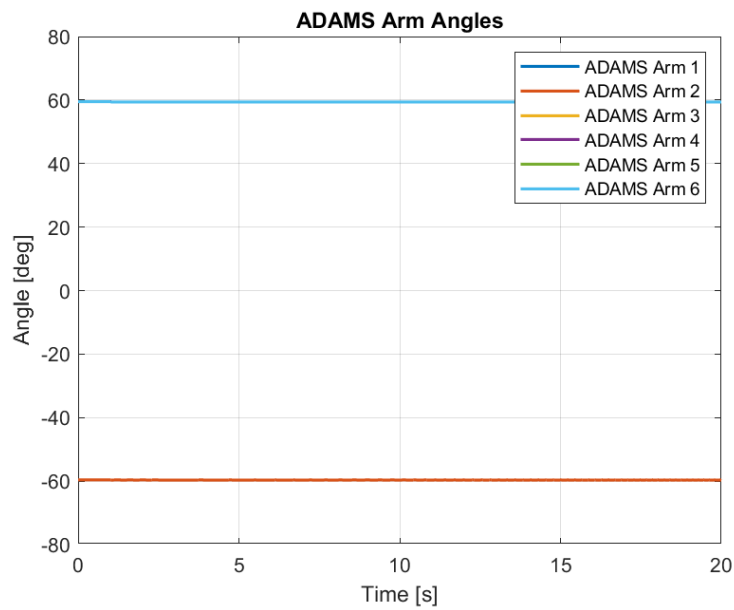


Figure 5-10. ADAMS Arm Angles for Case 1

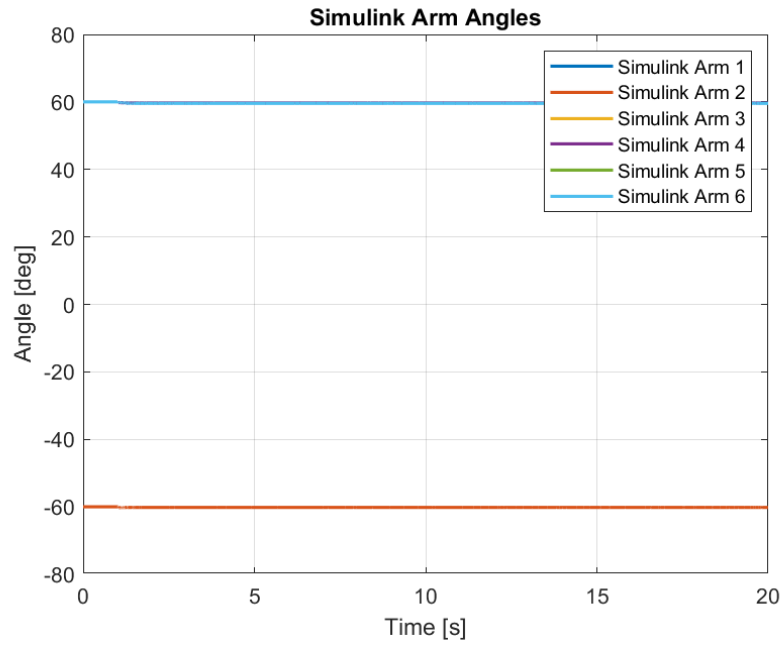


Figure 5-11. Simulink Arm Angles for Case 1

The results of each arm angle are compared between the two software and they are tabulated below.

Table 5-3. Comparison of Data of Arm Angles Produced between Models for the First Case

Parameters	MSE	ADAMS Max	Simulink Max	ADAMS Min	Simulink Min	ADAMS Mean	Simulink Mean
Arm Angle 1	0.0131	-59.6	-59.528	-59.7	-60.221	-59.6750	-59.6651
Arm Angle 2	0.0131	-59.6	-59.528	-59.7	-60.221	-59.6750	-59.6651
Arm Angle 3	0.1441	59.5	60	59.4	58.904	59.4051	59.0835
Arm Angle 4	0.1441	59.5	60	59.4	58.904	59.4051	59.0835
Arm Angle 5	0.2434	59.5	60	59.4	58.773	59.4050	58.9695
Arm Angle 6	0.2434	59.5	60	59.4	58.773	59.4050	58.9695

It should be noted that the ADAMS software starts the simulation from the static equilibrium. The arm angles are thus adjusted at the start in order to compensate the vertical tire force's effect on the rotation of the arm by the suspension. It is important to note however, the load distribution only effects the tire forces in Simulink because the system is treated as at rest initially and only the forces coming from tire deflection are considered when solving for the effect of the vertical tire forces. As seen from the arm angle values, the values are close and this assumption holds.

5.2 Case 2 – Road with a Single Bump

For the second case, a road profile input with a single bump is chosen. The characteristics of the bump are taken from APG standards as discussed in the road profile section of the third chapter. The bump has a height of 0.1 meters at maximum elevation and the bump length is 5.2 meters. The bump starts at a distance of 5.2 meters from center of gravity of the vehicle to allow the vehicle to speed up. For better visualization the initial position of the vehicle in ADAMS can be seen in figure 6-6.

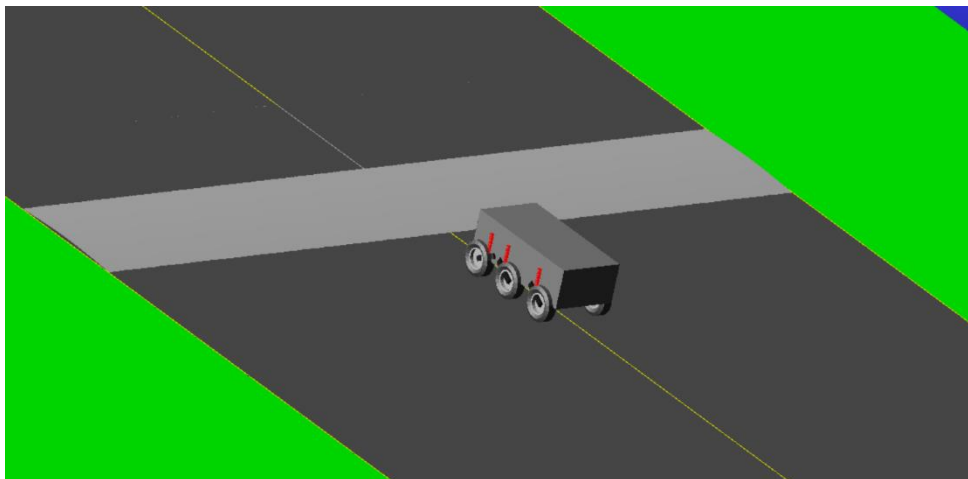


Figure 5-12. Initial position of the vehicle on the road with single bump in ADAMS

The vehicle's ride performance is the critical behavior in this case. As such, the vertical motion of the body, arm angles, load distribution and suspension forces will

be the main focus. As tire forces are directly affected by the load distribution, the change in the force generation of tires as the vehicle trespasses the bump are to be observed for this case as well.

However, firstly let us consider the translational velocity. In the first case the vehicle was able to speed up to 23.8 [m/s] in ADAMS and 24.9 [m/s] in Simulink at the end of the simulations.

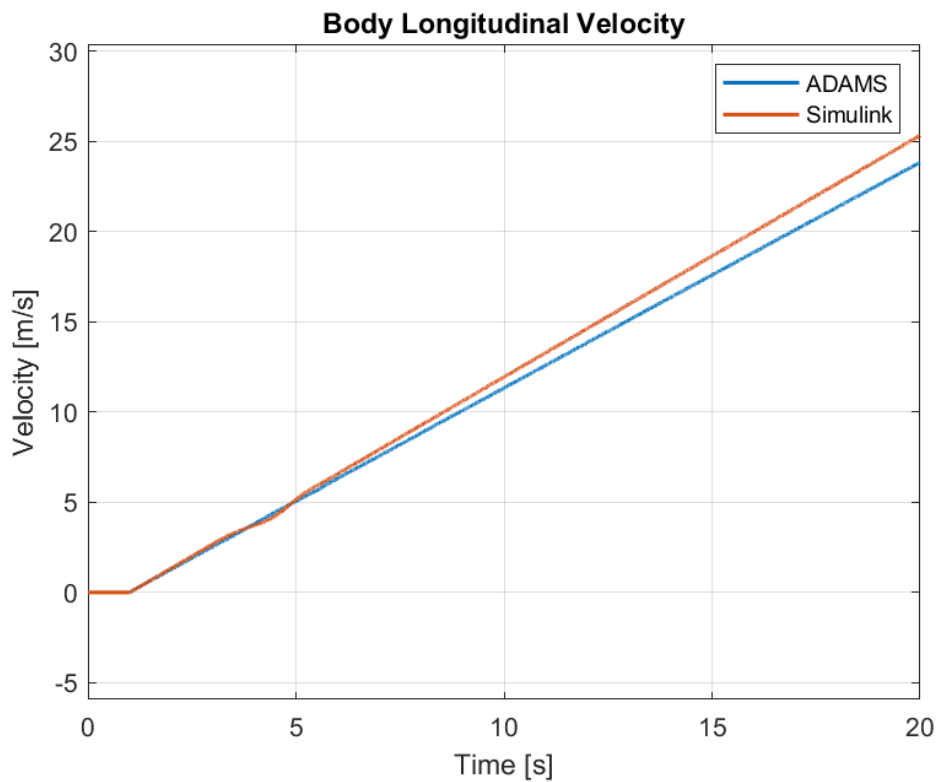


Figure 5-13. Plots of Longitudinal Velocity of Body for Case 2

Although the effect of the bump is more evident in Simulink, the values remain close to each other. At the end of Simulation, the ADAMS result yields a longitudinal velocity of 25.325 m/s and Simulink yields 23.831 m/s. The mean square error between the two data are 0.627 and mean values are 11.351 m/s and 11.977 m/s for ADAMS and Simulink, respectively.

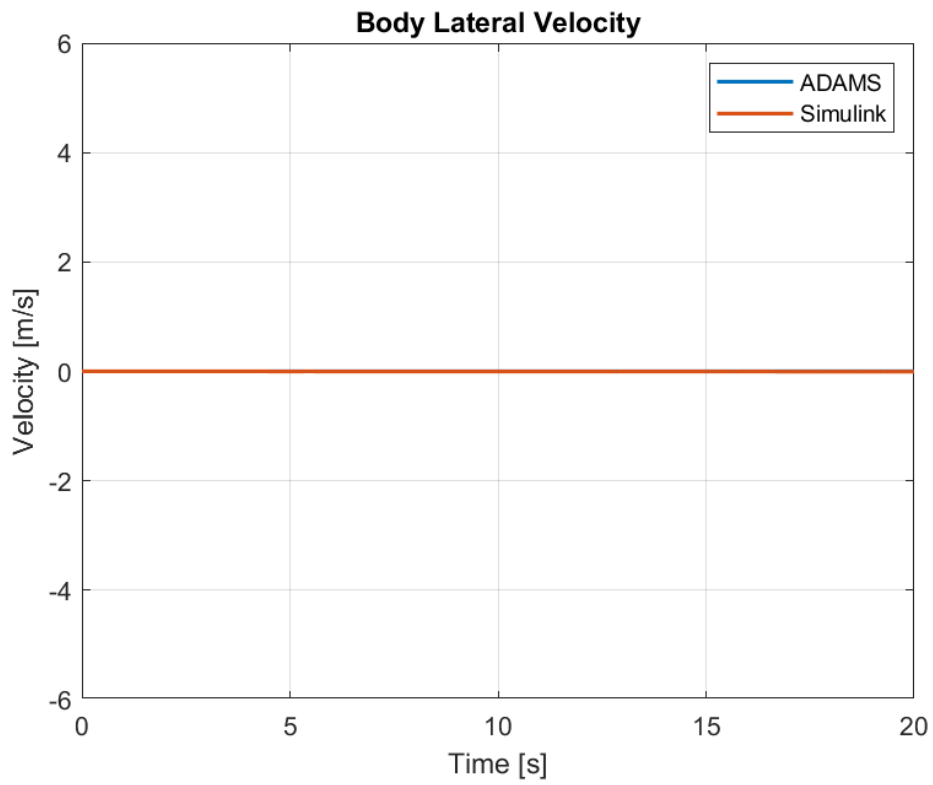


Figure 5-14. Plots of Lateral Velocity of Body for Case 2

Lateral velocity of the vehicle can be approximated to 0 throughout the simulations for both software similar to the first case.

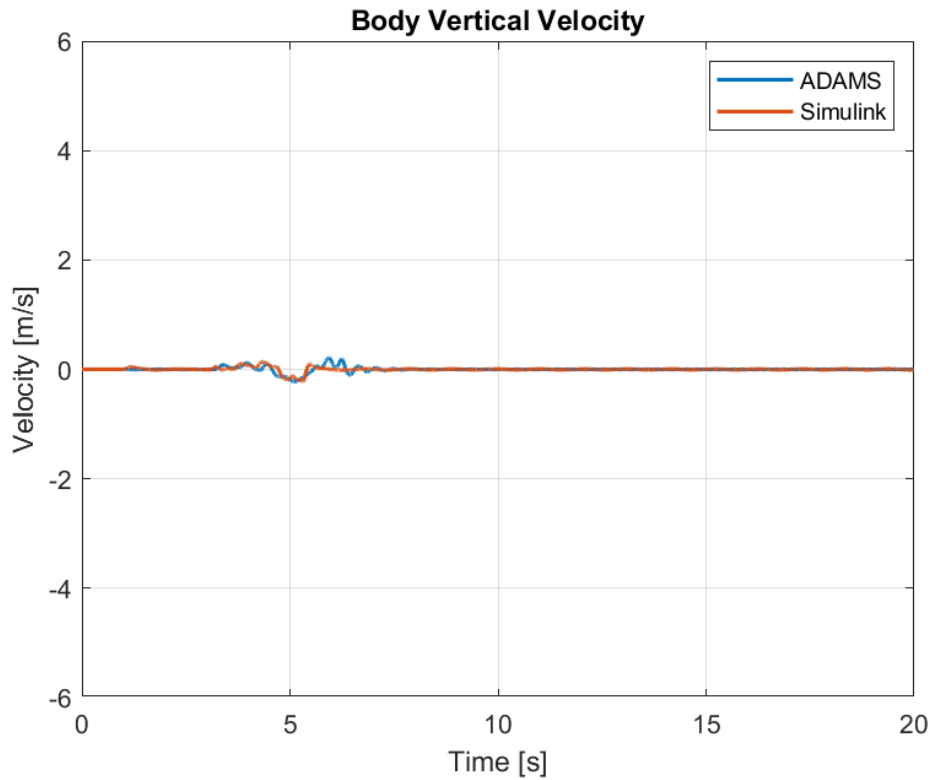


Figure 5-15. Plots of Vertical Velocity of the Body for Case 2

The vertical velocity of the vehicle is more important for this case as mentioned. For both simulations the vehicle shows the same behavior vertically. As the front tires reach the bump the center of gravity of the body moves upwards. The disturbance to the middle tires shows the same results but as the rear tires pass an opposite reaction is observed. The suspensions then work to damp the effect of the disturbances. Although the magnitude oscillations are not exactly the same, this level of difference can be accepted. As previously explained, the main difference comes from the fact that load distribution model in Simulink use approximations. However, the necessary assumptions made in load distribution still result in acceptable results. The mean square error between the datasets is 0.00122.

For translational velocity along the three axes the mean square error, maximum, minimum and mean values are shown in table 5-4.

Table 5-4. Comparison of Translational Velocity Data Produced between Models for Case 2

Parameter	MSE	ADAMS Max	Simulink Max	ADAMS Min	Simulink Min	ADAMS Mean	Simulink Mean
Long. Vel.	0.627	23.8	25.3	-9.8E-05	-2.3E-17	11.4	12.0
Lat. Vel.	1.3E-19	1.5E-12	1.8E-14	-7.5E-10	-1.7E-10	-3.5E-10	-3.1E-11
Vert. Vel.	0.00122	0.214	0.137	-0.222	-0.218	2.48E-05	5.26E-4

As a continuation of the translational velocity, the body displacements are to be explained next.

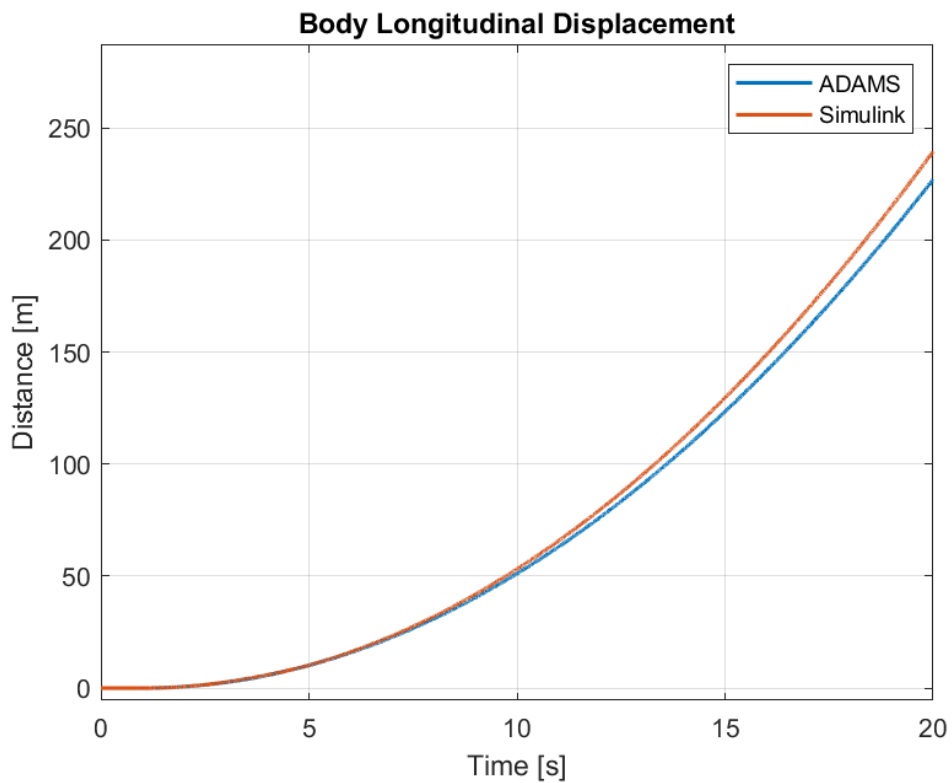


Figure 5-16. Plots of Longitudinal Displacement of the Body for Case 2

While reviewing the longitudinal velocity before, it was evident that the bump's effect on the vehicle was negligible in the longitudinal direction. In this case the

vehicle covers 227.0 meters and 239.5 meters in ADAMS and Simulink, respectively.

The lateral displacement is not shared as it is evident from the lateral velocity plot, its values are negligible but still, its statistical values can be found in table 5-5.

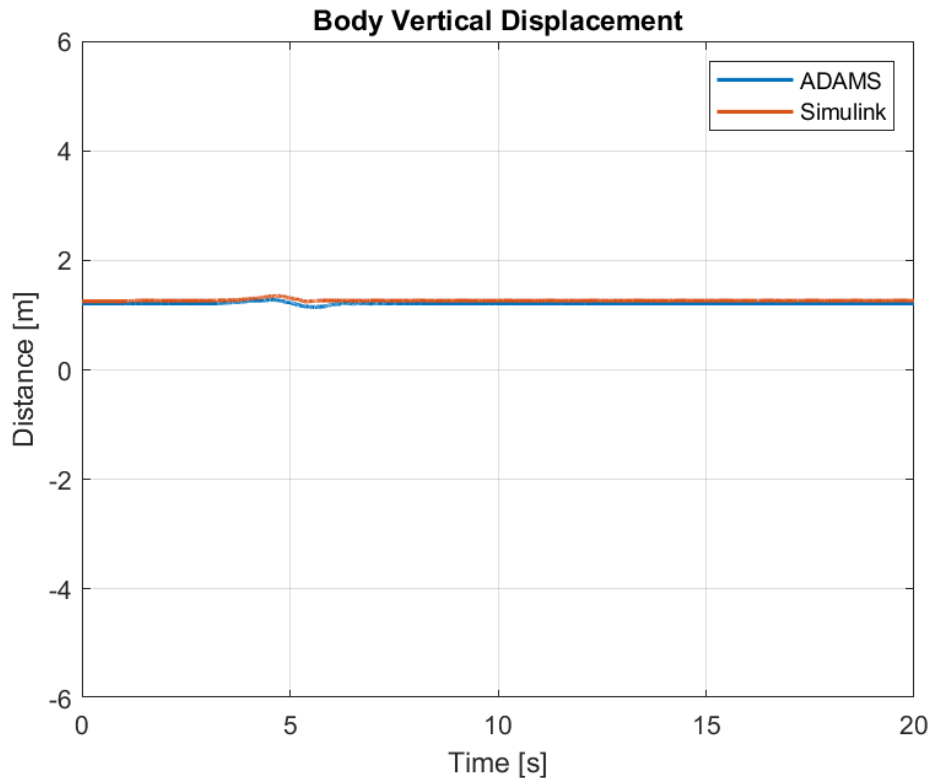


Figure 5-17. Plots of Vertical Displacement of the Body for Case 2

As further and direct proof of the vertical translational velocity results the vehicle can be seen to show the same behavior in both simulations. The center of gravity moves up while front and middle tires interact with the bump and consequently moves down while rear tires pass the bump. Again, the effect of oscillations can be seen here as well, which are more in magnitude in ADAMS. The mean square error between the datasets is 0.002957. The center of gravity experiences a maximum elevation of 1.280 meters in ADAMS and 1.349 meters in Simulink. The minimum values for vertical displacement are 1.147 meters and 1.247 meters in Simulink. The

mean values are 1.214 meters and 1.267 meters in ADAMS and Simulink, respectively.

The statistical data for displacements along the three axes can be seen in table 5.5.

Table 5-5. Comparison of Translational Displacement Data Produced between Models for Case 2

Parameter	MSE	ADAMS Max	Simulink Max	ADAMS Min	Simulink Min	ADAMS Mean	Simulink Mean
Long. Disp.	26.24	227.0	239.5	0.003763	-2.8E-18	72.013	75.514
Lat. Disp.	6.7E-05	1.1E-13	5.6E-08	-5.5E-14	-2.43E-2	6.3E-15	-4.89E-3
Vert. Disp.	0.002957	1.280	1.349	1.147	1.247	1.214	1.267

The translational accelerations are also in line with the translational velocities and displacements. As the main focus here is the vertical motion, its plot can be seen figure 5-18.

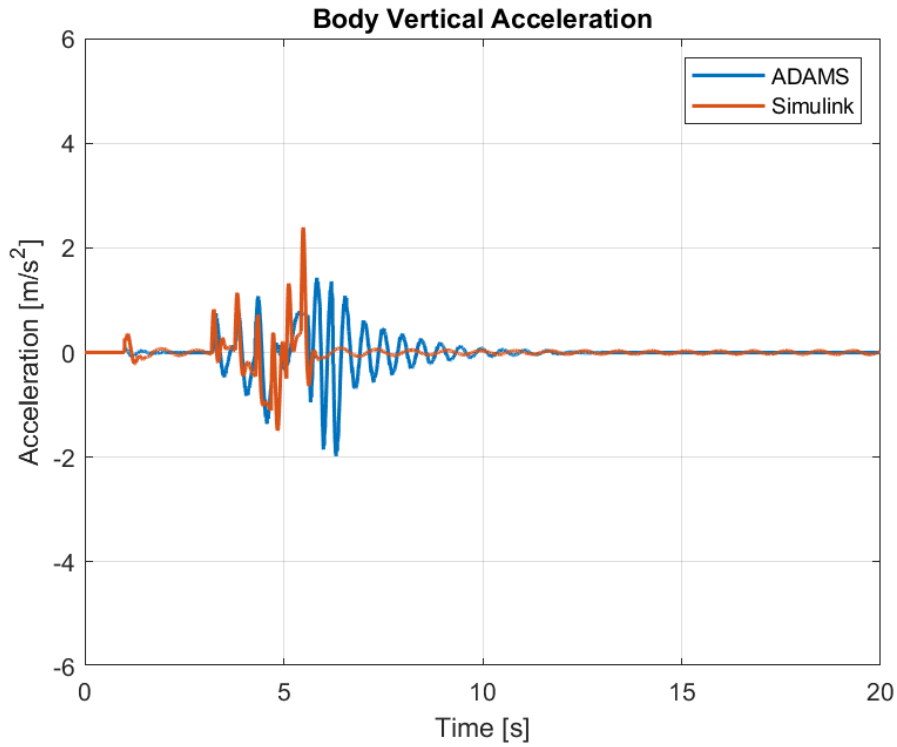


Figure 5-18. Plots of Vertical Acceleration of the Body for Case 2

Again, after 1 seconds, the torques are supplied to the tires and the traction forces induce a pitch motion which results in a shift in the center of gravity. The oscillations in this case are more severe as expected. However, as seen from the vertical velocity and displacement plots, the resulting behavior of the acceleration is not too severe and is damped shortly. The MSE value for results between ADAMS and Simulink models is 0.1117, respectively. The remaining statistical data can be found in table 5-6.

Table 5-6. Comparison of Translational Acceleration Data Produced between Models for Case 2

Parameter	MSE	ADAMS Max	Simulink Max	ADAMS Min	Simulink Min	ADAMS Mean	Simulink Mean
Long. Acc.	7.6E-3	1.610	1.578	-1.1E-4	-6.5E-16	1.192	1.152
Lat. Acc.	1.2E-5	2.4E-09	7.6E-4	-2.3E-09	-3.8E-05	-4.6E-12	2.6E-4
Vert. Acc.	0.1117	1.428	2.391	-1.981	-1.491	-2.3E-4	-3.5E-4

For this case, the rotations of the body are also of importance. Mainly the pitch motion of the body is expected to be more severe. However, firstly the roll angle of the vehicle can be seen in figure 5-19.

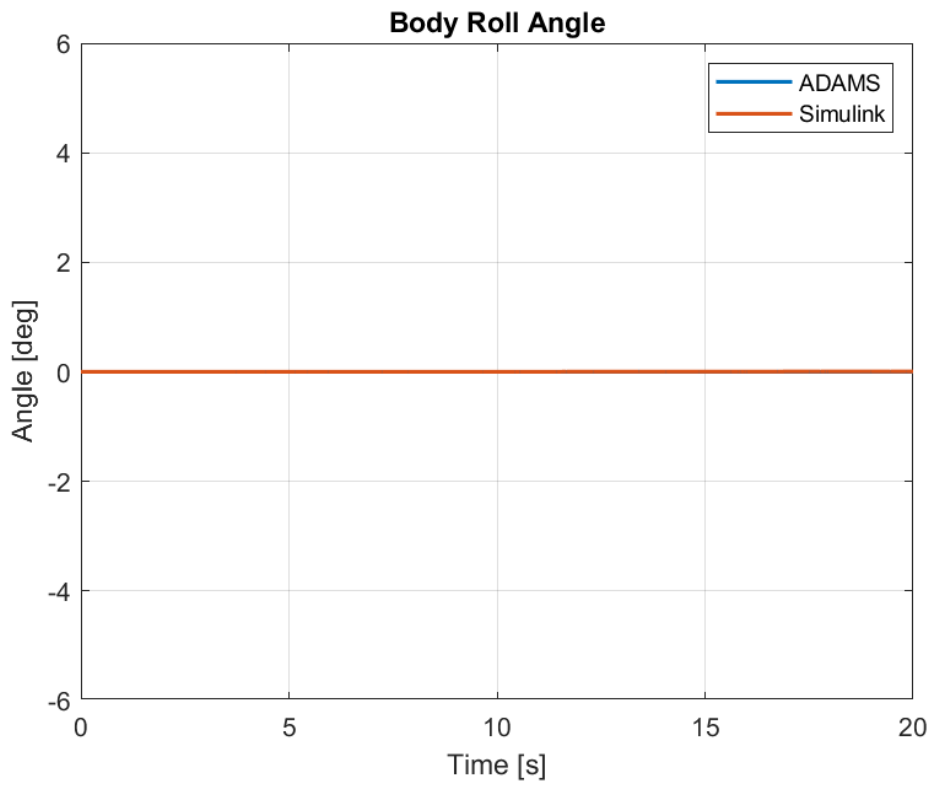


Figure 5-19. Plots of Roll Angle of the Body for Case 2

As expected, the values of the body roll angle are negligible in this case. However, the statistical data are still shared in table 5-7.

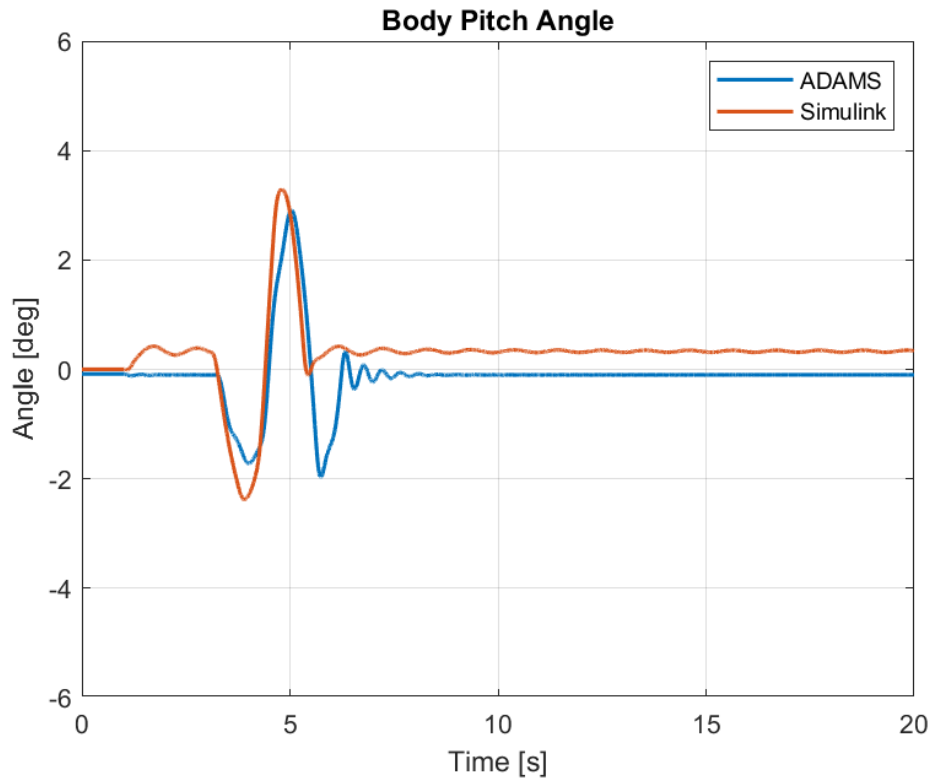


Figure 5-20. Plots of Pitch Angle of the Body for Case 2

As it could be interpreted from vertical translational motions, the pitch angle in ADAMS shows higher peaks but the angle remains in the range of -2 degrees and 3 degrees. Furthermore, the traction forces induce a positive pitch angle which is more evident in Simulink. Note that the positive pitch angle means the front of the vehicle is tilted downwards. This occurs because when the traction is present, front arms are extended towards the front end of the vehicle and as a result, the front end of the body is tilted downwards. The mean square error between the two datasets are 0.314. In ADAMS pitch angle shows a maximum value of 2.91 degrees and in Simulink a maximum value of 3.28 degrees. The minimum values are -1.96 and -2.37 degrees, in ADAMS and Simulink, respectively.

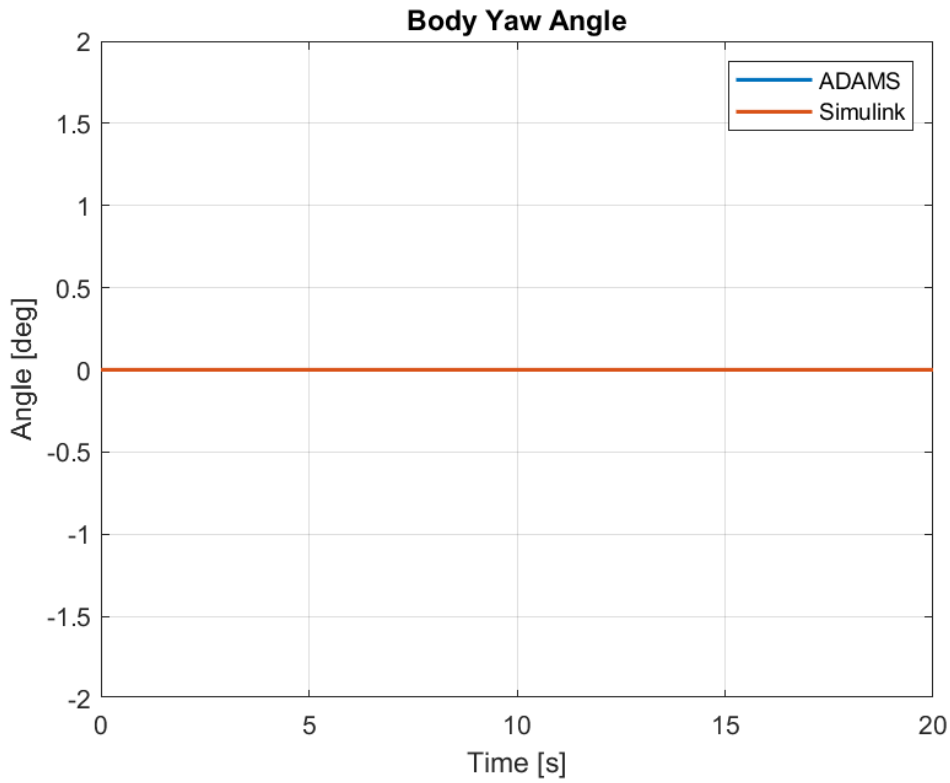


Figure 5-21. Plots of Yaw Angle of the Body for Case 2

Similar to roll angle, the values of yaw angle are negligible for this case as well. However, the statistical data for angular position results along the three axes can be seen in table 5-7.

Table 5-7. Comparison of Angular Position Data Produced between Models for Case 2

Parameter	MSE	ADAMS Max	Simulink Max	ADAMS Min	Simulink Min	ADAMS Mean	Simulink Mean
Roll Ang.	1.2E-05	1.9E-12	0.007203	-2.2E-12	-2.5E-05	-8.8E-15	0.002607
Pitch Ang.	0.3142	2.913	3.288	-1.967	-2.378	-0.1082	0.2836
Yaw Ang.	0.01239	6.7E-12	0.2431	-2.6E-12	-6.3E-20	3.0E-13	0.0826

The roll and yaw angular velocities can again be approximated to zero as well but still, their plots are shown in figures 5-22 and 5-24.

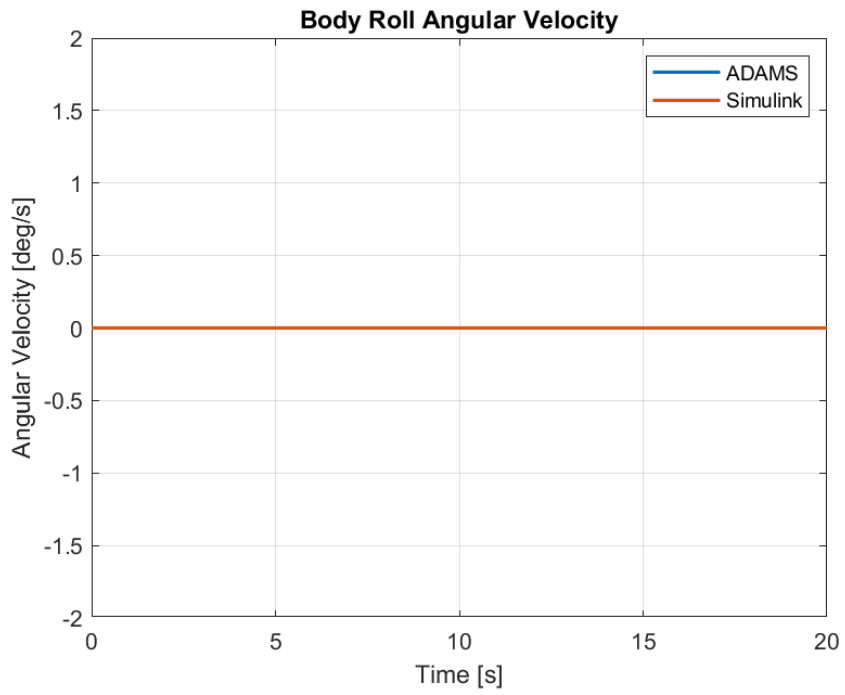


Figure 5-22. Plots of Roll Angular Velocity of the Body for Case 2

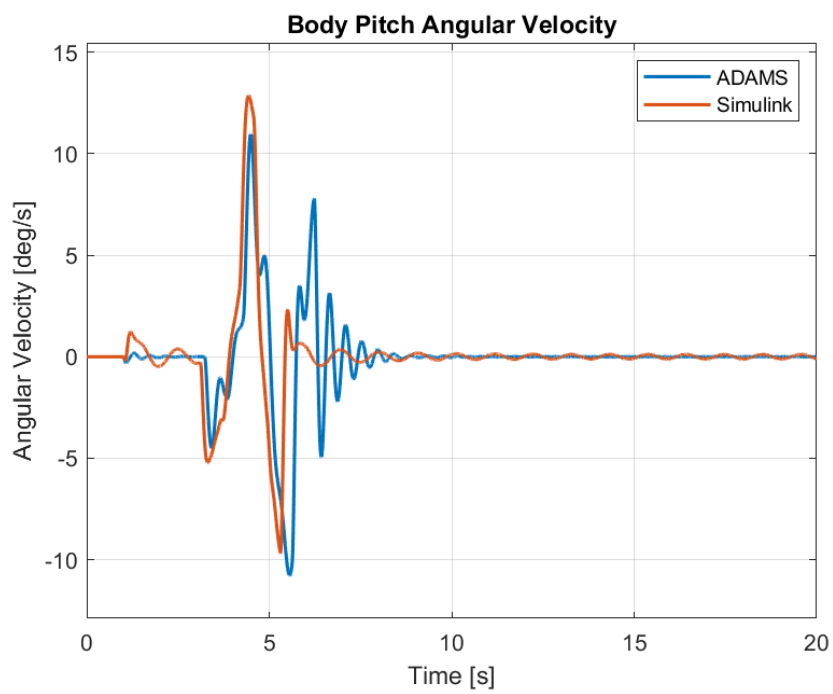


Figure 5-23. Plots of Pitch Angular Velocity of the Body for Case 2

Again, the body pitch angular velocity shows a more severe and oscillatory behavior in ADAMS compared to Simulink. However, the pitch motion is damped quickly again after the rear tires finish traversing the bump.

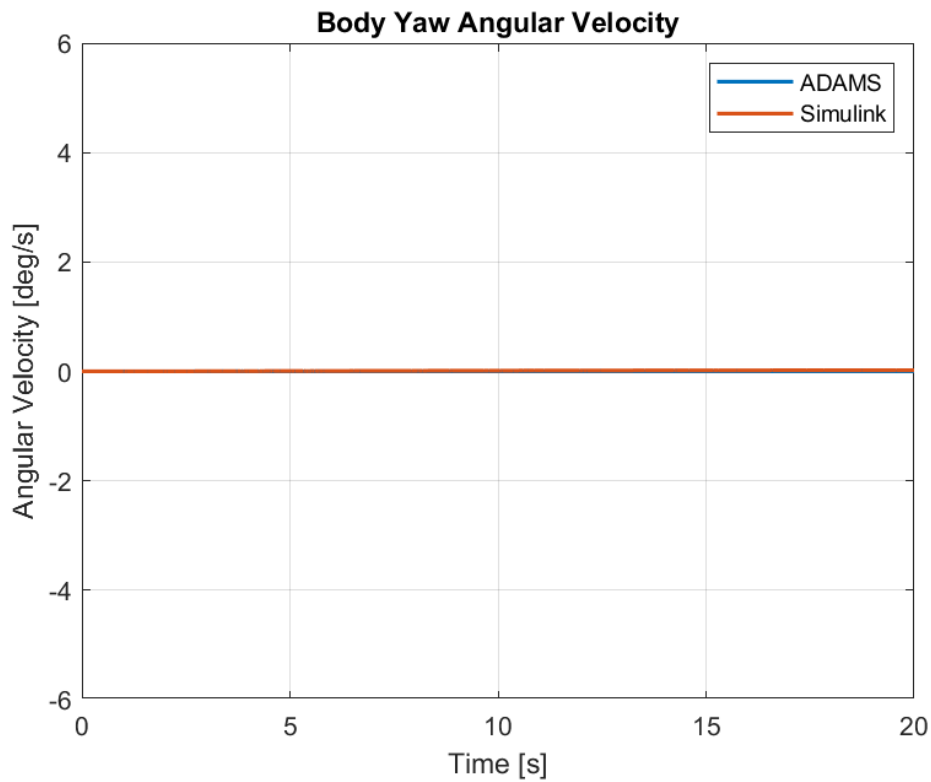


Figure 5-24. Plots of Yaw Angular Velocity of the Body for Case 2

The yaw velocity is close to zero as mentioned before.

Table 5-8. Comparison of Angular Velocity Data Produced between Models for Case 2

Parameter	MSE	ADAMS Max	Simulink Max	ADAMS Min	Simulink Min	ADAMS Mean	Simulink Mean
Roll Ang. Vel.	5.0E-7	1.6E-11	1.98E-3	-2.1E-11	-3.6E-3	3.6E-13	3.6E-4
Pitch Ang. Vel.	3.843	10.96	12.88	-10.78	-9.686	-9.1E-4	0.01705
Yaw Ang. Vel.	1.9E-4	7.7E-13	0.02165	0	-1.6E-19	3.8E-13	0.01216

Although the same case holds for roll and yaw accelerations, their plots will still be shared in the following figures.

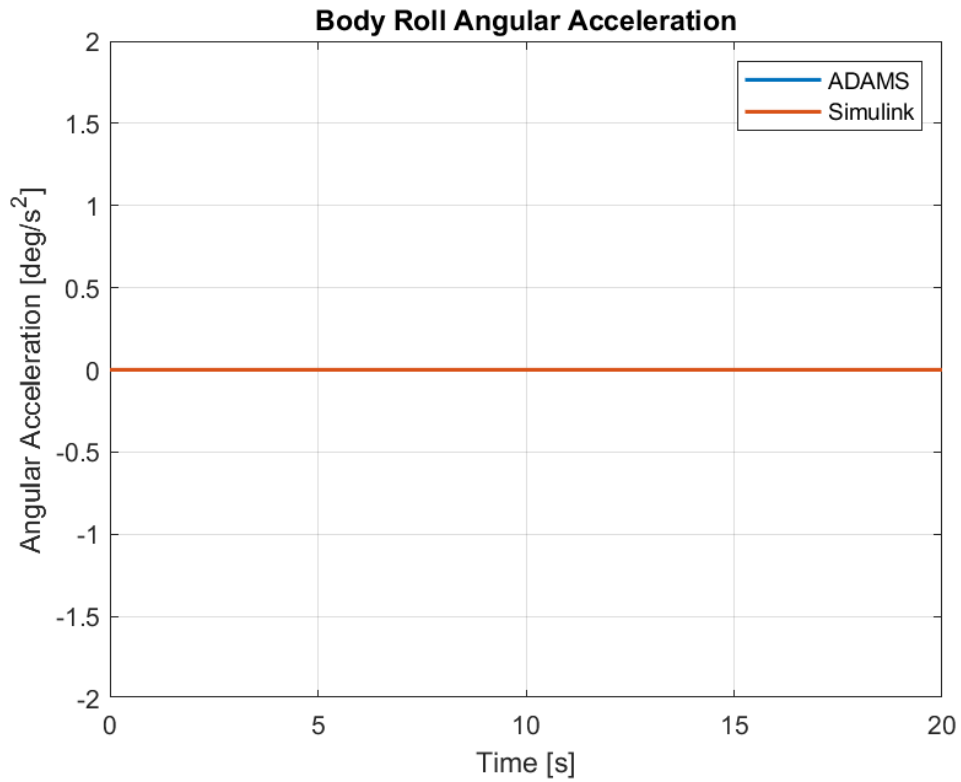


Figure 5-25. Plots of Roll Angular Acceleration of the Body for Case 2

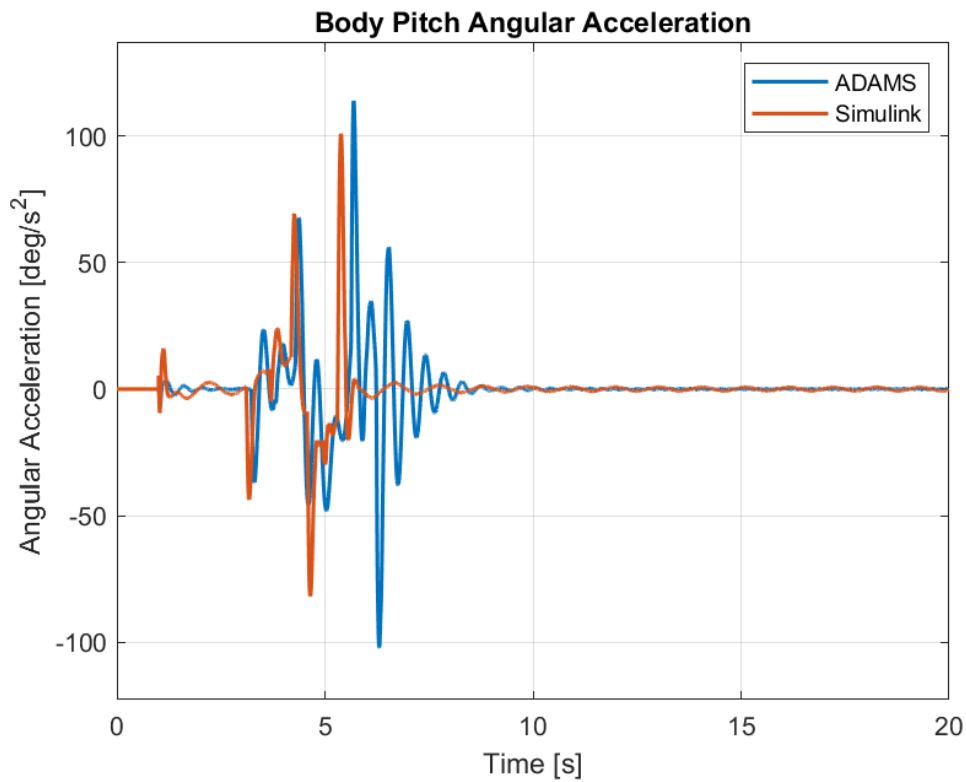


Figure 5-26. Plots of Pitch Angular Acceleration of the Body for Case 2

Contrary to the pitch angle and velocity, for the case of acceleration, Simulink shows a more extreme behavior. The selection of the solver step size also results in such an error. However, noting that the peaks are more frequent and higher in magnitude it results in more stable velocity and angle results. In other words, the pitch motion is seen to be damped more efficiently in Simulink. However, as evident from the previous figures, the resulting behaviors are similar. Remaining data are shown in table 5-9.

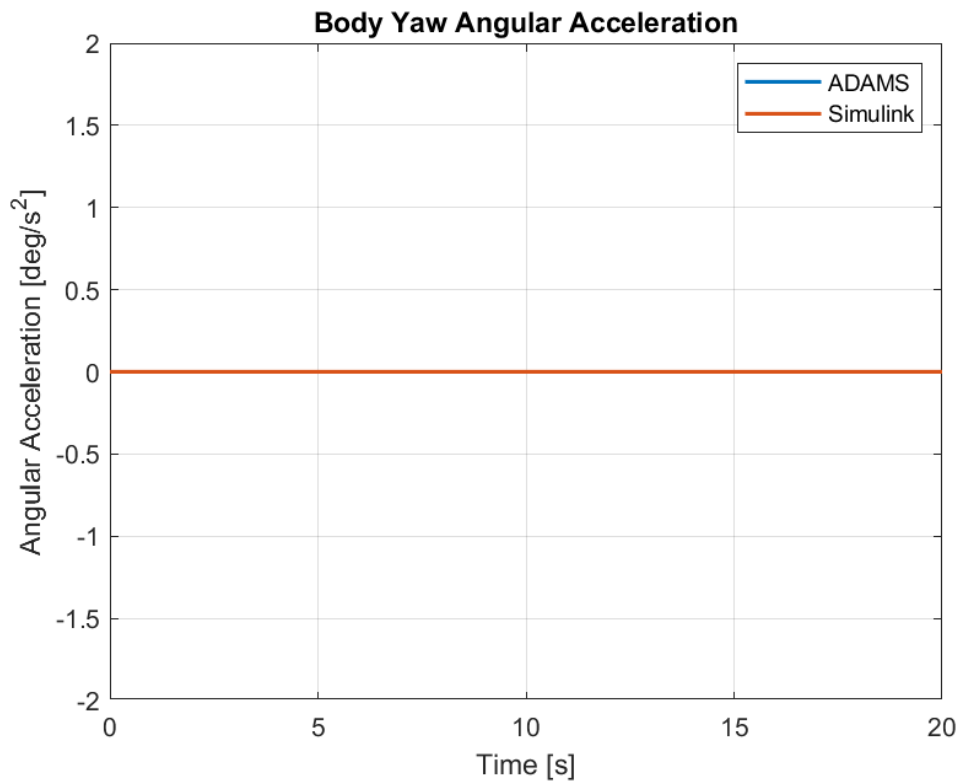


Figure 5-27. Plots of Yaw Angular Acceleration of the Body for Case 2

Table 5-9. Comparison of Angular Acceleration Data Produced between Models for Case 2

Parameter	MSE	ADAMS Max	Simulink Max	ADAMS Min	Simulink Min	ADAMS Mean	Simulink Mean
Roll Ang. Acc.	1.761	6.1E-10	0.0624	-6.6E-10	-0.823	-4.0E-12	8.1E-05
Pitch Ang. Acc.	298.3	113.9	100.9	-102.2	-81.88	1.5E-4	-0.00493
Yaw Ang. Acc.	8.6E-6	3.0E-10	0.12041	-2.9E-10	-0.0781	-2.9E-13	0.00108

Next, the behavior of the arms are to be considered. The arm angles are shown in figure 5-28 and 5-29 for ADAMS and Simulink, respectively.

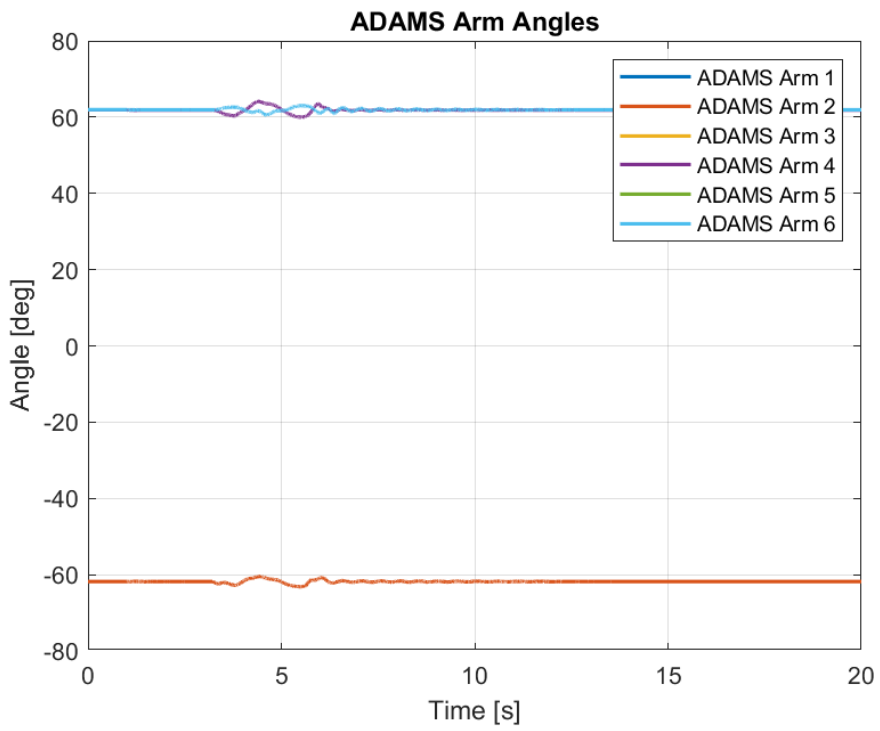


Figure 5-28. ADAMS Arm Angles for Case 2

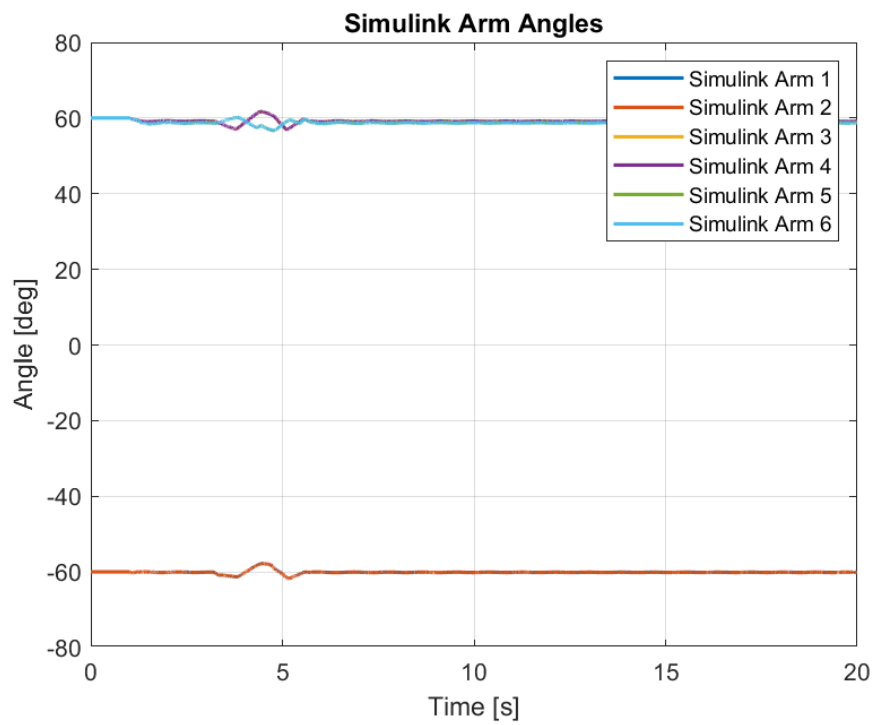


Figure 5-29. Simulink Arm Angles for Case 2

The resulting behaviors are the same for both simulations although there are differences in the magnitude and exact time of the effects. Table 5-10 which shows the statistical comparison of both software, however, shows that the behaviors are close enough. An important note to be made here is to revise the notation used for arm angles. The arm angles take a value of 0 degree when they are perpendicular to the ground, a value of 180 degrees when they are parallel to the ground and expanded to the rear and -180 degrees when expanded to the front of the vehicle. The plots show that the front and middle arms are further opened as front tires pass through the bump while an opposite behavior is observed in rear arms. As expected, while the rear tires pass through the bump, front and middle arms are then closed and rear arms are opened. As a result, they return approximately to their initial positions at the end. Here, opening means getting closer to being parallel to the ground.

Table 5-10. Comparison of Arm Angle Data Produced between Models for Case 2

Parameters	MSE	ADAMS Max	Simulink Max	ADAMS Min	Simulink Min	ADAMS Mean	Simulink Mean
Arm Angle 1	3.073	-60.512	-57.760	-63.150	-61.705	-61.820	-60.087
Arm Angle 2	3.053	-60.512	-57.759	-63.150	-61.706	-61.820	-60.092
Arm Angle 3	7.293	64.088	61.686	60.010	56.941	61.853	59.182
Arm Angle 4	7.261	64.088	61.687	60.010	56.942	61.853	59.188
Arm Angle 5	9.884	62.998	60.138	60.609	56.721	61.922	58.801
Arm Angle 6	9.846	62.998	60.138	60.609	56.723	61.922	58.807

The load distribution is also important for this case. The plots for the results of ADAMS and Simulink are shared in the following figures.

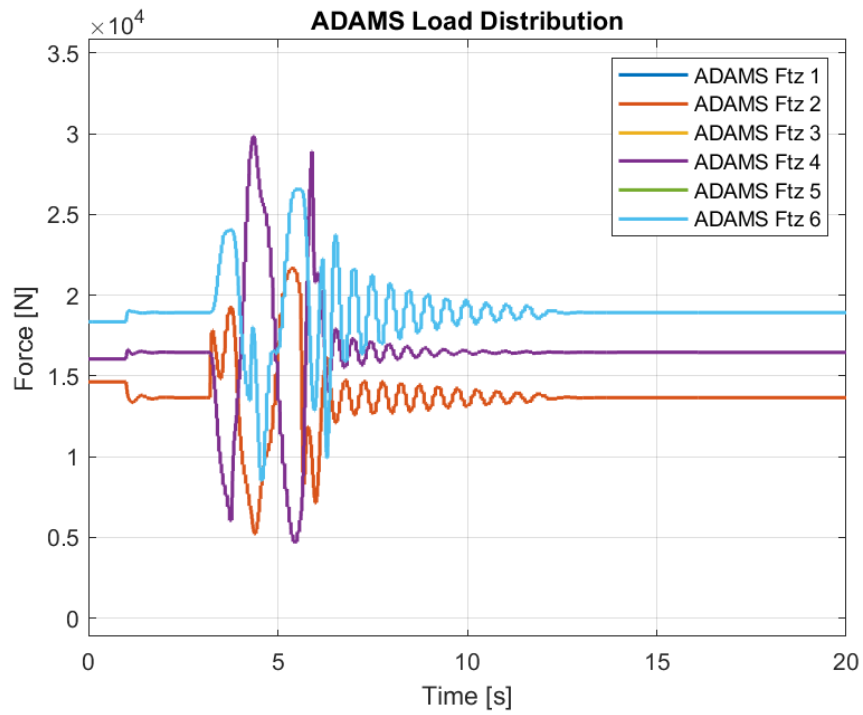


Figure 5-30. ADAMS Load Distribution for Case 2

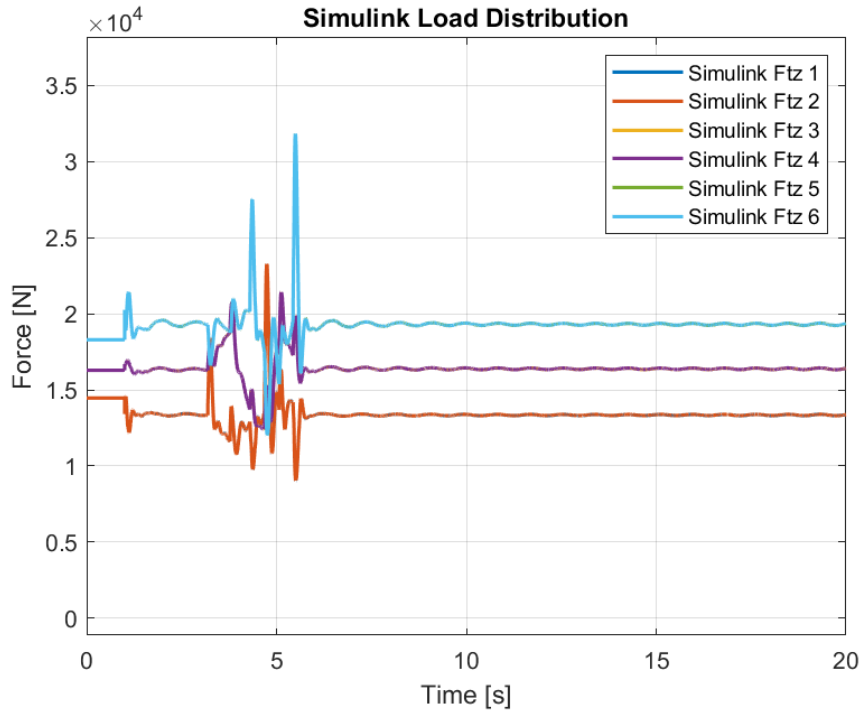


Figure 5-31. Simulink Load Distribution for Case 2

Again, it is important to revise that the Simulink solution to the load distribution is an approximation based on the vehicle motion and forces generated. ADAMS uses FEM in order to calculate the vertical tire forces. However, as the values and behavior of the load distribution in both models are similar, the remaining behaviors of the vehicle are seen to be close enough as well. This is further evidenced by making statistical comparisons between the results. The main difference caused by the load distribution is the total suspension torques.

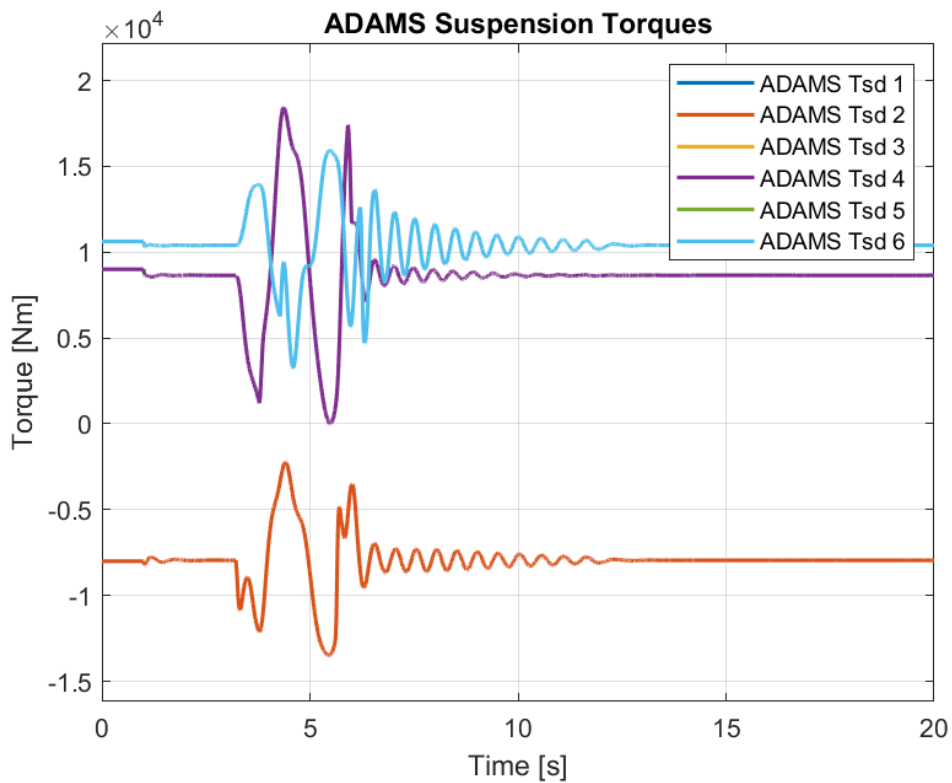


Figure 5-32. ADAMS Suspension Torques for Case 2

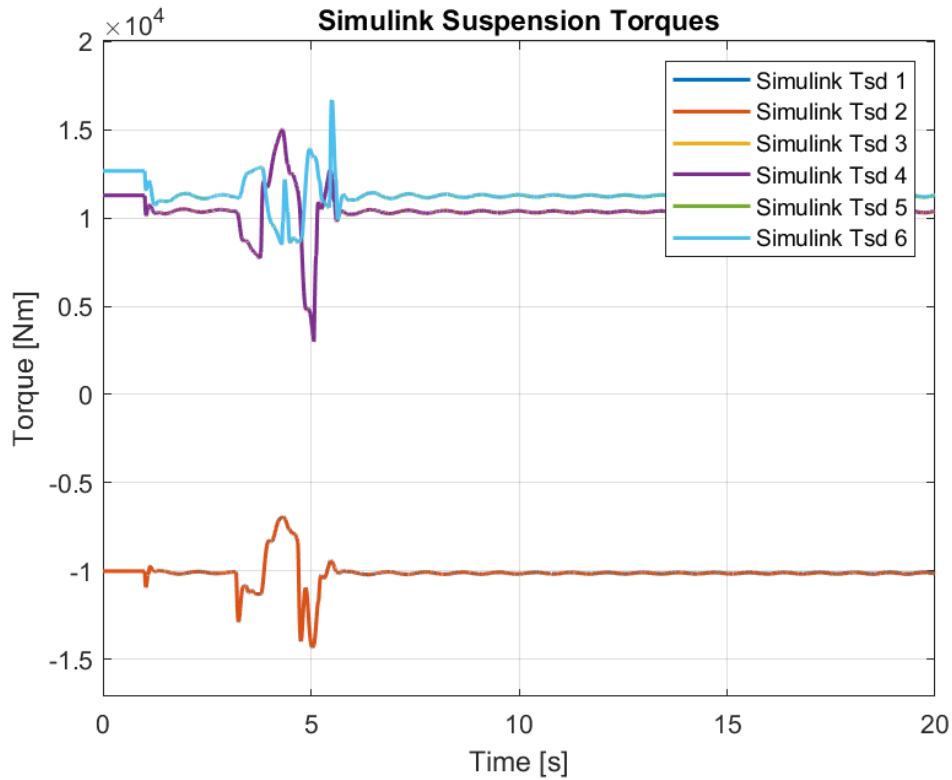


Figure 5-33. Simulink Suspension Torques for Case 2

The reason load distribution effects the suspension torques is that the suspensions try negating the effects of the vertical forces coming from tires. As the Simulink model is constructed as being at equilibrium position initially, only the disturbances coming from the tires effect the suspension. The force necessary to hold the equilibrium conditions change but as the dynamic behavior of the vehicle is the focus of this study, the response of the suspension is more important.

Furthermore, the results of the load distribution are fed directly to the tire module in Simulink and as can be seen from figures 5-34 and 5-35, they can be seen to be close.

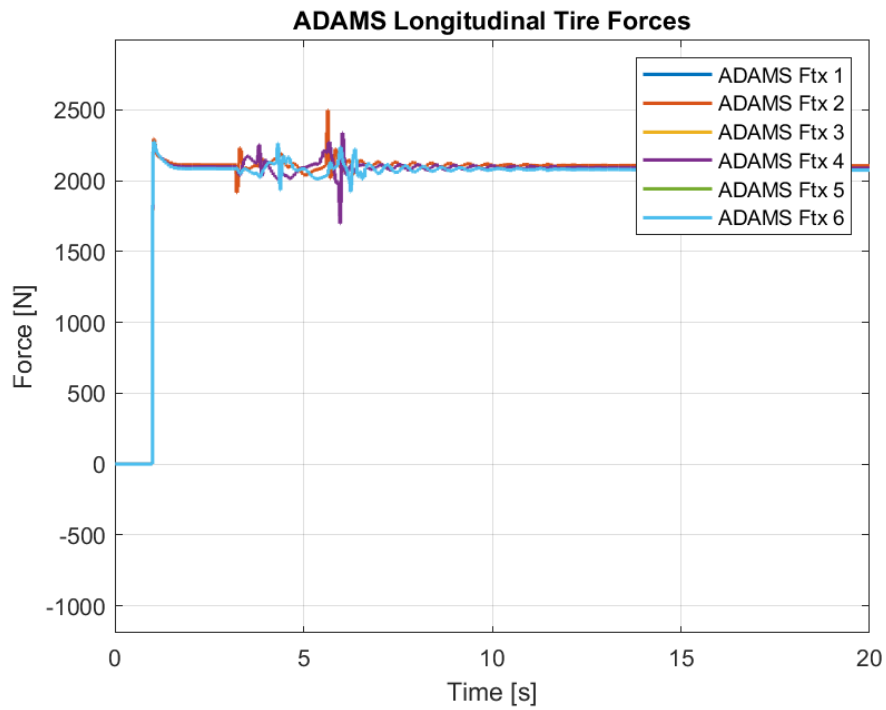


Figure 5-34. ADAMS Longitudinal Tire Forces for Case 2

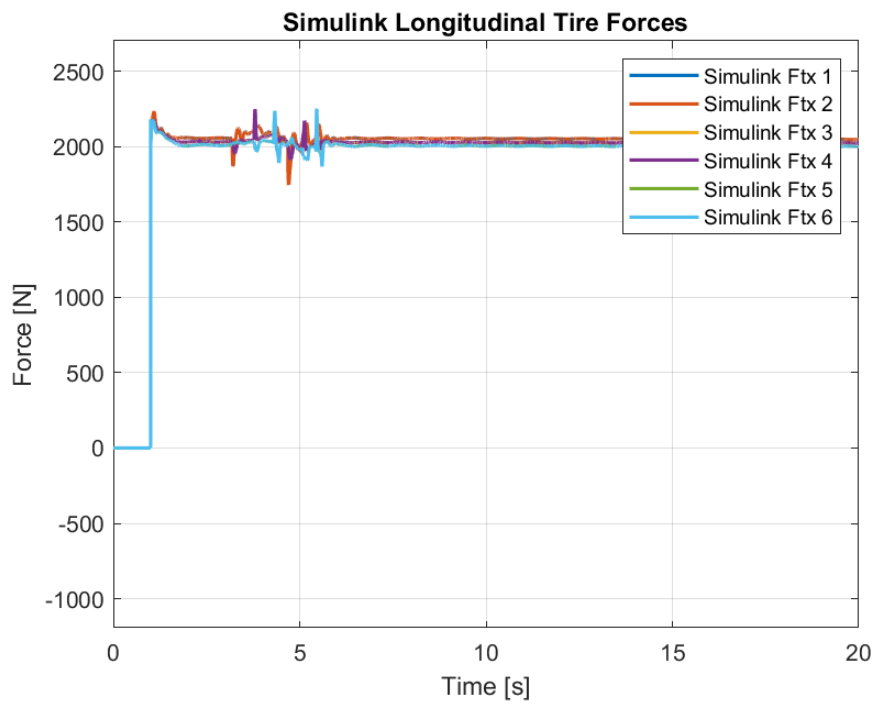


Figure 5-35. Simulink Longitudinal Tire Forces for Case 2

Table 5-11. Comparison of Longitudinal Tire Force Data Produced between Models for Case 2

Parameters	MSE	ADAMS Max	Simulink Max	ADAMS Min	Simulink Min	ADAMS Mean	Simulink Mean
Ftx 1	4465.6	2497.2	2235.6	0.0	0.0	2004.2	1952.6
Ftx 2	4469.8	2497.2	2235.6	0.0	0.0	2004.2	1952.5
Ftx 3	5699.9	2337.2	2249.1	-0.4	0.0	1990.3	1929.4
Ftx 4	5704.1	2337.2	2249.2	-0.4	0.0	1990.3	1929.4
Ftx 5	6458.4	2275.9	2251.6	-0.5	0.0	1977.9	1908.0
Ftx 6	6463.1	2275.9	2252.1	-0.5	0.0	1977.9	1907.9

5.3 Case 3 – Road with Irregularities

For the third road profile, a road with constant elevation difference is chosen. This road profile can be considered as an extension of the road profile with a single bump. The irregularities are modelled as the sine bump introduced in the previous case. However, in this case, the sine wave is constant throughout the road, starting at 5.2 meters ahead of the center of gravity of the vehicle. For better visualization, the road profile can be seen in the following figure, as presented in ADAMS software.

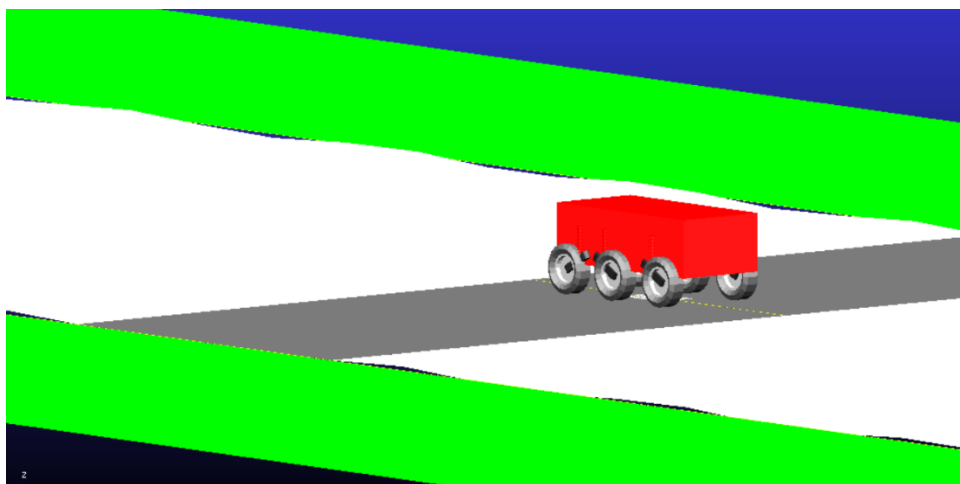


Figure 5-36. Initial Position of the vehicle on the road with gradient in ADAMS
Again, for tire input, a constant torque of 1500 Nm is supplied to each wheel.

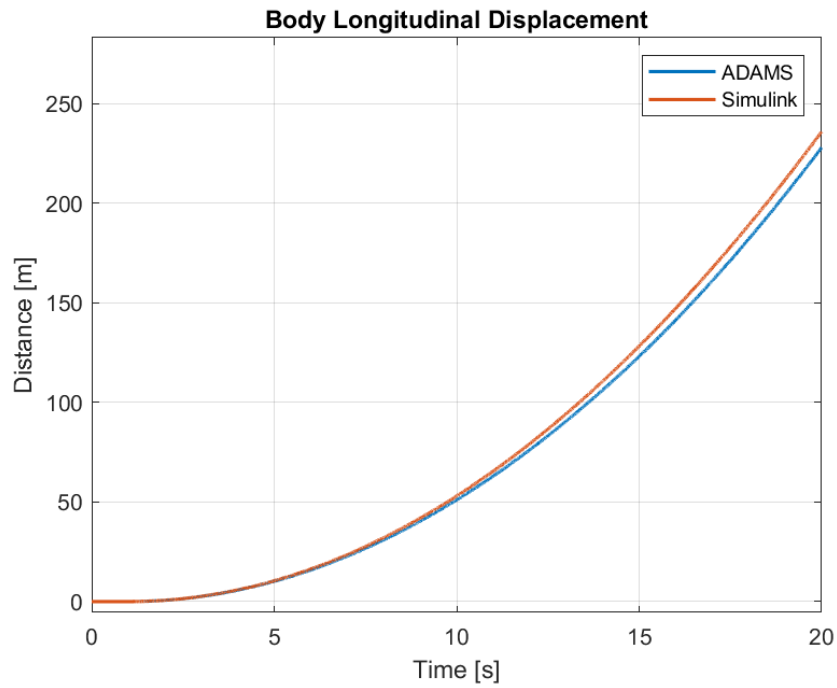


Figure 5-37. Plots of Longitudinal Displacement of Body for Case 3

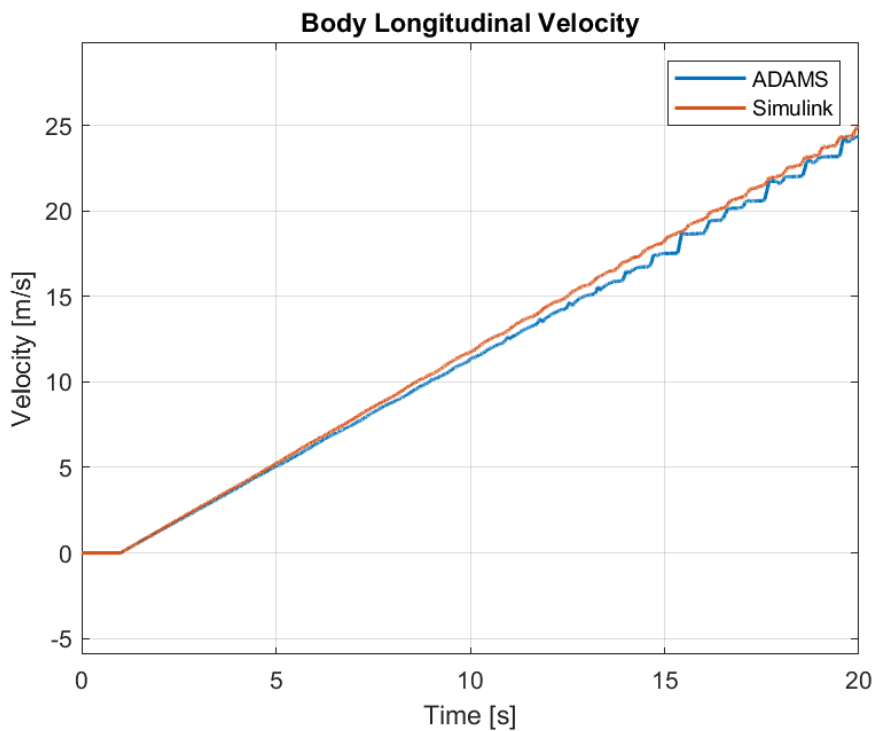


Figure 5-38. Plots of Longitudinal Velocity of Body for Case 3

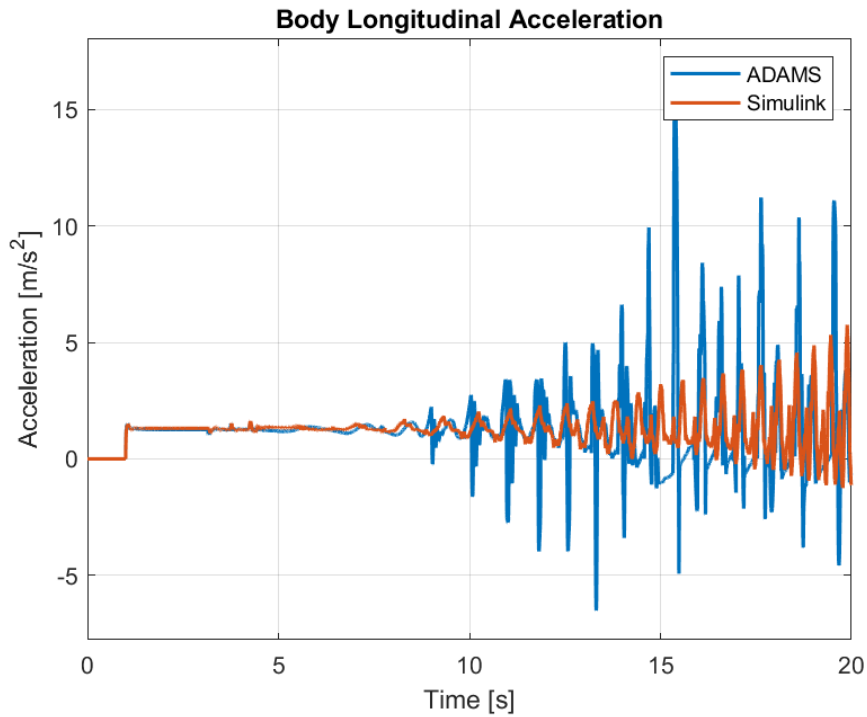


Figure 5-39. Plots of Longitudinal Acceleration of Body for Case 3

For the constant torque output, the longitudinal distance covered are similar to the first two cases. However, there is a slight deviation near the end of simulation between Simulink and ADAMS.

Table 5-12. Comparison of Longitudinal Motion Results Between Models for Case 3

Parameter	MSE	ADAMS Max	Simulink Max	ADAMS Min	Simulink Min	ADAMS Mean	Simulink Mean
Long. Disp.	14.75	228.0	235.9	0.003760	0	72.00	74.79
Long. Vel.	0.2295	24.34	24.89	-9.7E-05	0	11.40	11.79
Long. Acc.	3.461	15.05	5.756	-6.511	-1.246	1.215	1.243

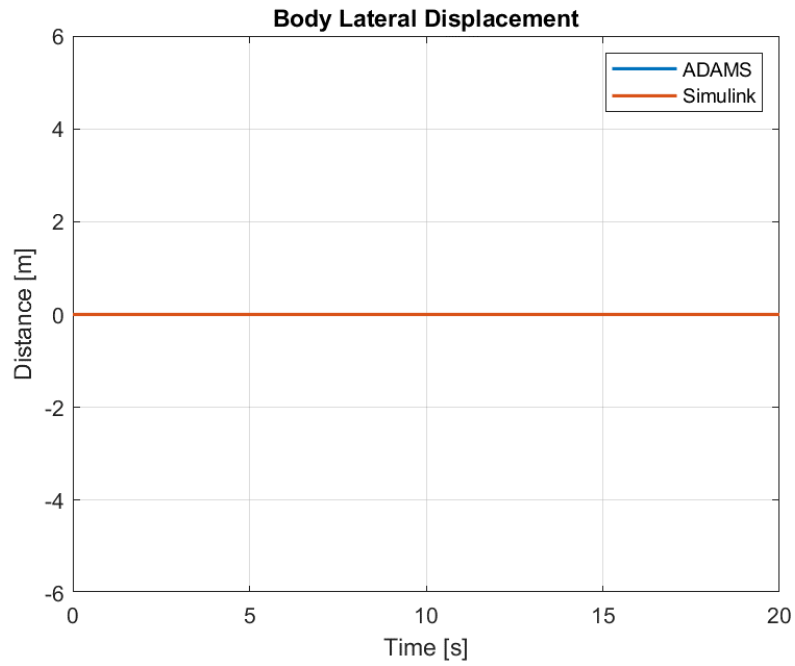


Figure 5-40. Plots of Lateral Displacement of the Body for Case 3

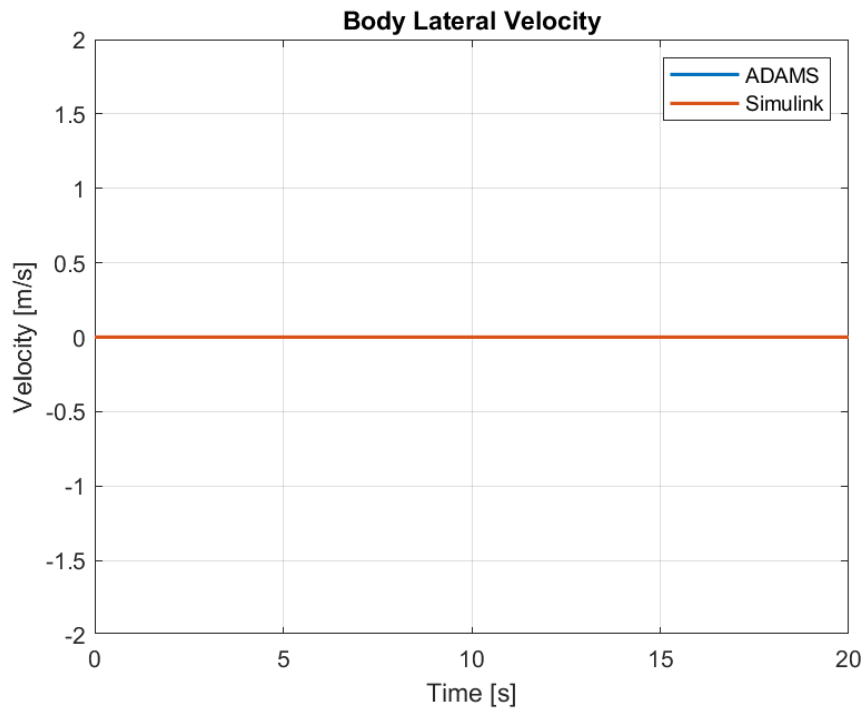


Figure 5-41. Plots of Lateral Velocity of the Body for Case 3

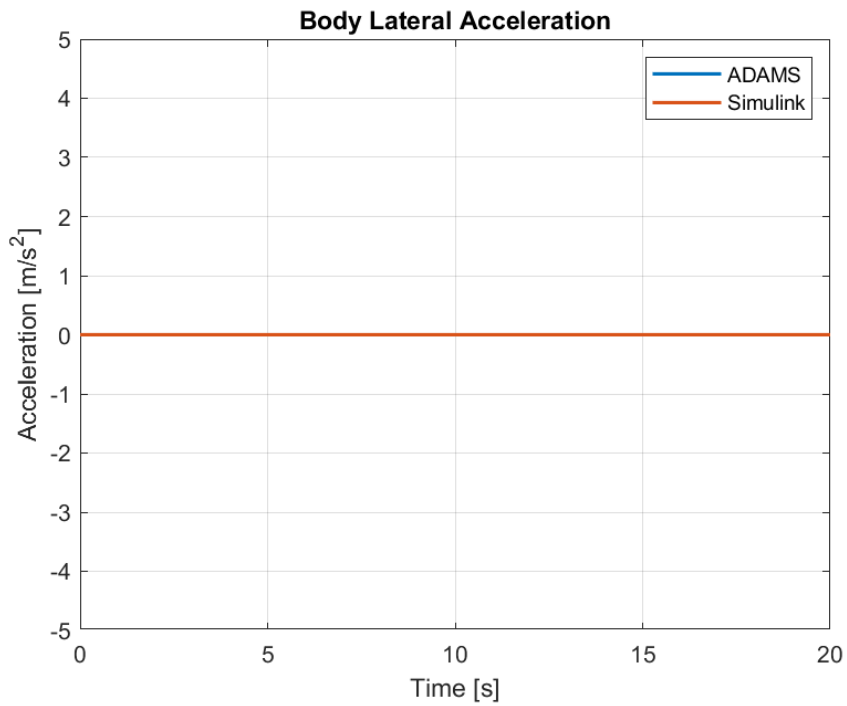


Figure 5-42. Plots of Lateral Acceleration of the Body for Case 3

Lateral displacement is again zero as expected. Since same torque are supplied to the wheels, there is no movement along the lateral axis. Because of this comparison table for the lateral table is not shared.

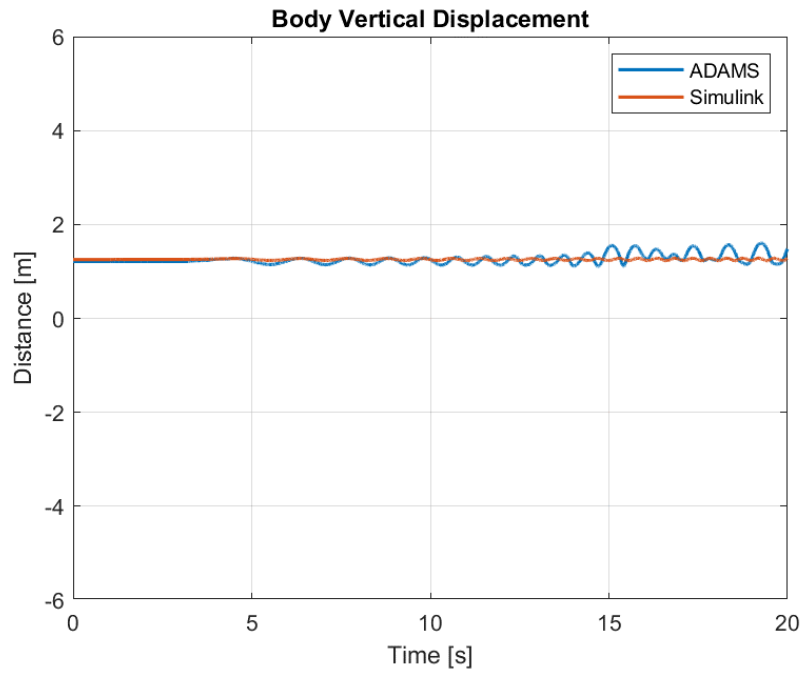


Figure 5-43. Plots of Vertical Displacement of the Body for Case 3

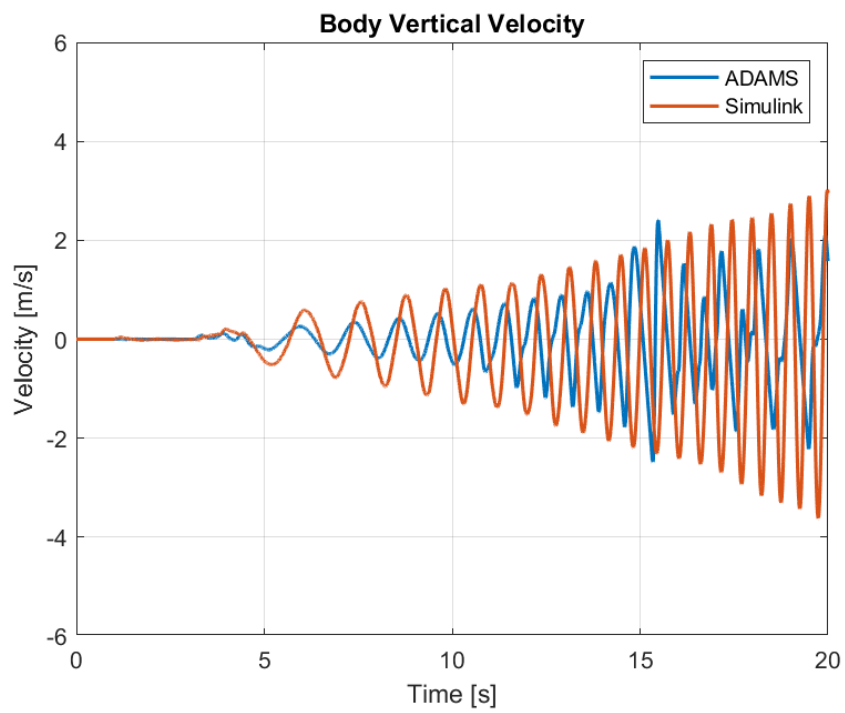


Figure 5-44. Plots of Vertical Velocity of the Body for Case 3

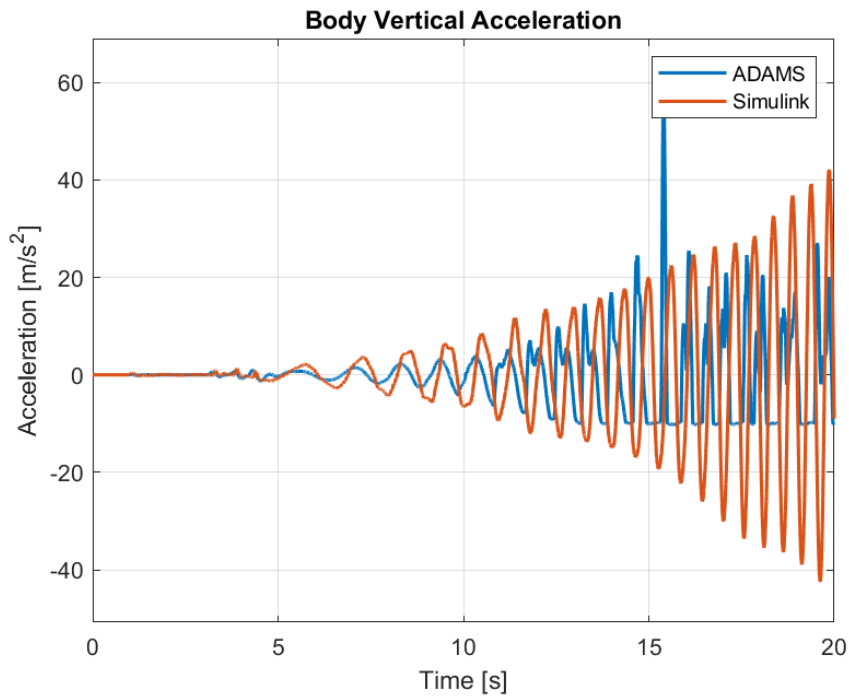


Figure 5-45. Plots of Vertical Acceleration of the Body for Case 3

In figure 5-43, the vertical displacement of the body is shown throughout the simulation. The change of position in vertical axis shows a sinusoidal behaviour at the start since the road profile is modeled as a sine wave. As the velocity of the vehicle increases, the frequency of the disturbance is increased as well. Near the 15 seconds mark deviations between the models can be observed. Due to the high difference between oscillations in vertical acceleration, a high mean square error value of 249.49 can be seen but the effect of these oscillations in velocity and position are low as the error between them are under 3 as it can be seen in the table 5-13.

Table 5-13. Comparison of Vertical Motion of the Body for Case 3

Parameter	MSE	ADAMS Max	Simulink Max	ADAMS Min	Simulink Min	ADAMS Mean	Simulink Mean
Vert. Disp.	0.0101	1.603	1.283	1.109	1.229	1.257	1.255
Vert. Vel.	2.161	2.411	3.023	-2.481	-3.620	0.0143	-0.1270
Vert. Acc.	249.4	57.52	42.13	-10.29	-42.48	0.06888	0.1628

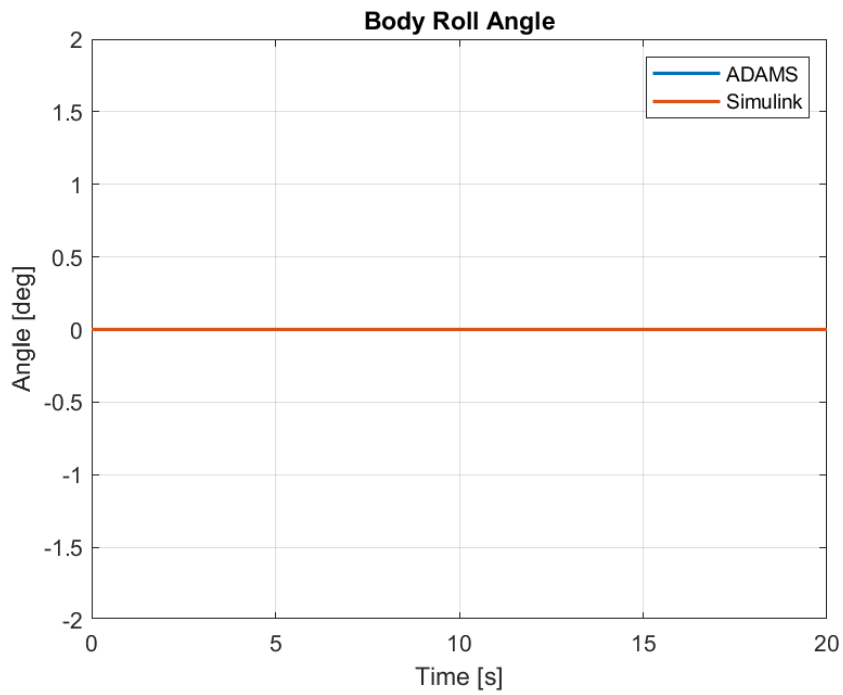


Figure 5-46. Plots of Roll Angle of the Body for Case 3

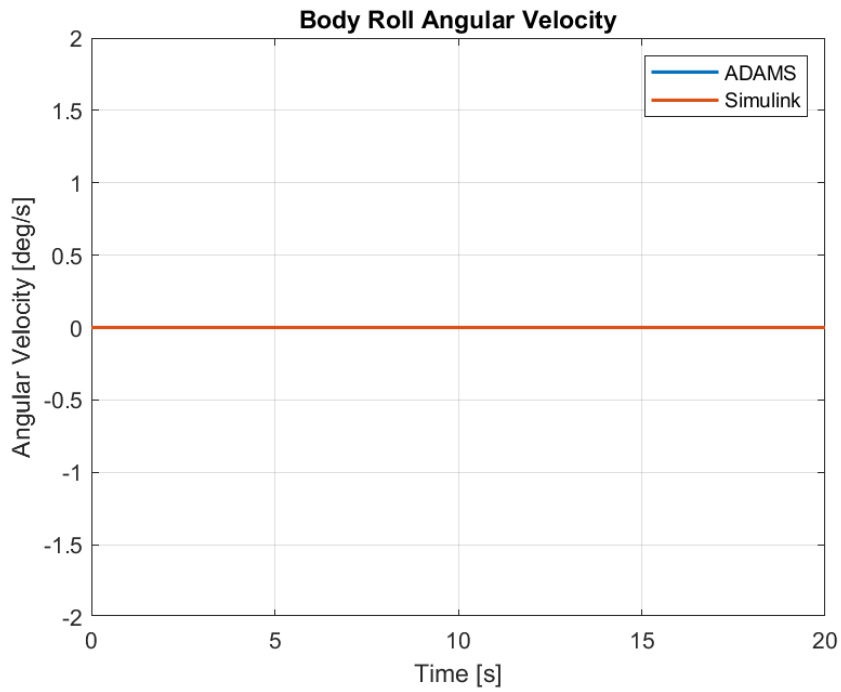


Figure 5-47. Plots of Roll Angular Velocity of the Body for Case 3

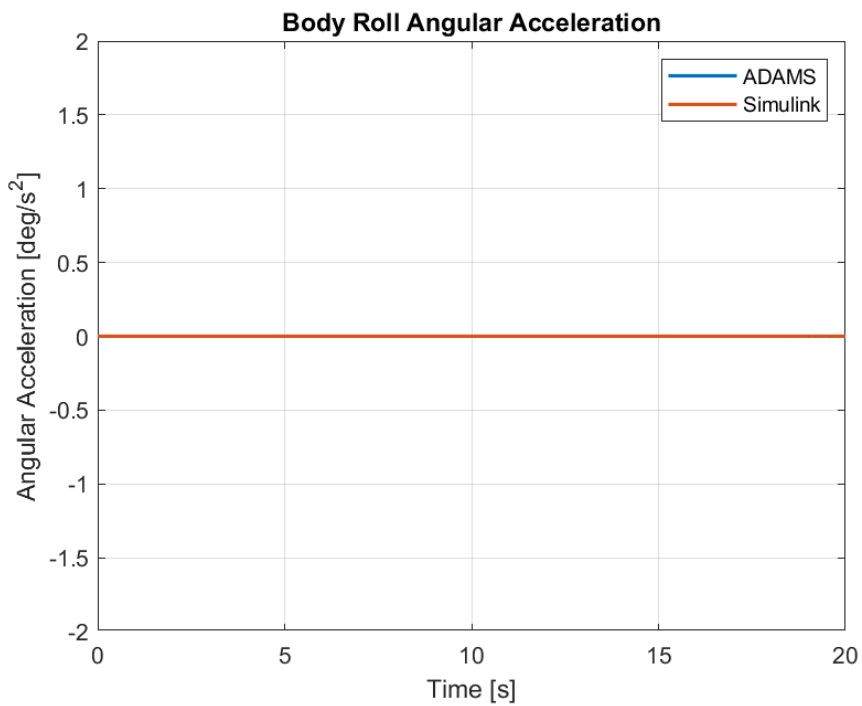


Figure 5-48. Plots of Roll Angular Acceleration of the Body for Case 3

Since the road profiles are the same for left and right tires and there is no steering motion, almost zero roll angle is produced in both models. Again, comparison table is not shared for roll angle as the values are in the powers of -10, they can be considered as errors in models with no result to the outcome.

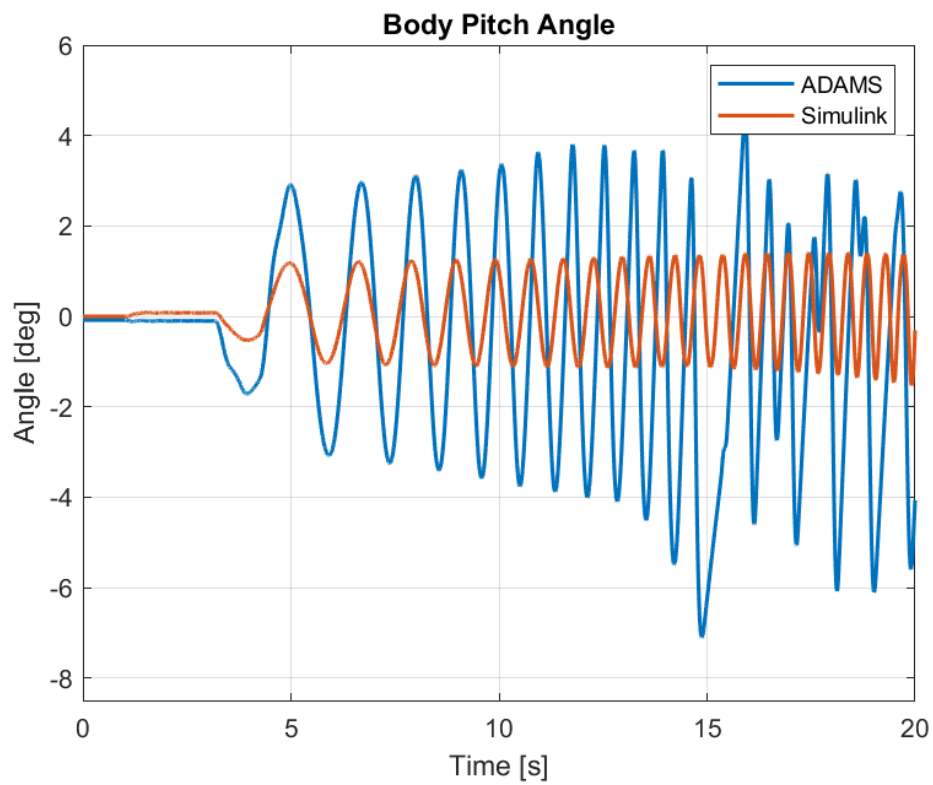


Figure 5-49. Plots of Pitch Angle of the Body for Case 3

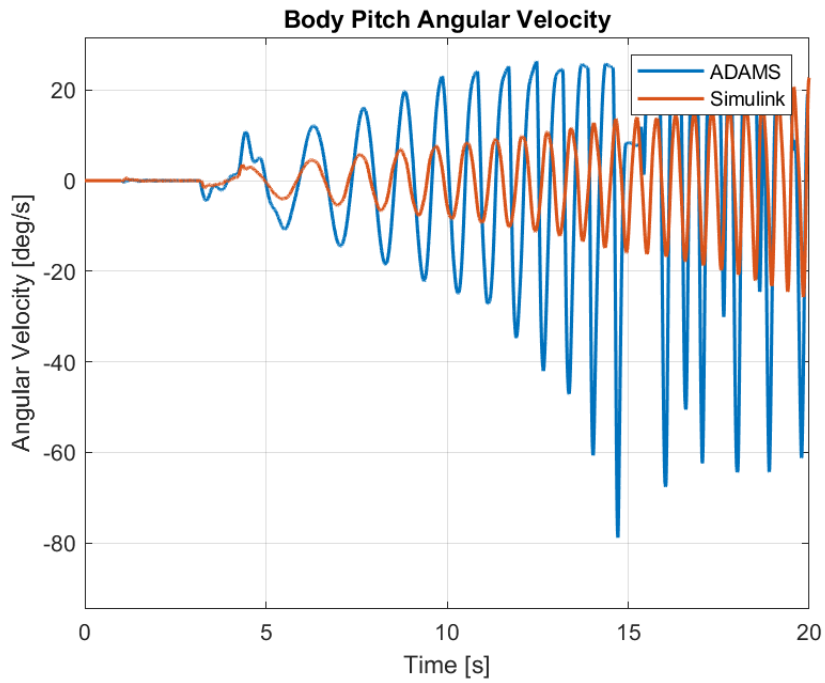


Figure 5-50. Plots of Pitch Angular Velocity of the Body for Case 3

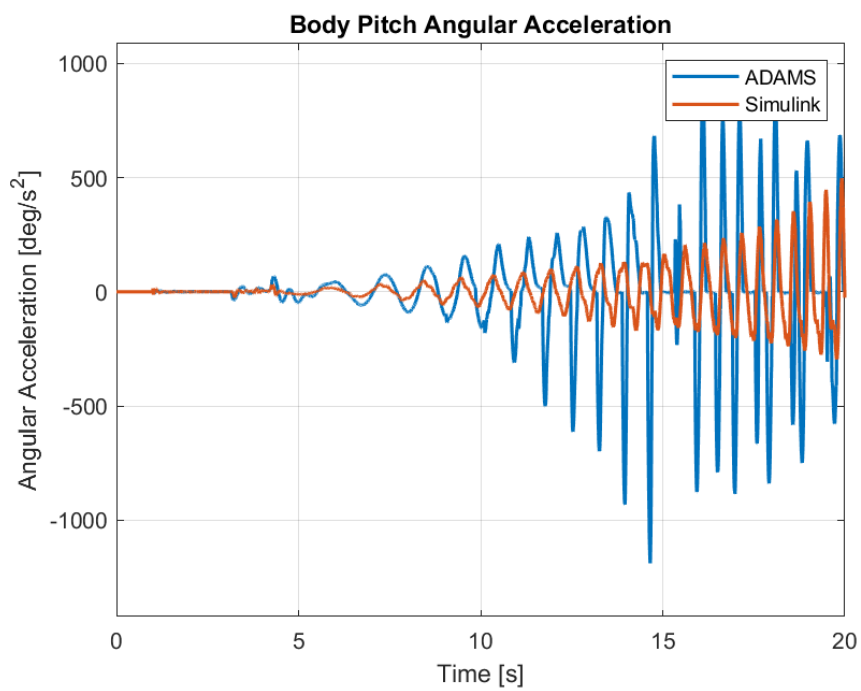


Figure 5-51. Plots of Pitch Angular Acceleration of the Body for Case 3

Due to the fact that road profile is modeled as a sine wave, the pitch angle produced in the models also represent a sinusoidal behavior. The amplitudes of the waves differ in the models but the frequencies remain the same as can be seen in figure x. The difference between the amplitudes are caused by the difference between the load distribution and the vertical forces produced in tires. As a result of different vertical forces, suspensions behave differently as well which will be illustrated in figure 5-57 and 5-58. The increasing oscillations are to be expected however, due to this system being an open loop one and the effect of the constant disturbances with increasing frequencies having a greater impact.

Table 5-14. Comparison of Pitch Motion of the Body for Case 3

Parameter	MSE	ADAMS Max	Simulink Max	ADAMS Min	Simulink Min	ADAMS Mean	Simulink Mean
Pitch Ang.	5.907	4.549	1.409	-7.103	-1.527	-0.5456	0.07949
Pitch Ang. Vel.	356.6	26.36	22.76	-78.82	-25.68	-0.1986	-0.01498
Pitch Ang. Acc.	54806.6	908.8	497.08	-1189.1	-297.2	0.9704	1.1441

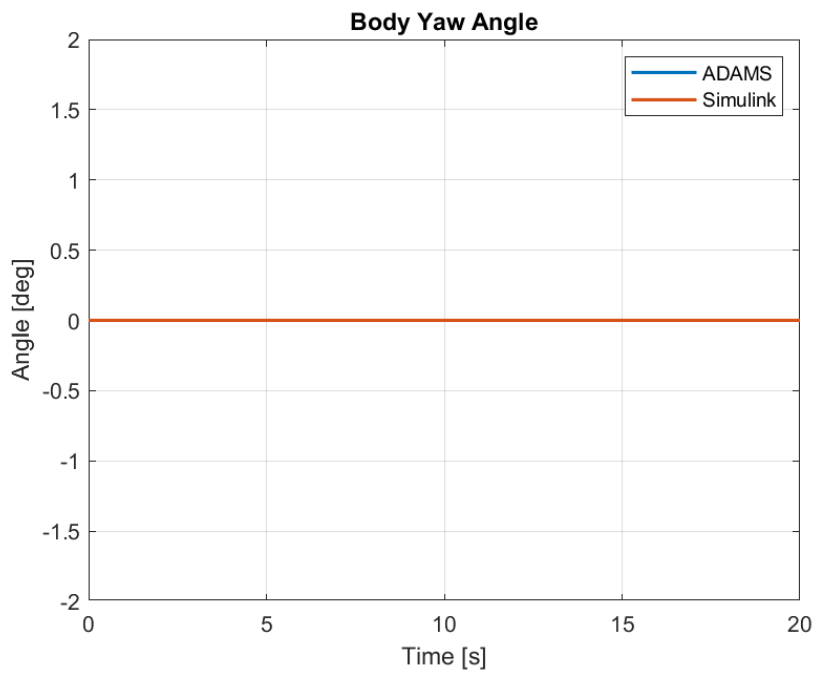


Figure 5-52. Plots of Yaw Angle of the Body for Case 3

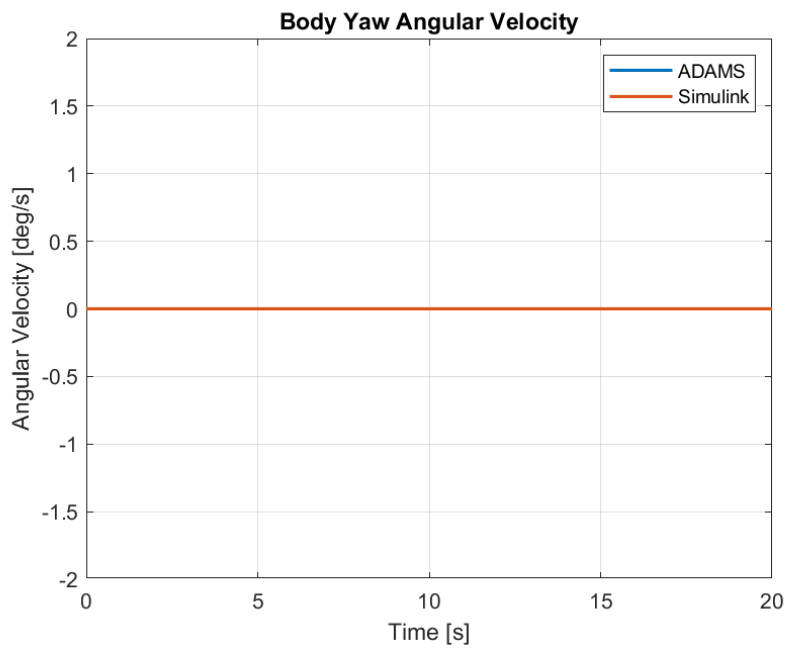


Figure 5-53. Plots of Yaw Angular Velocity of the Body for Case 3

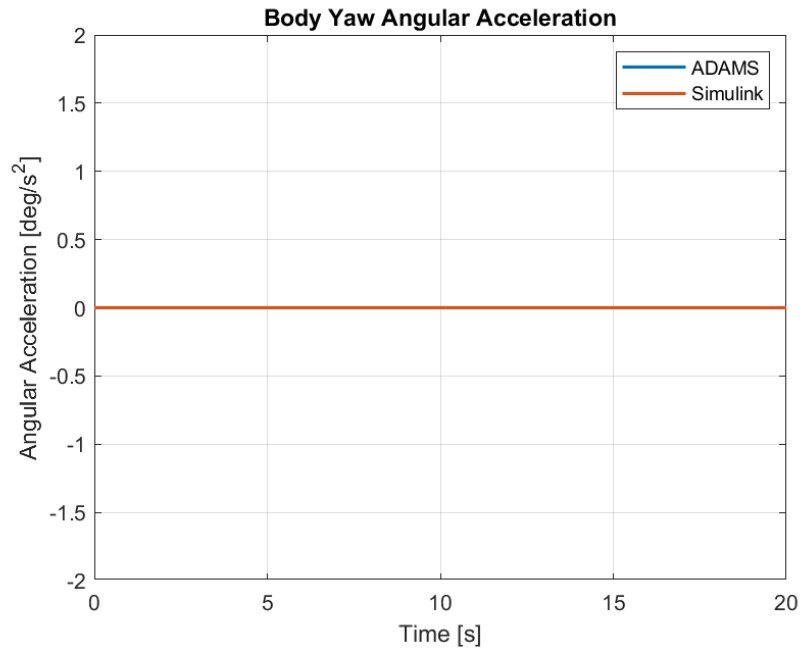


Figure 5-54. Plots of Yaw Angular Acceleration of the Body for Case 3

Similarly to lateral motions, no yaw angle is observed during the simulations.

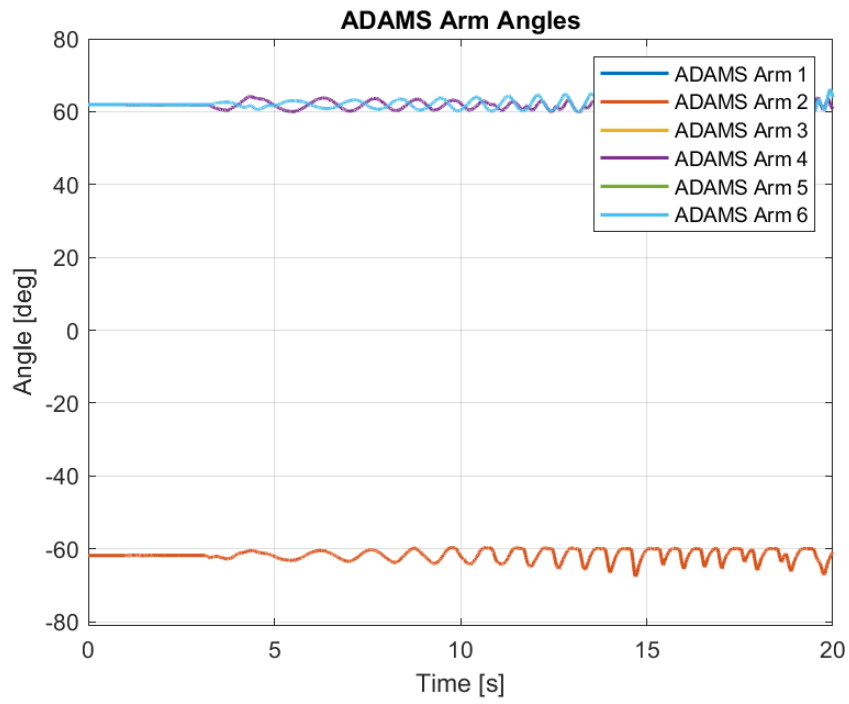


Figure 5-55. ADAMS Arm Angles for Case 3

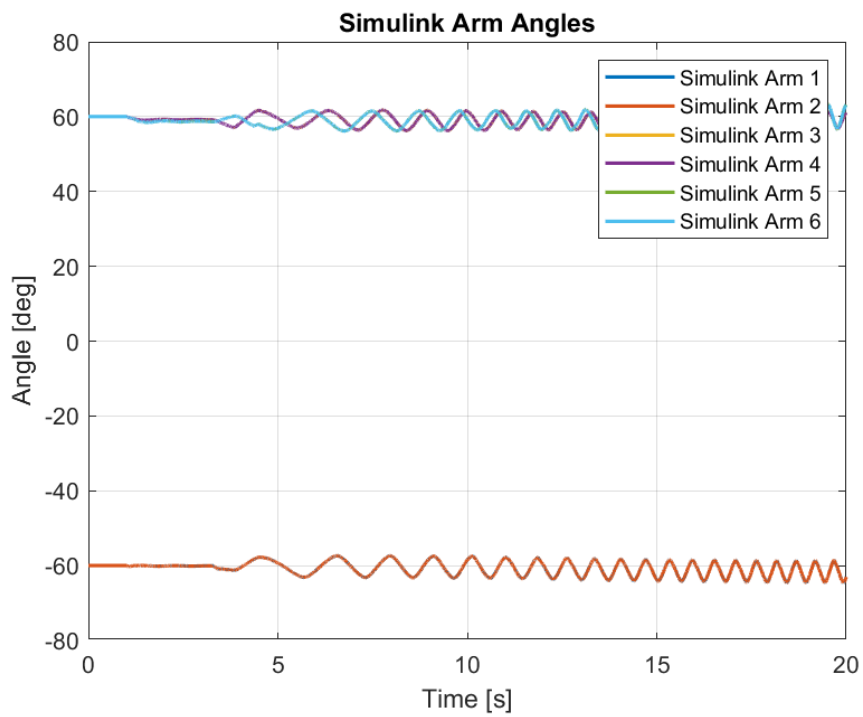


Figure 5-56. Simulink Arm Angles for Case 3

From figure 5-55 and 5-56, it can be seen that as the front arms interact with the bumps the angle they make with the vertical axis increase and they are further extended towards the front end of the vehicle. The middle and rear arm angles however, decrease at the same time. Then, as the middle and rear arms traverse the bump an opposite behavior is produced in each arm. The fact that front tires descend the bump as the middle and rear bumps start ascending results in a greater angle difference after the first bump.

The comparison table for both models considering the arm angles can be found below.

Table 5-15. Comparison of Arm Angles for Case 3

Parameters	MSE	ADAMS Max	Simulink Max	ADAMS Min	Simulink Min	ADAMS Mean	Simulink Mean
Arm Angle 1	8.979	-59.66	-57.35	-67.64	-64.57	-61.79	-60.69
Arm Angle 2	9.000	-59.66	-57.35	-67.64	-64.57	-61.79	-60.69
Arm Angle 3	8.904	65.86	61.78	59.20	56.23	61.52	59.06
Arm Angle 4	8.884	65.86	61.78	59.20	56.23	61.52	59.06
Arm Angle 5	14.75	66.21	63.24	59.91	56.16	61.97	59.12
Arm Angle 6	14.73	66.21	63.24	59.91	56.16	61.97	59.12

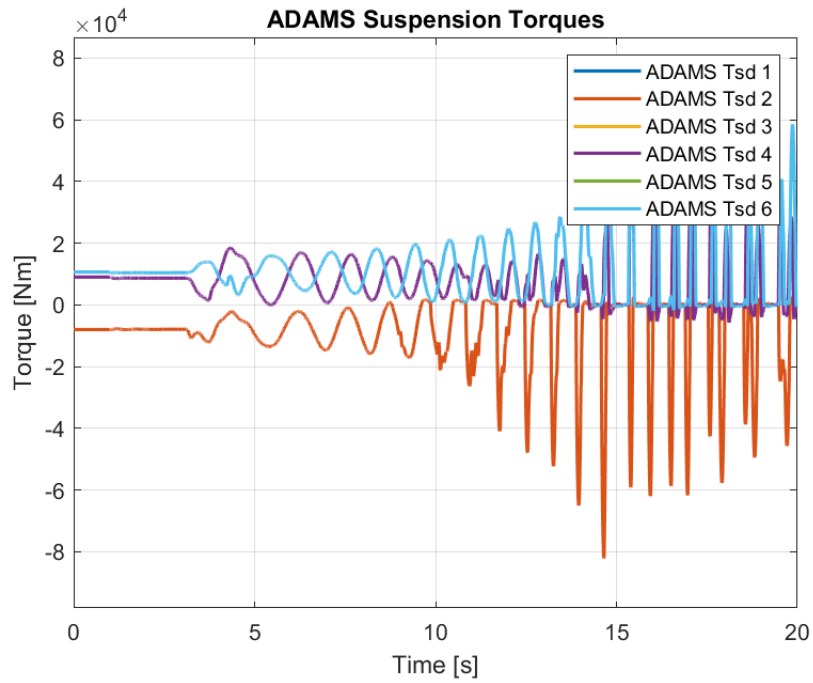


Figure 5-57. ADAMS Suspension Torques for Case 3

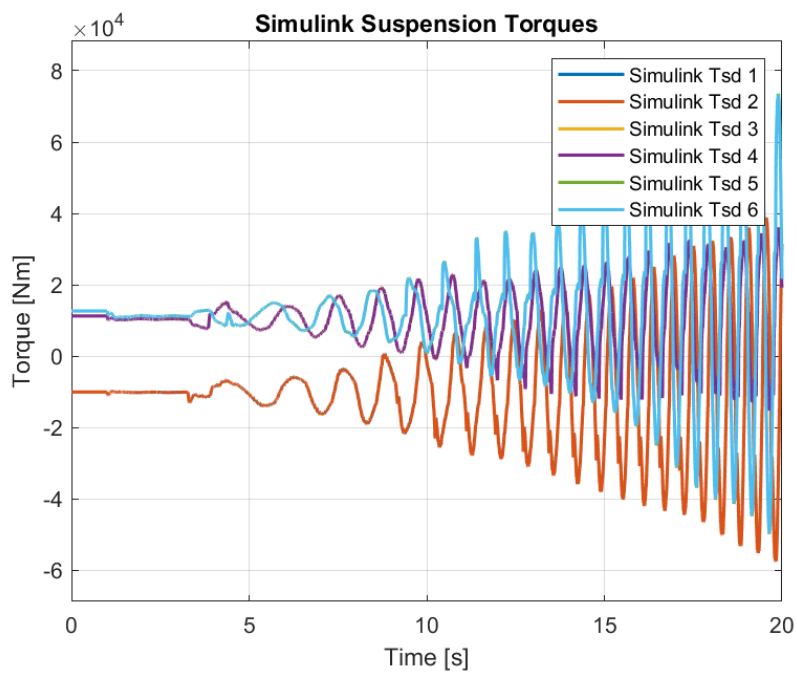


Figure 5-58. Simulink Suspension Torques for Case 3

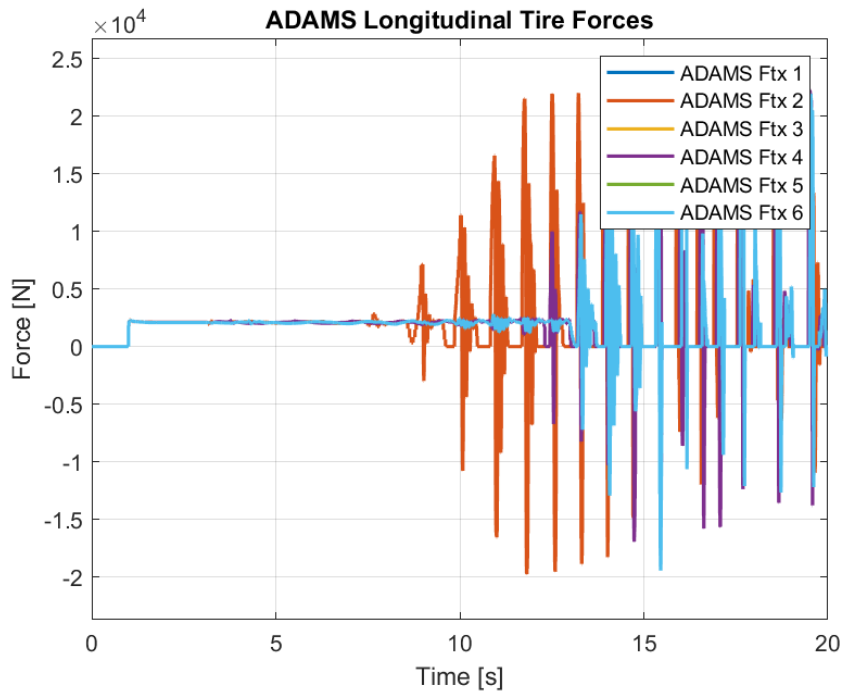


Figure 5-59. ADAMS Longitudinal Tire Forces for Case 3

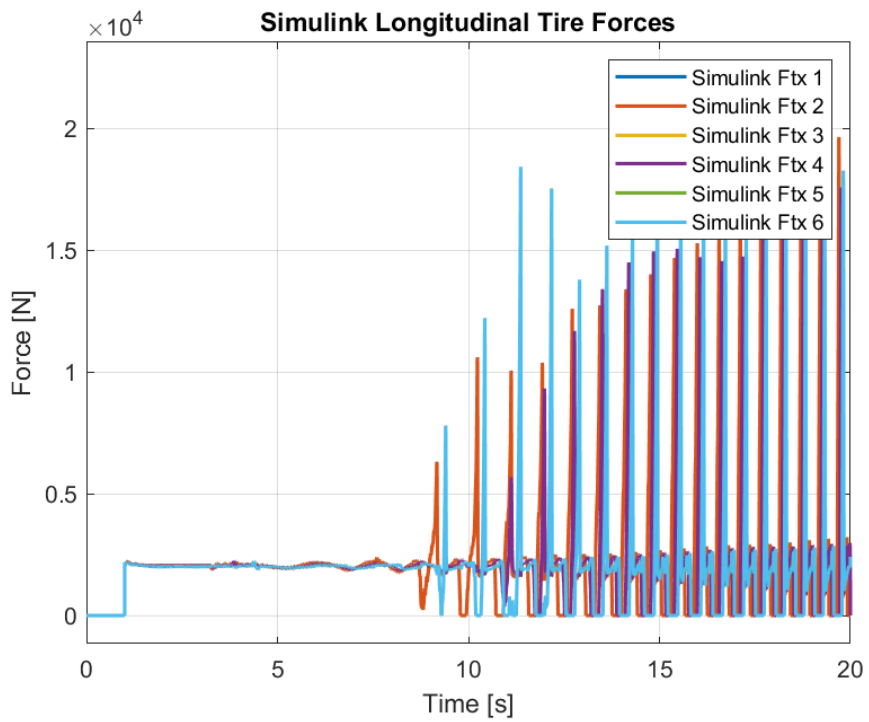


Figure 5-60. Simulink Longitudinal Tire Forces for Case 3

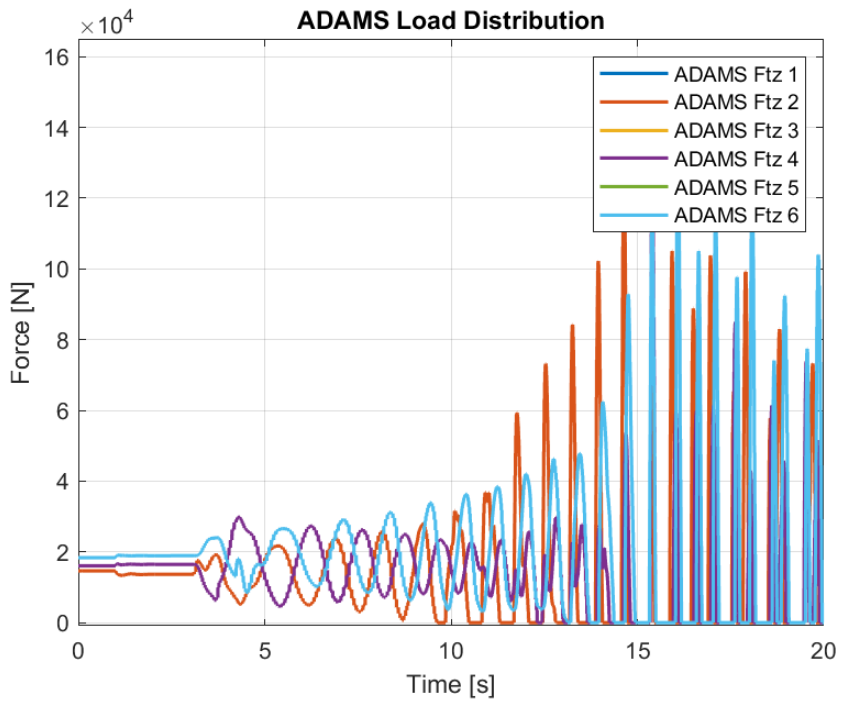


Figure 5-61. ADAMS Load Distribution for Case 3

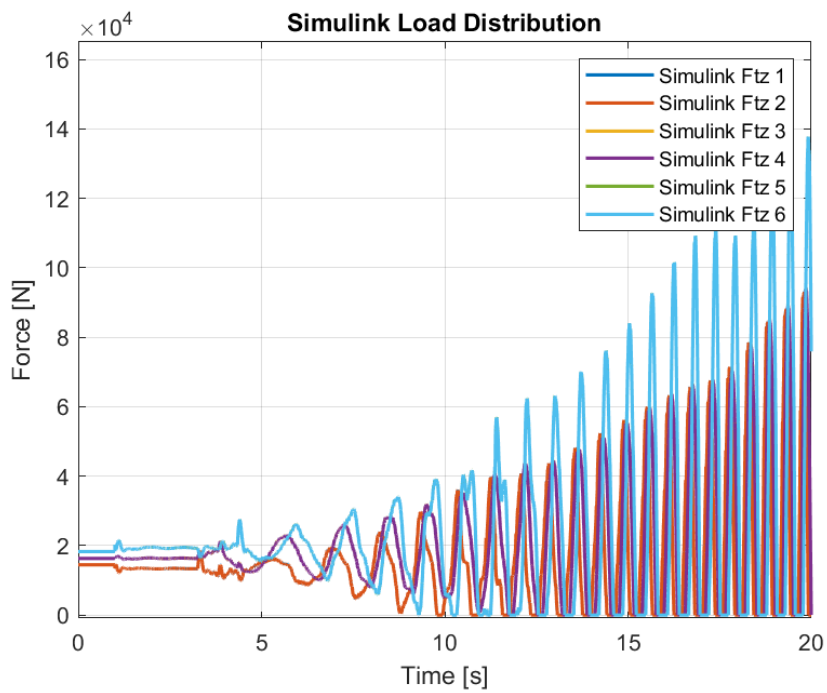


Figure 5-62. Simulink Load Distribution for Case 3

The load distribution behaves similarly in both models at the start of the simulation. However, as the vehicle starts interacting with the irregularities, oscillations with high amplitudes occur. This is expected as vehicle constantly runs into bumps while accelerating. In both models, the load distribution at front, middle and rear tires reach zero occasionally near the end of the simulation which means that for a road with irregularities as modeled in this study, the tires start losing contact with the ground while traversing this road profile.

5.4 Case 4 – Road with a Gradient Angle of 15°

For the fourth case, a road profile with a constant gradient is supplied to the models. The road profile is modeled according to the APG test track with 15° gradient which correspond to 26.79% gradient. The ramp profile is constructed in order to better test the performance of the vehicle. Different torque inputs are tested for this case. However, as the vehicle cannot climb the ramp with low torque levels, a constant torque of 6000 Nm is given as inputs to each wheel. The road profile as constructed in ADAMS software can be seen in figure 5-63. The ramp starts 5 meters ahead of the vehicle center of gravity so that it can gain traction before starting ascending.

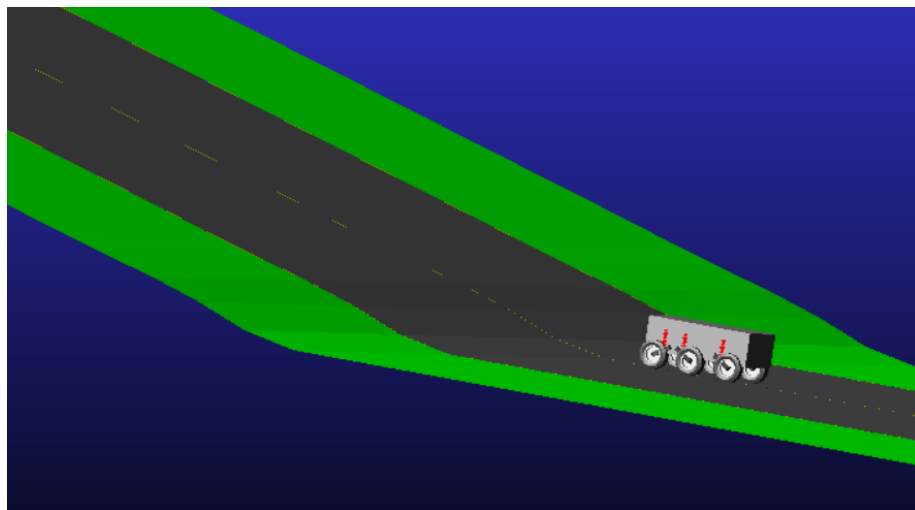


Figure 5-63. Ramp Road Profile in ADAMS

Firstly, the longitudinal motion of the body is to be examined as the performance is vital for this case.

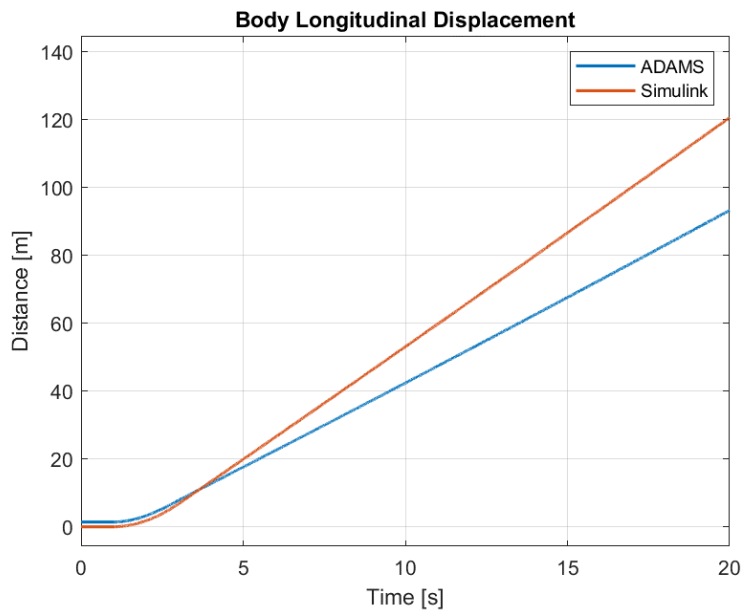


Figure 5-64. Plots of Longitudinal Displacement of the Body for Case 4

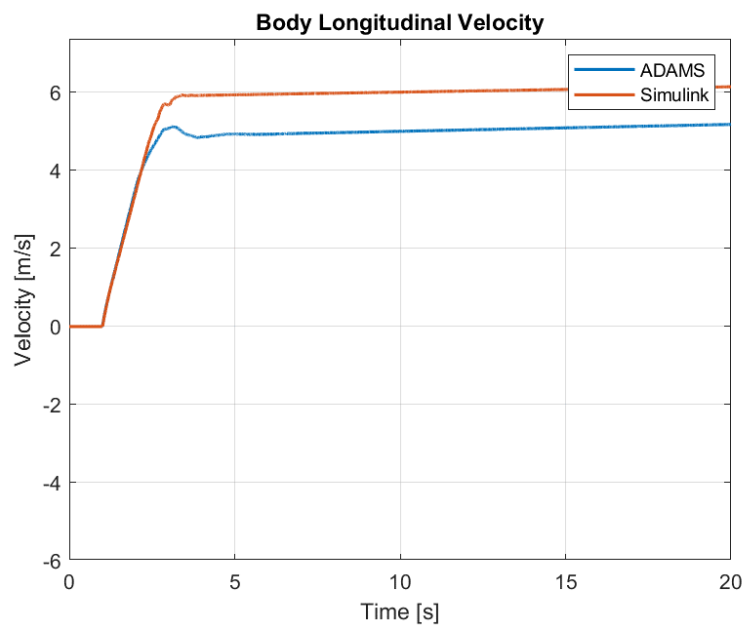


Figure 5-65. Plots of Longitudinal Velocity of the Body for Case 4

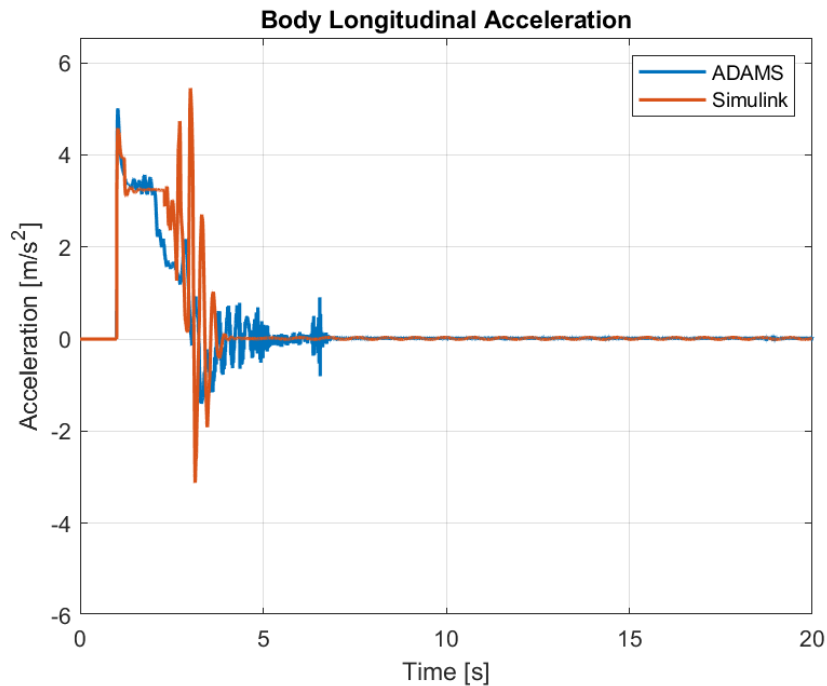


Figure 5-66. Plots of Longitudinal Acceleration of the Body for Case 4

From the figures depicting the longitudinal position, velocity and acceleration of the vehicle body, it can be seen that the vehicle gains traction until it encounters the ramp profile. Afterwards, the gradient resistance takes hold. For the Simulink, the constant torque of 6000 Nm supplied to the wheels is just enough to overcome the resistance and results in the acceleration to reach almost zero but has a positive value. This results in a slow increase in longitudinal velocity. If lower torques were to be supplied, it could be seen that the vehicle would eventually succumb to the resistances and start descending. The differences are again observed to be caused by the load distribution and tire models in softwares which will be explained more thoroughly in the following pages. However, due to these differences, different traction forces are produced in tires.

Table 5-16. Comparison of Translational Motion Along the Longitudinal Axis between Models for Case 5

Parameter	MSE	ADAMS Max	Simulink Max	ADAMS Min	Simulink Min	ADAMS Mean	Simulink Mean
Long. Disp.	205.1	93.28	120.6	1.416	-4.5E-17	43.05	54.04
Long. Vel.	0.8464	5.178	6.142	0	-9.5E-17	4.593	5.450
Long. Acc.	0.3465	5.014	5.452	-1.405	-3.123	0.2695	0.3341

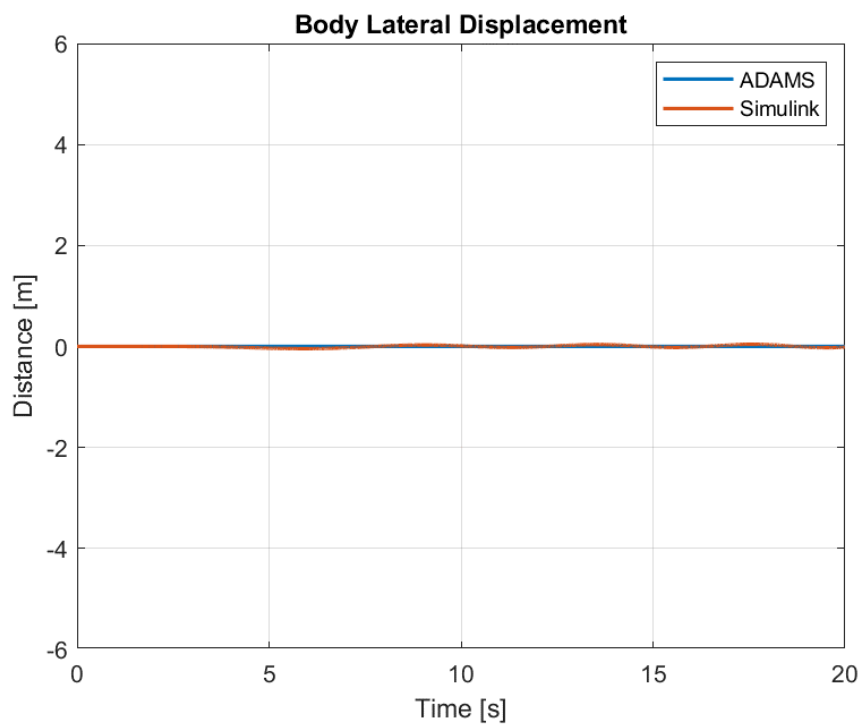


Figure 5-67. Plots of Lateral Displacement of the Body for Case 4

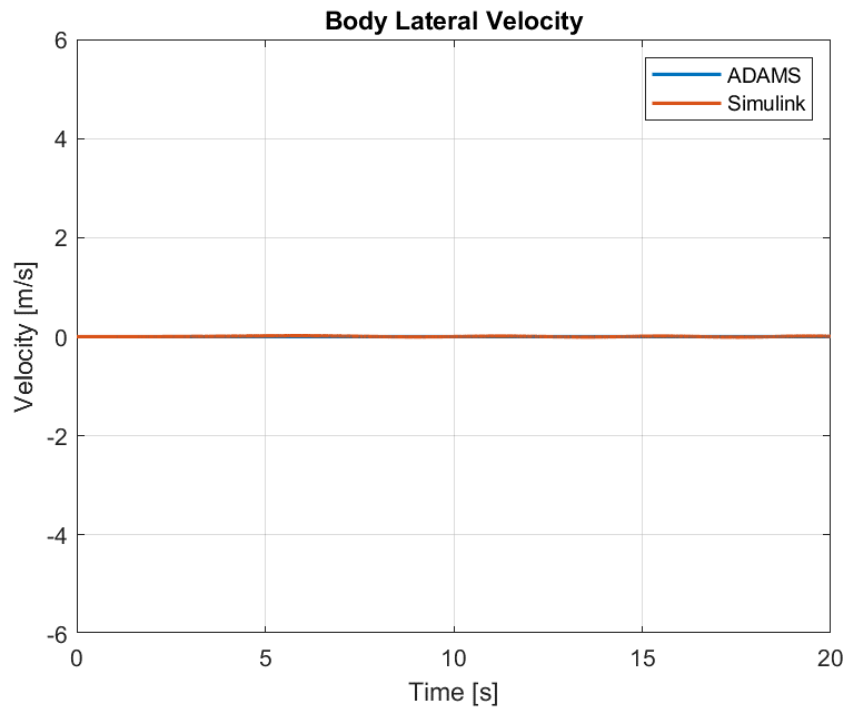


Figure 5-68. Plots of Lateral Velocity of the Body for Case 4

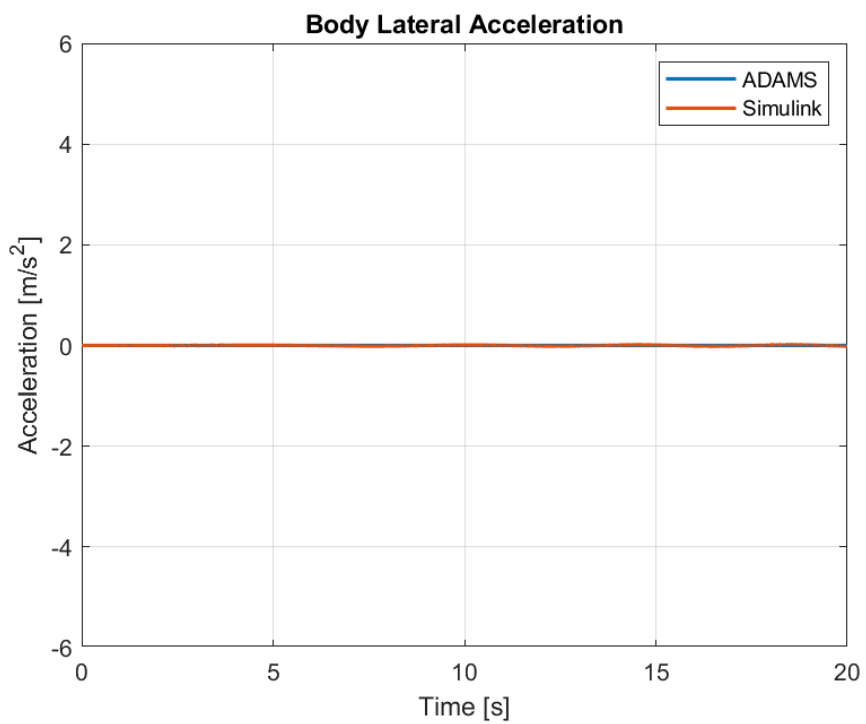


Figure 5-69. Plots of Lateral Acceleration of the Body for Case 4

Again almost zero motion along the lateral axis is produced for this case although some fluctuations can be seen from the plots. This can be considered as an error of the models constructed. Although disturbances are present because of the road profile, the left and rear tires should encounter the same disturbances at the same time.

Table 5-17. Comparison of Translational Motion Along the Lateral Axis between Models for Case 5

Parameter	MSE	ADAMS Max	Simulink Max	ADAMS Min	Simulink Min	ADAMS Mean	Simulink Mean
Lat. Disp.	5.0E-4	6.55E-14	0.04458	-1.8E-7	-0.04272	-6.5E-9	-3.56E-4
Lat. Vel.	8.6E-5	5.1E-12	0.02005	-2.6E-7	-0.00849	-9.0E-9	0.005448
Lat. Acc.	7.3E-5	1.5E-08	0.03946	-4.2E-7	-0.01808	-1.3E-8	0.000273

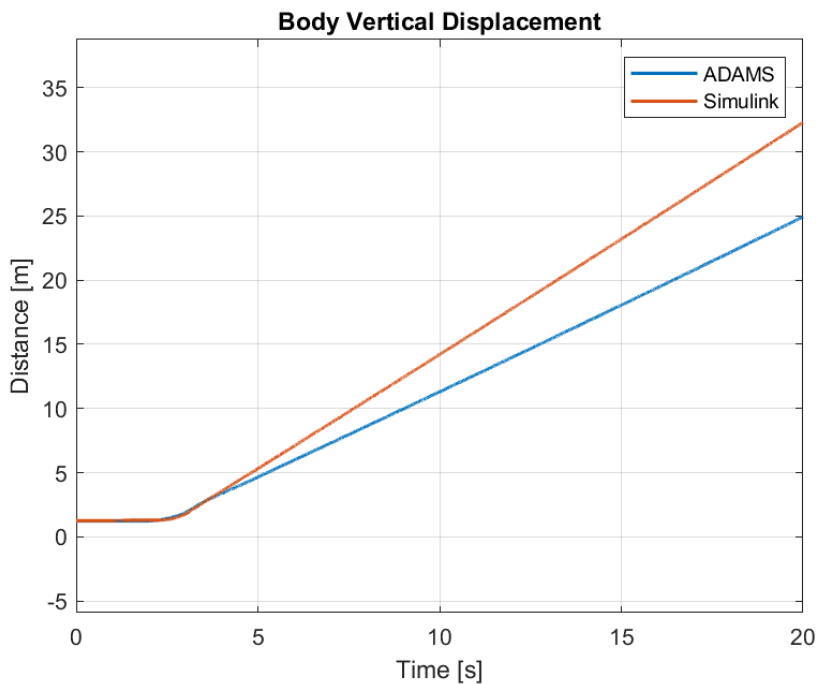


Figure 5-70. Plots of Vertical Displacement of the Body for Case 4

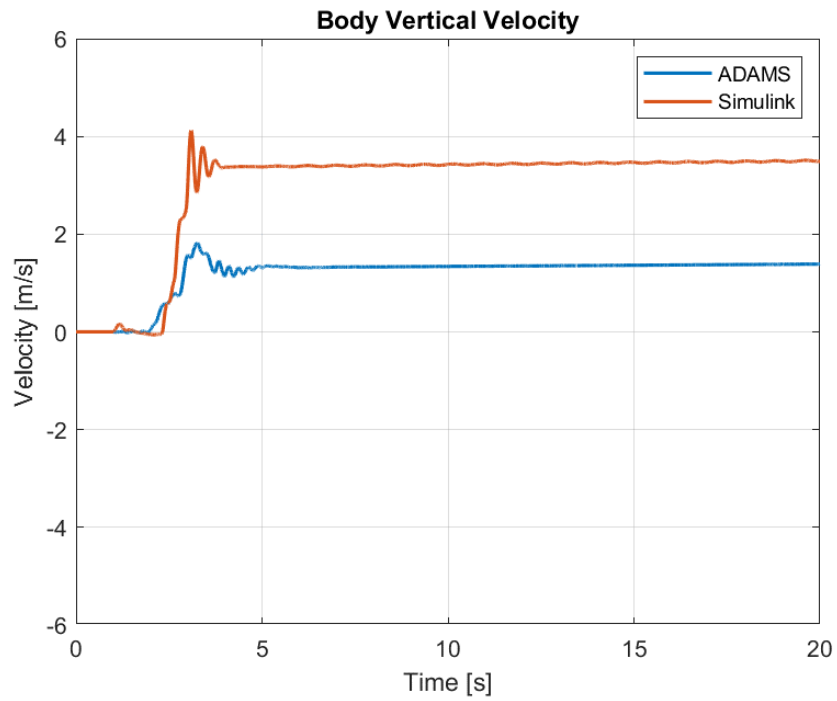


Figure 5-71. Plots of Vertical Velocity of the Body for Case 4

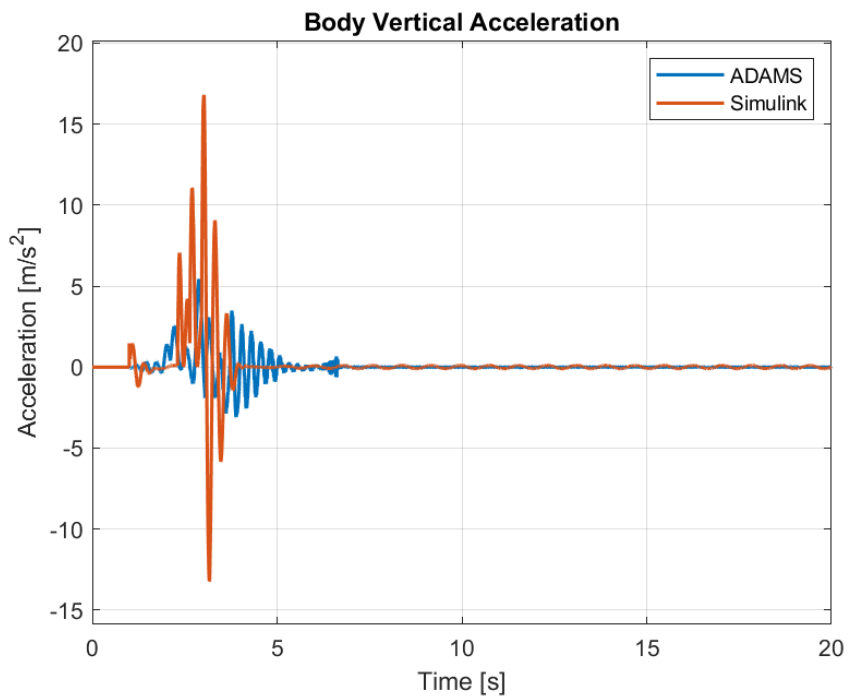


Figure 5-72. Plots of Vertical Acceleration of the Body for Case 4

Similar results are present for the vertical motion as the longitudinal motion. Because of the resistances, the vehicle start climbing the gradient more slowly. However, again a strong fluctuation is present in ADAMS. The reason is the same as explained while reviewing the longitudinal motion of the vehicle for this case which is the differences between the tire and ground interaction between the models. The vehicle is observed to be climbing 24.93 meters in the vertical direction in ADAMS and 32.29 meters in Simulink while covering a distance of 93.28 meters and 120.6 meters in ADAMS and Simulink, respectively. This means that the gradient calculated from the distance covered are 26.73% in Simulink and 26.77% in ADAMS, while the road profile supplied has a gradient of 26.79%. Due to the fact that the vehicle starts at a flat road at first, this is expected.

Table 5-18. Comparison of Translational Motion Along the Vertical Axis between Models for Case 4

Parameter	MSE	ADAMS Max	Simulink Max	ADAMS Min	Simulink Min	ADAMS Mean	Simulink Mean
Vert. Disp.	14.94	24.93	32.29	1.232	1.252	11.56	14.59
Vert. Vel.	3.719	1.821	4.122	-0.0153	-0.0573	1.185	2.970
Vert. Acc.	3.865	5.444	16.80	-3.101	-13.24	0.05913	0.1618

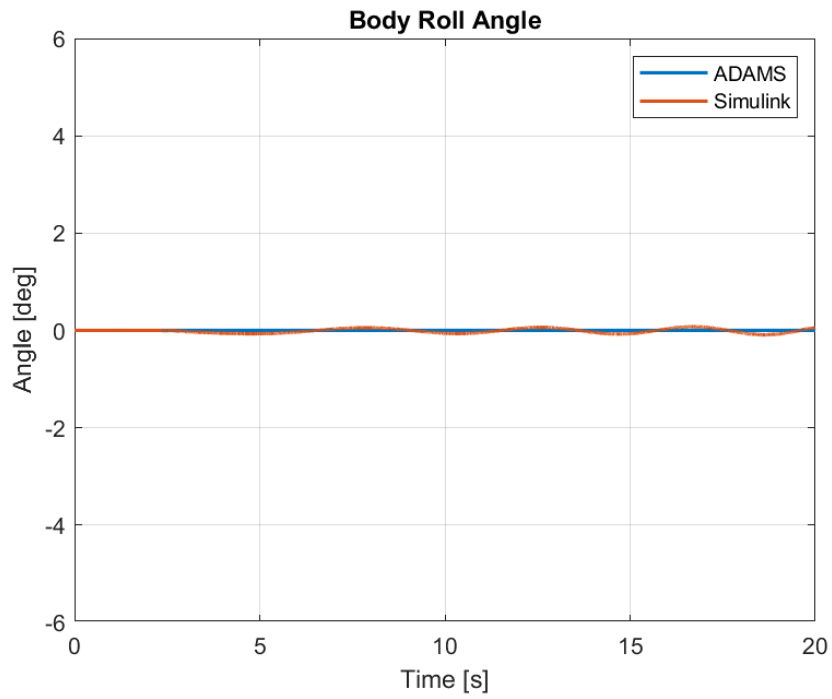


Figure 5-73. Plots of Roll Angle of the Body for Case 4

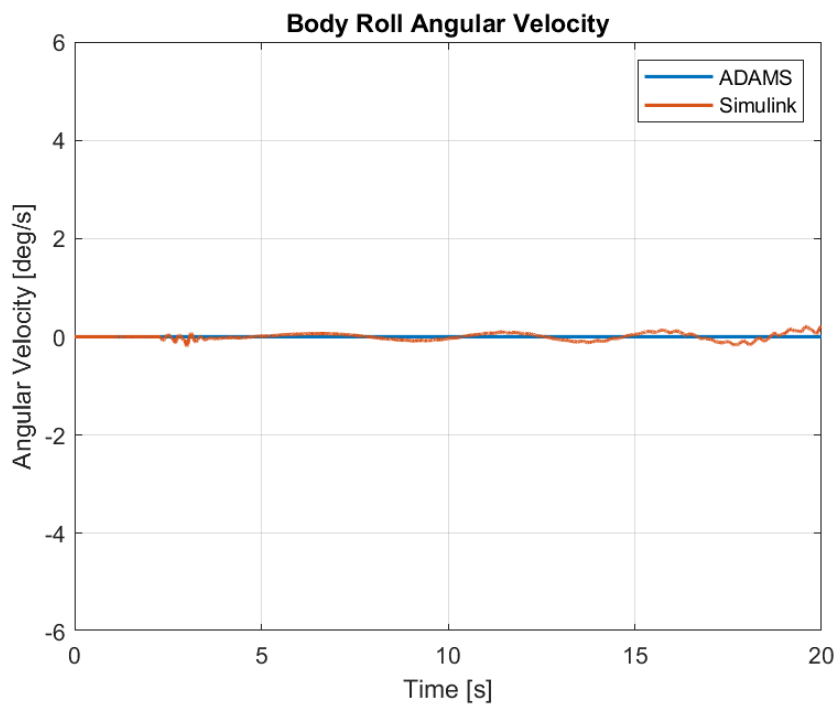


Figure 5-74. Plots of Roll Angular Velocity of the Body for Case 4

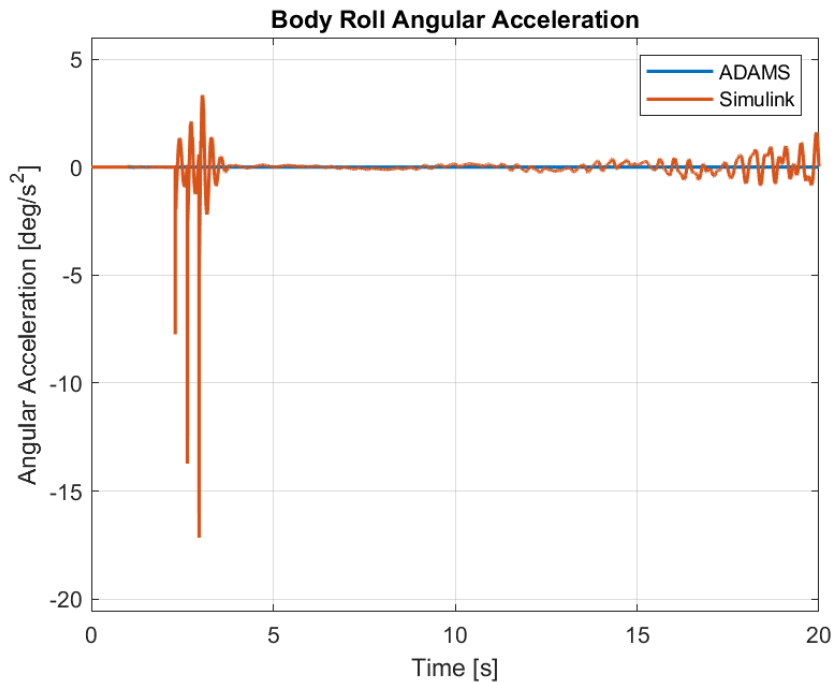


Figure 5-75. Plots of Roll Angular Acceleration of the Body for Case 4

For this case, no roll angle is expected as disturbance is expected as the left and right tires pass through the bumps at the same time. However, although damped quickly and the effect in the angular position and velocity is low, a strong oscillation in roll angular acceleration is present in Simulink. As the tire positions are found by integration and the model constructed is difficult for computers to handle, some errors can occur and the tires can interact with the bumps after a short delay. Again, the effects are damped quickly by the suspension systems.

Table 5-19. Comparison of Rotational Motion Along the Roll Axis between Models for Case 4

Parameter	MSE	ADAMS Max	Simulink Max	ADAMS Min	Simulink Min	ADAMS Mean	Simulink Mean
Roll Ang.	0.002097	4.4E-12	0.07772	-4.9E-07	-0.09158	-1.5E-08	-0.00993
Roll Ang. Vel.	0.004636	2.0E-06	0.2103	-1.6E-10	-0.1834	6.23E-08	0.002939
Roll Ang. Acc.	0.1958	1.9E-05	3.331	-4.2E-05	-17.15	9.08E-08	0.01041

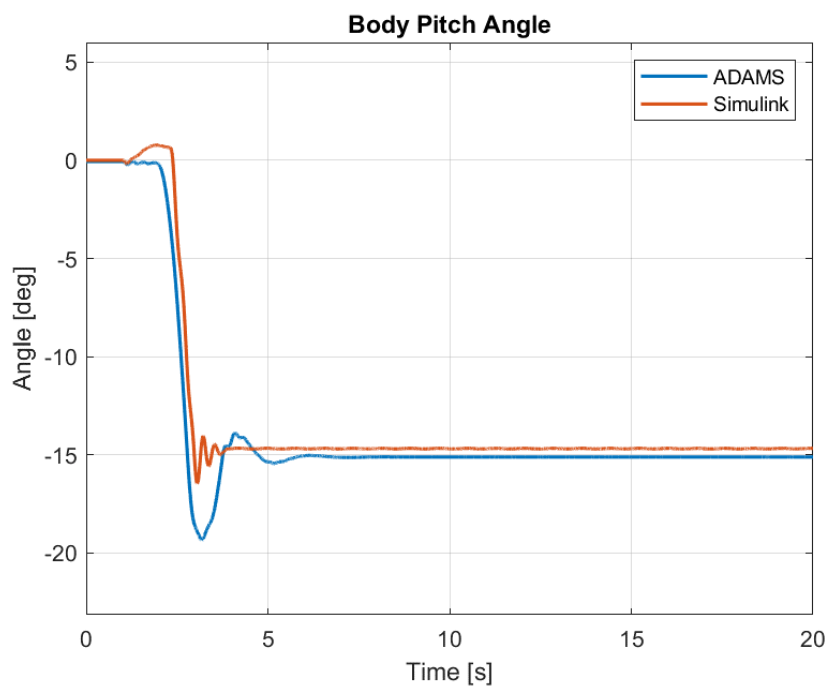


Figure 5-76. Plots of Pitch Angle of the Body for Case 4

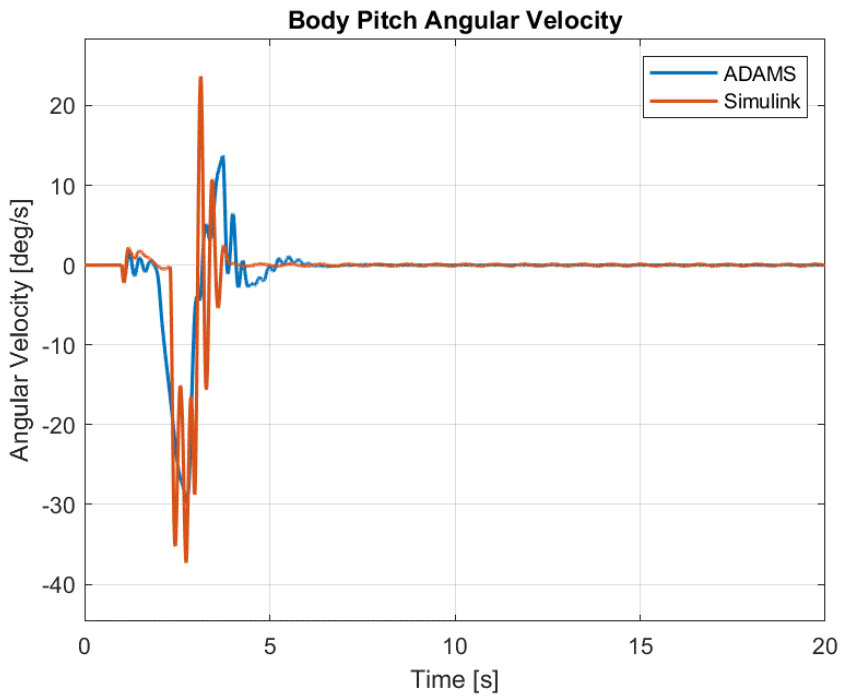


Figure 5-77. Plots of Pitch Angular Velocity of the Body for Case 4

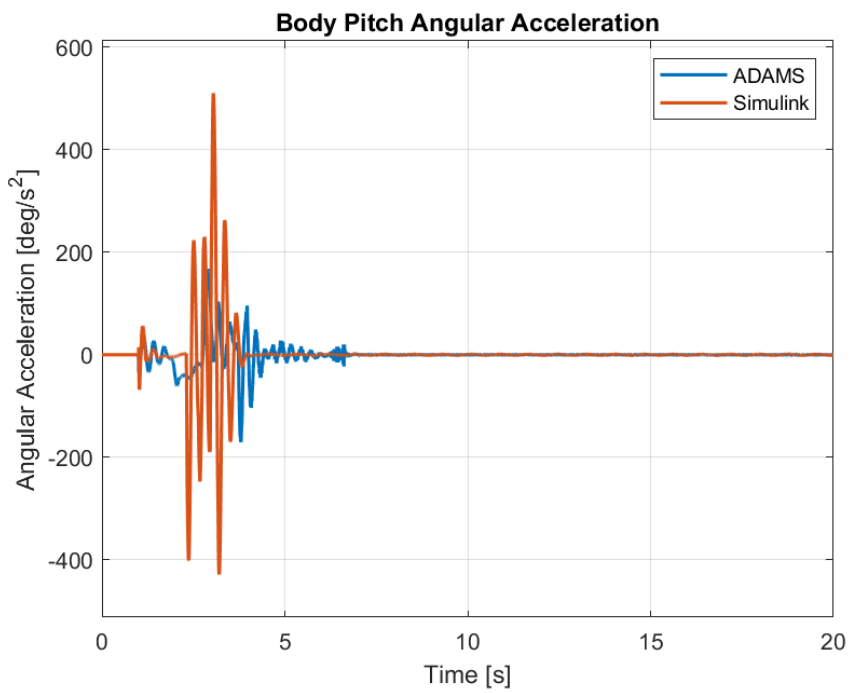


Figure 5-78. Plots of Pitch Angular Acceleration of the Body for Case 4

As that vehicle starts going up the ramp, a pitch angle is introduced to the system. After the rear tires encounter the ramp as well, the pitch angle remains constant. For both Simulink and ADAMS, the angular position is settled at almost 15 degrees after the vehicle completely enters the ramp, which is expected due to the fact that the road profile has a constant 15 degrees gradient. The oscillations which occur in Simulink for acceleration is again much greater than ADAMS. This is caused by the differences in load distribution and its effects on the suspension system.

Table 5-20. Comparison of Rotational Motion Along the Pitch Axis between Models for Case 4

Parameter	MSE	ADAMS Max	Simulink Max	ADAMS Min	Simulink Min	ADAMS Mean	Simulink Mean
Pitch Ang.	1.268	-0.05984	0.7697	-19.33	-16.47	-13.36	-12.72
Pitch Ang. Vel.	13.05	13.70	23.66	-29.73	-37.31	-0.7522	-0.7336
Pitch Ang. Acc.	3969.7	167.6	510.09	-170.6	-428.2	0.0005103	-0.002793

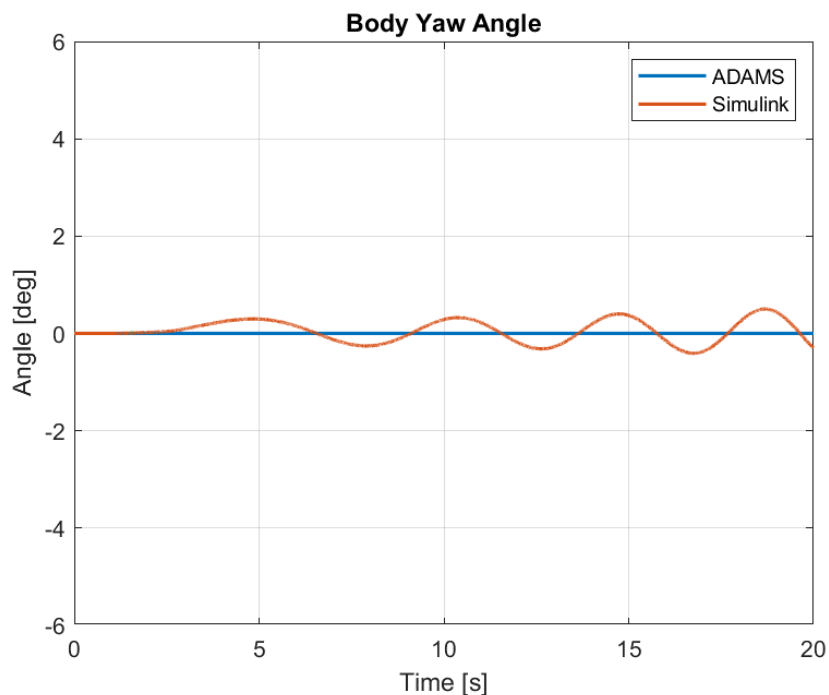


Figure 5-79. Plots of Yaw Angle of the Body for Case 4

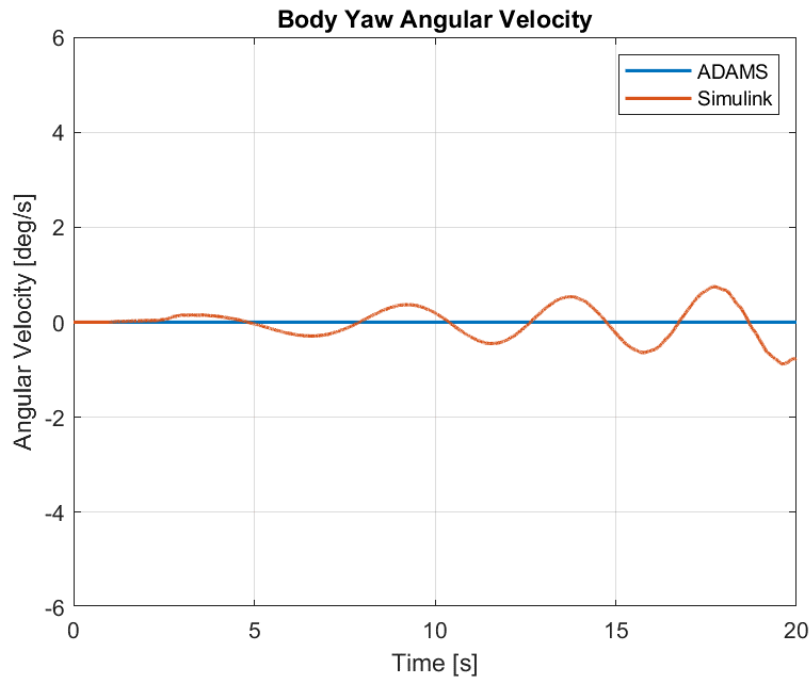


Figure 5-80. Plots of Yaw Angular Velocity of the Body for Case 4

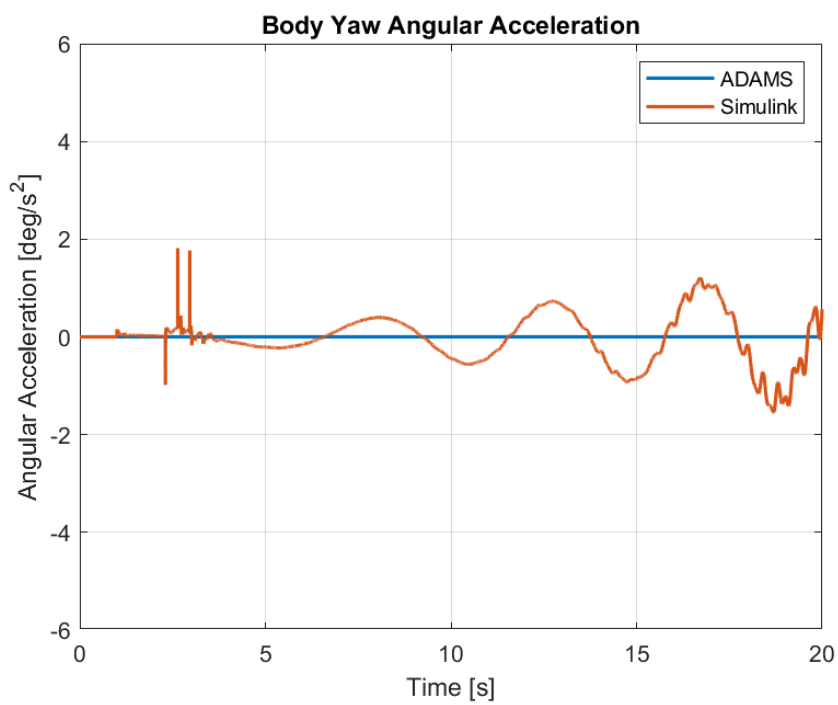


Figure 5-81. Plots of Yaw Angular Acceleration of the Body for Case 4

Similar to the roll angle, a deviation occurs in Simulink for yaw angle as well. This could be interpreted from the plots before as a lateral motion was present for the vehicle. However, again this is mostly caused by the error in calculation of the tire positions since the disturbances should effect the left and rear tires in the same manner.

Table 5-21. Comparison of Rotational Motion Along the Yaw Axis between Models for Case 4

Parameter	MSE	ADAMS Max	Simulink Max	ADAMS Min	Simulink Min	ADAMS Mean	Simulink Mean
Yaw Ang.	0.05394	-1.8E-11	0.5029	-6.8E-06	-0.4080	-2.2E-07	0.05354
Yaw Ang. Vel.	0.1179	7.2E-11	0.7483	-9.8E-06	-0.8799	-3.1E-07	-0.01492
Yaw Ang. Acc.	0.2515	1.0E-06	1.817	-2.3E-05	-1.5493	-4.9E-07	-0.03797

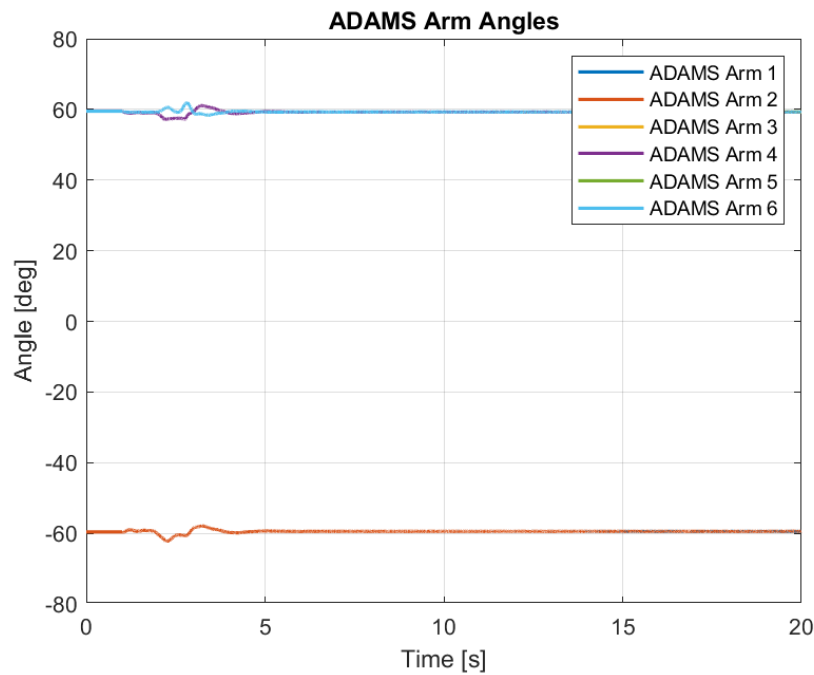


Figure 5-82. ADAMS Arm Angles for Case 4

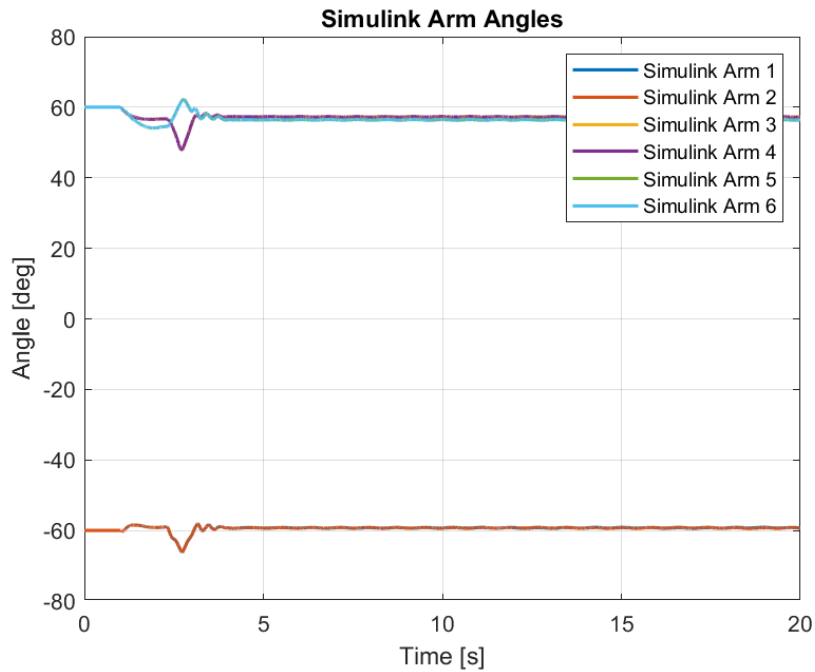


Figure 5-83. Simulink Arm Angles for Case 4

Similar to the previous cases, when the front arms first enter the ramp, they are extended and conversely, the middle and rear tires close up. However, after the vehicle completely enters the ramp profile, the suspensions are able to hold the arms in their original position. The amplitude of disturbance in Simulink is higher compared to the ADAMS model. The comparison of the results obtained can be found in the table below.

Table 5-22. Comparison of Arm Angles between Models for Case 4

Parameters	MSE	ADAMS Max	Simulink Max	ADAMS Min	Simulink Min	ADAMS Mean	Simulink Mean
Arm Angle 1	1.188	-59.96	-58.08	-60.30	-66.08	-60.14	-59.40
Arm Angle 2	1.179	-59.96	-58.09	-60.30	-66.11	-60.14	-59.40
Arm Angle 3	10.01	60.37	60	59.95	47.86	60.14	57.23
Arm Angle 4	9.927	60.37	60	59.95	47.87	60.14	57.24
Arm Angle 5	13.54	60.37	62.23	60.06	54.09	60.19	56.69
Arm Angle 6	13.45	60.37	62.22	60.06	54.09	60.19	56.70

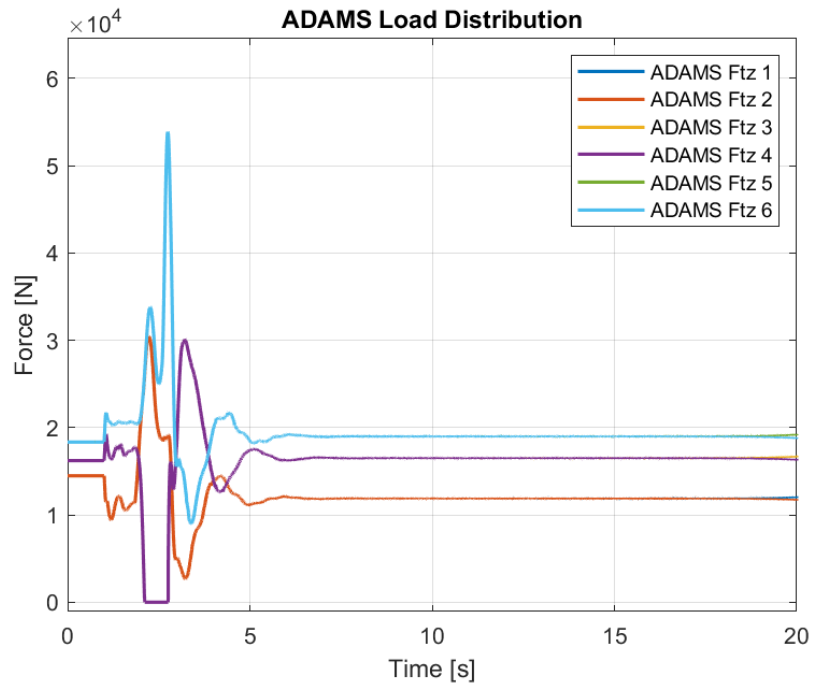


Figure 5-84. ADAMS Load Distribution for Case 4

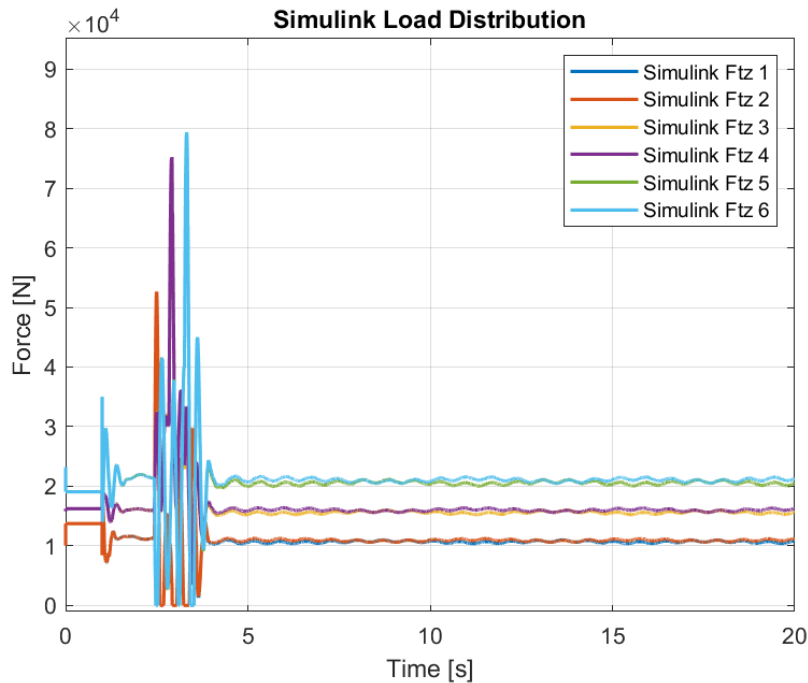


Figure 5-85. Simulink Load Distribution for Case 4

As mentioned before, the load distribution in models behave differently. Since the ADAMS model calculates the vertical forces in tires through its internal finite element calculations and the load distribution algorithm constructed in Simulink use approximation through the motion of the body, deviations are present. In ADAMS, the tire forces are distributed the same as it was in flat road but in Simulink, most of the load is acting on the rear tires once the vehicle reaches the ramp profile. This is the main cause of errors. The front and middle tires in Simulink cannot produce enough traction in this case to completely overcome the resistance.

Although mean values of the load distribution are close between the softwares, as the jumps are high in magnitude and occur at different times, the mean square error in this case is not calculated since its value is too high to be meaningful. This is also due to the fact that the magnitude of the forces considered are in the powers of four. However, in ADAMS the middle tires can be seen to lose contact with the road while in Simulink, the front and rear tires give zero values. This is also an error of the load distribution model constructed in Simulink.

Table 5-23. Comparison of Load Distribution between Models for Case 4

Parameters	ADAMS Max	Simulink Max	ADAMS Min	Simulink Min	ADAMS Mean	Simulink Mean
Load Dist. 1	28941.2	58017.2	0	0	12614.3	11908.7
Load Dist. 2	28941.2	58007.5	0	0	12614.3	11847.7
Load Dist. 3	41396.1	77503.0	0	0	15608.9	16716.0
Load Dist. 4	41396.1	77453.1	0	0	15608.9	16625.9
Load Dist. 5	55433.8	102892.7	1962.3	0	19662.7	20400.1
Load Dist. 6	55433.8	102838.4	1962.3	0	19662.7	20293.0

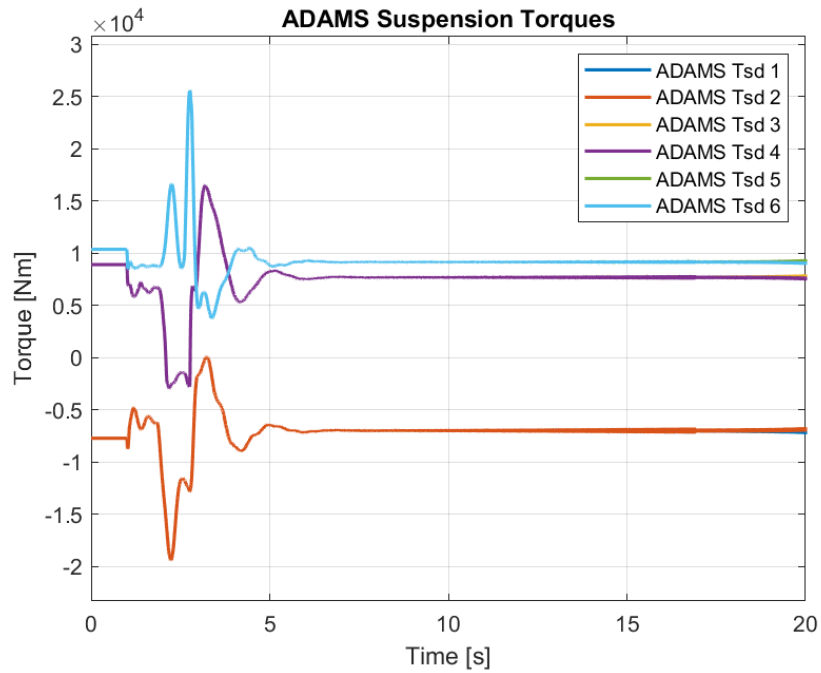


Figure 5-86. ADAMS Suspension Torques for Case 4

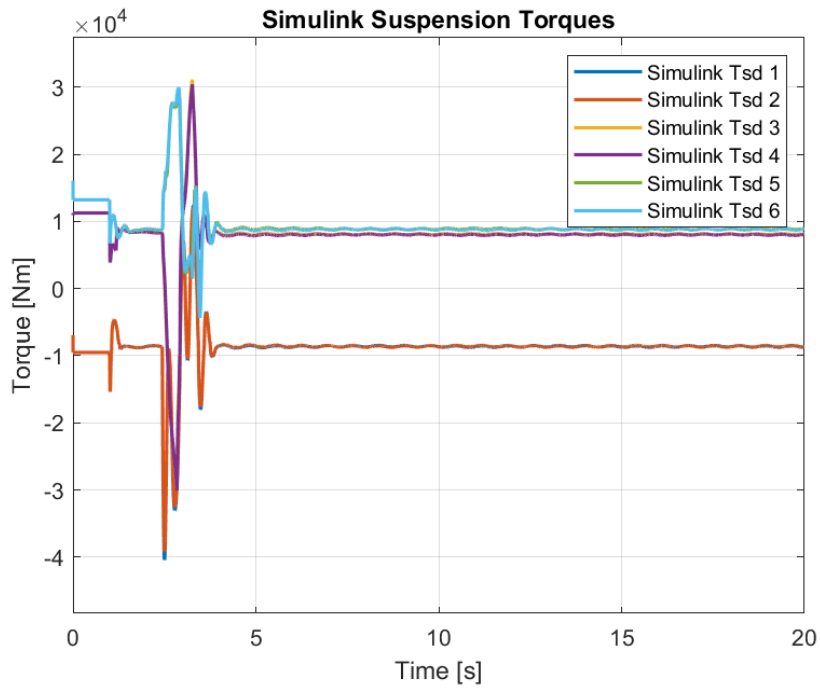


Figure 5-87. Simulink Suspension Torques for Case 4

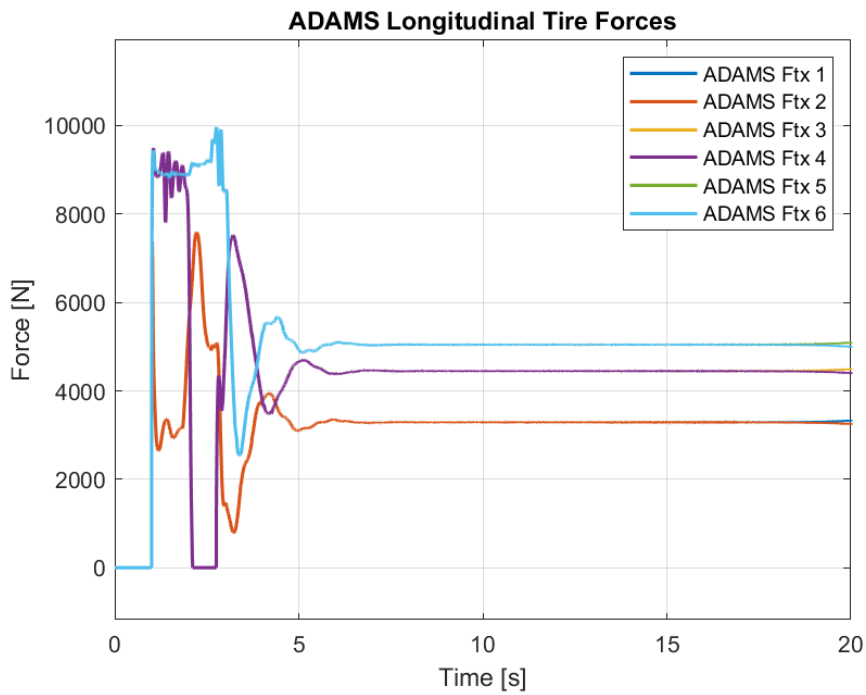


Figure 5-88. ADAMS Longitudinal Tire Forces for Case 4

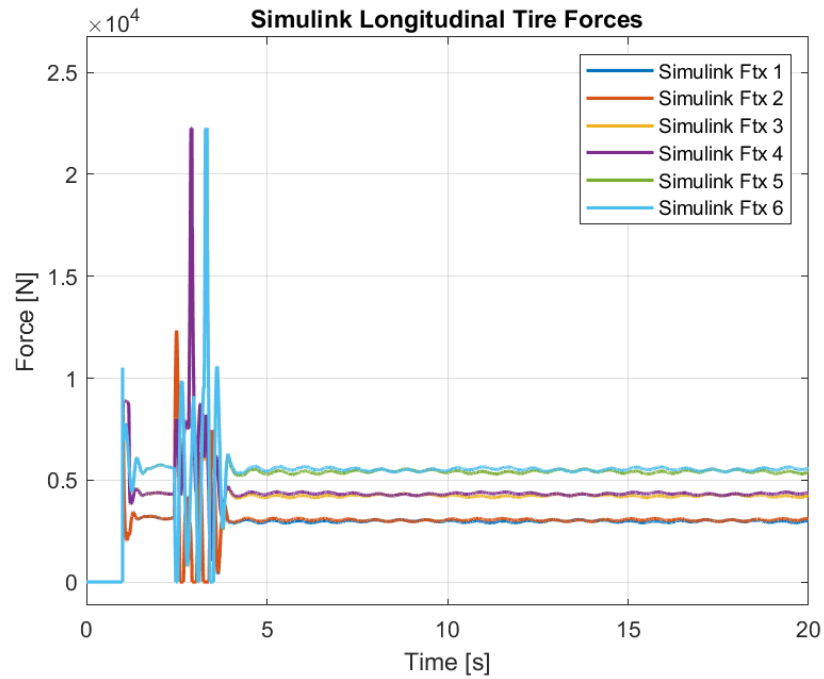


Figure 5-89. Simulink Longitudinal Tire Forces for Case 4

The differences in the traction forces and suspension torques are caused by the load distribution as discussed before. Due to high fluctuations in load distribution, the longitudinal tire forces can be seen to increase a value of 22278 at certain instants in Simulink while the maximum value obtained is 9834 in ADAMS. However, the mean values can be seen to be close enough despite the high fluctuations. The differences are caused due to the approximations made in Simulink while creating the dynamic load distribution model.

Table 5-24. Comparison of Longitudinal Tire Forces for Case 4

Parameters	ADAMS Max	Simulink Max	ADAMS Min	Simulink Min	ADAMS Mean	Simulink Mean
Ftx 1	7731.8	13887	0	-1.0E-13	3271.0	3083.4
Ftx 2	7731.8	13884	0	-1.0E-13	3271.0	3067.6
Ftx 3	9834.2	22278	-0.62585	-4.6E-13	4005.3	4316.9
Ftx 4	9834.2	22278	-0.62585	-4.6E-13	4005.3	4294.9
Ftx 5	10119	22276	-0.72587	-3.5E-13	5225.5	5315.1
Ftx 6	10119	22276	-0.72587	-3.5E-13	5225.5	5289.9

5.5 Case 5 – Steering with Different Torque Inputs

For the fifth case, steering is to be examined. By supplying left and right tires with different torque inputs, a yaw angle is desired to be produced in the vehicle due to the moment created by the different traction forces. Flat road profile is given to the vehicle and a constant torque of 1500 Nm and 4500 Nm is supplied to the left and right tires, respectively.

Although lateral motion is of interest in this case, longitudinal motion is also produced since the vehicle will be turning with respect to a center of curvature as the torque inputs have the same sign and different magnitudes.

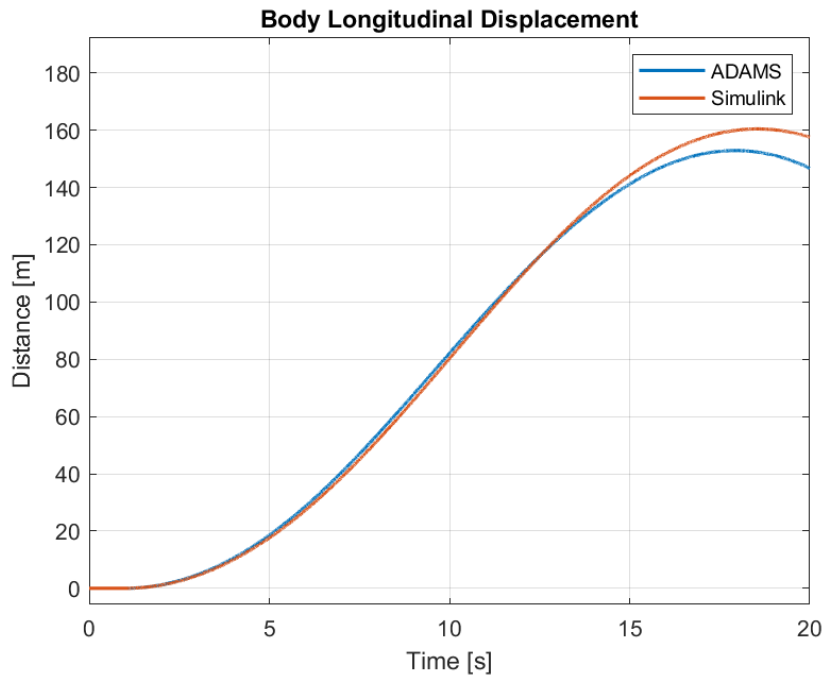


Figure 5-90. Plots of Longitudinal Displacement of the Body for Case 5

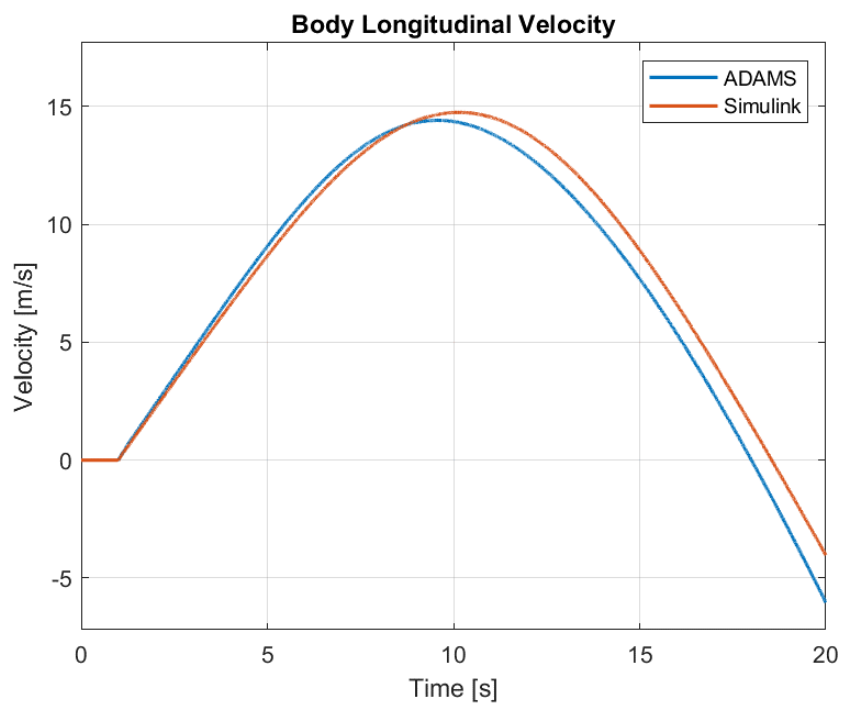


Figure 5-91. Plots of Longitudinal Velocity of the Body for Case 5

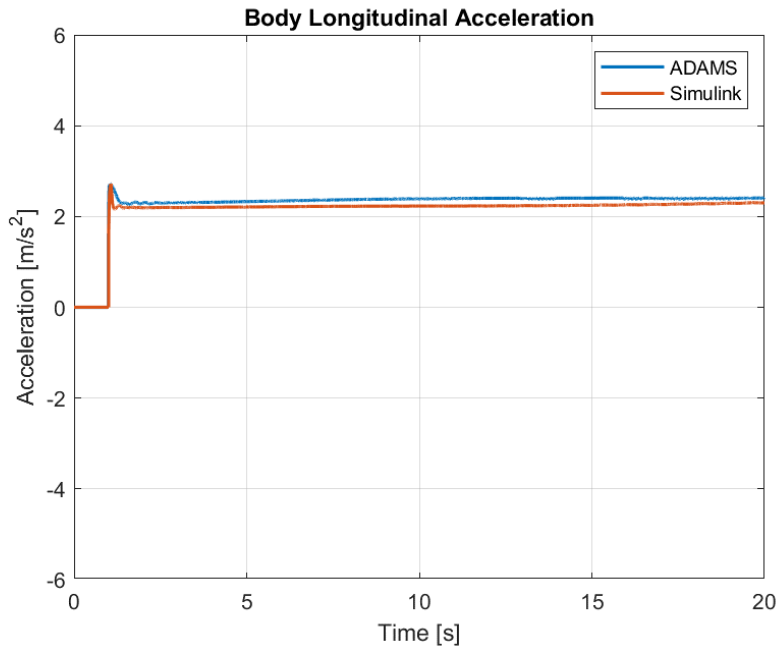


Figure 5-92. Plots of Longitudinal Acceleration of the Body for Case 5

As it can be interpreted from the plots, the behavior of the vehicle along the road are the same. The vehicle starts gaining traction at 1 second mark and it follows a circular trajectory. As a result the longitudinal velocity starts decreasing as the vehicle turns in inertial reference frame since the longitudinal axis of the body turns with the vehicle as well. The values in results show a deviation near the end but this is due to the differences between tire road interaction between the models. ADAMS uses its own algorithm which is a modified version of the Magic Formula.

Table 5-25. Comparison of Longitudinal Motion Between Models for Case 5

Parameter	MSE	ADAMS Max	Simulink Max	ADAMS Min	Simulink Min	ADAMS Mean	Simulink Mean
Long. Disp.	13.34	152.9	160.4	-2.477E-4	-4.5E-17	79.31	80.48
Long. Vel.	0.8233	14.41	14.74	-6.031	-4.026	7.368	7.876
Long. Acc.	0.0198	2.711	2.724	-1.064E-4	-6.5E-16	2.255	2.124

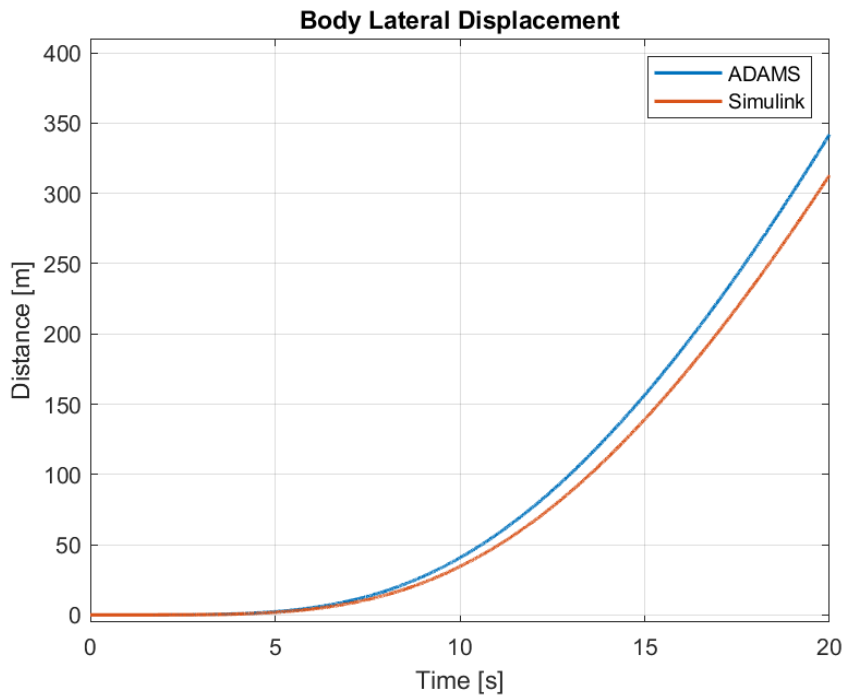


Figure 5-93. Plots of Lateral Displacement of the Body for Case 5

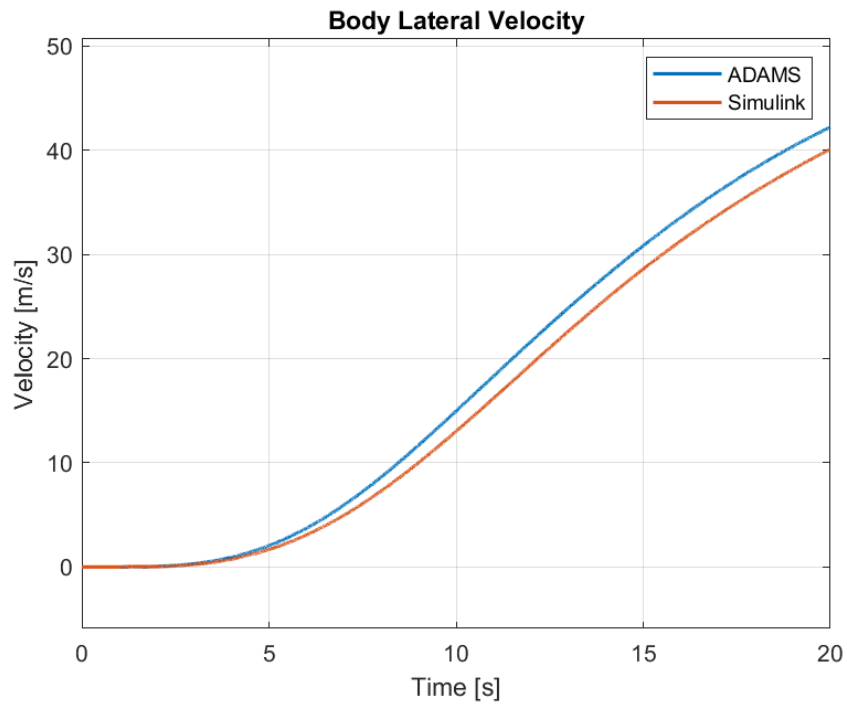


Figure 5-94. Plots of Lateral Velocity of the Body for Case 5

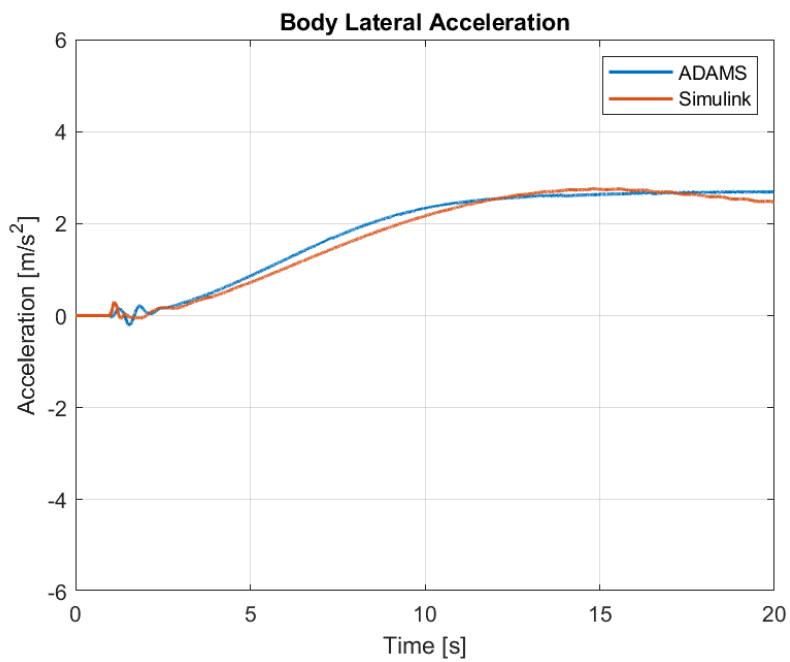


Figure 5-95. Plots of Lateral Acceleration of the Body for Case 5

A similar case is present for the lateral motion in this case. As the simulation continues, the lateral velocity increases since the longitudinal axis of the vehicle aligns with the lateral axis of the inertial reference frame as the vehicle turns. If the simulation was longer, a decrease in lateral displacement would have been seen when the vehicle rotates 180 degrees with respect to its original orientation. The reason for deviations are the same as explained while reviewing the longitudinal motion.

Table 5-26. Comparison of Lateral Motion Between Models for Case 5

Parameter	MSE	ADAMS Max	Simulink Max	ADAMS Min	Simulink Min	ADAMS Mean	Simulink Mean
Lat. Disp.	176.4	341.9	312.9	-1.674E-4	-1.3E-25	88.18	78.79
Lat. Vel.	2.829	42.23	40.11	-1.821E-3	-1.4E-22	17.06	15.65
Lat. Acc.	0.01895	2.703	2.754	-0.2123	-0.06232	1.787	1.717

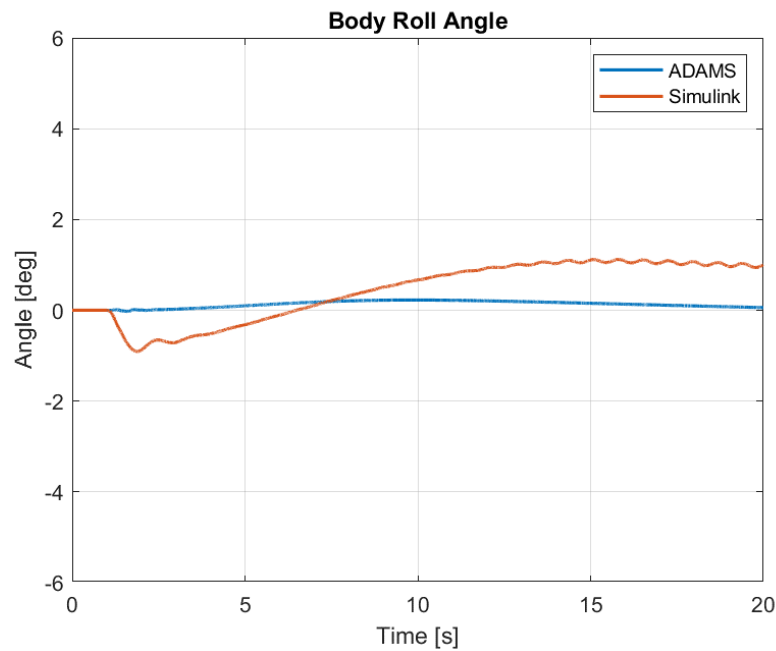


Figure 5-96. Plots of Roll Angle of the Body for Case 5

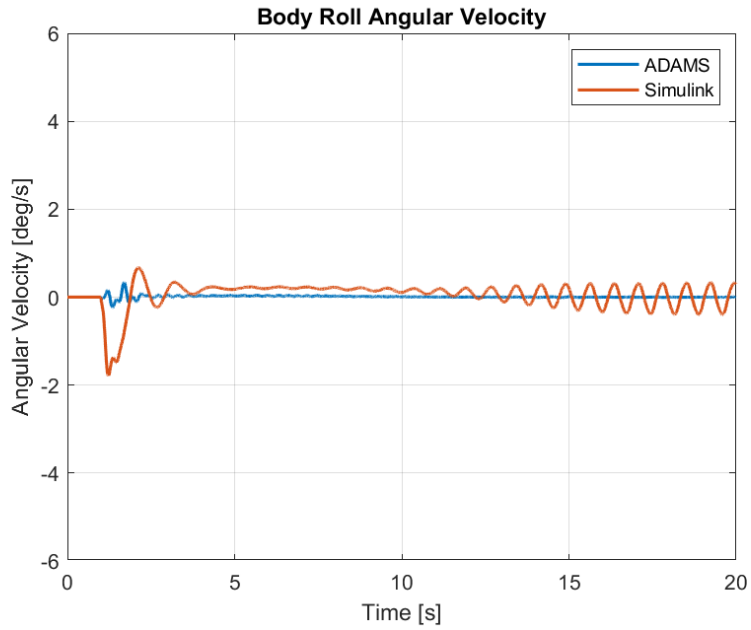


Figure 5-97. Plots of Roll Angular Velocity of the Body for Case 5

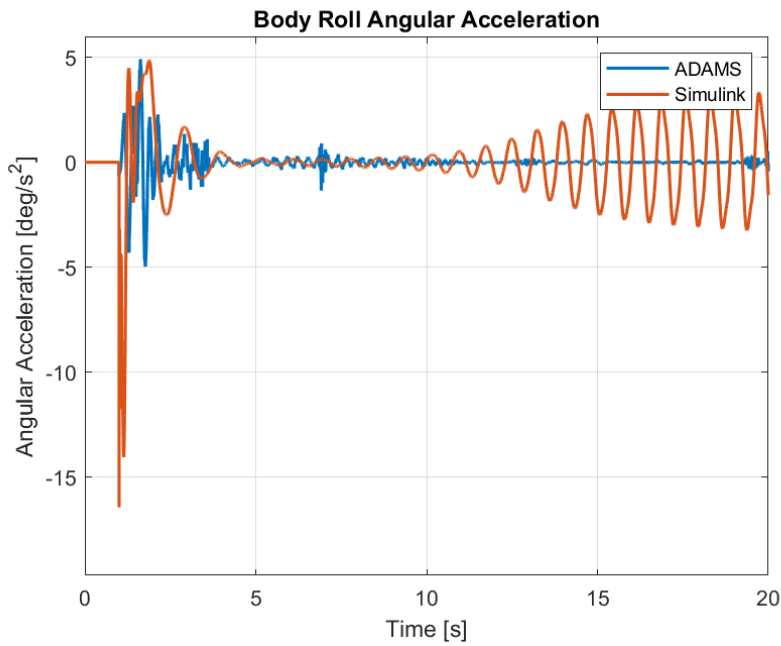


Figure 5-98. Plots of Roll Angular Acceleration of the Body for Case 5

A negative roll angle is produced in Simulink when different traction forces are applied. However, as the lateral acceleration increases, a positive roll angle can be observed in both models.

Table 5-27. Comparison of Roll Motion Between Models for Case 5

Parameter	MSE	ADAMS Max	Simulink Max	ADAMS Min	Simulink Min	ADAMS Mean	Simulink Mean
Roll Angle	0.4548	0.2269	1.121	-0.02271	-0.9057	0.1284	0.4314
Roll Ang. Vel.	0.09828	0.3365	0.6686	-0.2319	-1.784	0.01029	0.04985
Roll Ang. Acc.	3.609	4.922	4.871	-4.966	-16.45	-4.207E-4	0.01488

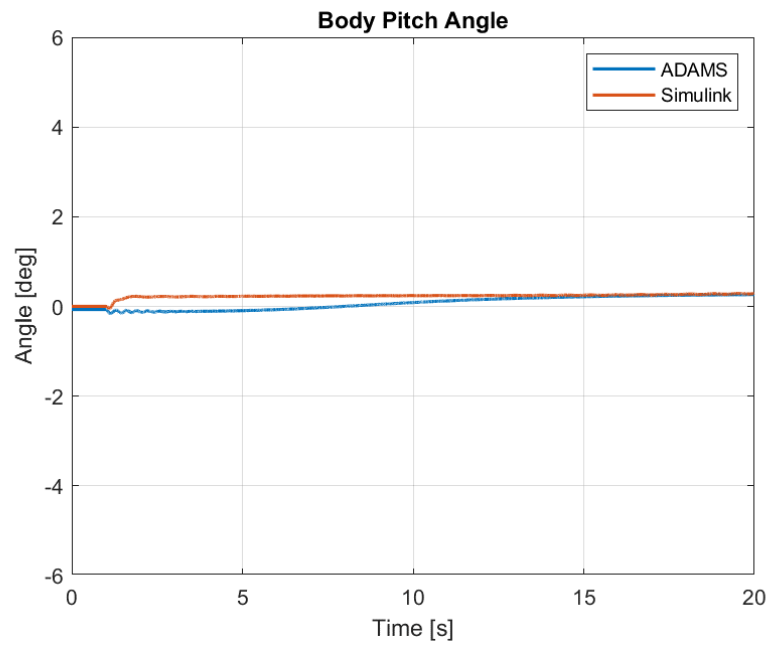


Figure 5-99. Plots of Pitch Angle of the Body for Case 5

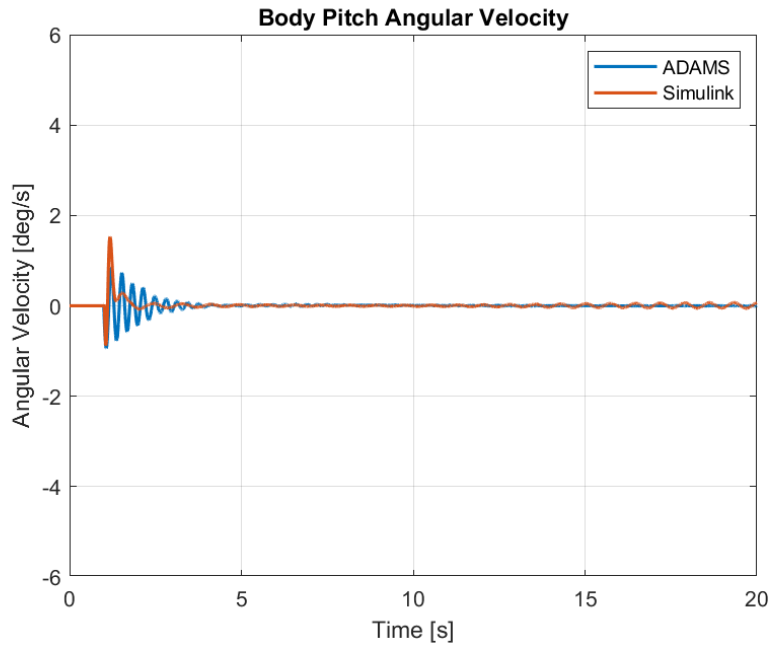


Figure 5-100. Plots of Pitch Angular Velocity of the Body for Case 5

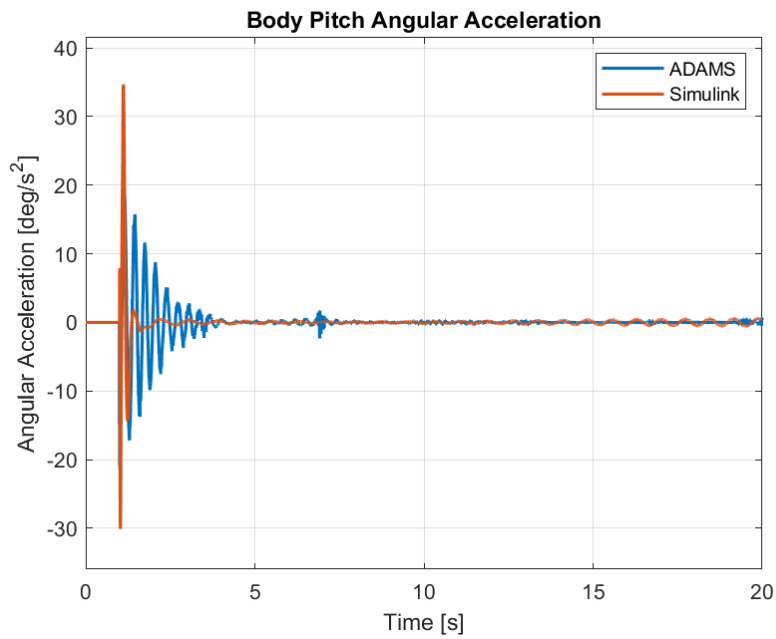


Figure 5-101. Plots of Pitch Angular Acceleration of the Body for Case 5

The pitch angles produced for this remain close as it can be seen from the errors. The pitch angle is settled at 0.284 deg in Simulink and 0.267 deg in ADAMS, the values remain close and a positive pitch angle can be observed. A similar case is present in velocity as well but for acceleration, while a maximum value of 19.01 deg/s² is obtained at the start of traction in ADAMS, Simulink model shows an acceleration of 34.68 deg/s². Frequent oscillations is present as the simulation continues in ADAMS for this case as well. However, its effects are negligible.

Table 5-28. Comparison of Pitch Motion Between Models for Case 5

Parameter	MSE	ADAMS Max	Simulink Max	ADAMS Min	Simulink Min	ADAMS Mean	Simulink Mean
Pitch Ang.	0.03827	0.2641	0.2907	-0.1593	-0.05131	0.07297	0.2265
Pitch Ang. Vel.	0.01563	0.8498	1.527	-0.9401	-0.8806	0.002909	0.01424
Pitch Ang. Acc.	5.195	19.01	34.68	-21.51	-30.09	-0.00153	0.003387

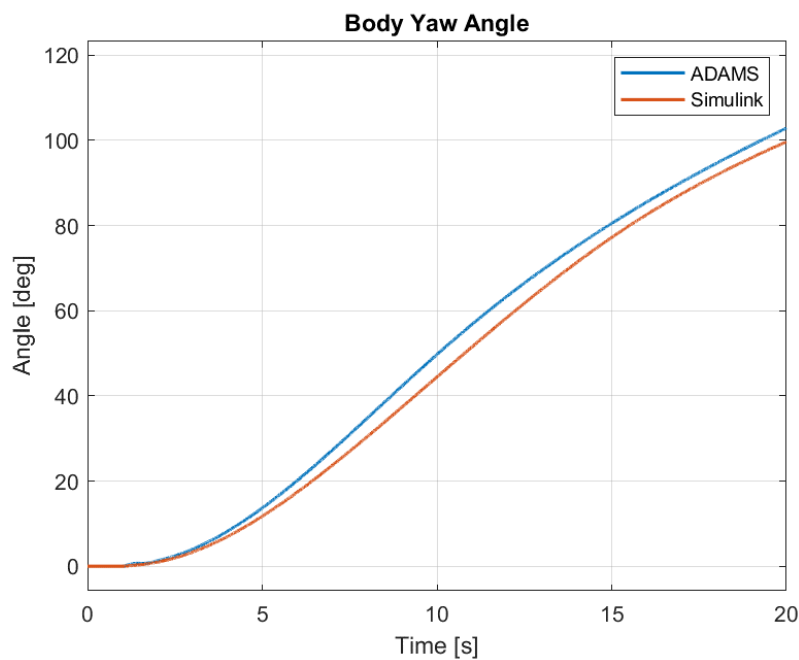


Figure 5-102. Plots of Yaw Angle of the Body for Case 5

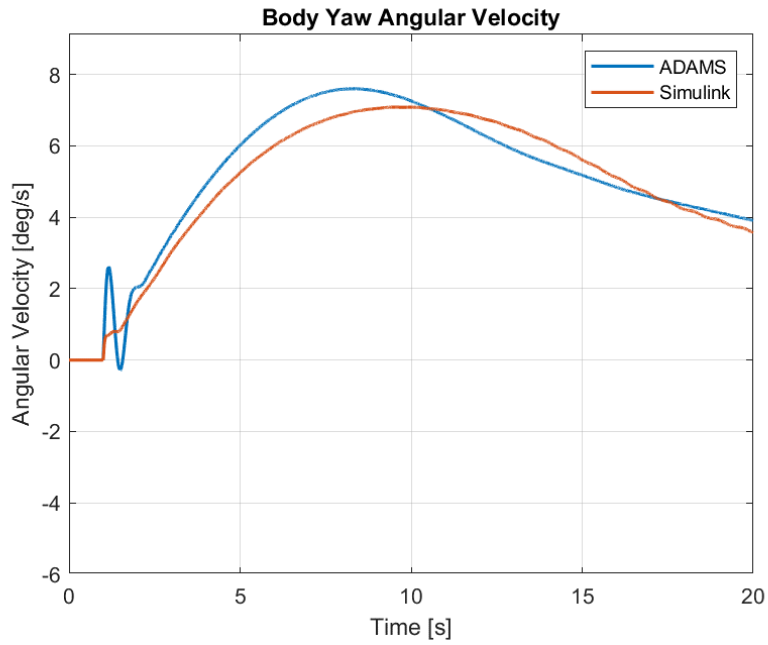


Figure 5-103. Plots of Yaw Angular Velocity of the Body for Case 5

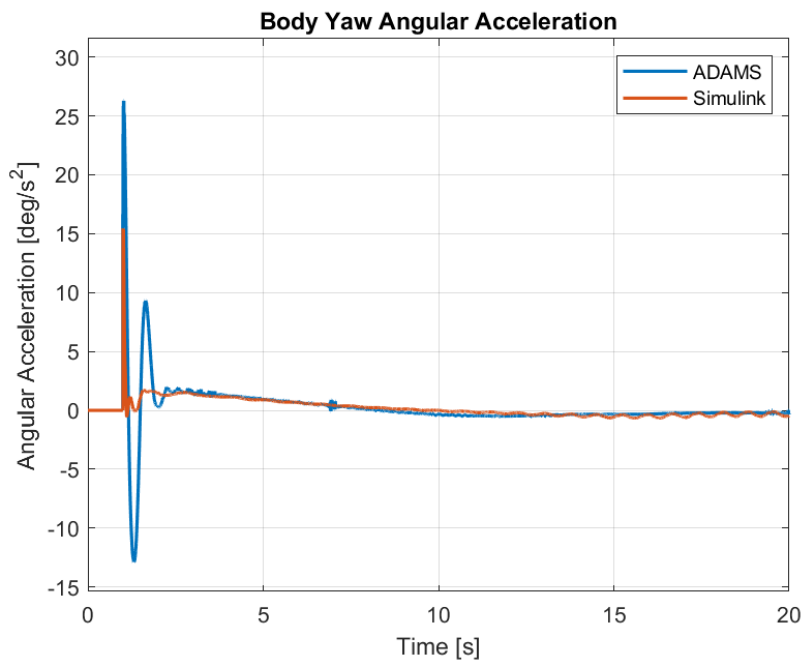


Figure 5-104. Plots of Yaw Angular Acceleration of the Body for Case 5

For a constant torque input of 4500 Nm and 1500 Nm to the right and left tires, respectively, the yaw angles at the end of the simulations are 99.64 degrees in Simulink and 102.8 degrees in ADAMS. Although the results show a similar behavior at the start, a deviation of 3.07% is present at the end. Since ADAMS and Simulink models have different calculation of tire-ground interaction this results in an error. Differences between load distribution also yield different tire forces and effect the behavior of the vehicle. Yaw velocity acts similarly but the error starts diminishing as the simulation progresses. Yaw acceleration plot shows a high peak of 26.29 deg/s² in ADAMS and 15.45 deg/s² when the torques are supplied to the tires at 1 second mark. ADAMS shows a high negative peak as well which can again be caused by the differences between tire-ground interactions. There are oscillations in the acceleration and velocity which are caused by the lateral resistive forces.

Table 5-29. Comparison of Yaw Motion Between Models for Case 5

Parameter	MSE	ADAMS Max	Simulink Max	ADAMS Min	Simulink Min	ADAMS Mean	Simulink Mean
Yaw Ang.	11.67	102.8	99.64	-1.1E-11	-2.6E-20	48.34	45.34
Yaw Ang. Vel.	0.2775	7.598	7.081	-0.2821	-1.2E-19	5.146	4.982
Yaw Ang. Acc.	3.493	26.29	15.45	-12.89	-0.6605	0.1962	0.1780

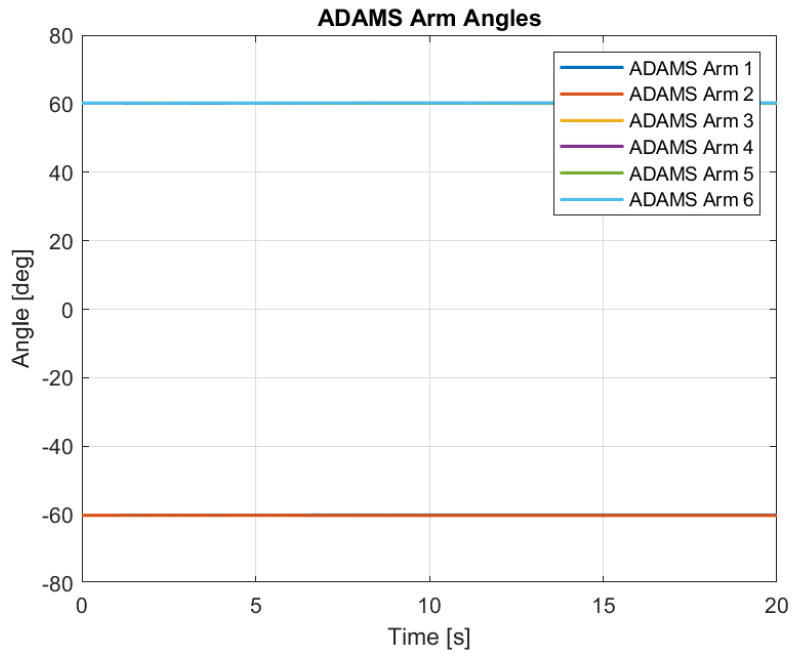


Figure 5-105. ADAMS Arm Angles for Case 5

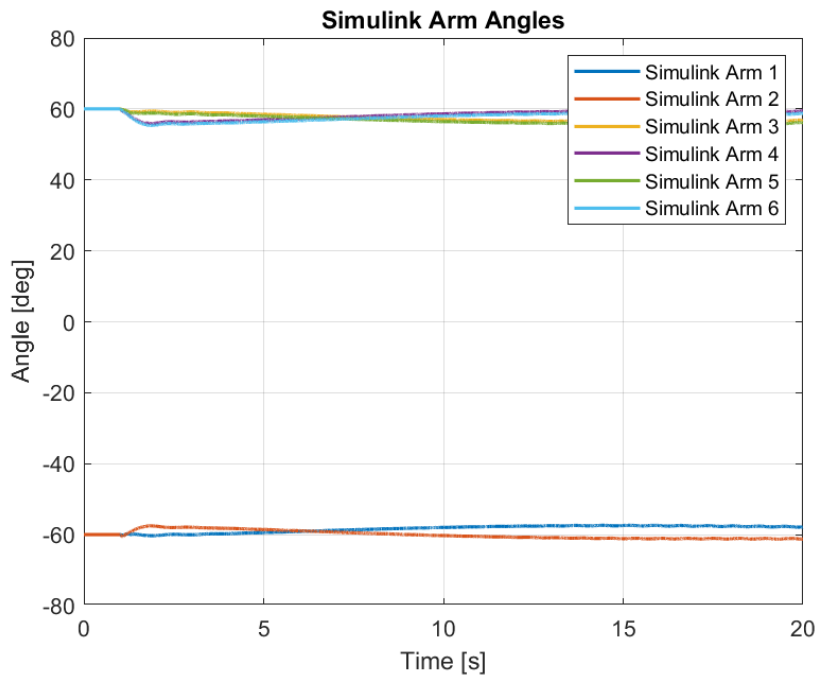


Figure 5-106. Simulink Arm Angles for Case 5

From figures 5-105 and 5-106, the arm angles can be seen to remain close to their original positions throughout the simulation. However, the right arms have a tendency to extend towards the rear end of the vehicle while the left arms exhibit an opposite behavior as they move towards the front end of the vehicle. The changes in arm angles in Simulink model are greater compared to the ADAMS model and the differences are reflected to the comparison table below. The main cause of errors are the approximations used while modelling the tire – ground interaction in Simulink.

Table 5-30. Comparison of Arm Angles Between Models for Case 5

Parameters	MSE	ADAMS Max	Simulink Max	ADAMS Min	Simulink Min	ADAMS Mean	Simulink Mean
Arm Angle 1	3.679	-60.08	-57.37	-60.15	-60.29	-60.10	-58.44
Arm Angle 2	1.295	-60.15	-57.54	-60.22	-61.27	-60.20	-59.98
Arm Angle 3	7.936	60.18	60.00	60.10	56.36	60.13	57.53
Arm Angle 4	4.441	60.20	60.00	60.13	55.91	60.18	58.41
Arm Angle 5	11.60	60.22	60.00	60.15	55.74	60.17	56.99
Arm Angle 6	6.938	60.24	60.00	60.18	55.36	60.22	57.86

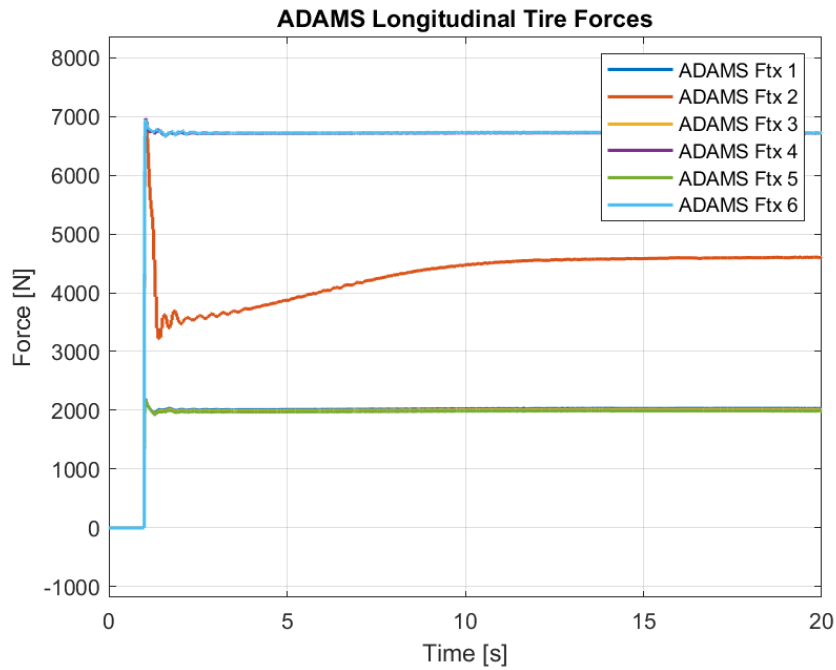


Figure 5-107. ADAMS Longitudinal Tire Forces for Case 5

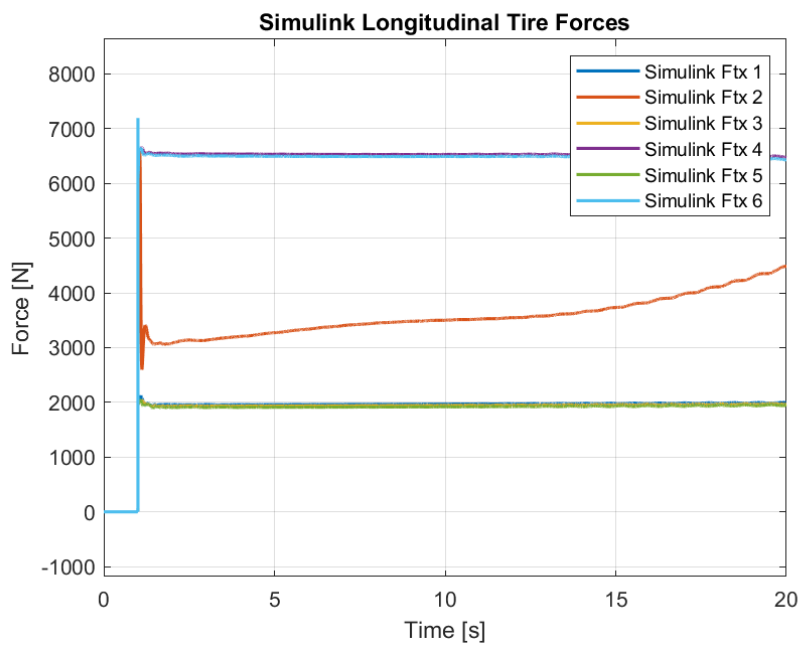


Figure 5-108. Simulink Longitudinal Tire Forces for Case 5

Table 5-31. Comparison of Longitudinal Tire Forces Between Models for Case 5

Parameters	ADAMS Max	Simulink Max	ADAMS Min	Simulink Min	ADAMS Mean	Simulink Mean
Ftx 1	2201.2	2127.2	0	-1.0E-13	1921.7	1872.3
Ftx 2	6912.8	6588.1	0	-1.0E-13	4103.5	3409.1
Ftx 3	2186.6	2057.2	-0.4364	-4.6E-13	1904.1	1850.2
Ftx 4	6967.9	6654.7	-0.4364	-4.6E-13	6383.8	6200.2
Ftx 5	2179.7	2198.1	-0.4999	-3.5E-13	1886.5	1827.9
Ftx 6	6950.4	7193.3	-0.4999	-3.5E-13	6390.2	6163.9

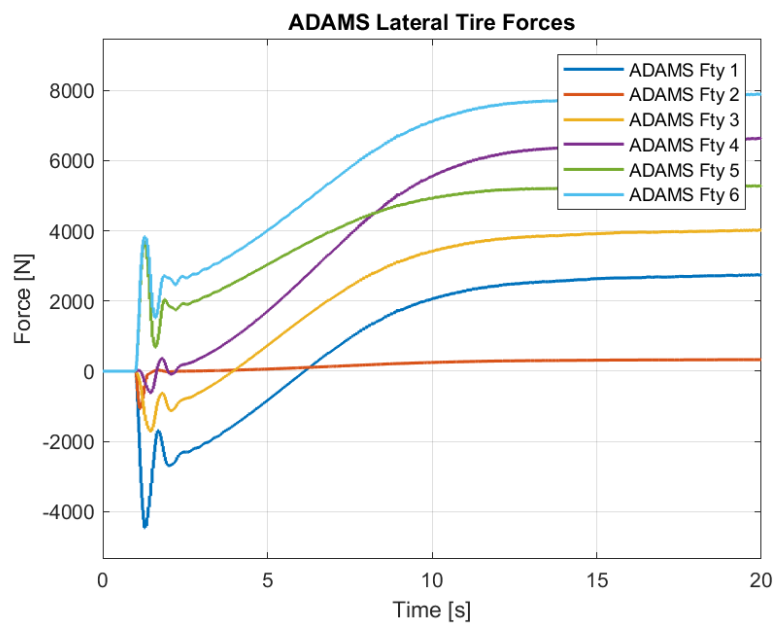


Figure 5-109. ADAMS Lateral Tire Forces for Case 5

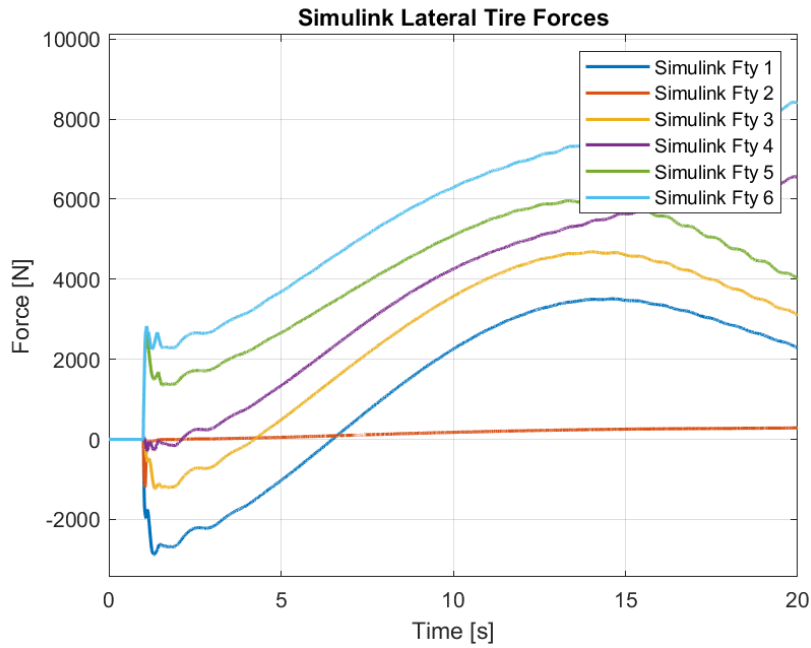


Figure 5-110. Simulink Lateral Tire Forces for Case 5

Table 5-32. Comparison of Lateral Tire Forces Between Models for Case 5

Parameters	ADAMS Max	Simulink Max	ADAMS Min	Simulink Min	ADAMS Mean	Simulink Mean
Fty 1	2752.1	3512.2	-4459.7	-2883.2	1088.6	1291.9
Fty 2	329.64	287.26	-1067.3	-1192.8	184.29	151.62
Fty 3	4024.6	4687.4	-1706.6	-1236.2	2420.9	2502.8
Fty 4	4024.6	4687.4	-1706.6	-1236.3	2420.9	2502.8
Fty 5	5283.0	5972.2	-1.1E-05	-3.8E-16	4078.2	4045.6
Fty 6	7895.9	8423.0	0	-3.8E-16	5875.2	5595.0

Although the tire forces produced exhibit the same behavior for both of the models, there are deviations caused by the load distribution and differences in the Magic Formula models employed. The right tires produce higher forces compared to the

left tires as the weight is distributed to the right side more while cornering as a result of the roll angle.

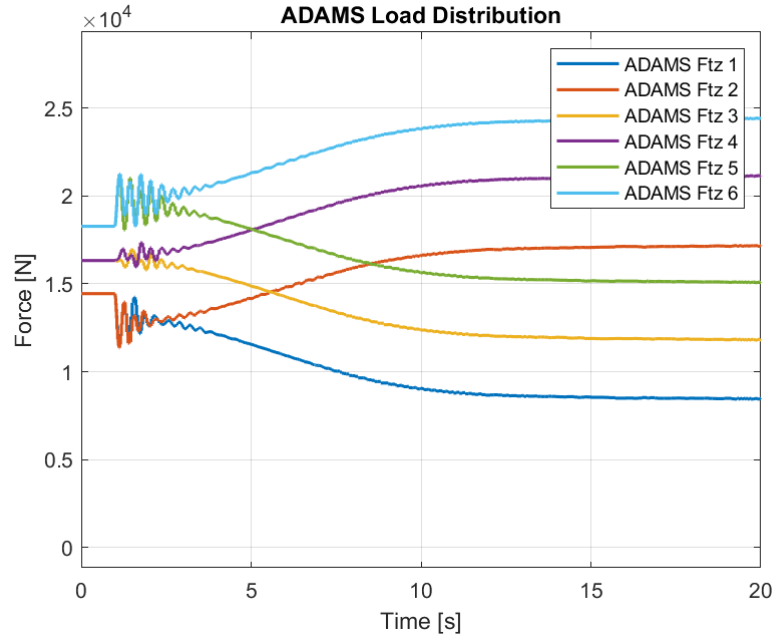


Figure 5-111. ADAMS Load Distribution for Case 5

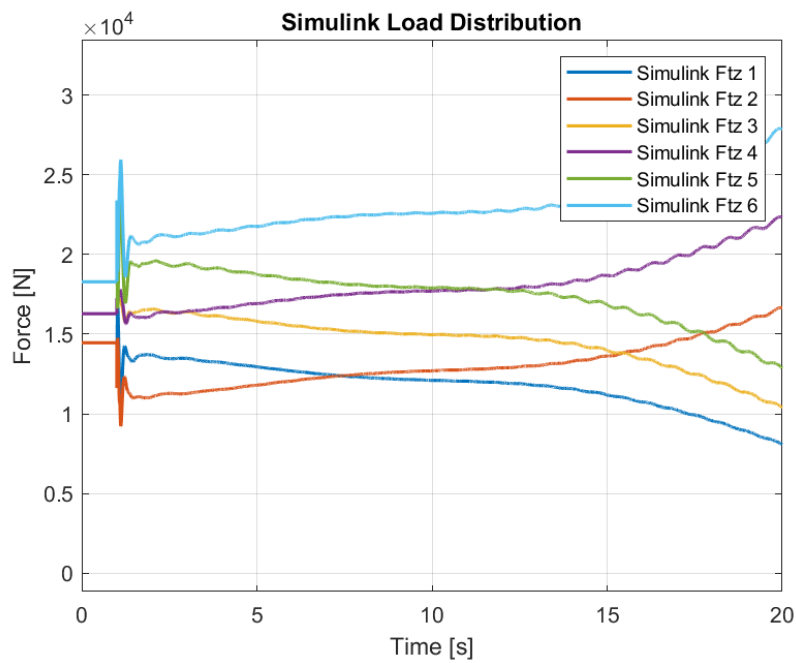


Figure 5-112. Simulink Load Distribution for Case 5

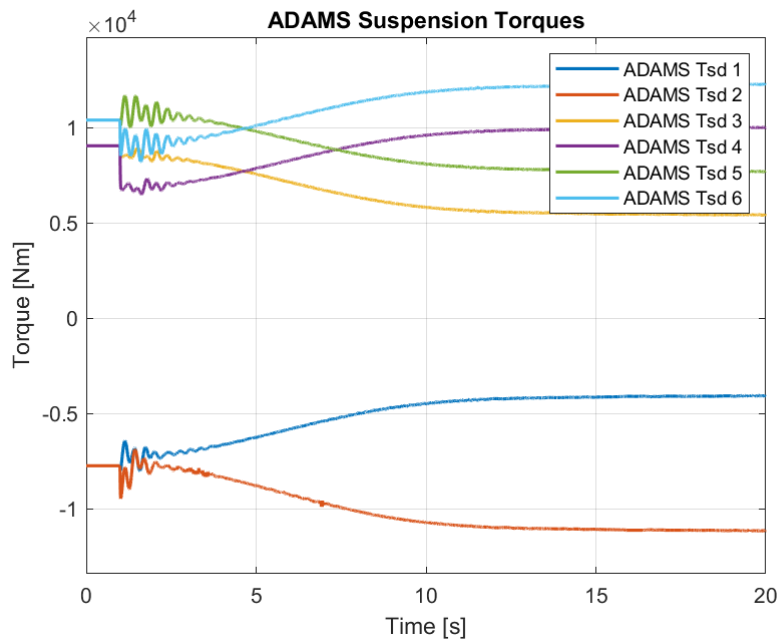


Figure 5-113. ADAMS Suspension Torques for Case 5

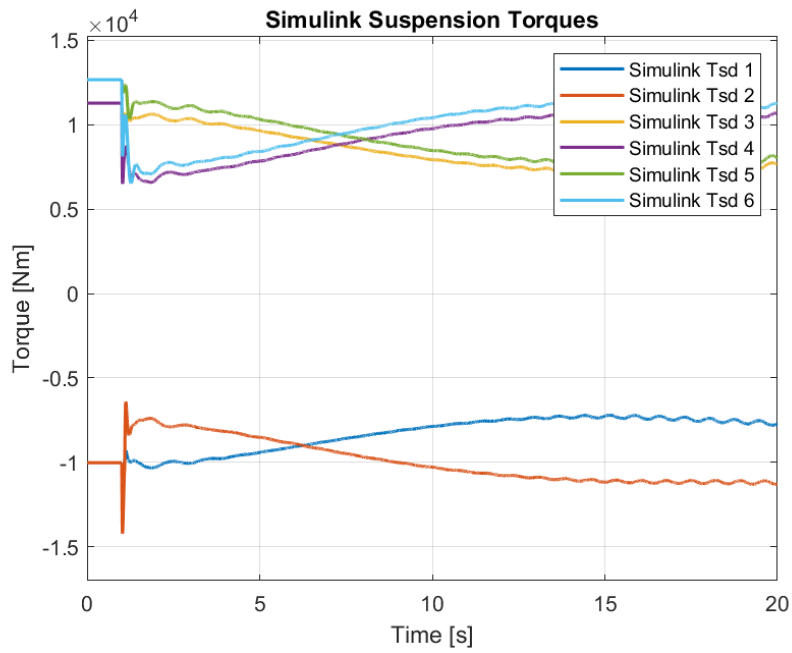


Figure 5-114. Simulink Suspension Torques for Case 5

5.6 Case 6 – Skid Steering Around Body Center of Gravity

For the sixth case, the rotation around the center of gravity is tested. As the vehicle considered in this study uses skid steering, by supplying each tire with torques equal in magnitude but opposite in signs, rotation around its own center is desired to be obtained. Since each tire is at equal lateral distance to the center of gravity of the body, traction forces which are opposite in left and right tires create a turning moment along the yaw axis. The lateral tire forces which however, create a resistance to the rotational motion. The road in this case is flat with 0.6 friction coefficient. The torque required to overcome the static friction is found to be 3100 Nm when supplied to the each tire. As a result, for this case, a torque input of 3500 Nm is supplied at 1 second mark.

Although we expect no translational motions, some slight deviations can occur due to the resistances and effects of the load distribution together with the suspension torques. So, the longitudinal translational motion will be considered first.

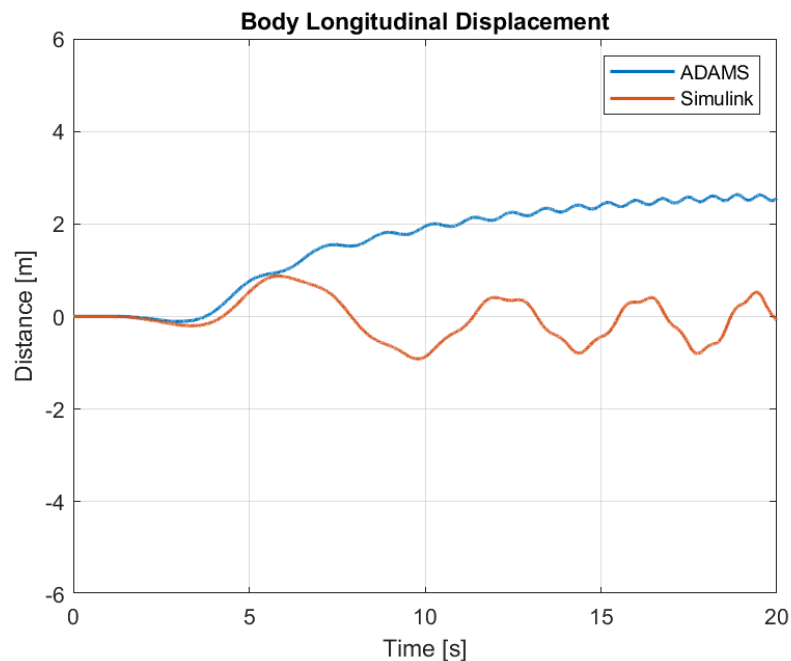


Figure 5-115. Plots of Longitudinal Displacement of the Body for Case 6

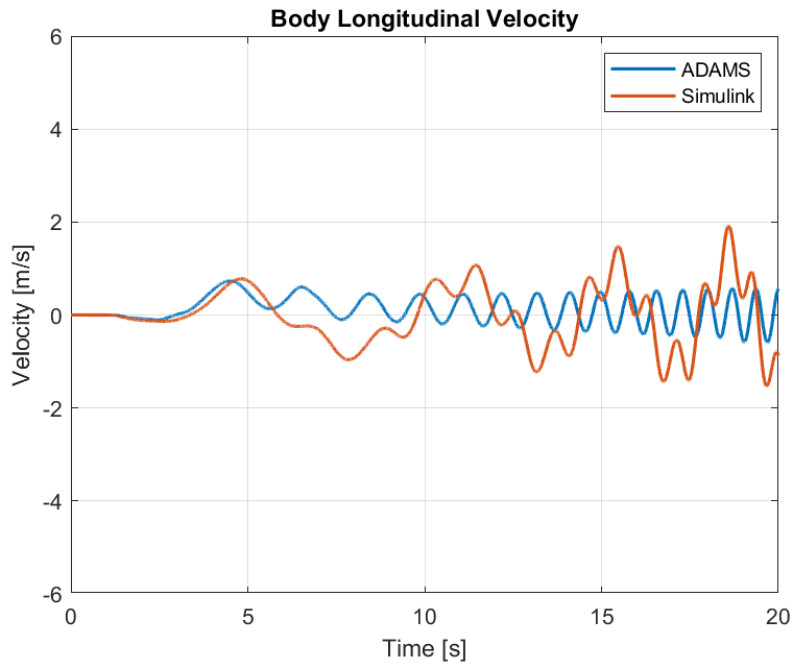


Figure 5-116. Plots of Longitudinal Velocity of the Body for Case 6

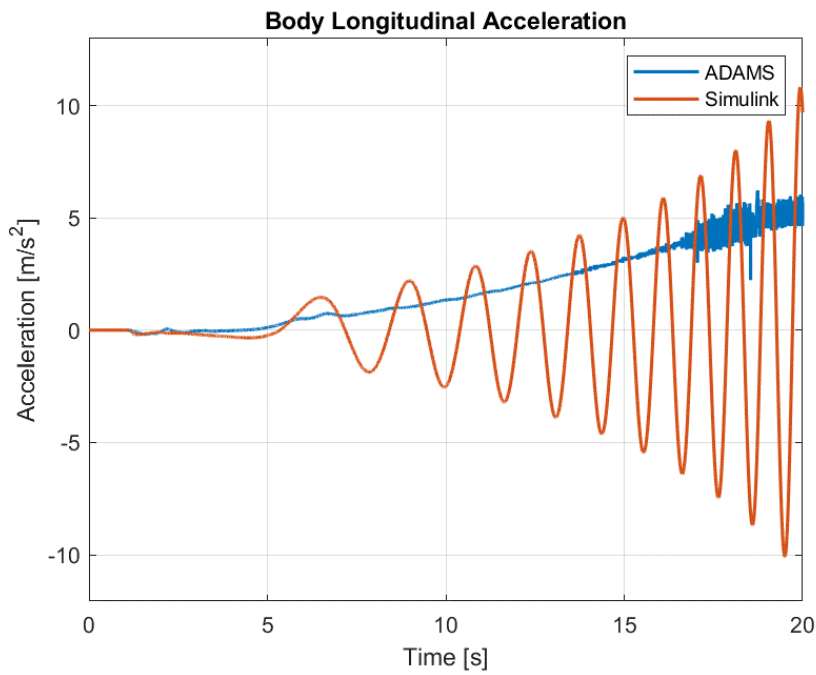


Figure 5-117. Plots of Longitudinal Acceleration of the Body for Case 6

In this case, no translational motion is expected since the vehicle is desired to be rotated around its own center of gravity. However, due to the resistances to motion, displacement along the longitudinal axis can be observed. At the start, until the vehicle can completely overcome the turning resistance it can be seen to move forward in ADAMS and backwards in Simulink. This is again, due to differences between tire and ground interaction. Although the velocity and acceleration show an oscillatory behaviour, the net displacement along the longitudinal axis is decreased. The oscillations are caused by the rotational motion of the vehicle since the motion is observed for the inertial reference frame in this case. As the vehicle's angular velocity increases the amplitudes of oscillations also increase.

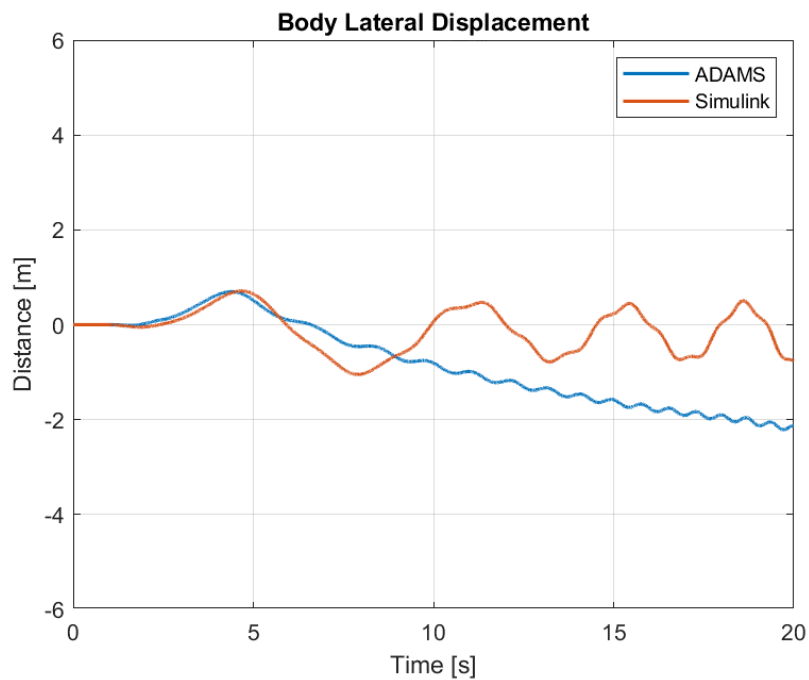


Figure 5-118. Plots of Lateral Displacement of the Body for Case 6

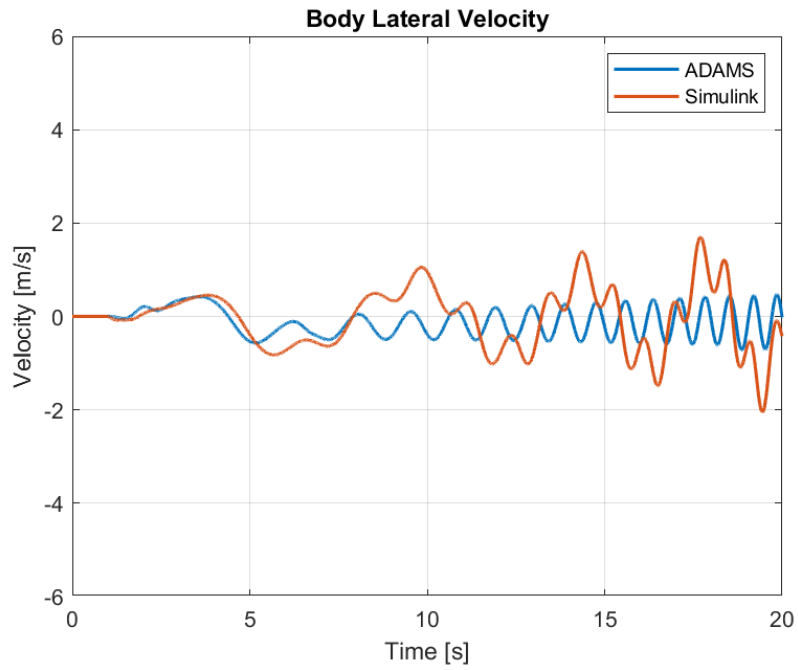


Figure 5-119. Plots of Lateral Velocity of the Body for Case 6

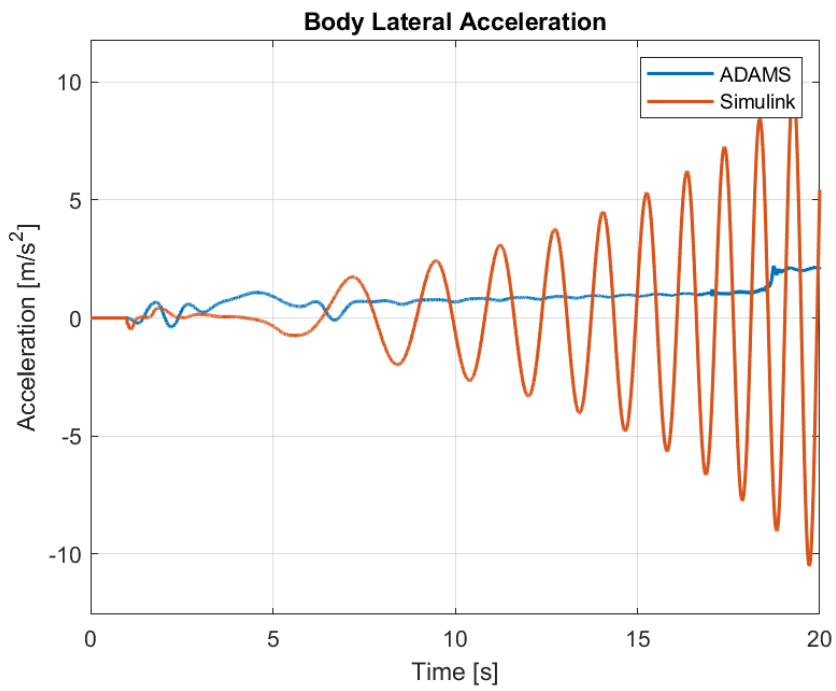


Figure 5-120. Plots of Lateral Acceleration of the Body for Case 6

A similar case holds for the lateral motion. The vehicle moves along the lateral axis while trying to overcome the resistances. As it rotates around its own center of gravity, it can be seen to move along the lateral axis as well but the displacement is of 2 meters in both softwares in a simulation of 20 seconds.

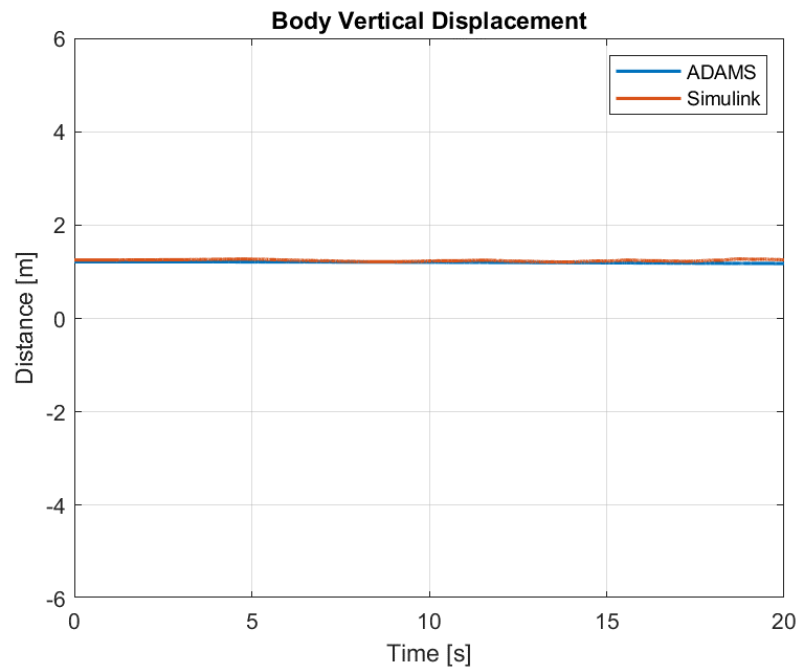


Figure 5-121. Plots of Vertical Displacement of the Body for Case 6

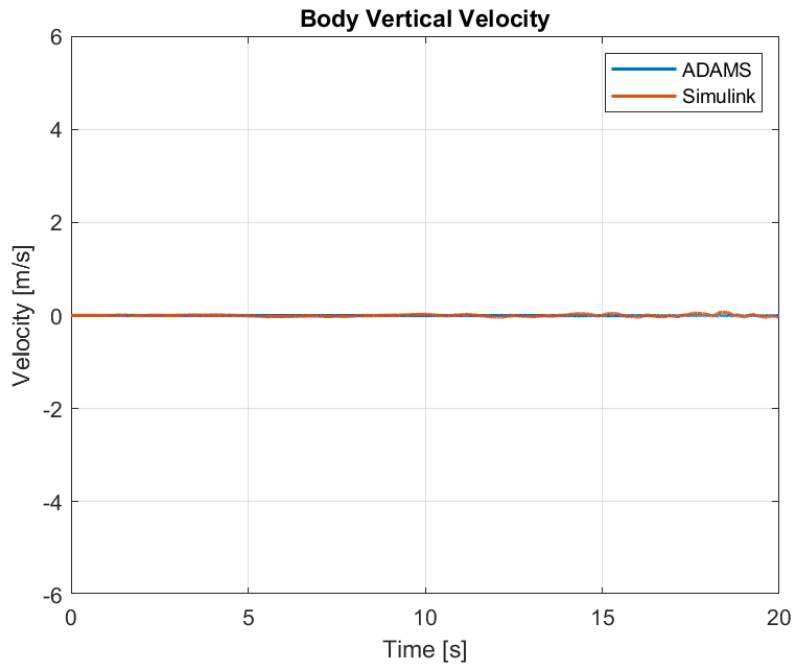


Figure 5-122. Plots of Vertical Velocity of the Body for Case 6

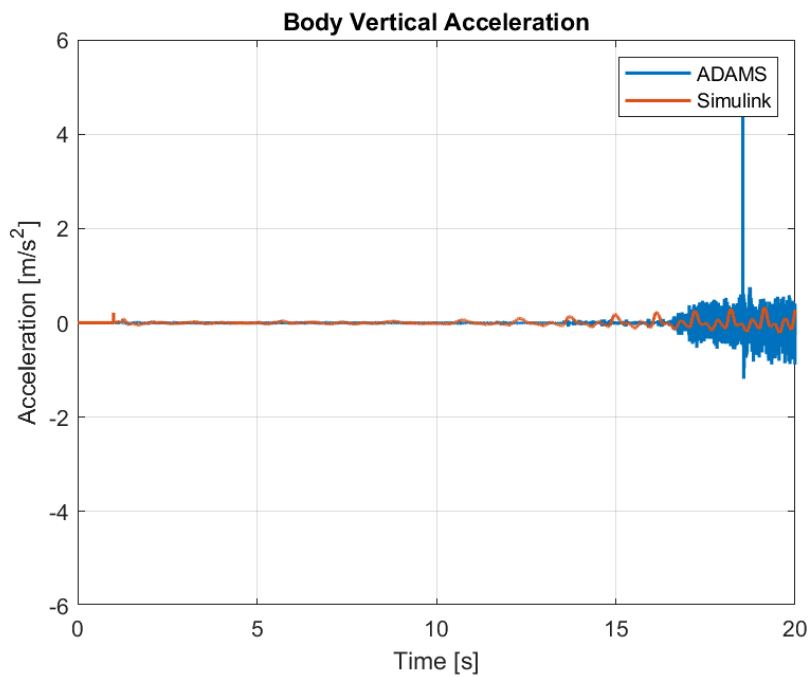


Figure 5-123. Plots of Vertical Acceleration of the Body for Case 6

For this case, vertical motion can be assumed to be almost zero. However, again, in ADAMS results, an oscillation is present near the end but these oscillations are caused by the solvers used in ADAMS. Although different solvers are tested with different parameters, these results are the best ones obtained.

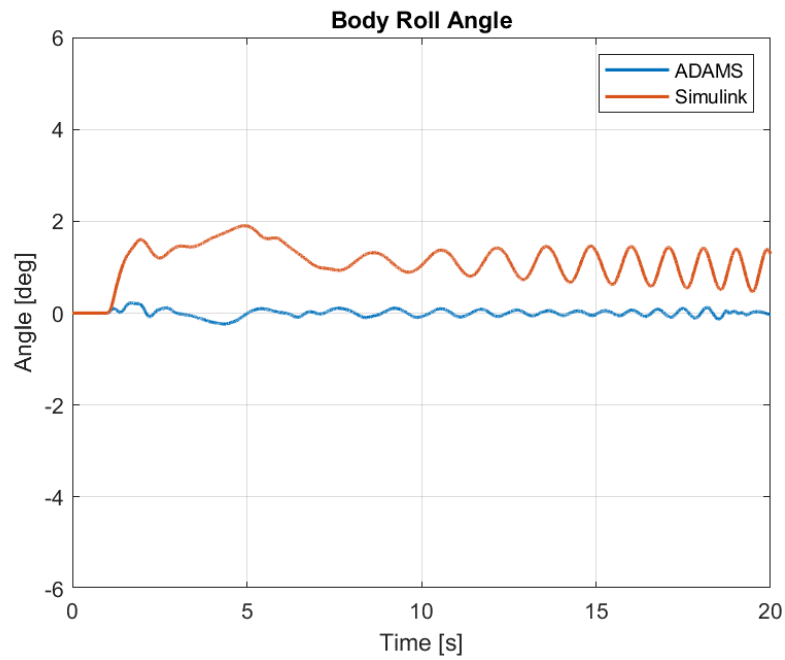


Figure 5-124. Plots of Roll Angle of the Body for Case 6

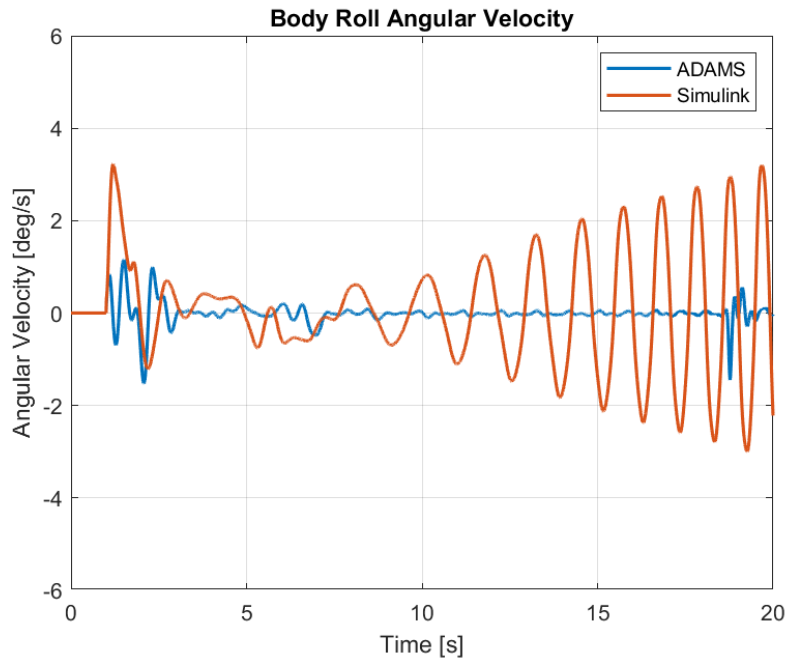


Figure 5-125. Plots of Roll Angular Velocity of the Body for Case 6

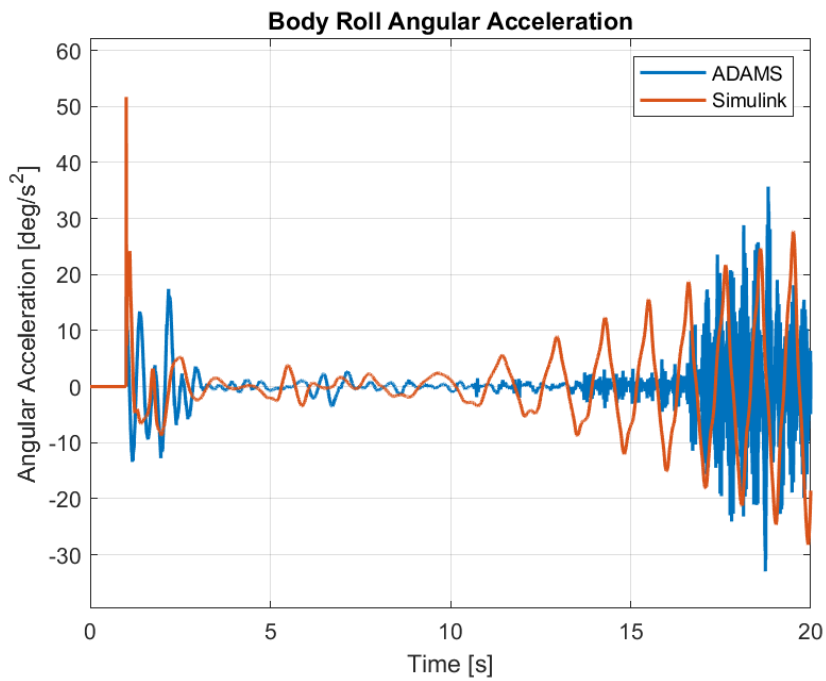


Figure 5-126. Plots of Roll Angular Acceleration of the Body for Case 6

As the vehicle rotates around its own axis, a roll motion is also produced due to the different forces produced in tires. Although the vehicle's roll angle is settled around 1 degrees in Simulink, the value is closer to 0 in ADAMS as it can be seen from the mean values in the following table.

Table 5-33. Comparison of Roll Motion Between Models for Case 6

Parameter	MSE	ADAMS Max	Simulink Max	ADAMS Min	Simulink Min	ADAMS Mean	Simulink Mean
Roll Ang.	1.437	0.2221	1.903	-0.2375	-5.2E-21	5.339E-4	1.116
Roll Ang. Vel.	1.522	1.152	3.224	-1.517	-2.998	-8.031E-3	0.06422
Roll Ang. Acc.	69.97	35.68	51.66	-32.98	-28.21	5.545E-3	-0.1123

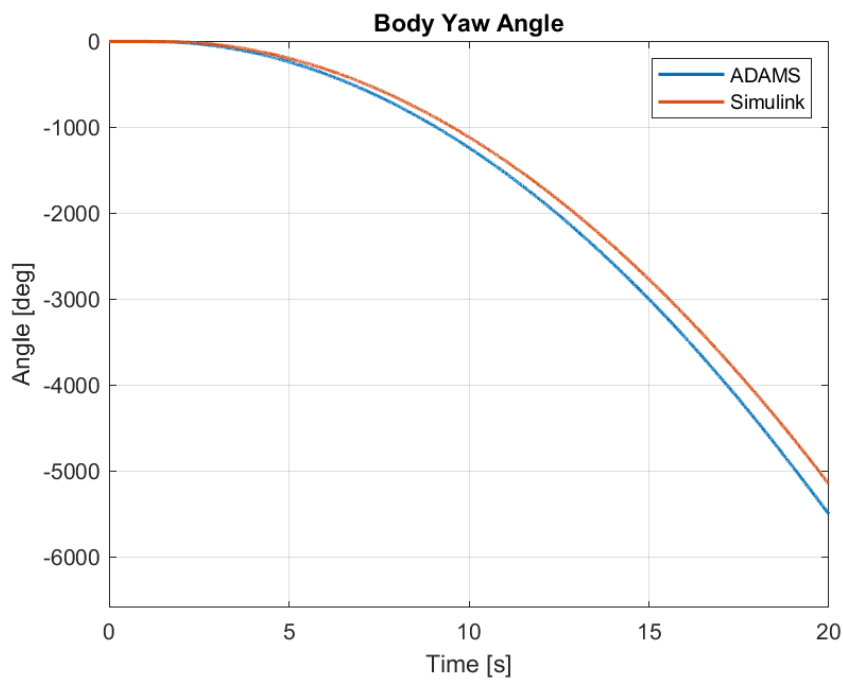


Figure 5-127. Plots of Yaw Angle of the Body for Case 6

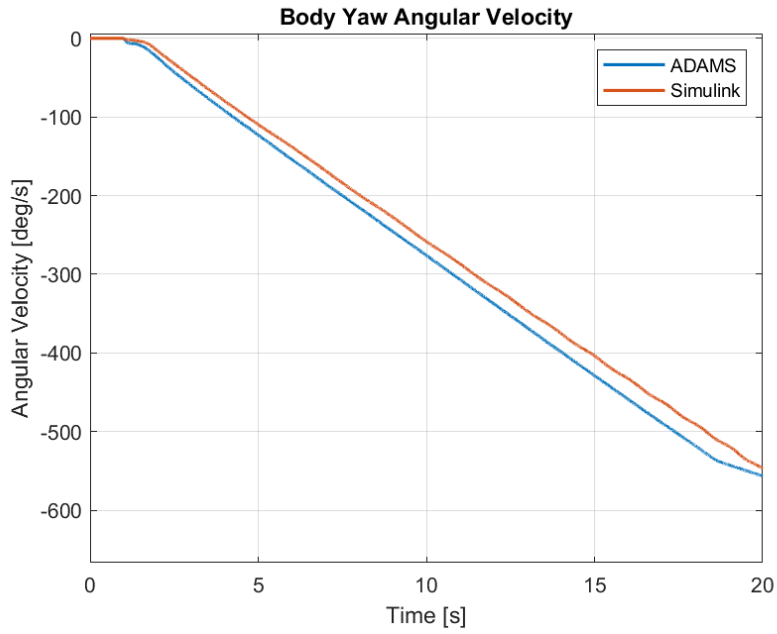


Figure 5-128. Plots of Yaw Angular Velocity of the Body for Case 6

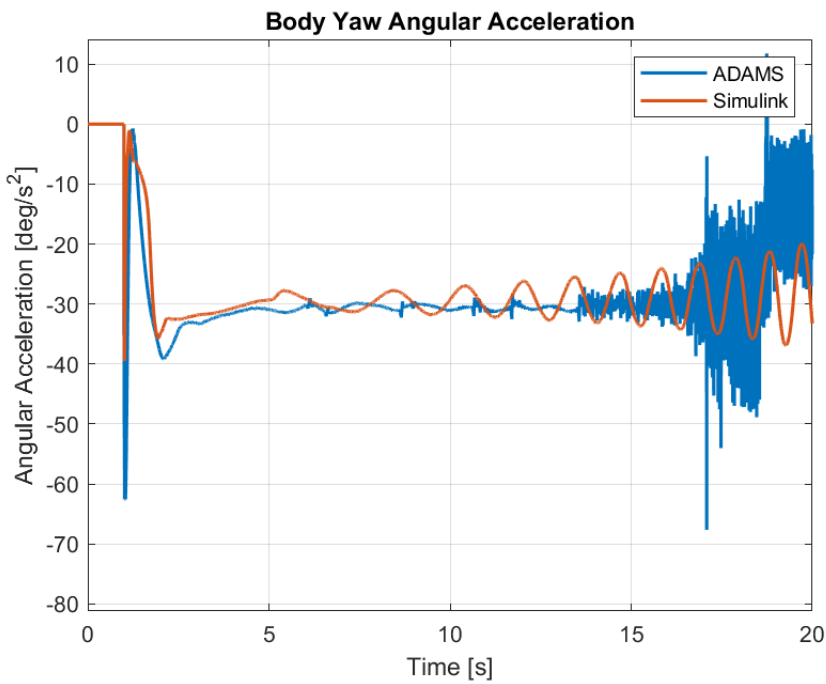


Figure 5-129. Plots of Yaw Angular Acceleration of the Body for Case 6

As constant torque of 3500 Nm with opposite signs is supplied to left and right tires, a constant yaw acceleration is produced in models. Although the data obtained from ADAMS seem to fluctuate constantly, the mean values of acceleration can be seen to be -27.8 and -27.3 for ADAMS and Simulink, respectively. Furthermore, the MSE between the results are high but the maximum, minimum and mean values can be seen to be close.

Table 5-34. Comparison of Yaw Motion Between Models for Case 6

Parameter	MSE	ADAMS Max	Simulink Max	ADAMS Min	Simulink Min	ADAMS Mean	Simulink Mean
Yaw Ang.	31584	7.1E-08	0	-5502.5	-5152.5	-1745.8	-1605.3
Yaw Ang. Vel.	355.18	5.5E-12	1.28E-19	-556.56	-547.15	-275.12	-257.63
Yaw Ang. Acc.	35.412	11.772	7.99E-18	-67.648	-39.501	-27.828	-27.357

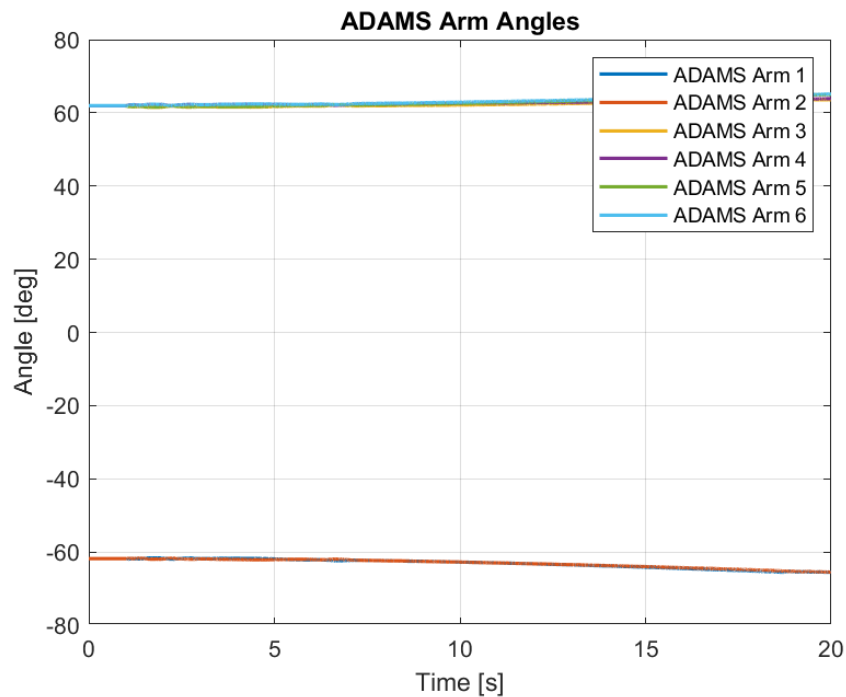


Figure 5-130. ADAMS Arm Angles for Case 6

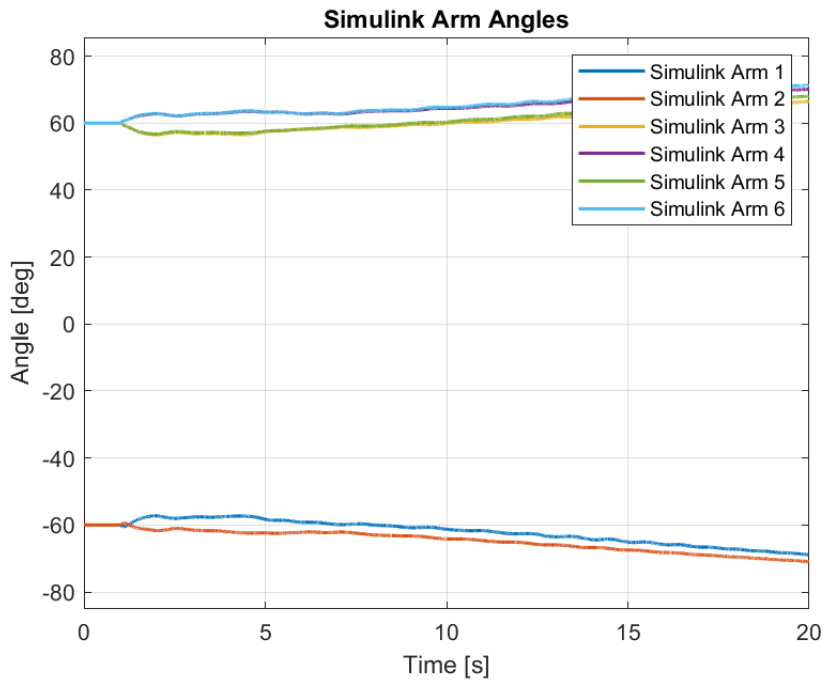


Figure 5-131. Simulink Arm Angles for Case 6

While the vehicle is constantly rotating around its own vertical axis and forces are produced constantly in opposite directions in tires, the arms tend to open constantly. The arms open up much more slowly in ADAMS compared to Simulink.

Table 5-35. Comparison of Arm Angles Between Models for Case 6

Parameters	MSE	ADAMS Max	Simulink Max	ADAMS Min	Simulink Min	ADAMS Mean	Simulink Mean
Arm Angle 1	6.143	-61.63	-57.27	-65.54	-68.83	-63.13	-62.02
Arm Angle 2	6.879	-61.65	-59.42	-65.49	-70.92	-63.08	-64.73
Arm Angle 3	8.174	63.65	66.47	61.49	56.47	62.34	60.64
Arm Angle 4	9.731	63.87	70.11	61.93	60.00	62.71	64.98
Arm Angle 5	7.925	64.98	68.04	61.57	56.72	62.89	61.29
Arm Angle 6	9.779	65.12	71.33	61.96	60.00	63.16	65.43

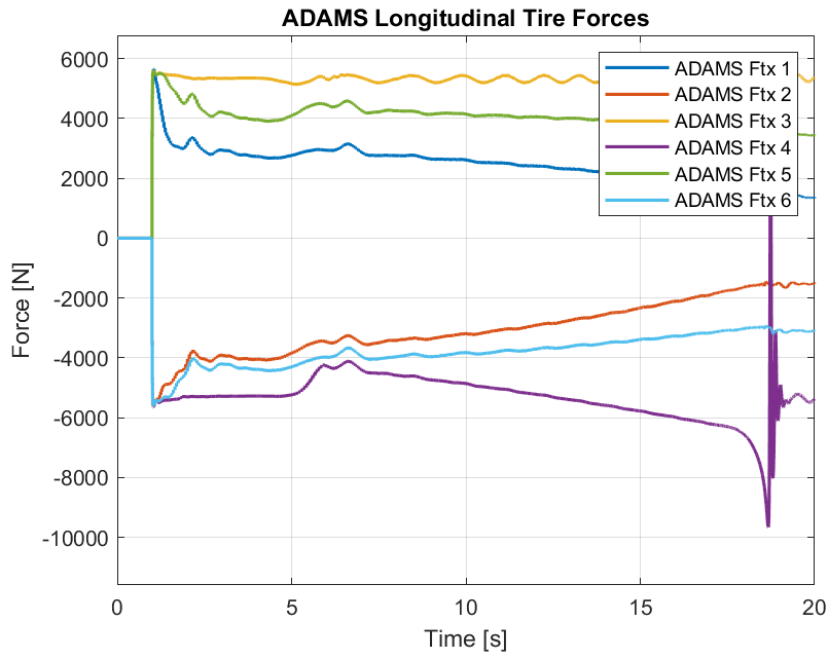


Figure 5-132. ADAMS Longitudinal Tire Forces for Case 6

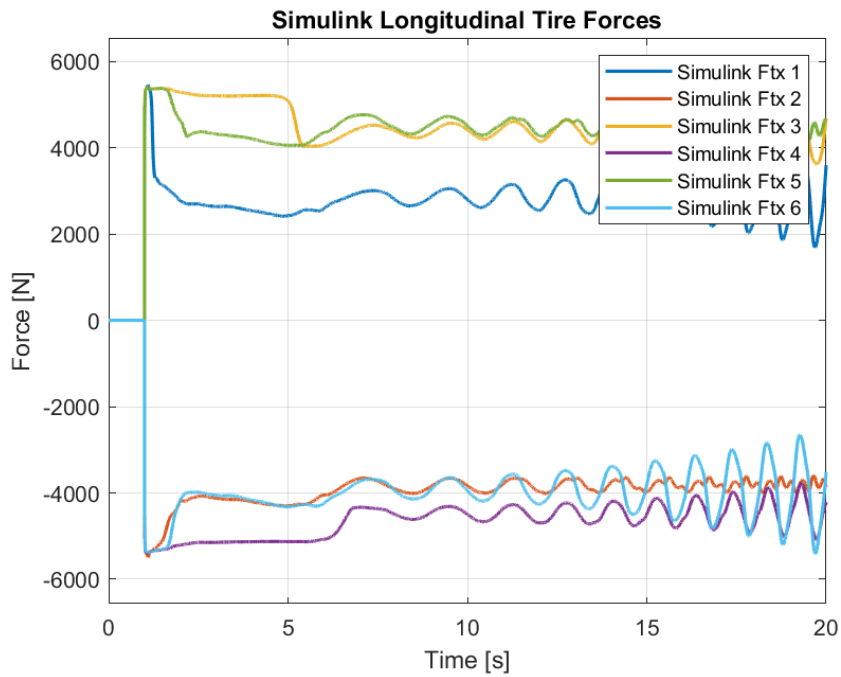


Figure 5-133. Simulink Longitudinal Tire Forces for Case 6

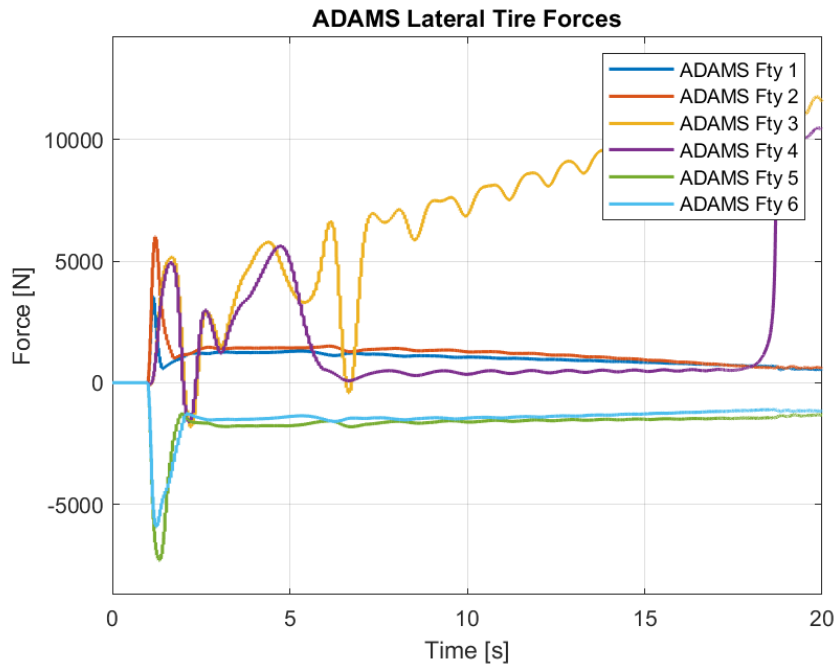


Figure 5-134. ADAMS Lateral Tire Forces for Case 6

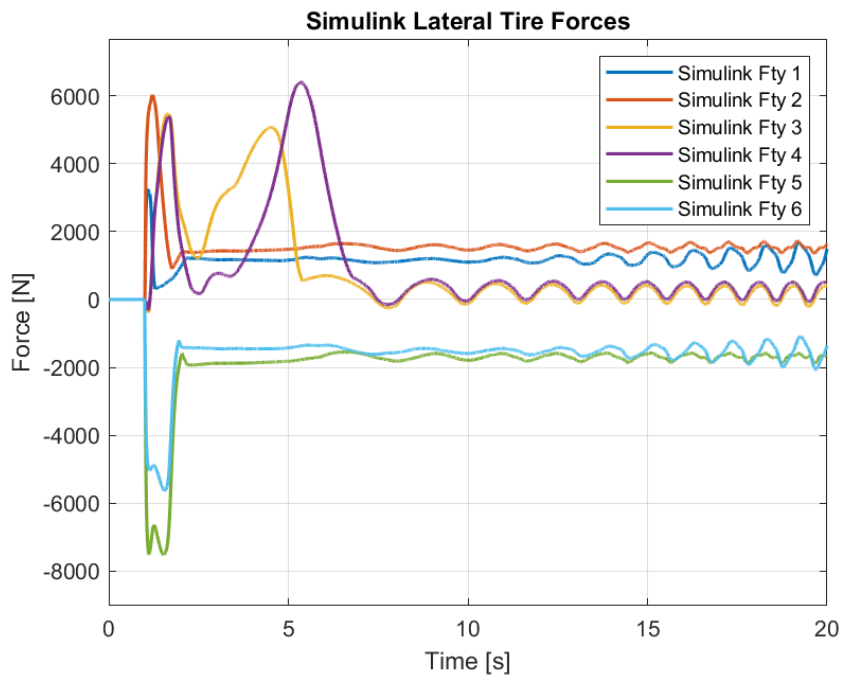


Figure 5-135. Simulink Lateral Tire Forces for Case 6

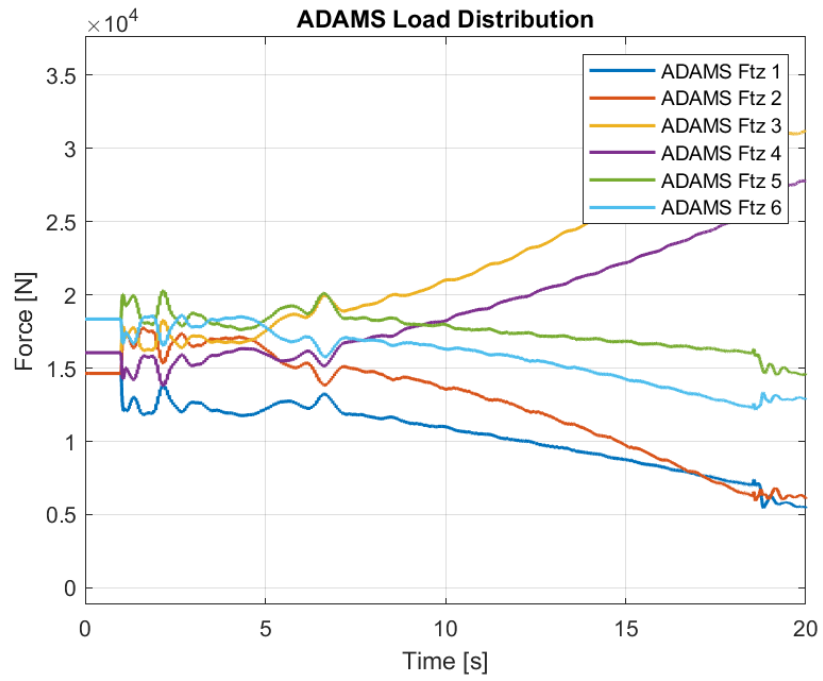


Figure 5-136. ADAMS Load Distribution Forces for Case 6

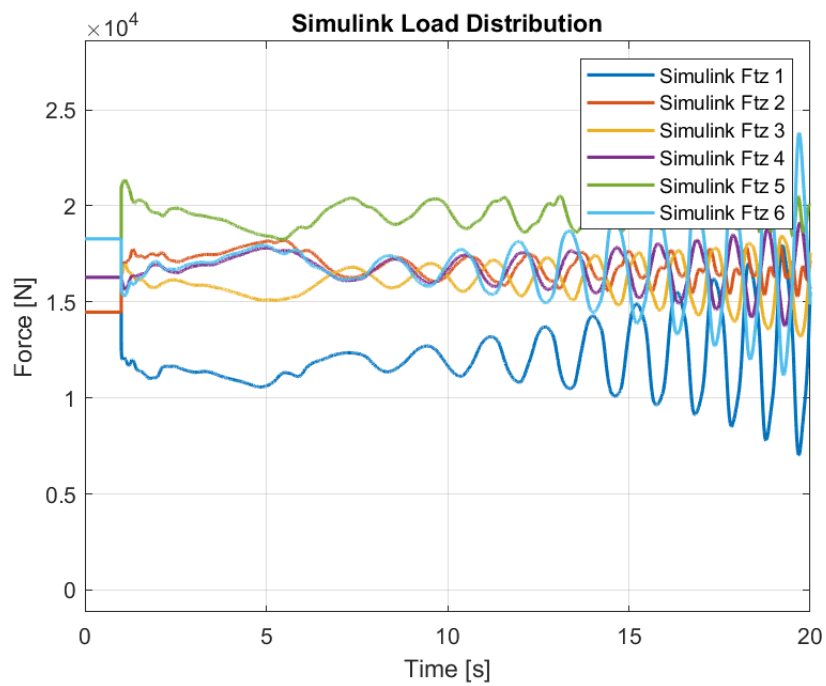


Figure 5-137. Simulink Load Distribution Forces for Case 6

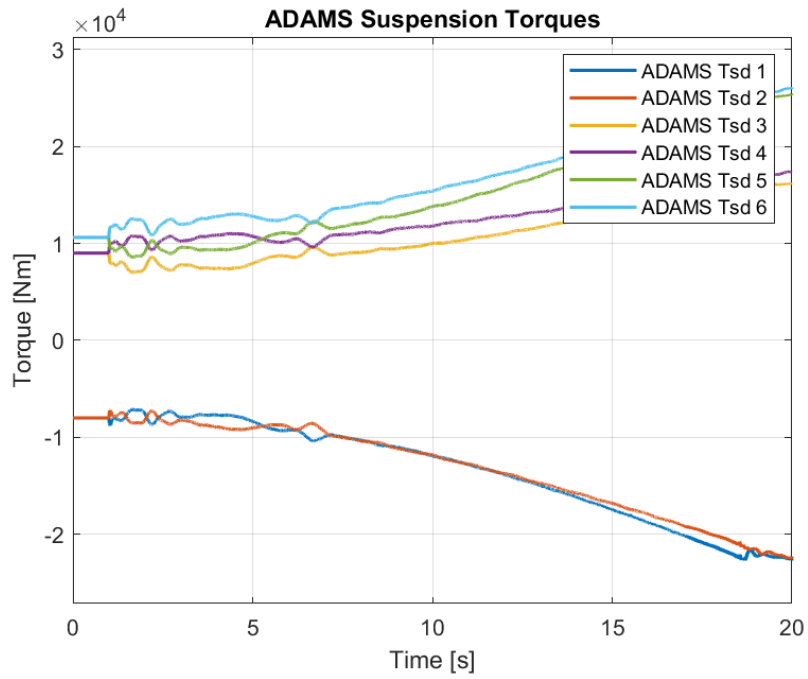


Figure 5-138. ADAMS Suspension Torques for Case 6

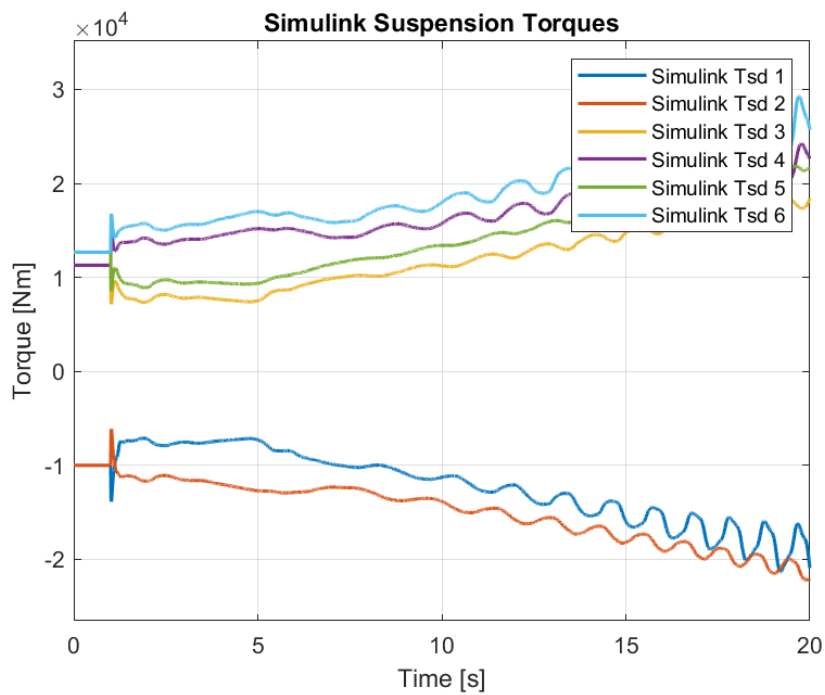


Figure 5-139. Simulink Suspension Torques for Case 6

Suspensions behave similarly between the models although the Simulink model shows a more oscillatory behavior. However, their mean values can be seen to be close. Note that the signs are opposite in front suspensions due to the direction of the torques applied. Magnitude of the torques applied are given in table

Table 5-36. Comparison of Suspension Torques Between Models For Case 6

Parameters	ADAMS Max	Simulink Max	ADAMS Min	Simulink Min	ADAMS Mean	Simulink Mean
Susp. Torque 1	8002.4	10640	4048.3	7203.5	5167.2	8363.9
Susp. Torque 2	11177	14220	6878.4	6400.4	10006	9960.7
Susp. Torque 3	9043.3	11280	5392.9	7164.5	6498.9	8520.7
Susp. Torque 4	10017	11280	6508.9	6501.6	9052.5	9471.1
Susp. Torque 5	11668	12669	7678.6	7600.7	8718.8	9128.1
Susp. Torque 6	12289	12669	8213.2	6530.4	11268	10129

CHAPTER 6

CONCLUSIONS AND FUTURE WORK

In the scope of this thesis the simulation of a 6x6 skid steered vehicle with articulated hydro-pneumatic suspension has been conducted to investigate the behavior of the vehicle under different road conditions for various movement scenarios. The results obtained from both MATLAB/Simulink and ADAMS are compared to inspect the accuracy of the created model.

The behavior of the 18 degrees-of-freedom model is investigated using dynamic equations of motion in MATLAB-Simulink for its sprung mass, arms and the tires using appropriate models. Models of the double-acting hydro-pneumatic suspension system are also created which increase the performance of the vehicle in off-road conditions.

The second model in the ADAMS environment is constructed to verify the results obtained. The responses of the vehicle regarding longitudinal, lateral, and vertical motions are shown to be similar along with the constructed load distribution algorithm and the suspension systems.

As it is mentioned in the dynamic modeling chapter the vehicle has 18 degrees-of-freedom consisting of several subsystems. It is important to emphasize that the suspension characteristics and load distribution share the most important role on this model because of their complex structure. In the future studies, results of these crucial sub-systems can be compared with the data obtained from real-life tests on the presented 6x6 vehicle once its production is completed. These sub-systems can then be improved upon. As observed from the results, the main source of error is due to the differences between the modeling of tire and ground contact between the two models. Load distribution algorithm in Simulink model which is an approximation

of the real-life case also cause errors. As such, improvements on the modeling of the tire-ground contact will be made in the future. Once the real-life tests can be performed, the tire parameters will be obtained and optimized to reflect the real-life behavior of the tires.

In addition to validation of the model, to achieve leveling adjustments and change suspension characteristics, control algorithms can be developed for the double-acting hydro-pneumatic suspension system. Especially for the climbing applications on steep slope road.

As a final step in this future work the model of the driveline, which is not considered in this study, can be implemented to the presented model, in order to validate the overall vehicle behavior under same input scenarios with the real-life prototype.

REFERENCES

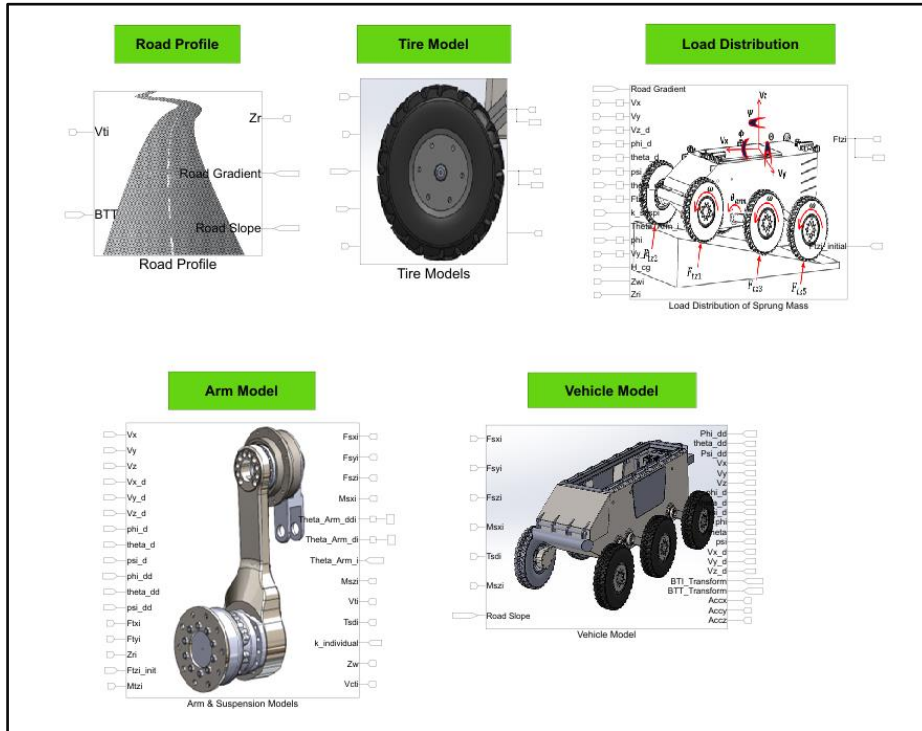
- [1]. Kale, A. (2020). Mobility Improvement of Wheeled Military Vehicles Using Preview Controlled Active Ride Height System (Master's thesis, METU).
- [2]. Tavoosi, V., Marzban Rad, J., & Mirzaei, R. (2018). Vertical Dynamics Modeling and Simulation of a Six-Wheel Unmanned Ground Vehicle. *Automotive Science and Engineering*, 8(2), 2709-2729.
- [3]. Pico, N., Park, S. H., Yi, J. S., & Moon, H. (2022). Six-Wheel Robot Design Methodology and Emergency Control to Prevent the Robot from Falling down the Stairs. *Applied Sciences*, 12(9), 4403.
- [4]. Chen, S., Li, X., Zhou, J., Wu, W., Yuan, S., & Liu, S. (2017). Modelling the vertical dynamics of unmanned ground vehicle with rocker suspension. In 2017 IEEE International Conference on Mechatronics and Automation (ICMA) (pp. 370-375). IEEE.
- [5]. Fauroux, J. C., Chapelle, F., & Bouzgarrou, B. C. (2006). A new principle for climbing wheeled robots: Serpentine climbing with the open WHEEL platform. In 2006 IEEE/RSJ International Conference on Intelligent Robots and Systems (pp. 3405-3410). IEEE.
- [6]. Seidla, A. (2008). Actively articulated suspension for a four-wheeled vehicle. In DS 50: Proceedings of NordDesign 2008 Conference, Tallinn, Estonia, 21.-23.08. 2008.
- [7]. Bayar, K. (2006). Modeling of the dynamics of multi-axle steered vehicles (Master's thesis, METU).
- [8]. Zhang, Y., Khajepour, A., & Huang, Y. (2018). Multi-axle/articulated bus dynamics modeling: a reconfigurable approach. *Vehicle System Dynamics*, 56(9), 1315-1343.
- [9]. Ni, J., & Hu, J. (2016). Dynamic modelling and experimental validation of a skid-steered vehicle in the pivotal steering condition. *Proceedings of the Institution of Mechanical Engineers, Part D: Journal of Automobile Engineering*, 231(2), 225-240.
- [10]. Ni, J., Hu, J., & Xiang, C. (2020). A review for design and dynamics control of unmanned ground vehicle. *Proceedings of the Institution of Mechanical Engineers, Part D: Journal of Automobile Engineering*, 235(4), 1084-1100.

- [11]. Fauroux, J. C., & Vaslin, P. P. P. (2010). Modeling, experimenting, and improving skid steering on a 6× 6 all-terrain mobile platform. *Journal of Field Robotics*, 27(2), 107-126.
- [12]. Yacoub, M., & Ali, A. (2020, August). Propulsion Dynamic Requirements Analysis for Multi-Axle Skid-Steer Wheeled Vehicles. In *International Design Engineering Technical Conferences and Computers and Information in Engineering Conference* (Vol. 83938, p. V004T04A002). American Society of Mechanical Engineers.
- [13]. Rajamani, R. (2005). *Vehicle Dynamics and Control*. Springer.
- [14]. Bayar, K., Wang, J., & Rizzoni, G. (2012). Development of a vehicle stability control strategy for a hybrid electric vehicle equipped with axle motors. *Proceedings of the Institution of Mechanical Engineers, Part D: Journal of automobile engineering*, 226(6), 795-814.
- [15]. Pacejka, H. (2005). *Tire and vehicle dynamics*. Elsevier.
- [16]. Kang, J., Kim, W., Yi, K., Jung, S., & Lee, J. (2010). Skid steering based driving control of a robotic vehicle with six in-wheel drives. *SAE International Journal of Passenger Cars-Mechanical Systems*, 3(2010-01-0087), 131-144.
- [17]. Unlusoy, Y. Samim. *Performance of Road Vehicles*. Lecture Notes.
- [18]. Karaođlan, M. U., & Kuralay, N. S. (2019). Determination of dynamic axle load using suspension deflection method for the load distribution optimisation of multi-axle vehicles. *International Journal of Vehicle Design*, 80(2-4), 89-102.
- [19]. Jazar, R. (2014). *Vehicle dynamics: Theory and application*. Cham: Springer.
- [20]. PUTGÜL, Y., & ALTIPARMAK, D. (2016). Taşıt Süspansiyon Sistemi Çeşitleri ve Ön Düzen Geometrisine Etkileri. *Politeknik Dergisi*, 19(2), 195-202.
- [21]. Bauer, W. (2011). *Hydropneumatic suspension systems* (pp. 19-66). Berlin: Springer.
- [22]. Kocakulak, T., Çokgünlü, S. A., & Konukseven, E. İ. (2019). 6x6 Taktik Tekerlekli Askeri Kara Platformu Üzerinde Kullanılacak Hidropnömatik Süspansiyon Sisteminin Modellenmesi ve Sistem Elemanlarının Sönümlenmeye Etkisinin İncelenmesi. In *International Symposium on Automotive Science and Technology* (pp. 99-110).
- [23]. Gardulski, J. (2007). Application of simulation researches in diagnostic's of vehicle hydropneumatic suspension. *Transport Problems*, 2(1), 13-21.

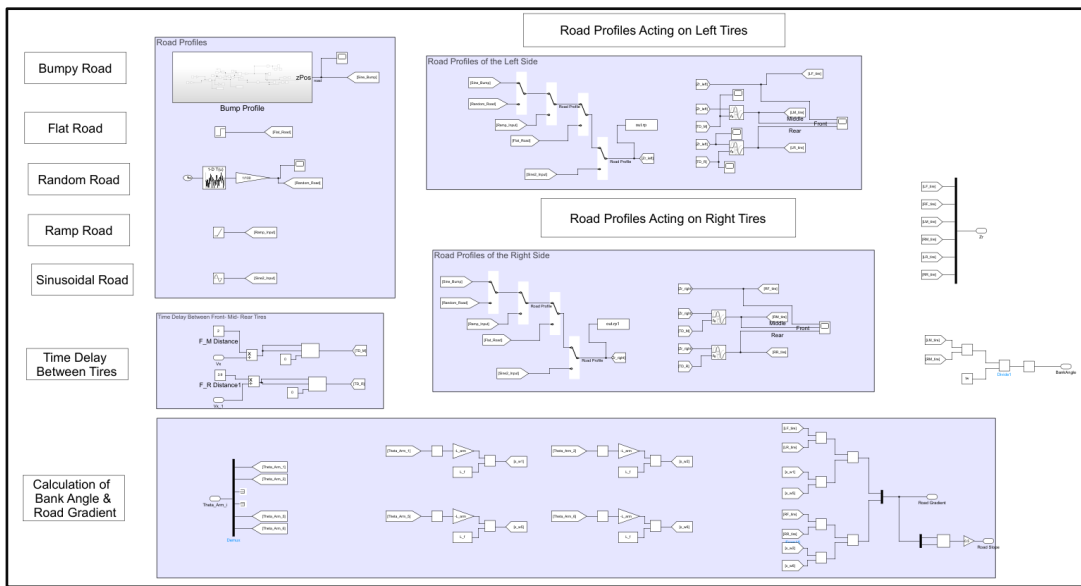
- [24]. Sağlam, F. (2016). Optimization of Ride Comfort for Vehicles Equipped With Passive and Active Hydro-Pneumatic Suspensions (Doctoral Thesis, METU).
- [25]. Joo, F. R. (1991). Dynamic analysis of a hydropneumatic suspension system (Master's thesis, 1991). Montr. al: Concordia University.
- [26]. Joo, S. H., & Lee, J. H. (2012). A dynamic modeling of 6× 6 skid type vehicle for real time traversability analysis over curved driving path. *Journal of Institute of Control, Robotics and Systems*, 18(4), 359-364.
- [27]. Kaloust, J. (2006). A robust nonlinear skid-steering control design applied to the MULE (6x6) unmanned ground vehicle. In *Unmanned Systems Technology VIII* (Vol. 6230, pp. 751-760). SPIE.
- [28]. Hillegass, M. J., Faller, J. G., Bounds, M. S., El-Gindy, M., & Chae, S. (2005, January). Validating the vertical dynamic performance of a multi-wheeled combat vehicle computer simulation model. In *ASME International Mechanical Engineering Congress and Exposition* (Vol. 42150, pp. 31-40).
- [29]. Kılıç, V. (2003). Generation of Deterministic Data From Signals of Known Power Spectral Density, ME 513 Vehicle Dynamics Term Project, METU.
- [30]. Pacejka, H. B. (2012). Tire characteristics and vehicle handling and stability. *Tyre and Vehicle Dynamics*, 2nd ed.; Elsevier: Amsterdam, The Netherlands, 1-60.
- [31]. Pacejka, H. B., & Besselink, I. J. M. (1997). Magic formula tyre model with transient properties. *Vehicle system dynamics*, 27(S1), 234-249.
- [32]. Sağlam, F., & Ünlüsoy, Y. S. (2014) Hidro-Pnömatik Süspansiyonlu Araçlar İçin Tümlüşük Sürüş Konforu ve Yükseklik Kontrolü. *OTEKON*, 14(7), 26-27.
- [33]. Reddy, C. V., Shankapal, S. R., & Gowda, M. H. (2014). Modelling and simulation of hydropneumatic suspension for a car. *SASTech-Technical Journal of RUAS*, 13(1), 24-30.
- [34]. Sağlam, F., & Ünlüsoy, Y. S. (2016). Birbirine Bağlı Hidro-Pnömatik Süspansiyon Sistemine Sahip Üç Aksli Bir Aracın Sürüş Konforu İçin Optimizasyonu. *OTEKON*, 16(8), 23-24.
- [35]. Oscarsson, M. (2015). A hydropneumatic suspension parameter study on heavy multi-axle vehicle handling.

APPENDIX

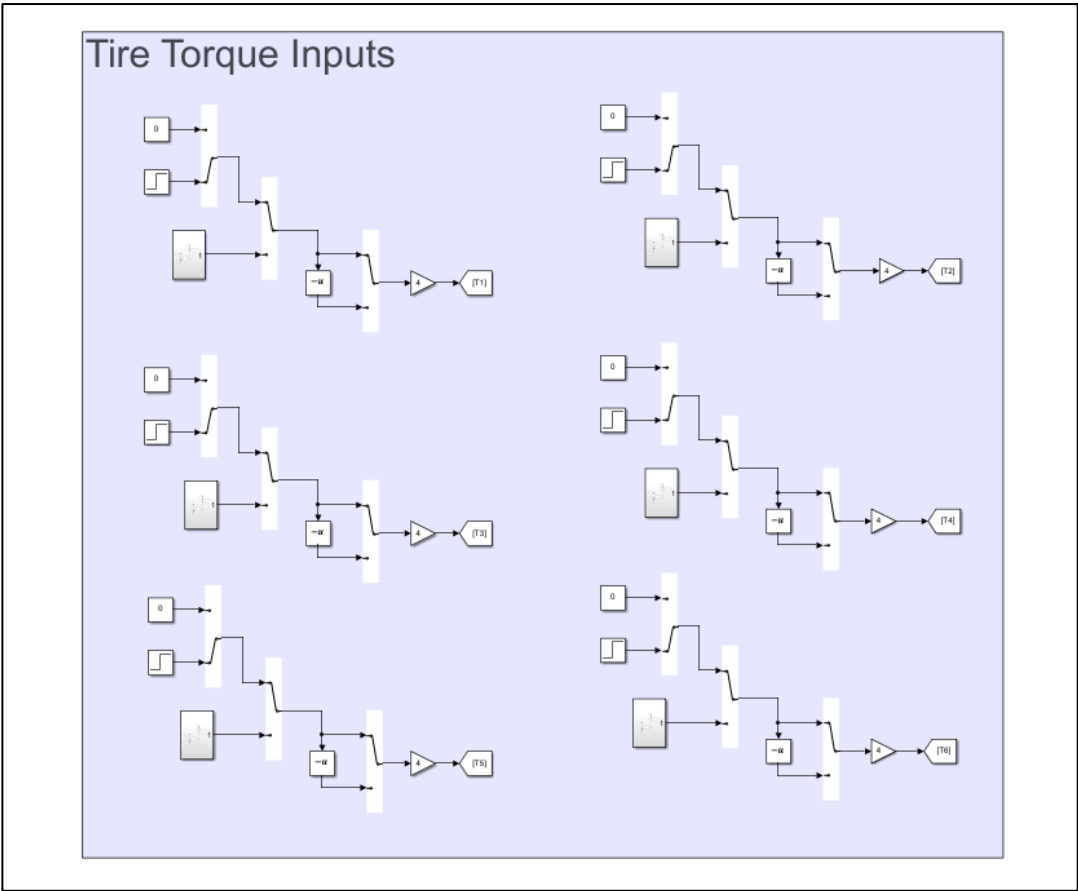
A. Simulink Model



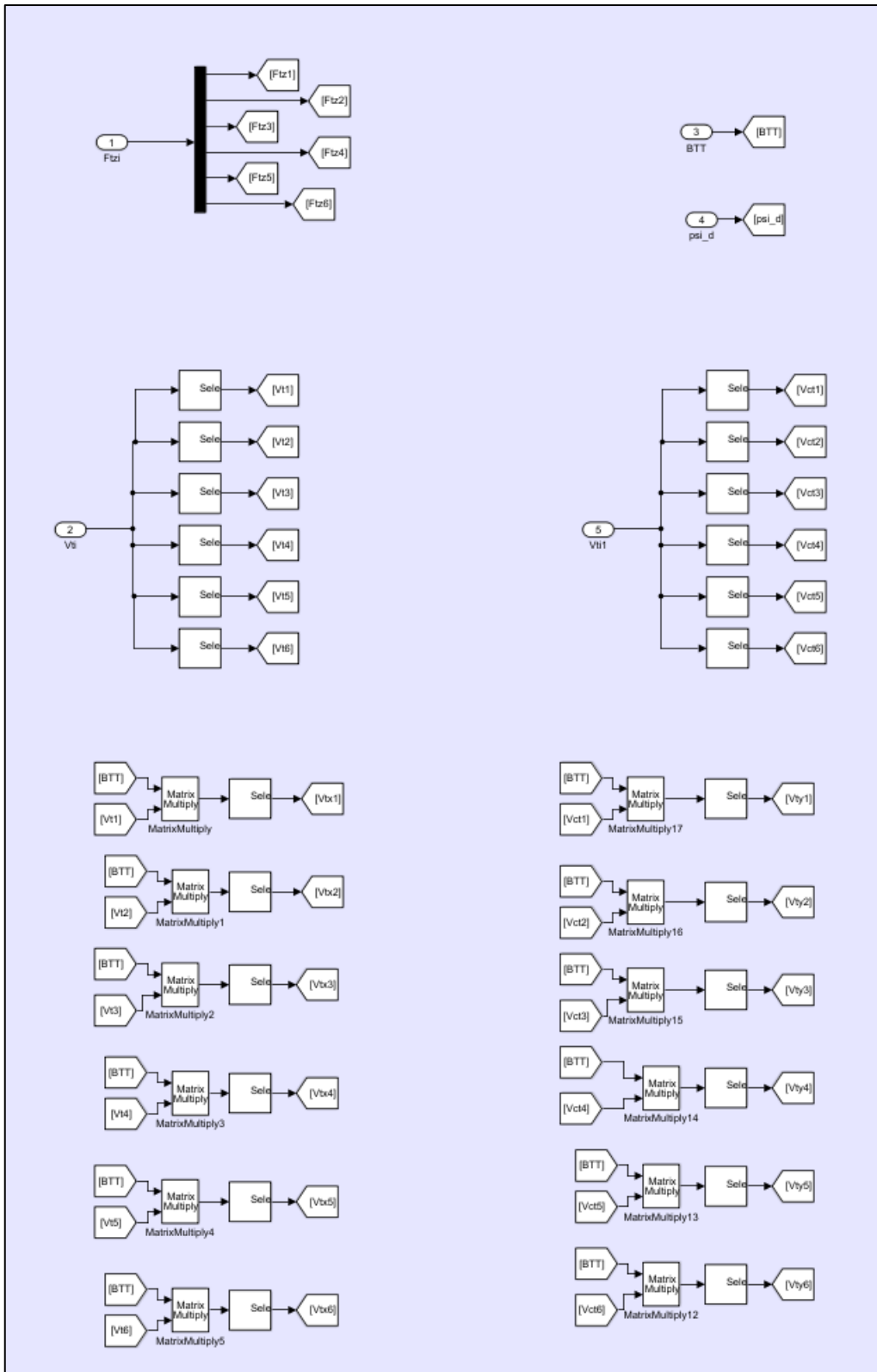
Appendix A - 1. Overview of the Vehicle Model in Simulink



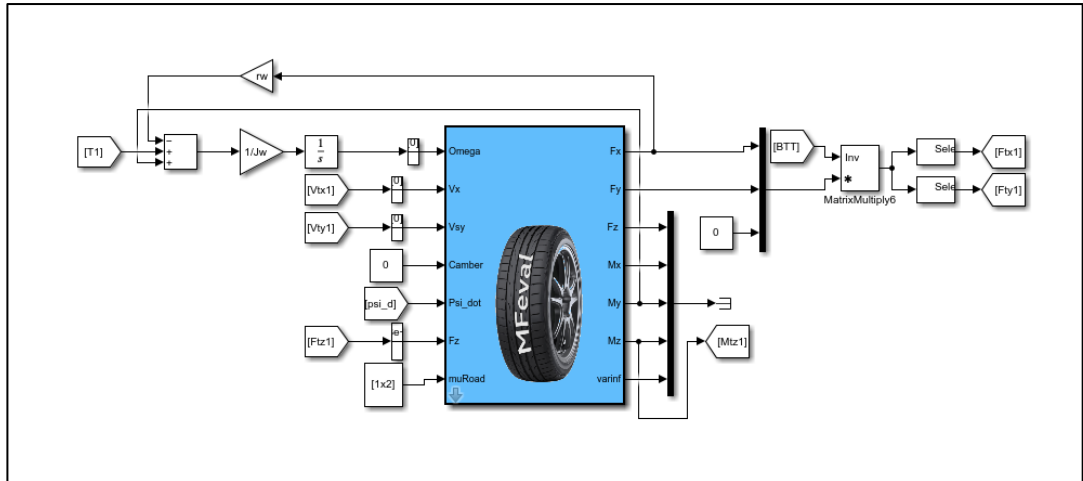
Appendix A - 2. Road Profile Subsystem in Simulink



Appendix A - 3. Torque Inputs to the Tires in Tire Subsystem of Simulink Model

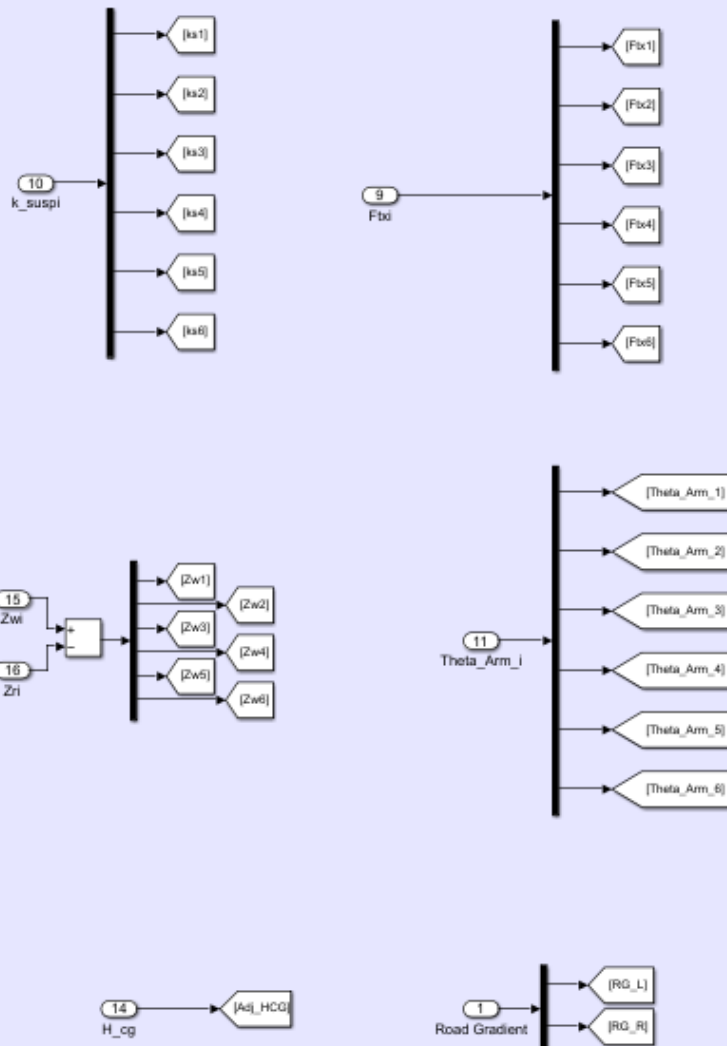


Appendix A - 4. Inputs to the Tire Model Subsystem in Simulink Model

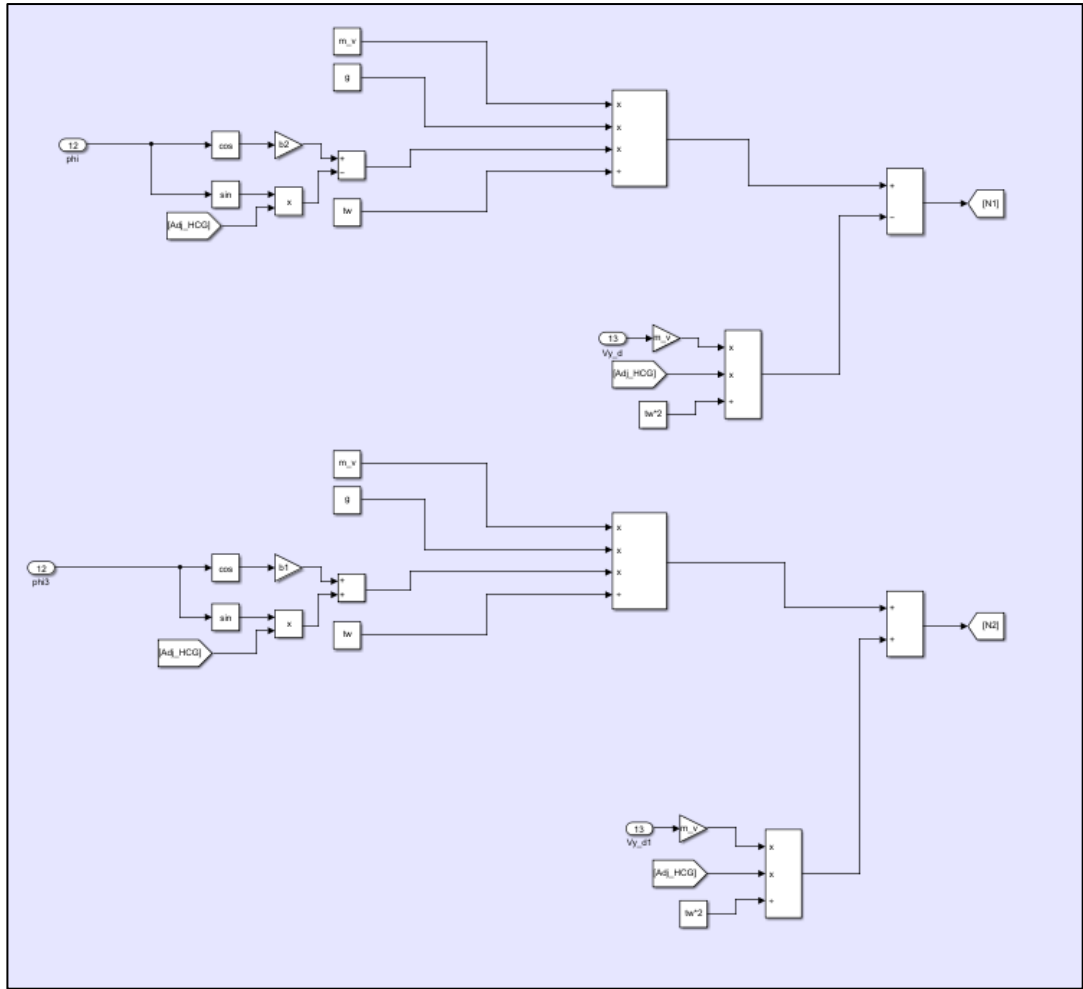


Appendix A - 5. Magic Formula Tire Model in Simulink with Wheel Dynamics Equation and Frame Transformation

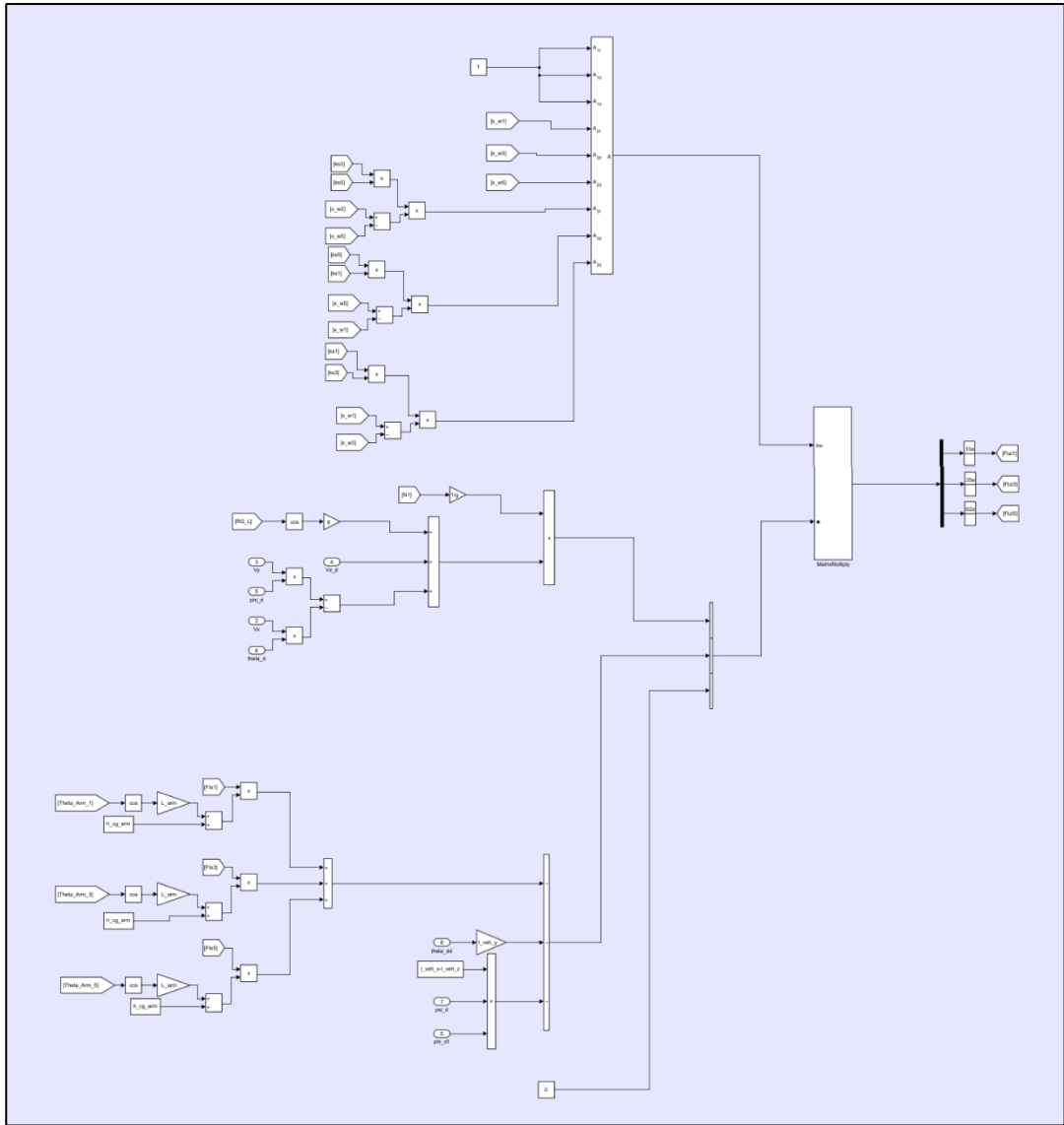
Inputs to the System



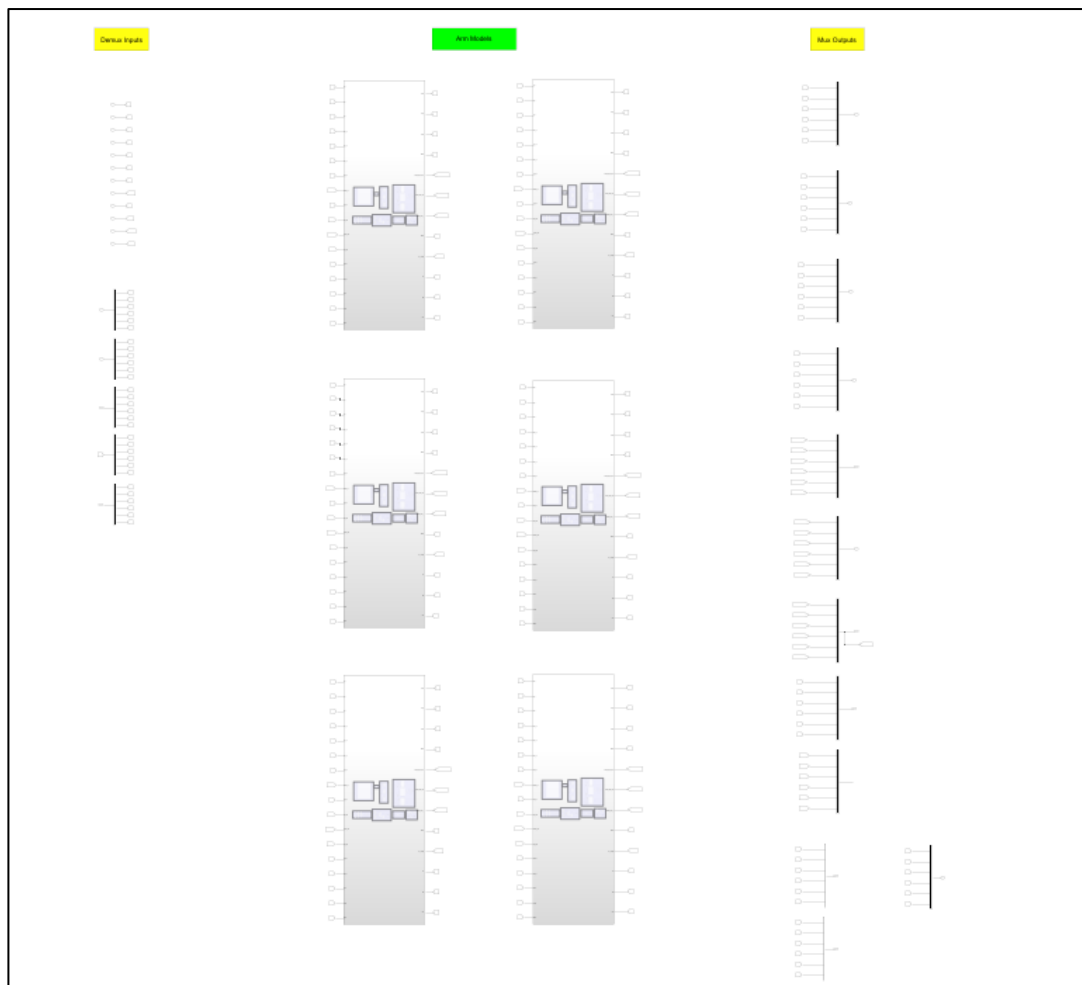
Appendix A - 6. Inputs to the Load Distribution Subsystem



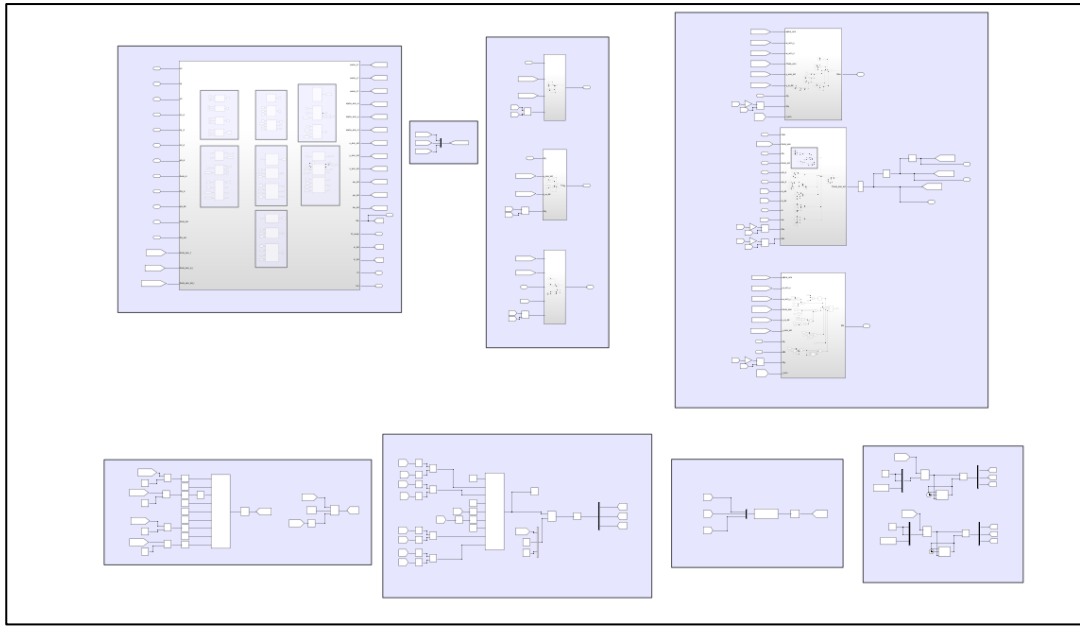
Appendix A - 7. Lateral Load Distribution Equations



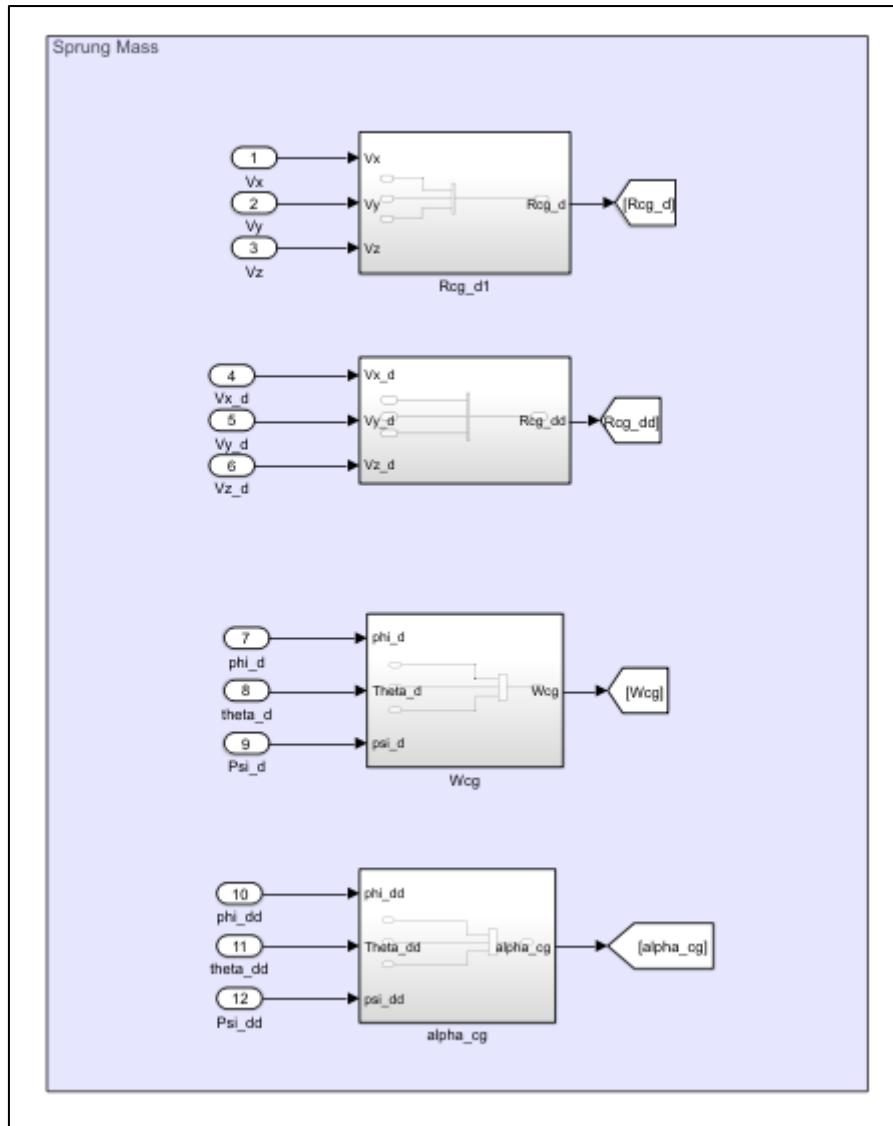
Appendix A - 8. Longitudinal Load Distribution Equations for Left Tires in Simulink



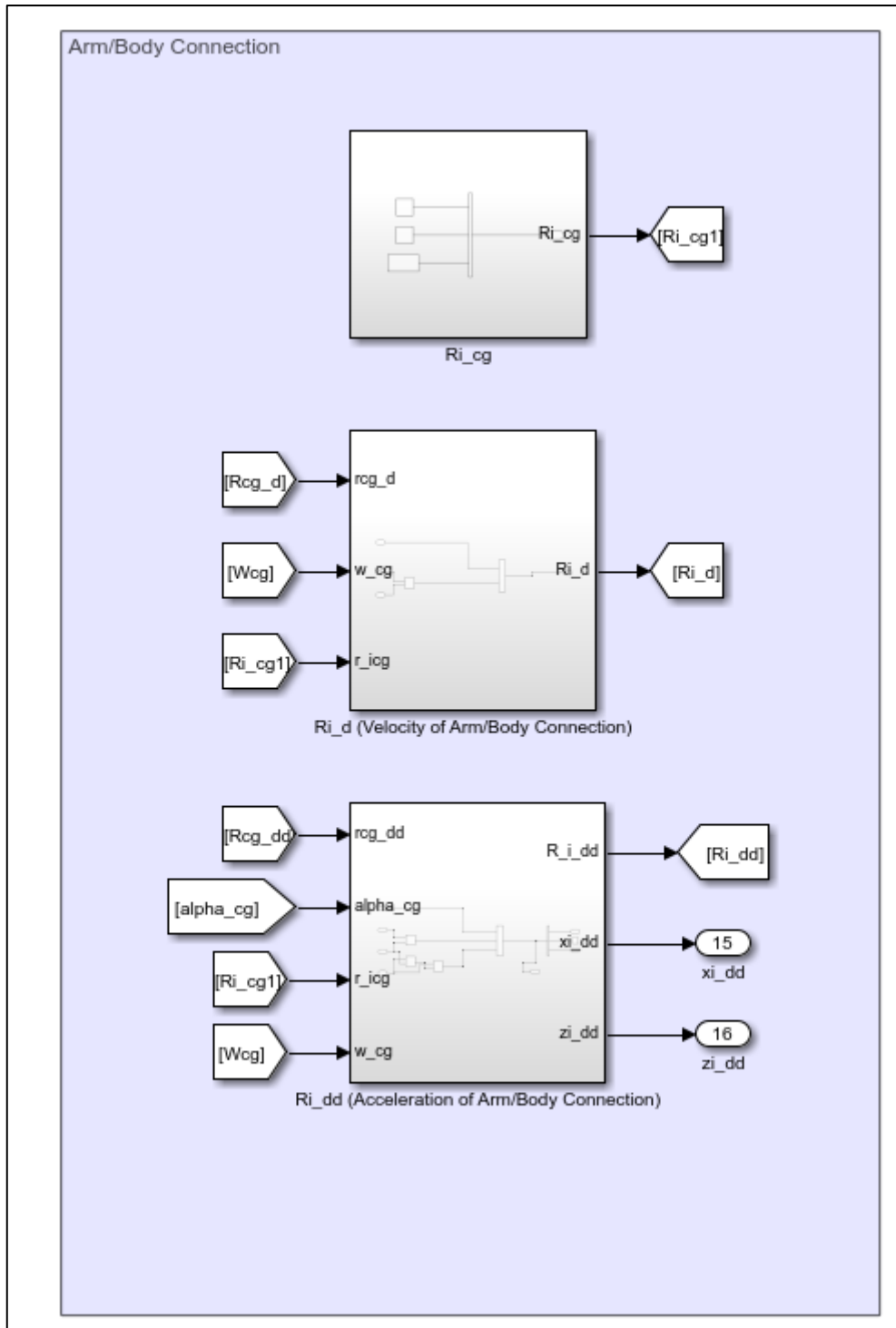
Appendix A - 9. Overview of the Arm Model Subsystem Containing Subsystems for Six Arms



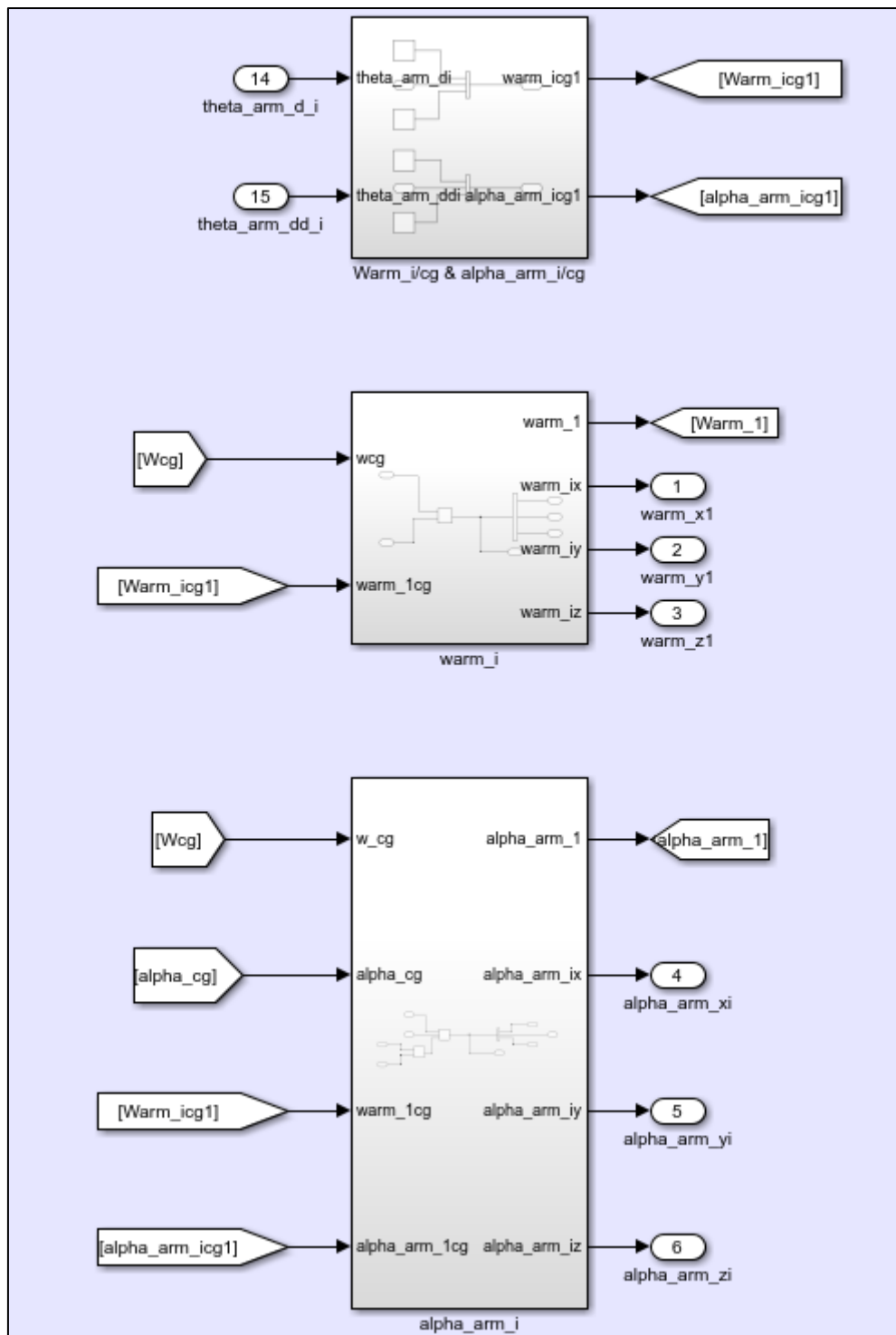
Appendix A - 10. Overview of a Single Arm Model Subsystem Containing Equations of Motions and Kinematic Relations



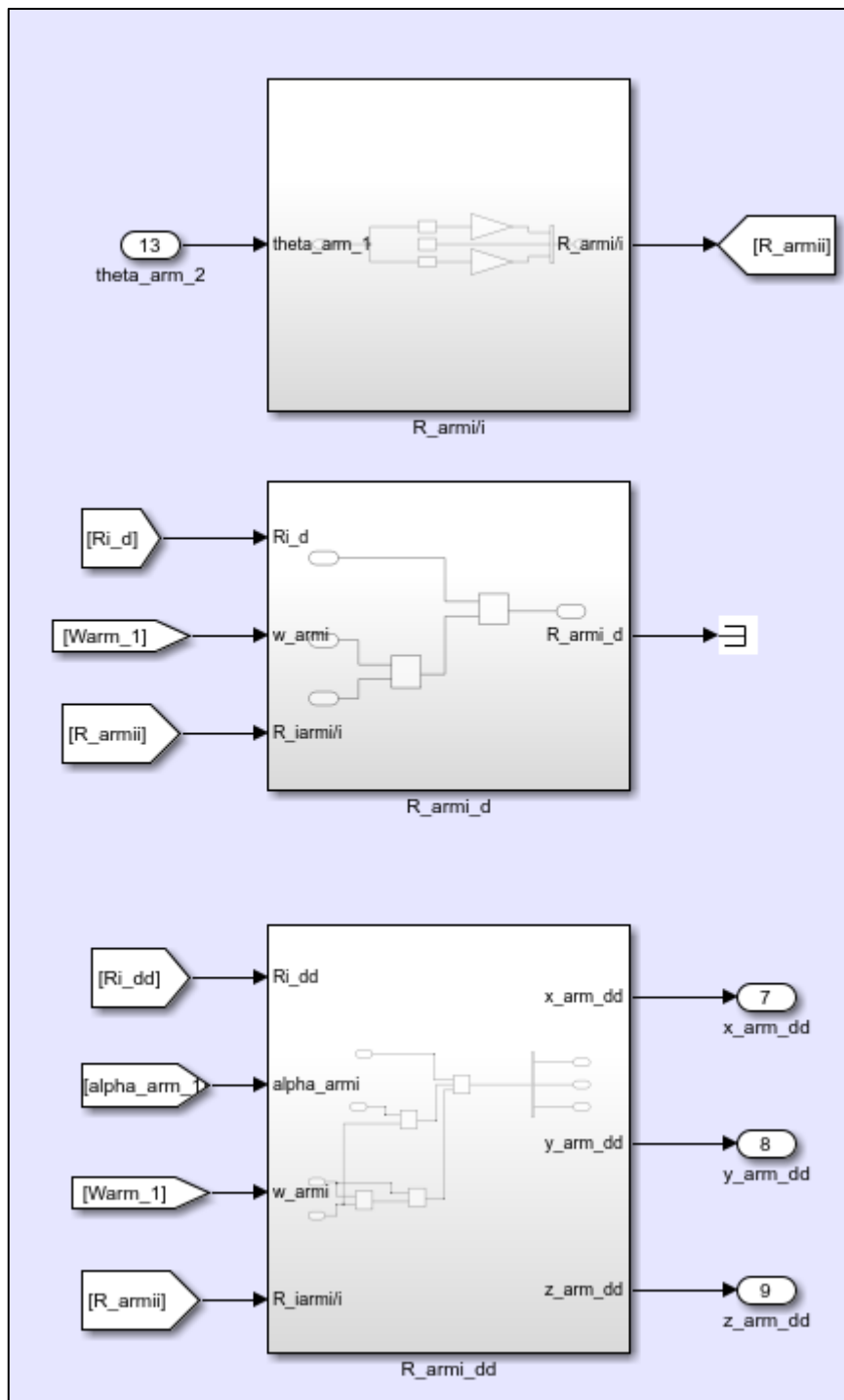
Appendix A - 11. Kinematic Relations for Gathering Body Motions



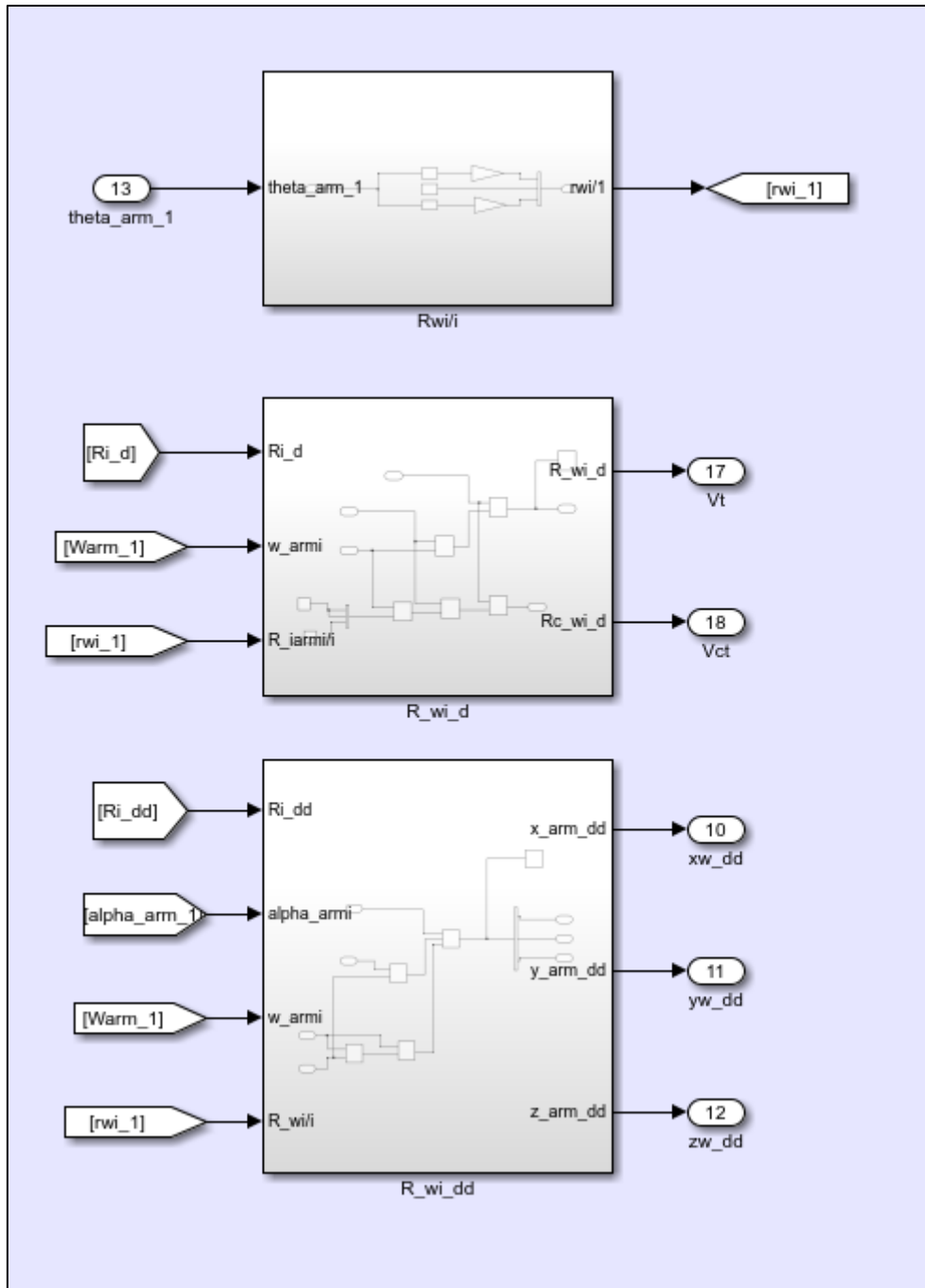
Appendix A - 12. Subsystems of Equations for Deriving Arm and Body Connections



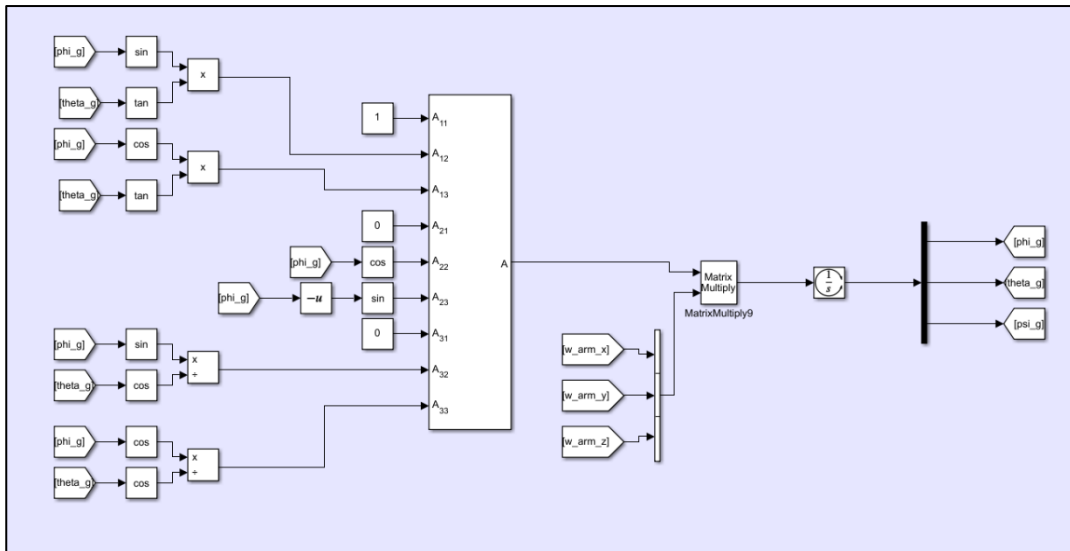
Appendix A - 13. Subsystems of Equations for Deriving Arm Rotational Motion using Kinematic Relations Between Body and Arms



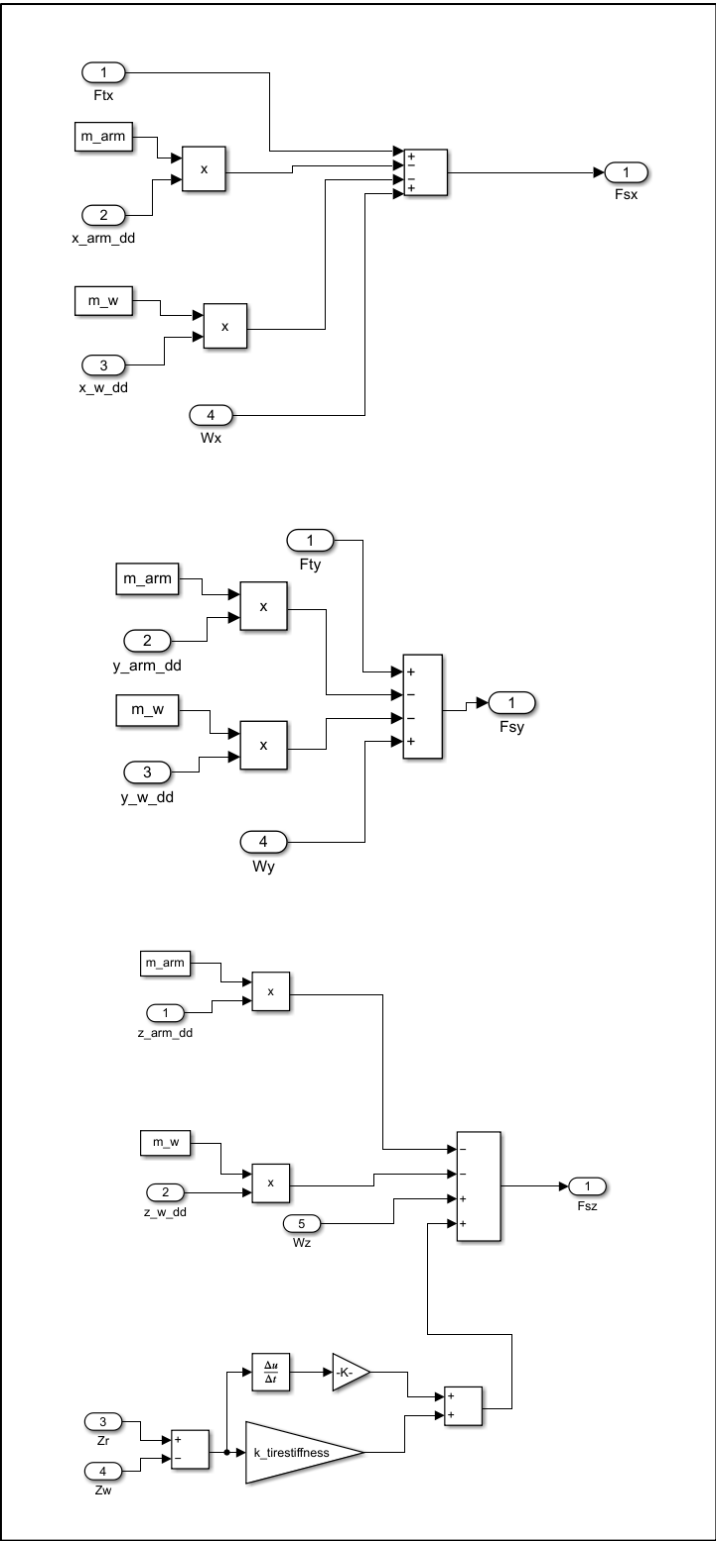
Appendix A - 14. Kinematic Relations for Deriving the Motion of Arm Center



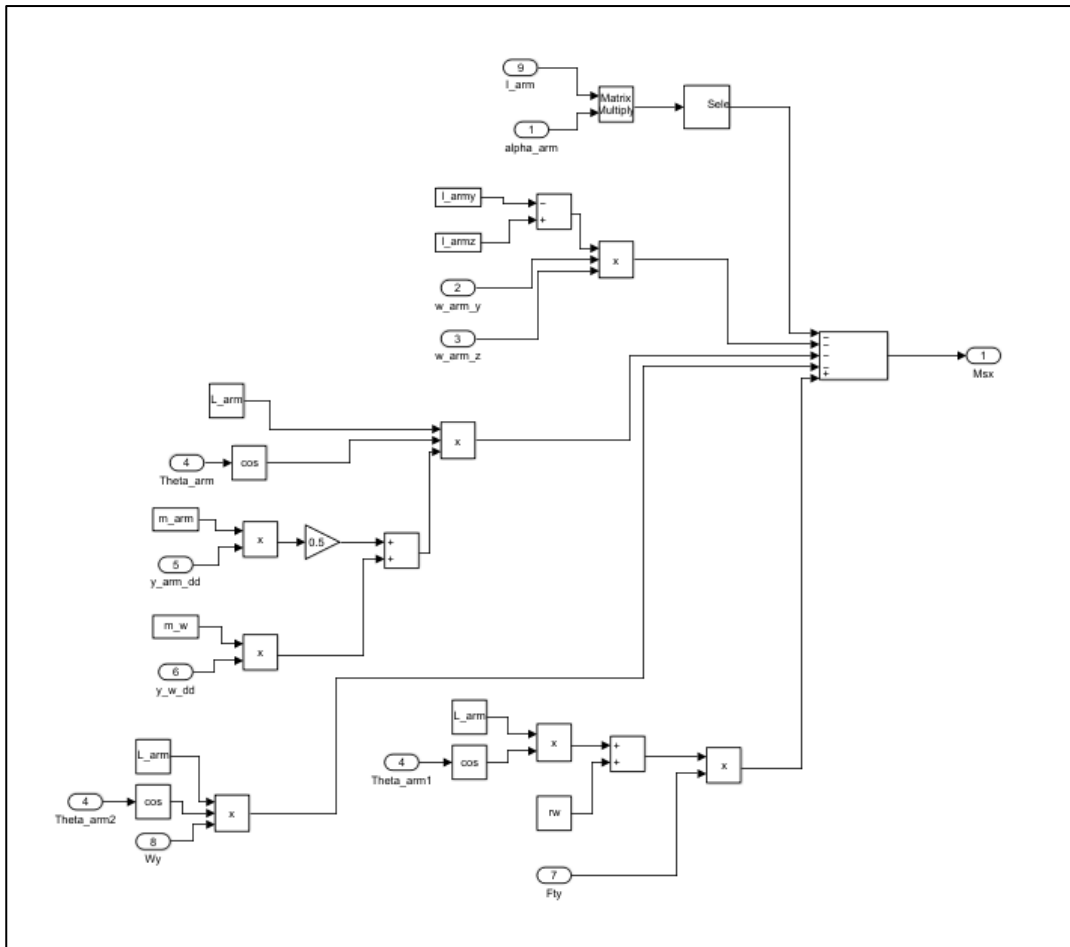
Appendix A - 15. Kinematic Relations for Deriving Motion of Tire Center and Tire Ground Contact Points



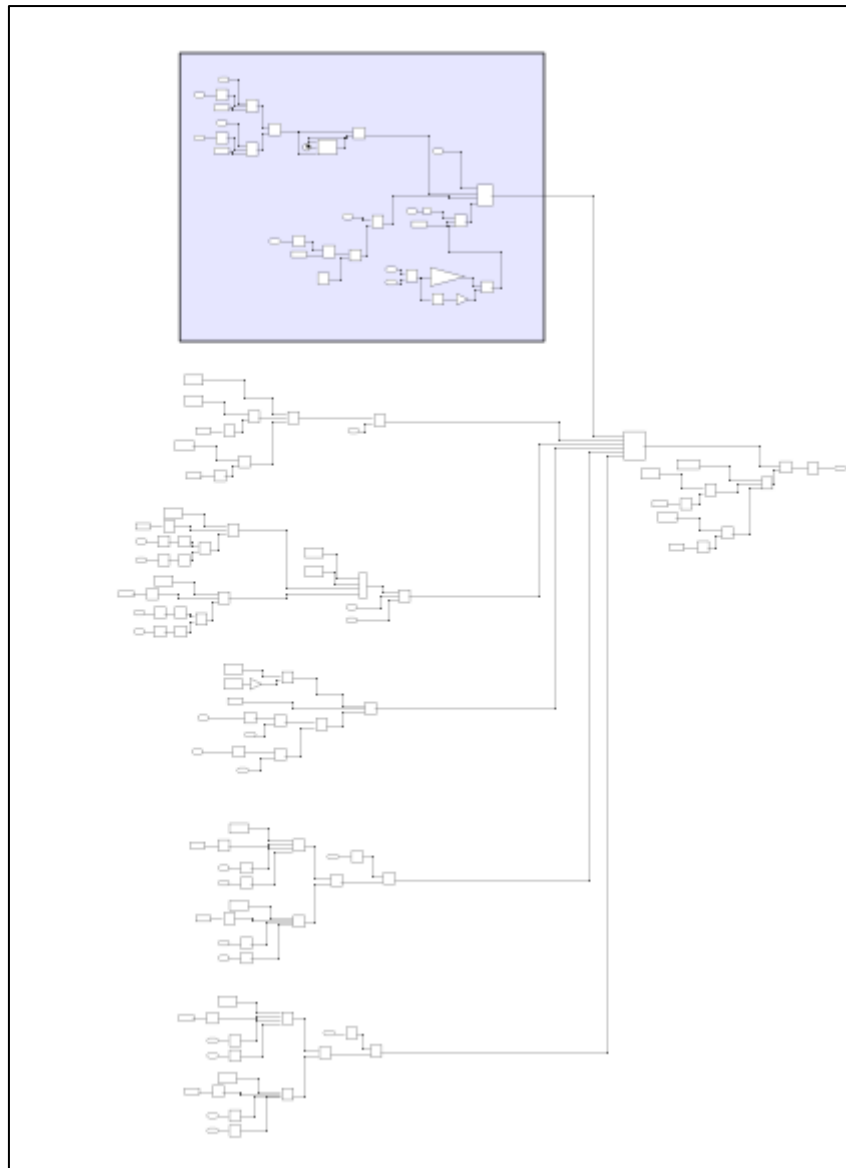
Appendix A - 16. Equations for Calculating Euler Angles for Arms



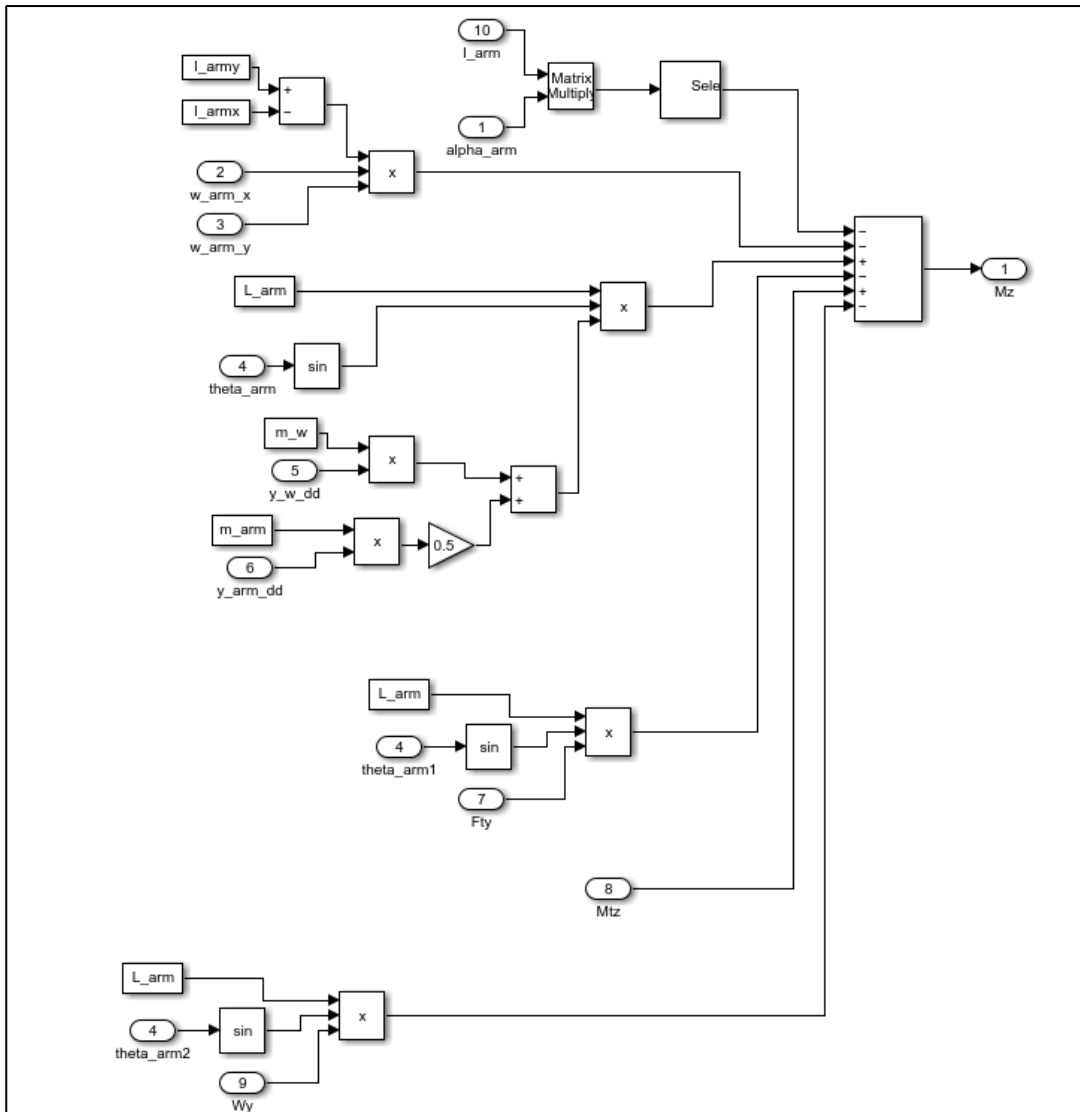
Appendix A - 17. Force Equations for Arms



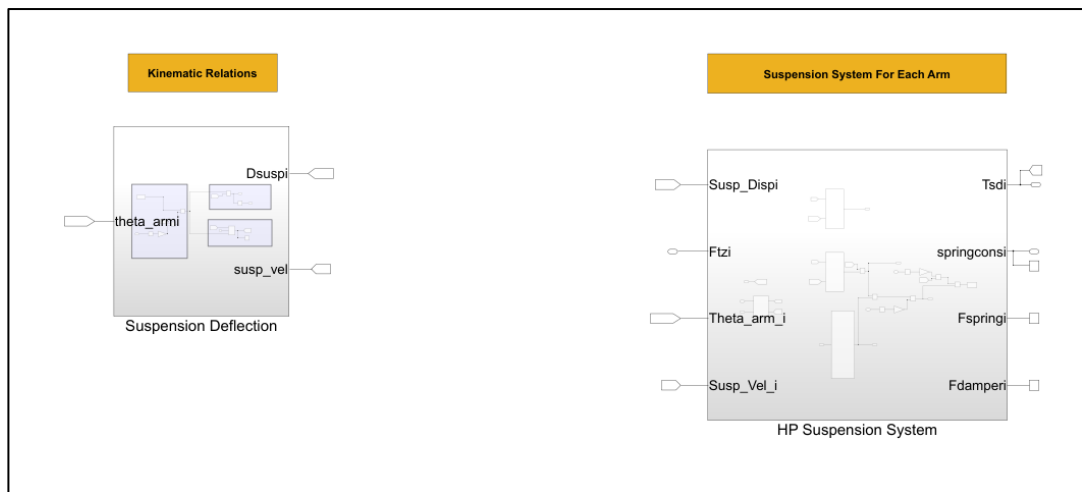
Appendix A - 18. Moment Equation Along The Longitudinal Axis for Arms



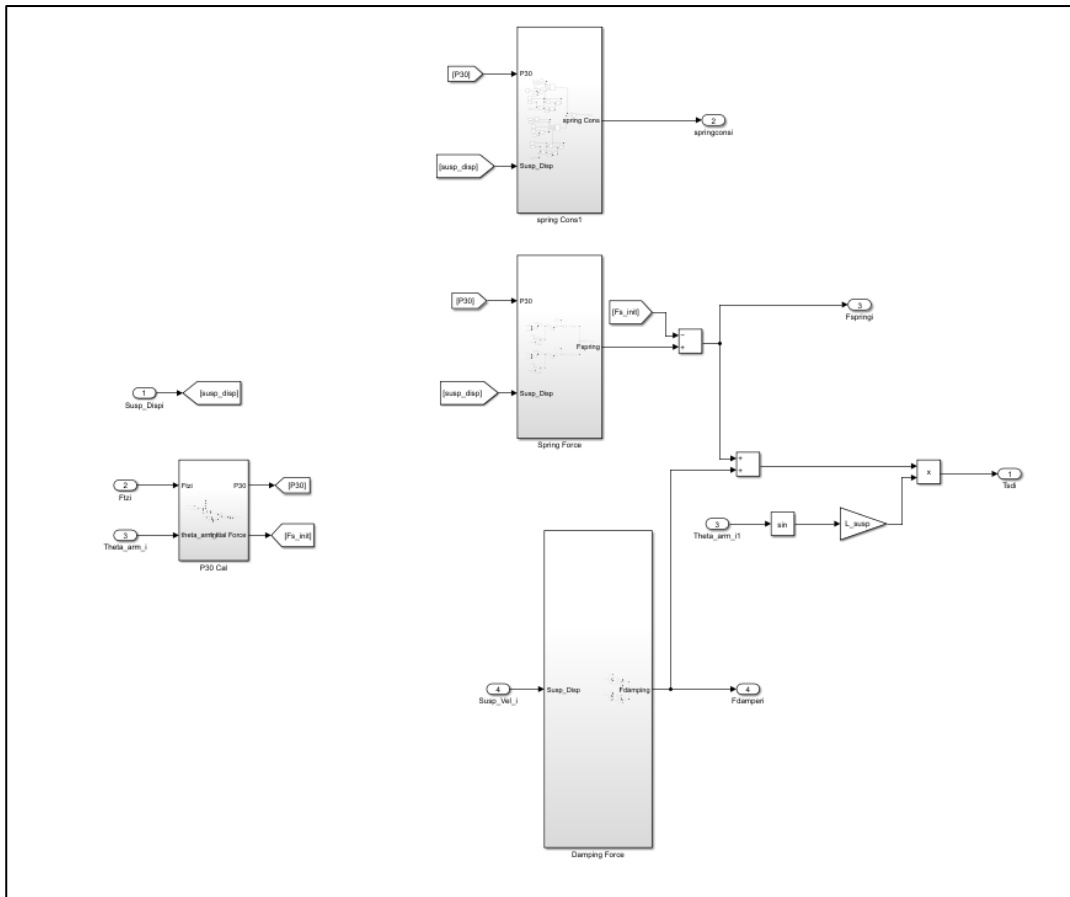
Appendix A - 19. Moment Equation Along the Lateral Axis for Arms



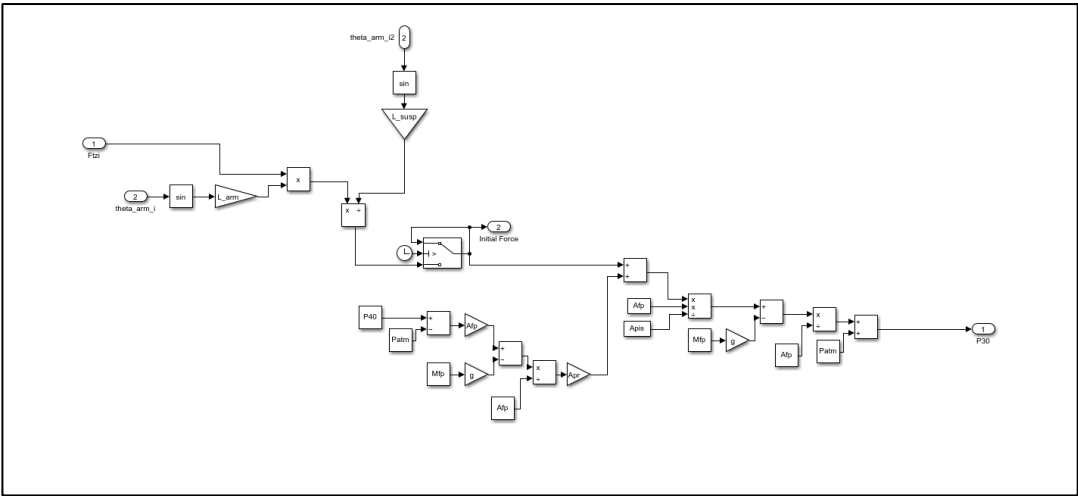
Appendix A - 20. Moment Equation Along the Vertical Axis for Arms



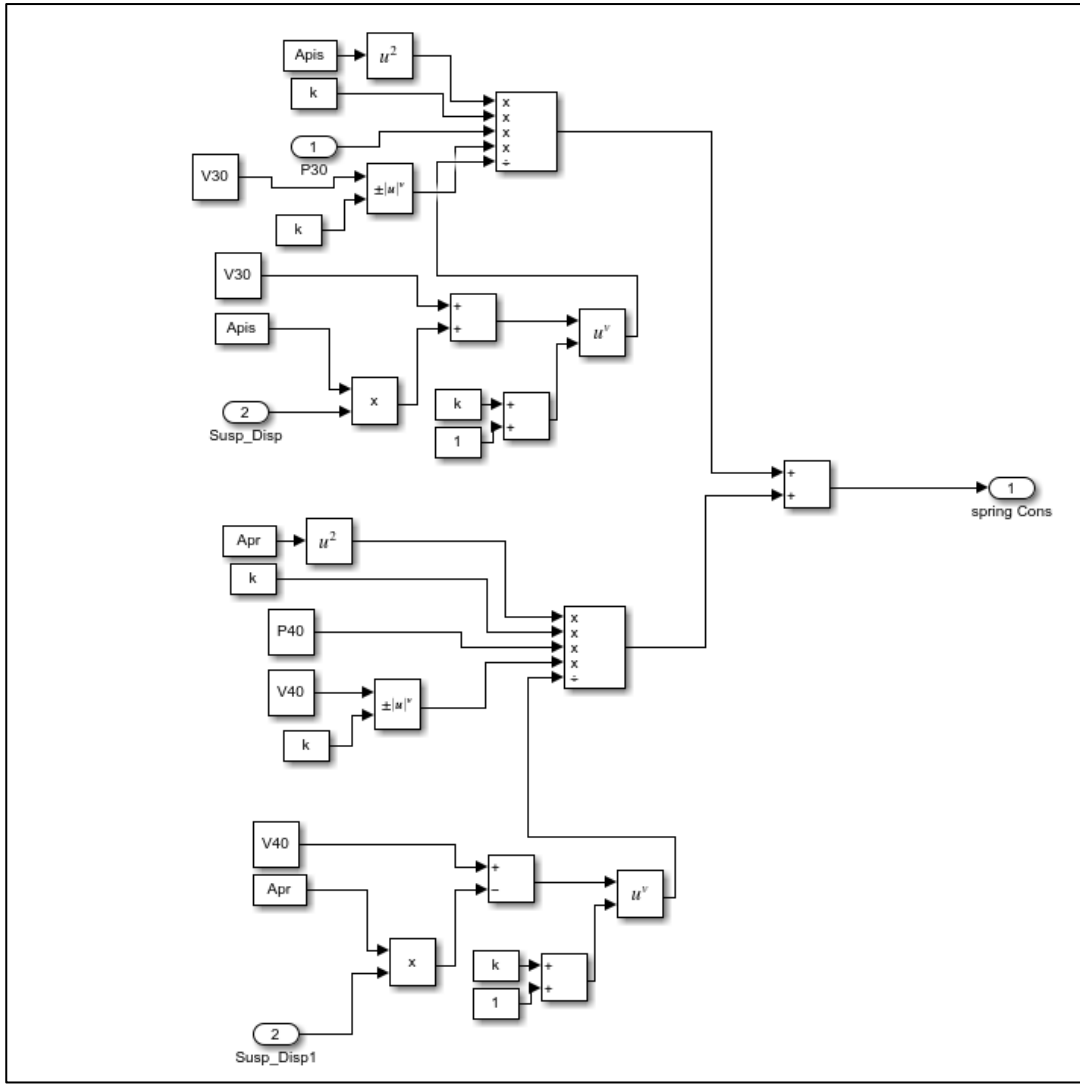
Appendix A - 21. Overview of the Suspension System



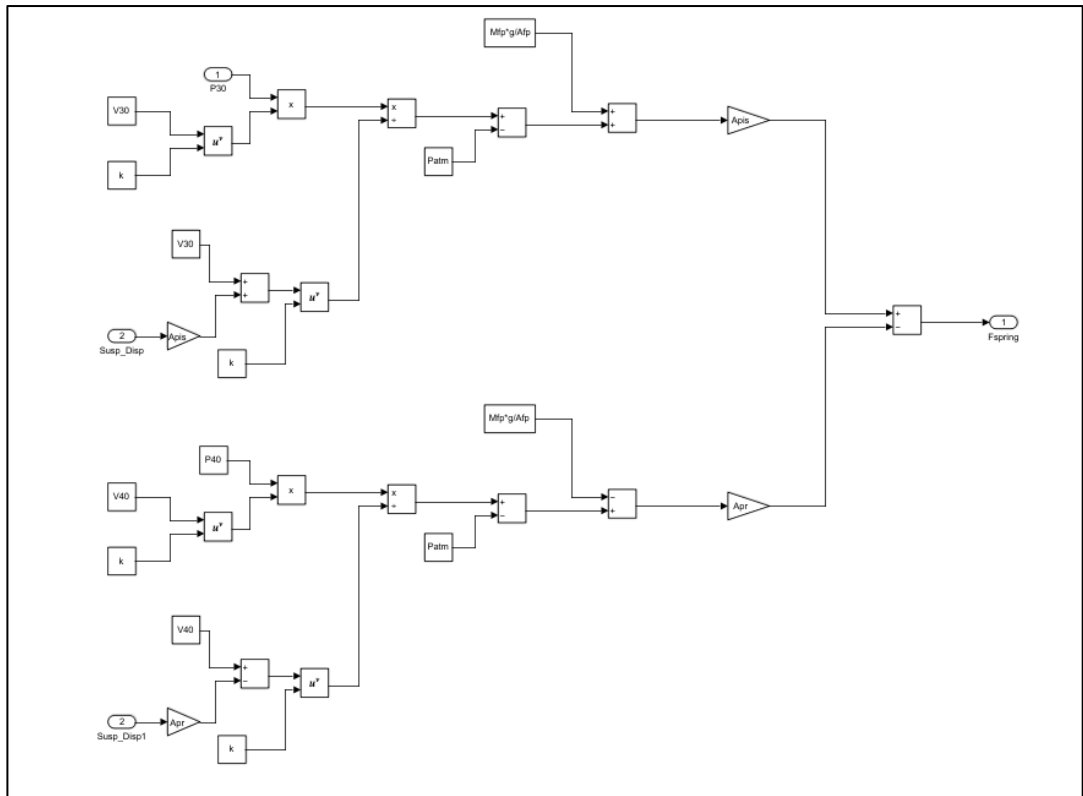
Appendix A - 22. Subsystems in the Suspension Model



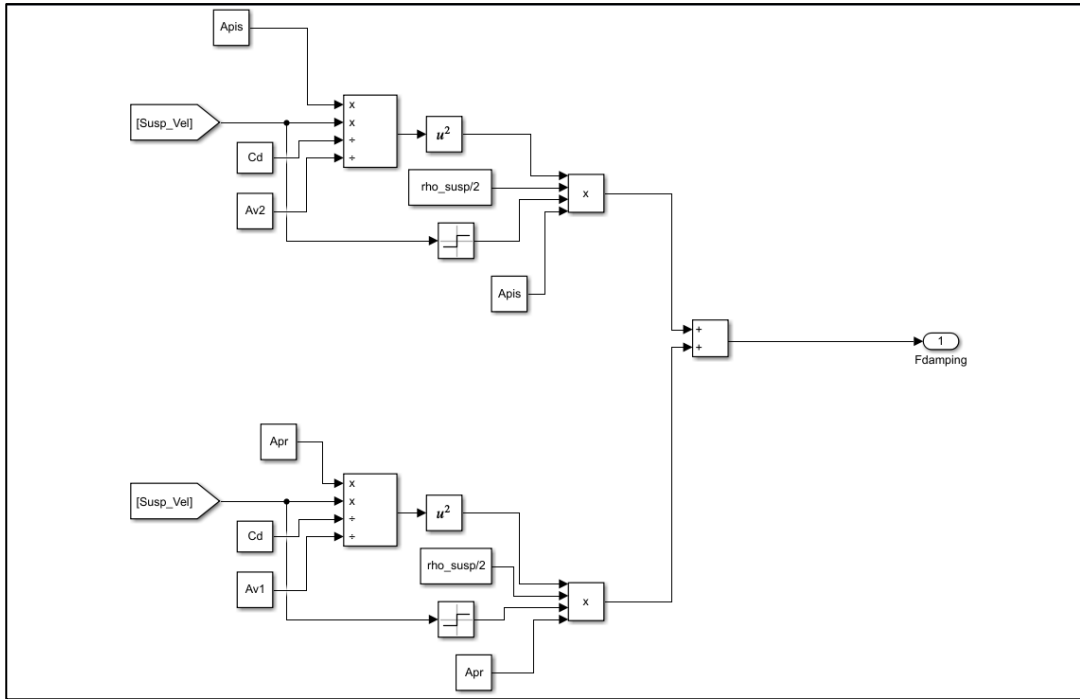
Appendix A - 23. Calculations of Initial Gas Pressure



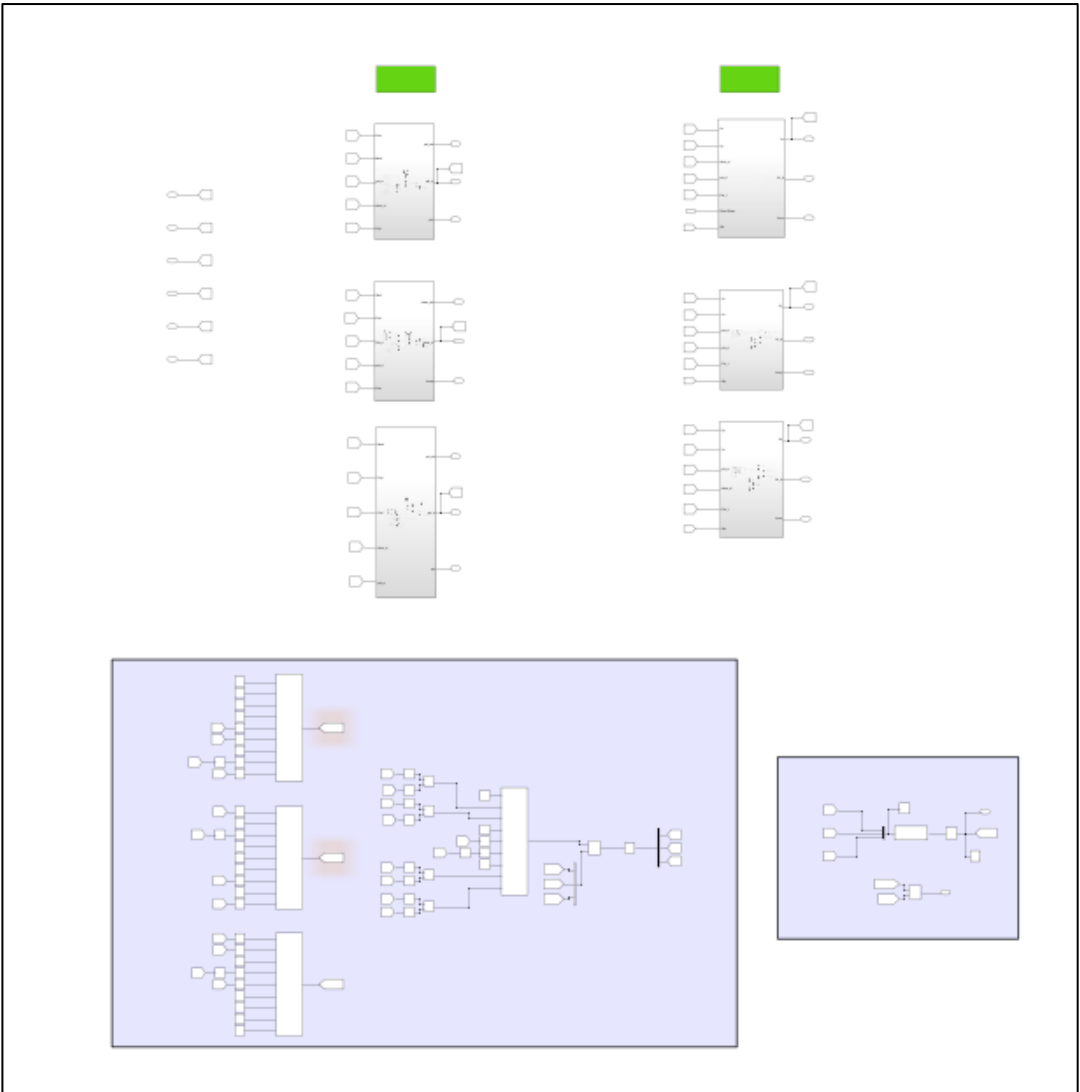
Appendix A - 24. Calculations for Spring Constant



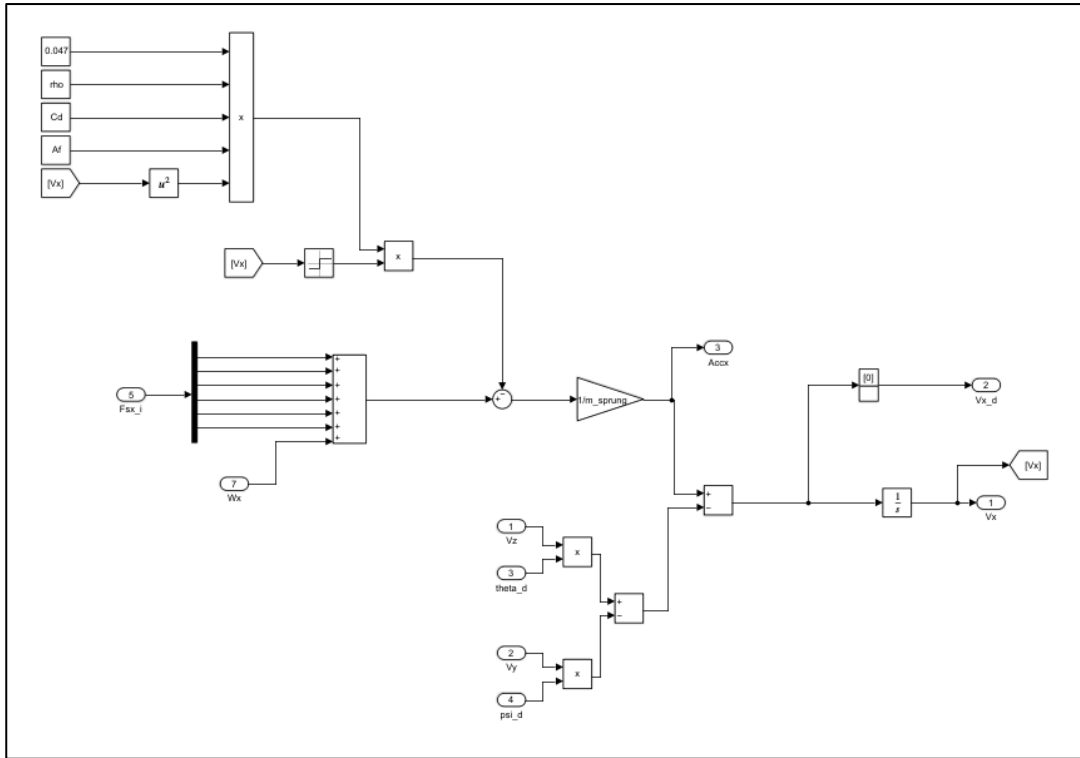
Appendix A - 25. Calculations of the Spring Force in Suspensions



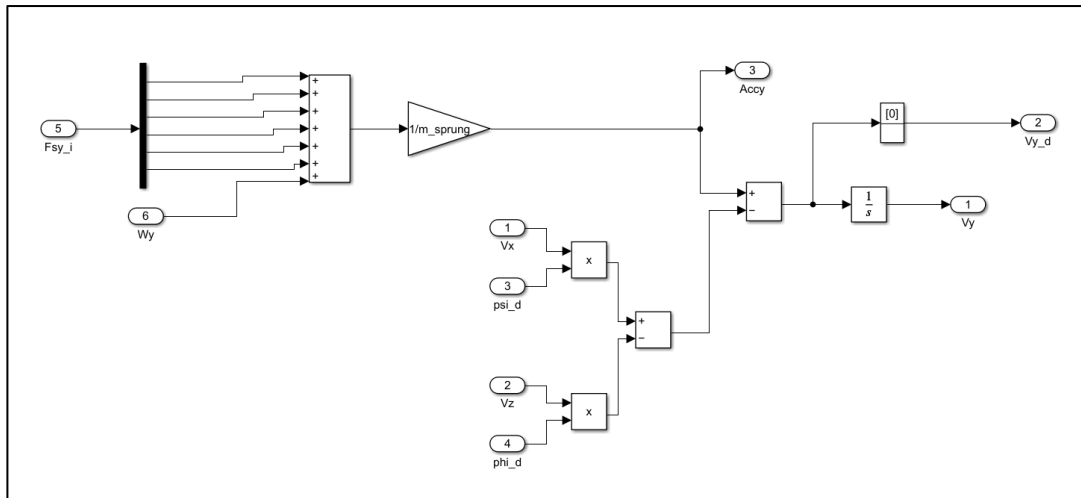
Appendix A - 26. Calculations of the Damping Force in Suspensions



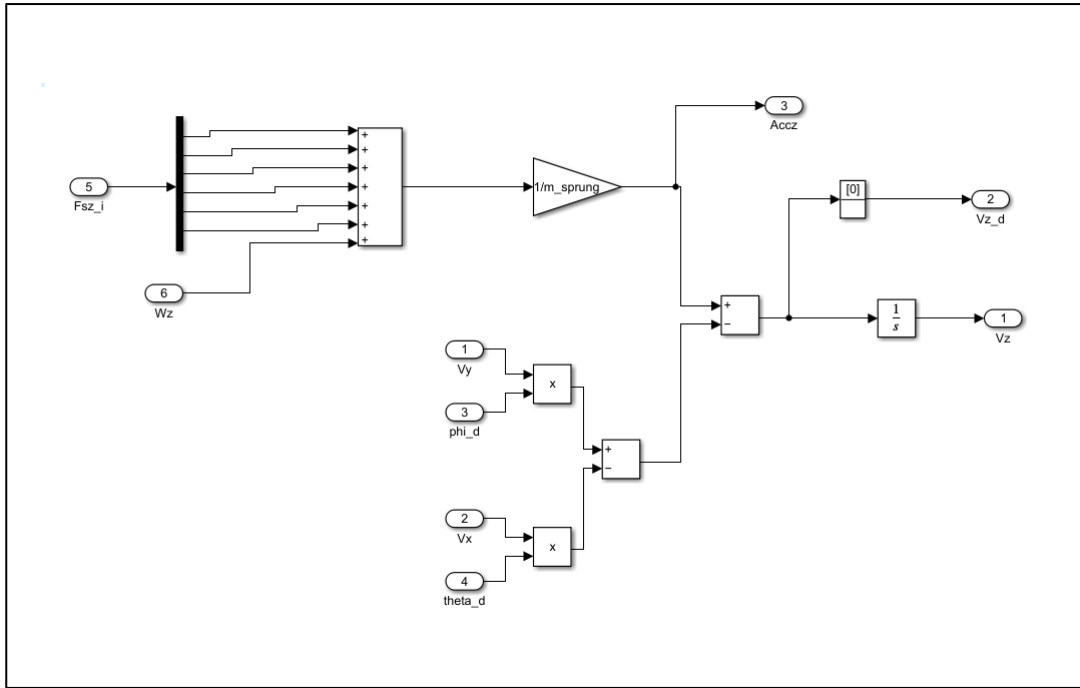
Appendix A - 27. Overview of the Vehicle Body Subsystem



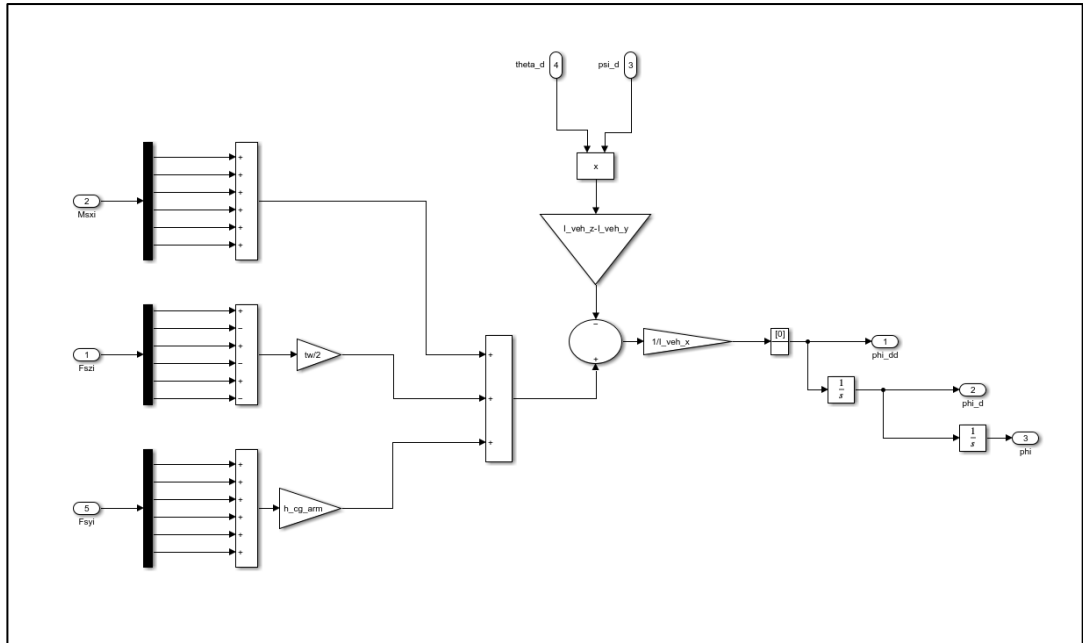
Appendix A - 28. Translational Equation of Motion Along the Longitudinal Axis



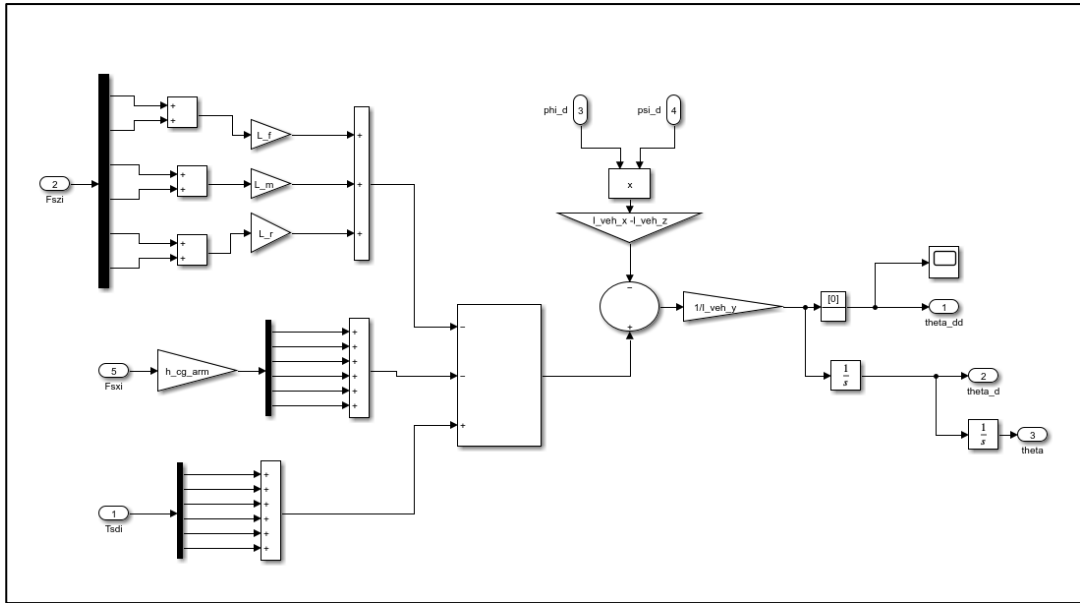
Appendix A - 29. Translational Equation of Motion Along the Lateral Axis



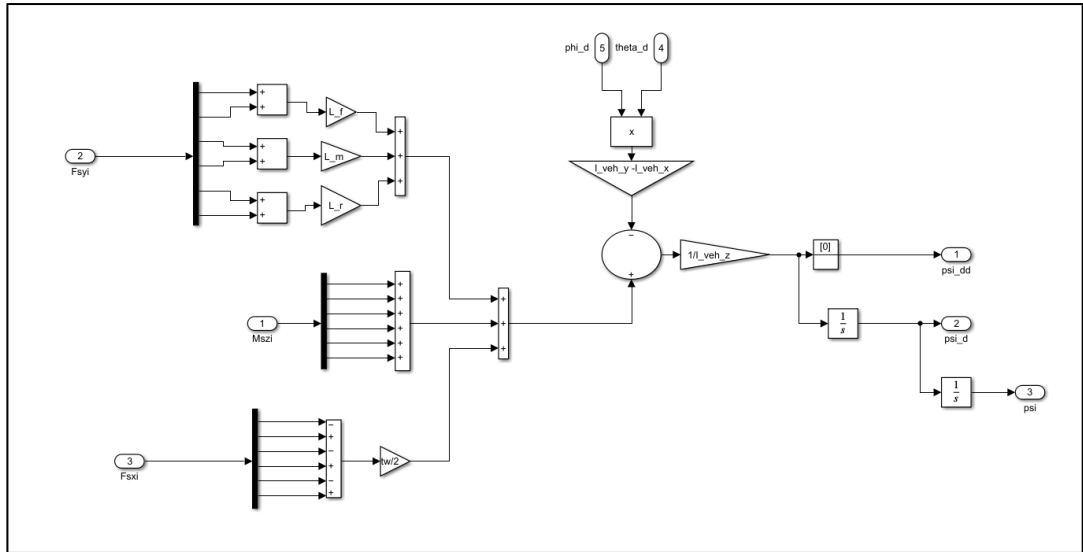
Appendix A - 30. Translational Equation of Motion Along the Vertical Axis



Appendix A - 31. Rotational Equation of Motion Along the Longitudinal Axis



Appendix A - 32. Rotational Equation of Motion Along the Lateral Axis



Appendix A - 33. Rotational Equation of Motion Along the Vertical Axis

B. MatLab Code

```
%%%%%%%%%%%%%%%%%%%%%%%%%%%%%%%%%%%%%%%%%%%%%%%%%%%%%%%%%%%%%%%%%%%%%%%% 6x6 Skid Steered Vehicle %%%%%%%%%%%%%%%%%%%%%%%%%%%%%%%%%%%%%%%%%%%%%%%%%%%%%%%%%%%%%%%%%%%%%%%%%
```

List of the Parameters

```
clc, clear all, close all
LoP = readtable('List of Parameters.xlsx'); % To Read the Parameters from Excel
File
load('susp_road.mat'); % To Read the Random Road Profile

Par = table2array(LoP(:,2));
Jw = Par(1); % [kg.m^2] Tire inertia
Ri = Par(3); % [m] Dynamic tire radius
rw= Ri;
I_armx = Par(14); % [kg.m^2] Moment of Inertia of the Arm Rod About Roll Axis
I_army = Par(15); % [kg.m^2] Moment of Inertia of the Arm Rod About Pitch
Axis
I_armz = Par(16); % [kg.m^2] Moment of Inertia of the Arm Rod About Yaw
Axis
L_arm = Par(17); % [m] Length of the Arm Rod
L_sus = Par(18); % [m] Length Between the Connection of the
Suspension and Connection of the Arm Rod
tw = Par(19); % [m] Track Width
L_m = Par(20); % [m] Length Between the Center of Mass and Middle Rod Axle
L_f = Par(21); % [m] Length Between the Center of Mass and Front Rod Axle
L_r = Par(22); % [m] Length Between the Center of Mass and Rear Rod Axle
I_veh_x = Par(24); % [kg.m^2] Moment of Inertia of the Vehicle About
the Roll Axis
I_veh_y = Par(25); % [kg.m^2] Moment of Inertia of the Vehicle About
the pitch Axis
I_veh_z = Par(26); % [kg.m^2] Moment of Inertia of the Vehicle About
the yaw Axis
m_arm = 130; % [kg] Arm mass
m_w = 270; % [kg] Tire mass
m_sprung = 7600; % [kg] Sprung Mass
m_v = 10000; % [kg] Total mass
```

```
b1 = tw/2; b2 = tw/2;
fr=0.12;
rho = 1.227;
m_v = 10000;
Af= 3.5;
rw = 0.65;
h_s = 1.330; %Height of the sprung mass [m]
h_cg_top = h_s/3; %Distance b/w CG and bottom of vehicle [m]
h_arms = 0.241; %Distance b/w arm and bottom of the vehicle [m]
```

```

h_cg_arm = h_cg_top - h_arms;
A_s = 0.7;
rho_susp = 800;
k = 1.4;

%%%%%%%%%% Road Profile Inputs %%%%%%%%%%%
X_bump1 = linspace(0,5.2,1000);
Z_bump1 = 0.1*sin(2*pi/10.4*X_bump1);
X_bump1 = [-200,X_bump1+5,200];
Z_bump1 = [0,Z_bump1,0];
X_bump2 = [linspace(-500,-5.2,1000), linspace(-5.19,5.19,100),
linspace(5.2,500,1000)];
Z_bump2 = [-0.1*sin(2*pi/10.4*X_bump2(1:1000)),linspace(0,0,100),-
0.1*sin(2*pi/10.4*X_bump2(1101:end))];
%%%%%%%%%%

%%%%%%%%%% Suspension Connection Coordinates %%%%%%%%%%%
xsusp1 = L_f;
xsusp2 = xsusp1;
xsusp3 = L_m;
xsusp4 = xsusp3;
xsusp5 = L_r;
xsusp6 = xsusp5;
ysusp1 = tw/2;
ysusp2 = -ysusp1;
ysusp3 = ysusp1;
ysusp4 = ysusp2;
ysusp5 = ysusp3;
ysusp6 = ysusp4;
zsusp1 = 1.116 - 1.7/3;
zsusp2 = zsusp1; zsusp3 = zsusp1; zsusp4 = zsusp1; zsusp5 = zsusp1;
zsusp6 = zsusp1;
%%%%%%%%%%

%%%%%%%%%% -Pacejka Magic Formula Tyre Parameters%%%%%%%%%%
% 315/80 R22.5
k_tirestiffness = 1e6;
% Longitudinal Tyre Parameters
PCX1           = 1.7204           ;%Shape factor Cfx for longitudinal
force
PDX1           = 0.77751         ;%Longitudinal friction Mux at
Fznom
PDX2           = -0.24431        ;%Variation of friction Mux with
load
PDX3           = -0.00015908     ;%Variation of friction Mux with
camber
PEX1           = 0.46659         ;%Longitudinal curvature Efx at
Fznom
PEX2           = 0.393           ;%Variation of curvature Efx with
load
PEX3           = 0.076024        ;%Variation of curvature Efx with
load squared

```

```

PEX4                = 2.6509e-006      ;%Factor in curvature Efx while
driving
PKX1                = 14.848           ;%Longitudinal slip stiffness
Kfx/Fz at Fznom
PKX2                = -9.8161         ;%Variation of slip stiffness
Kfx/Fz with load
PKX3                = 0.15818         ;%Exponent in slip stiffness Kfx/Fz
with load
PHX1                = -0.00088873     ;%Horizontal shift Shx at Fznom
PHX2                = -0.00067818     ;%Variation of shift Shx with load
PVX1                = -5.5714e-007    ;%Vertical shift SvX/Fz at Fznom
PVX2                = 6.2972e-006     ;%Variation of shift SvX/Fz with
load
RBX1                = 11.13           ;%Slope factor for combined slip Fx
reduction
RBX2                = -12.494         ;%Variation of slope Fx reduction
with kappa
RCX1                = 0.97505         ;%Shape factor for combined slip Fx
reduction
REX1                = -0.37196        ;%Curvature factor of combined Fx
REX2                = 0.0017379       ;%Curvature factor of combined Fx
with load
RHX1                = 0.0045181       ;%Shift factor for combined slip Fx
reduction
PTX1                = 1.5             ;%Relaxation length SigKap0/Fz at
Fznom
PTX2                = 1.4             ;%Variation of SigKap0/Fz with load
PTX3                = 1               ;%Variation of SigKap0/Fz with
exponent of load
PTX4                = 0.1             ;%Low speed damping

% Lateral Tire Parameters
PCY1                = 1.5874          ;%Shape factor Cfy for lateral
forces
PDY1                = 0.73957         ;%Lateral friction Muy
PDY2                = -0.075004       ;%Variation of friction Muy with
load
PDY3                = -8.0362        ;%Variation of friction Muy with
squared camber
PEY1                = 0.37562         ;%Lateral curvature Efy at Fznom
PEY2                = -0.069325       ;%Variation of curvature Efy with
load
PEY3                = 0.29168        ;%Zero order camber dependency of
curvature Efy
PEY4                = 11.559         ;%Variation of curvature Efy with
camber
PKY1                = -10.289         ;%Maximum value of stiffness
Kfy/Fznom
PKY2                = 3.3343         ;%Load at which Kfy reaches maximum
value
PKY3                = -0.25732       ;%Variation of Kfy/Fznom with
camber

```

```

PHY1 = 0.0056509 ;%Horizontal shift Shy at Fznom
PHY2 = -0.0020257 ;%Variation of shift Shy with load
PHY3 = -0.038716 ;%Variation of shift Shy with
camber
PVY1 = 0.015216 ;%Vertical shift in Svy/Fz at Fznom
PVY2 = -0.010365 ;%Variation of shift Svy/Fz with
load
PVY3 = -0.31373 ;%Variation of shift Svy/Fz with
camber
PVY4 = -0.055766 ;%Variation of shift Svy/Fz with
camber and load
RBY1 = 13.271 ;%Slope factor for combined Fy
reduction
RBY2 = 5.2405 ;%Variation of slope Fy reduction
with alpha
RBY3 = 1.1547e-005 ;%Shift term for alpha in slope Fy
reduction
RCY1 = 1.01 ;%Shape factor for combined Fy
reduction
REY1 = 0.010513 ;%Curvature factor of combined Fy
REY2 = 5.9816e-005 ;%Curvature factor of combined Fy
with load
RHY1 = 0.028005 ;%Shift factor for combined Fy
reduction
RHY2 = -4.8794e-005 ;%Shift factor for combined Fy
reduction with load
RVY1 = 0.0066878 ;%Kappa induced side force
Svyk/Muy*Fz at Fznom
RVY2 = -0.042813 ;%Variation of Svyk/Muy*Fz with
load
RVY3 = -0.16227 ;%Variation of Svyk/Muy*Fz with
camber
RVY4 = -0.019796 ;%Variation of Svyk/Muy*Fz with
alpha
RVY5 = 1.9 ;%Variation of Svyk/Muy*Fz with
kappa
RVY6 = -7.8097 ;%Variation of Svyk/Muy*Fz with
atan(kappa)
PTY1 = 1.2 ;%Peak value of relaxation length
SigAlp0/R0
PTY2 = 2.5 ;%Value of Fz/Fznom where SigAlp0
is extreme
FNOMIN = 35000 ;%Nominal wheel load
Lambda_mat2 = ones(27,1);

Apis = 0.015; Apr = Apis - Ar;

```

Loading the ADAMS & Simulink Data

```
ADAMS_AngAcc = readtable('C:\Users\user\Desktop\METU\MatLab\Total Vehicle Model\Last with
simscape\Results\LeftSinewave2(1500_1500)\ADAMS\AngAcc.csv', 'Range', 'B4:G20004', 'ReadVariableNames', false);
ADAMS_AngAcc_x = table2array(ADAMS_AngAcc(:,1));
ADAMS_AngAcc_y = table2array(ADAMS_AngAcc(:,2));
ADAMS_AngAcc_z = table2array(ADAMS_AngAcc(:,3));

ADAMS_AngPos = readtable('C:\Users\user\Desktop\METU\MatLab\Total Vehicle Model\Last with
simscape\Results\LeftSinewave2(1500_1500)\ADAMS\AngPos.csv', 'Range', 'B4:G20004', 'ReadVariableNames', false);
ADAMS_AngPos_x = table2array(ADAMS_AngPos(:,1));
ADAMS_AngPos_y = table2array(ADAMS_AngPos(:,2));
ADAMS_AngPos_z = table2array(ADAMS_AngPos(:,3));

ADAMS_AngVel = readtable('C:\Users\user\Desktop\METU\MatLab\Total Vehicle Model\Last with
simscape\Results\LeftSinewave2(1500_1500)\ADAMS\AngVel.csv', 'Range', 'B4:G20004', 'ReadVariableNames', false);
ADAMS_AngVel_x = table2array(ADAMS_AngVel(:,1));
ADAMS_AngVel_y = table2array(ADAMS_AngVel(:,2));
ADAMS_AngVel_z = table2array(ADAMS_AngVel(:,3));

ADAMS_ArmAng = readtable('C:\Users\user\Desktop\METU\MatLab\Total Vehicle Model\Last with
simscape\Results\LeftSinewave2(1500_1500)\ADAMS\ArmAng.csv', 'Range', 'B4:G20004', 'ReadVariableNames', false);
ADAMS_ArmAng_1 = table2array(ADAMS_ArmAng(:,1));
ADAMS_ArmAng_2 = table2array(ADAMS_ArmAng(:,2));
ADAMS_ArmAng_3 = table2array(ADAMS_ArmAng(:,3));
ADAMS_ArmAng_4 = table2array(ADAMS_ArmAng(:,4));
ADAMS_ArmAng_5 = table2array(ADAMS_ArmAng(:,5));
ADAMS_ArmAng_6 = table2array(ADAMS_ArmAng(:,6));

ADAMS_BodyDisp = readtable('C:\Users\user\Desktop\METU\MatLab\Total Vehicle Model\Last with
simscape\Results\LeftSinewave2(1500_1500)\ADAMS\BodyDisp.csv', 'Range', 'B4:G20004', 'ReadVariableNames', false);
ADAMS_BodyDisp_x = table2array(ADAMS_BodyDisp(:,1));
ADAMS_BodyDisp_y = table2array(ADAMS_BodyDisp(:,2));
ADAMS_BodyDisp_z = table2array(ADAMS_BodyDisp(:,3));

ADAMS_Ftxi = readtable('C:\Users\user\Desktop\METU\MatLab\Total Vehicle Model\Last with
simscape\Results\LeftSinewave2(1500_1500)\ADAMS\Ftxi.csv', 'Range', 'B4:G20004', 'ReadVariableNames', false);
ADAMS_Ftxi_1 = table2array(ADAMS_Ftxi(:,1));
ADAMS_Ftxi_2 = table2array(ADAMS_Ftxi(:,2));
ADAMS_Ftxi_3 = table2array(ADAMS_Ftxi(:,3));
```



```

ADAMS_Ftxi_4 = table2array(ADAMS_Ftxi(:,4));
ADAMS_Ftxi_5 = table2array(ADAMS_Ftxi(:,5));
ADAMS_Ftxi_6 = table2array(ADAMS_Ftxi(:,6));

ADAMS_Ftyi = readtable('C:\Users\user\Desktop\METU\MatLab\Total Vehicle Model\Last
with
simscape\Results\LeftSinewave2(1500_1500)\ADAMS\Ftyi.csv','Range','B4:G20004','Read
VariableNames',false);
ADAMS_Ftyi_1 = table2array(ADAMS_Ftyi(:,1));
ADAMS_Ftyi_2 = table2array(ADAMS_Ftyi(:,2));
ADAMS_Ftyi_3 = table2array(ADAMS_Ftyi(:,3));
ADAMS_Ftyi_4 = table2array(ADAMS_Ftyi(:,4));
ADAMS_Ftyi_5 = table2array(ADAMS_Ftyi(:,5));
ADAMS_Ftyi_6 = table2array(ADAMS_Ftyi(:,6));

ADAMS_LoadDist = readtable('C:\Users\user\Desktop\METU\MatLab\Total Vehicle
Model\Last with
simscape\Results\LeftSinewave2(1500_1500)\ADAMS\LoadDist.csv','Range','B4:G20004','
ReadVariableNames',false);
ADAMS_LoadDist_1 = table2array(ADAMS_LoadDist(:,1));
ADAMS_LoadDist_2 = table2array(ADAMS_LoadDist(:,2));
ADAMS_LoadDist_3 = table2array(ADAMS_LoadDist(:,3));
ADAMS_LoadDist_4 = table2array(ADAMS_LoadDist(:,4));
ADAMS_LoadDist_5 = table2array(ADAMS_LoadDist(:,5));
ADAMS_LoadDist_6 = table2array(ADAMS_LoadDist(:,6));

ADAMS_Tsdi = readtable('C:\Users\user\Desktop\METU\MatLab\Total Vehicle Model\Last
with
simscape\Results\LeftSinewave2(1500_1500)\ADAMS\Tsdi.csv','Range','B4:G20004','Read
VariableNames',false);
ADAMS_Tsdi_1 = table2array(ADAMS_Tsdi(:,1));
ADAMS_Tsdi_2 = table2array(ADAMS_Tsdi(:,2));
ADAMS_Tsdi_3 = table2array(ADAMS_Tsdi(:,3));
ADAMS_Tsdi_4 = table2array(ADAMS_Tsdi(:,4));
ADAMS_Tsdi_5 = table2array(ADAMS_Tsdi(:,5));
ADAMS_Tsdi_6 = table2array(ADAMS_Tsdi(:,6));

ADAMS_TransVel = readtable('C:\Users\user\Desktop\METU\MatLab\Total Vehicle
Model\Last with
simscape\Results\LeftSinewave2(1500_1500)\ADAMS\TransVel.csv','Range','B4:G20004','
ReadVariableNames',false);
ADAMS_TransVel_x = table2array(ADAMS_TransVel(:,1));
ADAMS_TransVel_y = table2array(ADAMS_TransVel(:,2));
ADAMS_TransVel_z = table2array(ADAMS_TransVel(:,3));

ADAMS_TransAcc = readtable('C:\Users\user\Desktop\METU\MatLab\Total Vehicle
Model\Last with
simscape\Results\LeftSinewave2(1500_1500)\ADAMS\TransAcc.csv','Range','B4:G20004','
ReadVariableNames',false);
ADAMS_TransAcc_x = table2array(ADAMS_TransAcc(:,1));
ADAMS_TransAcc_y = table2array(ADAMS_TransAcc(:,2));
ADAMS_TransAcc_z = table2array(ADAMS_TransAcc(:,3));

```

```

Simulink_AngAcc = readtable('C:\Users\user\Desktop\METU\MatLab\Total Vehicle
Model\Last with Simscape\Results\LeftSinewave2(1500_1500)\Simulink\AngAcc.csv');
Simulink_AngAcc_x = table2array(Simulink_AngAcc(:,1));
Simulink_AngAcc_y = table2array(Simulink_AngAcc(:,2));
Simulink_AngAcc_z = table2array(Simulink_AngAcc(:,3));

Simulink_AngPos = readtable('C:\Users\user\Desktop\METU\MatLab\Total Vehicle
Model\Last with Simscape\Results\LeftSinewave2(1500_1500)\Simulink\AngPos.csv');
Simulink_AngPos_x = table2array(Simulink_AngPos(:,1));
Simulink_AngPos_y = table2array(Simulink_AngPos(:,2));
Simulink_AngPos_z = table2array(Simulink_AngPos(:,3));

Simulink_AngVel = readtable('C:\Users\user\Desktop\METU\MatLab\Total Vehicle
Model\Last with Simscape\Results\LeftSinewave2(1500_1500)\Simulink\AngVel.csv');
Simulink_AngVel_x = table2array(Simulink_AngVel(:,1));
Simulink_AngVel_y = table2array(Simulink_AngVel(:,2));
Simulink_AngVel_z = table2array(Simulink_AngVel(:,3));

Simulink_ArmAng = readtable('C:\Users\user\Desktop\METU\MatLab\Total Vehicle
Model\Last with Simscape\Results\LeftSinewave2(1500_1500)\Simulink\ArmAng.csv');
Simulink_ArmAng_1 = table2array(Simulink_ArmAng(:,1));
Simulink_ArmAng_2 = table2array(Simulink_ArmAng(:,2));
Simulink_ArmAng_3 = table2array(Simulink_ArmAng(:,3));
Simulink_ArmAng_4 = table2array(Simulink_ArmAng(:,4));
Simulink_ArmAng_5 = table2array(Simulink_ArmAng(:,5));
Simulink_ArmAng_6 = table2array(Simulink_ArmAng(:,6));

Simulink_BodyDisp = readtable('C:\Users\user\Desktop\METU\MatLab\Total Vehicle
Model\Last with Simscape\Results\LeftSinewave2(1500_1500)\Simulink\BodyDisp.csv');
Simulink_BodyDisp_x = table2array(Simulink_BodyDisp(:,1));
Simulink_BodyDisp_y = table2array(Simulink_BodyDisp(:,2));
Simulink_BodyDisp_z = table2array(Simulink_BodyDisp(:,3));

Simulink_Ftxi = readtable('C:\Users\user\Desktop\METU\MatLab\Total Vehicle
Model\Last with Simscape\Results\LeftSinewave2(1500_1500)\Simulink\Ftxi.csv');
Simulink_Ftxi_1 = table2array(Simulink_Ftxi(:,1));
Simulink_Ftxi_2 = table2array(Simulink_Ftxi(:,2));
Simulink_Ftxi_3 = table2array(Simulink_Ftxi(:,3));
Simulink_Ftxi_4 = table2array(Simulink_Ftxi(:,4));
Simulink_Ftxi_5 = table2array(Simulink_Ftxi(:,5));
Simulink_Ftxi_6 = table2array(Simulink_Ftxi(:,6));

Simulink_Ftyi = readtable('C:\Users\user\Desktop\METU\MatLab\Total Vehicle
Model\Last with Simscape\Results\LeftSinewave2(1500_1500)\Simulink\Ftyi.csv');
Simulink_Ftyi_1 = table2array(Simulink_Ftyi(:,1));
Simulink_Ftyi_2 = table2array(Simulink_Ftyi(:,2));
Simulink_Ftyi_3 = table2array(Simulink_Ftyi(:,3));
Simulink_Ftyi_4 = table2array(Simulink_Ftyi(:,4));
Simulink_Ftyi_5 = table2array(Simulink_Ftyi(:,5));
Simulink_Ftyi_6 = table2array(Simulink_Ftyi(:,6));

```

```

Simulink_LoadDist = readtable('C:\Users\user\Desktop\METU\MatLab\Total Vehicle
Model\Last with Simscape\Results\LeftSinewave2(1500_1500)\Simulink\LoadDist.csv');
Simulink_LoadDist_1 = table2array(Simulink_LoadDist(:,1));
Simulink_LoadDist_2 = table2array(Simulink_LoadDist(:,2));
Simulink_LoadDist_3 = table2array(Simulink_LoadDist(:,3));
Simulink_LoadDist_4 = table2array(Simulink_LoadDist(:,4));
Simulink_LoadDist_5 = table2array(Simulink_LoadDist(:,5));
Simulink_LoadDist_6 = table2array(Simulink_LoadDist(:,6));

Simulink_Tsdi = readtable('C:\Users\user\Desktop\METU\MatLab\Total Vehicle
Model\Last with Simscape\Results\LeftSinewave2(1500_1500)\Simulink\Tsdi.csv');
Simulink_Tsdi_1 = table2array(Simulink_Tsdi(:,1));
Simulink_Tsdi_2 = table2array(Simulink_Tsdi(:,2));
Simulink_Tsdi_3 = table2array(Simulink_Tsdi(:,3));
Simulink_Tsdi_4 = table2array(Simulink_Tsdi(:,4));
Simulink_Tsdi_5 = table2array(Simulink_Tsdi(:,5));
Simulink_Tsdi_6 = table2array(Simulink_Tsdi(:,6));

Simulink_TransVel = readtable('C:\Users\user\Desktop\METU\MatLab\Total Vehicle
Model\Last with Simscape\Results\LeftSinewave2(1500_1500)\Simulink\TransVel.csv');
Simulink_TransVel_x = table2array(Simulink_TransVel(:,1));
Simulink_TransVel_y = table2array(Simulink_TransVel(:,2));
Simulink_TransVel_z = table2array(Simulink_TransVel(:,3));

Simulink_TransAcc = readtable('C:\Users\user\Desktop\METU\MatLab\Total Vehicle
Model\Last with Simscape\Results\LeftSinewave2(1500_1500)\Simulink\TransAcc.csv');
Simulink_TransAcc_x = table2array(Simulink_TransAcc(:,1));
Simulink_TransAcc_y = table2array(Simulink_TransAcc(:,2));
Simulink_TransAcc_z = table2array(Simulink_TransAcc(:,3));

t = linspace(0,20,20/0.001+1);

```

Plotting and Error Calculation Body Displacement

```
fig1 = figure(1);
plot(t,ADAMS_BodyDisp_x,t,Simulink_BodyDisp_x,'Linewidth',1.5)
xlabel('Time [s]')
ylabel('Distance [m]')
ylim([min(min(min(ADAMS_BodyDisp_x,Simulink_BodyDisp_x),-5))*1.2
1.2*max(max(max(ADAMS_BodyDisp_x,Simulink_BodyDisp_x),5))])
title('Body Longitudinal Displacement')
legend('ADAMS','Simulink')
grid on

saveas(fig1,'C:\Users\user\Desktop\METU\MatLab\Total Vehicle Model\Last with
simscape\Results\LeftSinewave2(1500_1500)\BodyDispX.png')
MSE_BodyDisp_x = immse(ADAMS_BodyDisp_x,Simulink_BodyDisp_x);
Max_BodyDisp_x = [max(ADAMS_BodyDisp_x),max(Simulink_BodyDisp_x)];
Min_BodyDisp_x = [min(ADAMS_BodyDisp_x),min(Simulink_BodyDisp_x)];
Mean_BodyDisp_x = [mean(ADAMS_BodyDisp_x),mean(Simulink_BodyDisp_x)];

T_BodyDisp_x = table(MSE_BodyDisp_x,Max_BodyDisp_x,Min_BodyDisp_x,Mean_BodyDisp_x,
'VariableNames', {'MSE', 'Max', 'Min', 'Mean'});
writetable(T_BodyDisp_x, 'C:\Users\user\Desktop\METU\MatLab\Total Vehicle
Model\Last with simscape\Results\LeftSinewave2(1500_1500)\BodyDisp_x.csv',
'WriteVariableNames', true)

fig2 = figure(2);
plot(t,ADAMS_BodyDisp_y,t,Simulink_BodyDisp_y,'Linewidth',1.5)
xlabel('Time [s]')
ylabel('Distance [m]')
ylim([min(min(min(ADAMS_BodyDisp_y,Simulink_BodyDisp_y),-5))*1.2
1.2*max(max(max(ADAMS_BodyDisp_y,Simulink_BodyDisp_y),5))])
title('Body Lateral Displacement')
legend('ADAMS','Simulink')
grid on

saveas(fig2,'C:\Users\user\Desktop\METU\MatLab\Total Vehicle Model\Last with
simscape\Results\LeftSinewave2(1500_1500)\BodyDispY.png')

MSE_BodyDisp_y = immse(ADAMS_BodyDisp_y,Simulink_BodyDisp_y);
Max_BodyDisp_y = [max(ADAMS_BodyDisp_y),max(Simulink_BodyDisp_y)];
Min_BodyDisp_y = [min(ADAMS_BodyDisp_y),min(Simulink_BodyDisp_y)];
Mean_BodyDisp_y = [mean(ADAMS_BodyDisp_y),mean(Simulink_BodyDisp_y)];

T_BodyDisp_y = table(MSE_BodyDisp_y,Max_BodyDisp_y,Min_BodyDisp_y,Mean_BodyDisp_y,
'VariableNames', {'MSE', 'Max', 'Min', 'Mean'});
writetable(T_BodyDisp_y, 'C:\Users\user\Desktop\METU\MatLab\Total Vehicle
Model\Last with simscape\Results\LeftSinewave2(1500_1500)\BodyDisp_y.csv',
'WriteVariableNames', true)

Simulink_BodyDisp_z = Simulink_BodyDisp_z+1.2523
fig3 = figure(3);
```

```

plot(t,ADAMS_BodyDisp_z,t,Simulink_BodyDisp_z,'Linewidth',1.5)
xlabel('Time [s]')
ylabel('Distance [m]')
ylim([min(min(min(ADAMS_BodyDisp_z,Simulink_BodyDisp_z),-5))*1.2
1.2*max(max(max(ADAMS_BodyDisp_z,Simulink_BodyDisp_z),5))])
title('Body Vertical Displacement')
legend('ADAMS','Simulink')
grid on

saveas(fig3,'C:\Users\user\Desktop\METU\MatLab\Total Vehicle Model\Last with
simscape\Results\LeftSinewave2(1500_1500)\BodyDispZ.png')
MSE_BodyDisp_z = immse(ADAMS_BodyDisp_z,Simulink_BodyDisp_z);
Max_BodyDisp_z = [max(ADAMS_BodyDisp_z),max(Simulink_BodyDisp_z)];
Min_BodyDisp_z = [min(ADAMS_BodyDisp_z),min(Simulink_BodyDisp_z)];
Mean_BodyDisp_z = [mean(ADAMS_BodyDisp_z),mean(Simulink_BodyDisp_z)];

T_BodyDisp_z = table(MSE_BodyDisp_z,Max_BodyDisp_z,Min_BodyDisp_z,Mean_BodyDisp_z,
'VariableNames', {'MSE', 'Max', 'Min', 'Mean'});
writetable(T_BodyDisp_z, 'C:\Users\user\Desktop\METU\MatLab\Total Vehicle
Model\Last with simscape\Results\LeftSinewave2(1500_1500)\BodyDisp_z.csv',
'WriteVariableNames', true)

```

Translational Velocity

```

fig4 = figure(4);
plot(t,ADAMS_TransVel_x,t,Simulink_TransVel_x,'Linewidth',1.5)
xlabel('Time [s]')
ylabel('velocity [m/s]')
ylim([min(min(min(ADAMS_TransVel_x,Simulink_TransVel_x),-5))*1.2
1.2*max(max(max(ADAMS_TransVel_x,Simulink_TransVel_x),5))])
title('Body Longitudinal velocity')
legend('ADAMS','Simulink')
grid on

saveas(fig4,'C:\Users\user\Desktop\METU\MatLab\Total Vehicle Model\Last with
simscape\Results\LeftSinewave2(1500_1500)\TransVelX.png')

MSE_TransVel_x = immse(ADAMS_TransVel_x,Simulink_TransVel_x);
Max_TransVel_x = [max(ADAMS_TransVel_x),max(Simulink_TransVel_x)];
Min_TransVel_x = [min(ADAMS_TransVel_x),min(Simulink_TransVel_x)];
Mean_TransVel_x = [mean(ADAMS_TransVel_x),mean(Simulink_TransVel_x)];

T_TransVel_x = table(MSE_TransVel_x,Max_TransVel_x,Min_TransVel_x,Mean_TransVel_x,
'VariableNames', {'MSE', 'Max', 'Min', 'Mean'});
writetable(T_TransVel_x, 'C:\Users\user\Desktop\METU\MatLab\Total Vehicle
Model\Last with simscape\Results\LeftSinewave2(1500_1500)\TransVel_x.csv',
'WriteVariableNames', true)

fig5 = figure(5);
plot(t,ADAMS_TransVel_y,t,Simulink_TransVel_y,'Linewidth',1.5)
xlabel('Time [s]')

```

```

ylabel('Velocity [m/s]')
ylim([min(min(min(ADAMS_TransVel_y,Simulink_TransVel_y),-5))*1.2
1.2*max(max(max(ADAMS_TransVel_y,Simulink_TransVel_y),5))])
title('Body Lateral Velocity')
legend('ADAMS','Simulink')
grid on

saveas(fig5,'C:\Users\user\Desktop\METU\MatLab\Total Vehicle Model\Last with
simscape\Results\LeftSinewave2(1500_1500)\TransvelY.png')

MSE_TransVel_y = immse(ADAMS_TransVel_y,Simulink_TransVel_y);
Max_TransVel_y = [max(ADAMS_TransVel_y),max(Simulink_TransVel_y)];
Min_TransVel_y = [min(ADAMS_TransVel_y),min(Simulink_TransVel_y)];
Mean_TransVel_y = [mean(ADAMS_TransVel_y),mean(Simulink_TransVel_y)];

T_TransVel_y = table(MSE_TransVel_y,Max_TransVel_y,Min_TransVel_y,Mean_TransVel_y,
'VariableNames', {'MSE', 'Max','Min','Mean'});
writetable(T_TransVel_y, 'C:\Users\user\Desktop\METU\MatLab\Total Vehicle
Model\Last with simscape\Results\LeftSinewave2(1500_1500)\Transvel_y.csv',
'writevariableNames', true)

fig6 = figure(6);
plot(t,ADAMS_TransVel_z,t,Simulink_TransVel_z,'Linewidth',1.5)
xlabel('Time [s]')
ylabel('Velocity [m/s]')
ylim([min(min(min(ADAMS_TransVel_z,Simulink_TransVel_z),-5))*1.2
1.2*max(max(max(ADAMS_TransVel_z,Simulink_TransVel_z),5))])
title('Body Vertical Velocity')
legend('ADAMS','Simulink')
grid on

saveas(fig6,'C:\Users\user\Desktop\METU\MatLab\Total Vehicle Model\Last with
simscape\Results\LeftSinewave2(1500_1500)\TransvelZ.png')

MSE_TransVel_z = immse(ADAMS_TransVel_z,Simulink_TransVel_z);
Max_TransVel_z = [max(ADAMS_TransVel_z),max(Simulink_TransVel_z)];
Min_TransVel_z = [min(ADAMS_TransVel_z),min(Simulink_TransVel_z)];
Mean_TransVel_z = [mean(ADAMS_TransVel_z),mean(Simulink_TransVel_z)];

T_TransVel_z = table(MSE_TransVel_z,Max_TransVel_z,Min_TransVel_z,Mean_TransVel_z,
'VariableNames', {'MSE', 'Max','Min','Mean'});
writetable(T_TransVel_z, 'C:\Users\user\Desktop\METU\MatLab\Total Vehicle
Model\Last with simscape\Results\LeftSinewave2(1500_1500)\Transvel_z.csv',
'writevariableNames', true)

```

Translational Acceleration

```

fig7 = figure(7);
plot(t,ADAMS_TransAcc_x,t,Simulink_TransAcc_x,'Linewidth',1.5)
xlabel('Time [s]')
ylabel('Acceleration [m/s^2]')
ylim([min(min(min(ADAMS_TransAcc_x,Simulink_TransAcc_x),-5))*1.2

```

```

1.2*max(max(max(ADAMS_TransAcc_x,Simulink_TransAcc_x),5))]]
title('Body Longitudinal Acceleration')
legend('ADAMS','Simulink')
grid on

saveas(fig7,'C:\Users\user\Desktop\METU\MatLab\Total Vehicle Model\Last with
simscape\Results\LeftSinewave2(1500_1500)\TransAccX.png')

MSE_TransAcc_x = immse(ADAMS_TransAcc_x,Simulink_TransAcc_x);
Max_TransAcc_x = [max(ADAMS_TransAcc_x),max(Simulink_TransAcc_x)];
Min_TransAcc_x = [min(ADAMS_TransAcc_x),min(Simulink_TransAcc_x)];
Mean_TransAcc_x = [mean(ADAMS_TransAcc_x),mean(Simulink_TransAcc_x)];

T_TransAcc_x = table(MSE_TransAcc_x,Max_TransAcc_x,Min_TransAcc_x,Mean_TransAcc_x,
'VariableNames', {'MSE', 'Max', 'Min', 'Mean'});
writetable(T_TransAcc_x, 'C:\Users\user\Desktop\METU\MatLab\Total Vehicle
Model\Last with simscape\Results\LeftSinewave2(1500_1500)\TransAcc_x.csv',
'writeVariableNames', true)

fig8 = figure(8);
plot(t,ADAMS_TransAcc_y,t,Simulink_TransAcc_y,'Linewidth',1.5)
xlabel('Time [s]')
ylabel('Acceleration [m/s^2]')
ylim([min(min(min(ADAMS_TransAcc_y,Simulink_TransAcc_y),-5))*1.2
1.2*max(max(max(ADAMS_TransAcc_y,Simulink_TransAcc_y),5))]]
title('Body Lateral Acceleration')
legend('ADAMS','Simulink')
grid on

saveas(fig8,'C:\Users\user\Desktop\METU\MatLab\Total Vehicle Model\Last with
simscape\Results\LeftSinewave2(1500_1500)\TransAccY.png')

MSE_TransAcc_y = immse(ADAMS_TransAcc_y,Simulink_TransAcc_y);
Max_TransAcc_y = [max(ADAMS_TransAcc_y),max(Simulink_TransAcc_y)];
Min_TransAcc_y = [min(ADAMS_TransAcc_y),min(Simulink_TransAcc_y)];
Mean_TransAcc_y = [mean(ADAMS_TransAcc_y),mean(Simulink_TransAcc_y)];

T_TransAcc_y = table(MSE_TransAcc_y,Max_TransAcc_y,Min_TransAcc_y,Mean_TransAcc_y,
'VariableNames', {'MSE', 'Max', 'Min', 'Mean'});
writetable(T_TransAcc_y, 'C:\Users\user\Desktop\METU\MatLab\Total Vehicle
Model\Last with simscape\Results\LeftSinewave2(1500_1500)\TransAcc_y.csv',
'writeVariableNames', true)

fig9 = figure(9);
plot(t,ADAMS_TransAcc_z,t,Simulink_TransAcc_z,'Linewidth',1.5)
xlabel('Time [s]')
ylabel('Acceleration [m/s^2]')
ylim([min(min(min(ADAMS_TransAcc_z,Simulink_TransAcc_z),-5))*1.2
1.2*max(max(max(ADAMS_TransAcc_z,Simulink_TransAcc_z),5))]]
title('Body Vertical Acceleration')

```

```

Legend('ADAMS','Simulink')
grid on

saveas(fig9,'C:\Users\user\Desktop\METU\MatLab\Total Vehicle Model\Last with
simscape\Results\LeftSinewave2(1500_1500)\TransAccZ.png')

MSE_TransAcc_z = immse(ADAMS_TransAcc_z,Simulink_TransAcc_z);
Max_TransAcc_z = [max(ADAMS_TransAcc_z),max(Simulink_TransAcc_z)];
Min_TransAcc_z = [min(ADAMS_TransAcc_z),min(Simulink_TransAcc_z)];
Mean_TransAcc_z = [mean(ADAMS_TransAcc_z),mean(Simulink_TransAcc_z)];

T_TransAcc_z = table(MSE_TransAcc_z,Max_TransAcc_z,Min_TransAcc_z,Mean_TransAcc_z,
'VariableNames', {'MSE', 'Max','Min','Mean'});
writetable(T_TransAcc_z, 'C:\Users\user\Desktop\METU\MatLab\Total Vehicle
Model\Last with simscape\Results\LeftSinewave2(1500_1500)\TransAcc_z.csv',
'writevariableNames', true)

```

Angular Position

```

fig10 = figure(10);
plot(t,ADAMS_AngPos_x,t,Simulink_AngPos_x,'Linewidth',1.5)
xlabel('Time [s]')
ylabel('Angle [deg]')
ylim([min(min(min(ADAMS_AngPos_x,Simulink_AngPos_x),-5))*1.2
1.2*max(max(max(ADAMS_AngPos_x,Simulink_AngPos_x),5))])
title('Body Roll Angle')
legend('ADAMS','Simulink')
grid on

saveas(fig10,'C:\Users\user\Desktop\METU\MatLab\Total Vehicle Model\Last with
simscape\Results\LeftSinewave2(1500_1500)\AngPosX.png')

MSE_AngPos_x = immse(ADAMS_AngPos_x,Simulink_AngPos_x);
Max_AngPos_x = [max(ADAMS_AngPos_x),max(Simulink_AngPos_x)];
Min_AngPos_x = [min(ADAMS_AngPos_x),min(Simulink_AngPos_x)];
Mean_AngPos_x = [mean(ADAMS_AngPos_x),mean(Simulink_AngPos_x)];

T_AngPos_x = table(MSE_AngPos_x,Max_AngPos_x,Min_AngPos_x,Mean_AngPos_x,
'VariableNames', {'MSE', 'Max','Min','Mean'});
writetable(T_AngPos_x, 'C:\Users\user\Desktop\METU\MatLab\Total Vehicle Model\Last
with simscape\Results\LeftSinewave2(1500_1500)\AngPos_x.csv', 'writevariableNames',
true)

fig11 = figure(11);
plot(t,ADAMS_AngPos_y,t,Simulink_AngPos_y,'Linewidth',1.5)
xlabel('Time [s]')
ylabel('Angle [deg]')
ylim([min(min(min(ADAMS_AngPos_y,Simulink_AngPos_y),-5))*1.2
1.2*max(max(max(ADAMS_AngPos_y,Simulink_AngPos_y),5))])
title('Body Pitch Angle')
legend('ADAMS','Simulink')
grid on

```



```

saveas(fig11, 'C:\Users\user\Desktop\METU\MatLab\Total Vehicle Model\Last with
simscape\Results\LeftSinewave2(1500_1500)\AngPosY.png')

MSE_AngPos_y = immse(ADAMS_AngPos_y, Simulink_AngPos_y);
Max_AngPos_y = [max(ADAMS_AngPos_y), max(Simulink_AngPos_y)];
Min_AngPos_y = [min(ADAMS_AngPos_y), min(Simulink_AngPos_y)];
Mean_AngPos_y = [mean(ADAMS_AngPos_y), mean(Simulink_AngPos_y)];

T_AngPos_y = table(MSE_AngPos_y, Max_AngPos_y, Min_AngPos_y, Mean_AngPos_y,
'VariableNames', {'MSE', 'Max', 'Min', 'Mean'});
writetable(T_AngPos_y, 'C:\Users\user\Desktop\METU\MatLab\Total Vehicle Model\Last
with simscape\Results\LeftSinewave2(1500_1500)\AngPos_y.csv', 'WritevariableNames',
true)

fig12 = figure(12);
plot(t, ADAMS_AngPos_z, t, Simulink_AngPos_z, 'Linewidth', 1.5)
xlabel('Time [s]')
ylabel('Angle [deg]')
ylim([min(min(min(ADAMS_AngPos_z, Simulink_AngPos_z), -5))*1.2
1.2*max(max(max(ADAMS_AngPos_z, Simulink_AngPos_z), 5))])
title('Body Yaw Angle')
legend('ADAMS', 'Simulink')
grid on

saveas(fig12, 'C:\Users\user\Desktop\METU\MatLab\Total Vehicle Model\Last with
simscape\Results\LeftSinewave2(1500_1500)\AngPosZ.png')

MSE_AngPos_z = immse(ADAMS_AngPos_z, Simulink_AngPos_z);
Max_AngPos_z = [max(ADAMS_AngPos_z), max(Simulink_AngPos_z)];
Min_AngPos_z = [min(ADAMS_AngPos_z), min(Simulink_AngPos_z)];
Mean_AngPos_z = [mean(ADAMS_AngPos_z), mean(Simulink_AngPos_z)];

T_AngPos_z = table(MSE_AngPos_z, Max_AngPos_z, Min_AngPos_z, Mean_AngPos_z,
'VariableNames', {'MSE', 'Max', 'Min', 'Mean'});
writetable(T_AngPos_z, 'C:\Users\user\Desktop\METU\MatLab\Total Vehicle Model\Last
with simscape\Results\LeftSinewave2(1500_1500)\AngPos_z.csv', 'WritevariableNames',
true)

```

Angular Velocity

```

fig13 = figure(13);
plot(t, ADAMS_AngVel_x, t, Simulink_AngVel_x, 'Linewidth', 1.5)
xlabel('Time [s]')
ylabel('Angular velocity [deg/s]')
ylim([min(min(min(ADAMS_AngVel_x, Simulink_AngVel_x), -5))*1.2
1.2*max(max(max(ADAMS_AngVel_x, Simulink_AngVel_x), 5))])
title('Body Roll Angular velocity')
legend('ADAMS', 'Simulink')
grid on

```

```

saveas(fig13,'C:\Users\user\Desktop\METU\MatLab\Total Vehicle Model\Last with
simscape\Results\LeftSinewave2(1500_1500)\AngVelx.png')

MSE_AngVel_x = immse(ADAMS_AngVel_x,Simulink_AngVel_x);
Max_AngVel_x = [max(ADAMS_AngVel_x),max(Simulink_AngVel_x)];
Min_AngVel_x = [min(ADAMS_AngVel_x),min(Simulink_AngVel_x)];
Mean_AngVel_x = [mean(ADAMS_AngVel_x),mean(Simulink_AngVel_x)];

T_AngVel_x = table(MSE_AngVel_x,Max_AngVel_x,Min_AngVel_x,Mean_AngVel_x,
'VariableNames', {'MSE', 'Max','Min','Mean'});
writetable(T_AngVel_x, 'C:\Users\user\Desktop\METU\MatLab\Total Vehicle Model\Last
with simscape\Results\LeftSinewave2(1500_1500)\AngVel_x.csv', 'writevariableNames',
true)

fig14 = figure(14);
plot(t,ADAMS_AngVel_y,t,Simulink_AngVel_y,'Linewidth',1.5)
xlabel('Time [s]')
ylabel('Angular velocity [deg/s]')
ylim([min(min(min(ADAMS_AngVel_y,Simulink_AngVel_y),-5))*1.2
1.2*max(max(max(ADAMS_AngVel_y,Simulink_AngVel_y),5))])
title('Body Pitch Angular velocity')
legend('ADAMS','Simulink')
grid on

saveas(fig14,'C:\Users\user\Desktop\METU\MatLab\Total Vehicle Model\Last with
simscape\Results\LeftSinewave2(1500_1500)\AngVelY.png')

MSE_AngVel_y = immse(ADAMS_AngVel_y,Simulink_AngVel_y);
Max_AngVel_y = [max(ADAMS_AngVel_y),max(Simulink_AngVel_y)];
Min_AngVel_y = [min(ADAMS_AngVel_y),min(Simulink_AngVel_y)];
Mean_AngVel_y = [mean(ADAMS_AngVel_y),mean(Simulink_AngVel_y)];

T_AngVel_y = table(MSE_AngVel_y,Max_AngVel_y,Min_AngVel_y,Mean_AngVel_y,
'VariableNames', {'MSE', 'Max','Min','Mean'});
writetable(T_AngVel_y, 'C:\Users\user\Desktop\METU\MatLab\Total Vehicle Model\Last
with simscape\Results\LeftSinewave2(1500_1500)\AngVel_y.csv', 'writevariableNames',
true)

fig15 = figure(15);
plot(t,ADAMS_AngVel_z,t,Simulink_AngVel_z,'Linewidth',1.5)
xlabel('Time [s]')
ylabel('Angular velocity [deg/s]')
ylim([min(min(min(ADAMS_AngVel_z,Simulink_AngVel_z),-5))*1.2
1.2*max(max(max(ADAMS_AngVel_z,Simulink_AngVel_z),5))])
title('Body Yaw Angular velocity')
legend('ADAMS','Simulink')
grid on

saveas(fig15,'C:\Users\user\Desktop\METU\MatLab\Total Vehicle Model\Last with
simscape\Results\LeftSinewave2(1500_1500)\AngVelZ.png')

```

```

MSE_AngVel_z = immse(ADAMS_AngVel_z,Simulink_AngVel_z);
Max_AngVel_z = [max(ADAMS_AngVel_z),max(Simulink_AngVel_z)];
Min_AngVel_z = [min(ADAMS_AngVel_z),min(Simulink_AngVel_z)];
Mean_AngVel_z = [mean(ADAMS_AngVel_z),mean(Simulink_AngVel_z)];

T_AngVel_z = table(MSE_AngVel_z,Max_AngVel_z,Min_AngVel_z,Mean_AngVel_z,
'VariableNames', {'MSE', 'Max','Min','Mean'});
writetable(T_AngVel_z, 'C:\Users\user\Desktop\METU\MatLab\Total Vehicle Model\Last
with simscape\Results\LeftSinewave2(1500_1500)\AngVel_z.csv', 'writevariableNames',
true)

```

Angular Acceleration

```

fig16 = figure(16);
plot(t,ADAMS_AngAcc_x,t,Simulink_AngAcc_x,'Linewidth',1.5)
xlabel('Time [s]')
ylabel('Angular Acceleration [deg/s^2]')
ylim([min(min(min(ADAMS_AngAcc_x,Simulink_AngAcc_x),-5))*1.2
1.2*max(max(max(ADAMS_AngAcc_x,Simulink_AngAcc_x),5))])
title('Body Roll Angular Acceleration')
legend('ADAMS','Simulink')
grid on

saveas(fig16,'C:\Users\user\Desktop\METU\MatLab\Total Vehicle Model\Last with
simscape\Results\LeftSinewave2(1500_1500)\AngAccX.png')

MSE_AngAcc_x = immse(ADAMS_AngAcc_x,Simulink_AngAcc_x);
Max_AngAcc_x = [max(ADAMS_AngAcc_x),max(Simulink_AngAcc_x)];
Min_AngAcc_x = [min(ADAMS_AngAcc_x),min(Simulink_AngAcc_x)];
Mean_AngAcc_x = [mean(ADAMS_AngAcc_x),mean(Simulink_AngAcc_x)];

T_AngAcc_x = table(MSE_AngAcc_x,Max_AngAcc_x,Min_AngAcc_x,Mean_AngAcc_x,
'VariableNames', {'MSE', 'Max','Min','Mean'});
writetable(T_AngAcc_x, 'C:\Users\user\Desktop\METU\MatLab\Total Vehicle Model\Last
with simscape\Results\LeftSinewave2(1500_1500)\AngAcc_x.csv', 'writevariableNames',
true)

fig17 = figure(17);
plot(t,ADAMS_AngAcc_y,t,Simulink_AngAcc_y,'Linewidth',1.5)
xlabel('Time [s]')
ylabel('Angular Acceleration [deg/s^2]')
ylim([min(min(min(ADAMS_AngAcc_y,Simulink_AngAcc_y),-5))*1.2
1.2*max(max(max(ADAMS_AngAcc_y,Simulink_AngAcc_y),5))])
title('Body Pitch Angular Acceleration')
legend('ADAMS','Simulink')
grid on

saveas(fig17,'C:\Users\user\Desktop\METU\MatLab\Total Vehicle Model\Last with
simscape\Results\LeftSinewave2(1500_1500)\AngAccY.png')

MSE_AngAcc_y = immse(ADAMS_AngAcc_y,Simulink_AngAcc_y);

```

```

Max_AngAcc_y = [max(ADAMS_AngAcc_y),max(Simulink_AngAcc_y)];
Min_AngAcc_y = [min(ADAMS_AngAcc_y),min(Simulink_AngAcc_y)];
Mean_AngAcc_y = [mean(ADAMS_AngAcc_y),mean(Simulink_AngAcc_y)];

T_AngAcc_y = table(MSE_AngAcc_y,Max_AngAcc_y,Min_AngAcc_y,Mean_AngAcc_y,
'VariableNames', {'MSE', 'Max','Min','Mean'});
writetable(T_AngAcc_y, 'C:\Users\user\Desktop\METU\MatLab\Total Vehicle Model\Last
with Simscape\Results\LeftSinewave2(1500_1500)\AngAcc_y.csv', 'writevariableNames',
true)

fig18 = figure(18);
plot(t,ADAMS_AngAcc_z,t,Simulink_AngAcc_z,'Linewidth',1.5)
xlabel('Time [s]')
ylabel('Angular Acceleration [deg/s^2]')
ylim([min(min(min(ADAMS_AngAcc_z,Simulink_AngAcc_z),-5))*1.2
1.2*max(max(max(ADAMS_AngAcc_z,Simulink_AngAcc_z),5))])
title('Body Yaw Angular Acceleration')
legend('ADAMS','Simulink')
grid on

saveas(fig18,'C:\Users\user\Desktop\METU\MatLab\Total Vehicle Model\Last with
Simscape\Results\LeftSinewave2(1500_1500)\AngAccZ.png')

MSE_AngAcc_z = immse(ADAMS_AngAcc_z,Simulink_AngAcc_z);
Max_AngAcc_z = [max(ADAMS_AngAcc_z),max(Simulink_AngAcc_z)];
Min_AngAcc_z = [min(ADAMS_AngAcc_z),min(Simulink_AngAcc_z)];
Mean_AngAcc_z = [mean(ADAMS_AngAcc_z),mean(Simulink_AngAcc_z)];

T_AngAcc_z = table(MSE_AngAcc_z,Max_AngAcc_z,Min_AngAcc_z,Mean_AngAcc_z,
'VariableNames', {'MSE', 'Max','Min','Mean'});
writetable(T_AngAcc_z, 'C:\Users\user\Desktop\METU\MatLab\Total Vehicle Model\Last
with Simscape\Results\LeftSinewave2(1500_1500)\AngAcc_z.csv', 'writevariableNames',
true)

```

Arm Angles

```

fig19 = figure(19);
plot(t,table2array(ADAMS_ArmAng),'Linewidth',1.5)
xlabel('Time [s]')
ylabel('Angle [deg]')
title('ADAMS Arm Angles')
ylim([min(min(min(table2array(ADAMS_ArmAng))),-80/1.2)*1.2
max(max(max(table2array(ADAMS_ArmAng)),80/1.2))*1.2])
legend('ADAMS Arm 1','ADAMS Arm 2','ADAMS Arm 3','ADAMS Arm 4','ADAMS Arm 5','ADAMS
Arm 6')
grid on

saveas(fig19,'C:\Users\user\Desktop\METU\MatLab\Total Vehicle Model\Last with
Simscape\Results\LeftSinewave2(1500_1500)\ArmAng_ADAMS.png')

fig20 = figure(20);

```

```

plot(t,table2array(Simulink_ArmAng),'Linewidth',1.5)
xlabel('Time [s]')
ylabel('Angle [deg]')
ylim([min(min(min(table2array(Simulink_ArmAng)),-80/1.2))*1.2
max(max(max(table2array(Simulink_ArmAng)),80/1.2))*1.2])
title('Simulink Arm Angles')
legend('Simulink Arm 1','Simulink Arm 2','Simulink Arm 3','Simulink Arm
4','Simulink Arm 5','Simulink Arm 6')
grid on

saveas(fig20,'C:\Users\user\Desktop\METU\MatLab\Total Vehicle Model\Last with
simscape\Results\LeftSinewave2(1500_1500)\ArmAng_Simulink.png')

MSE_ArmAng_1 = immse(ADAMS_ArmAng_1,Simulink_ArmAng_1);
Max_ArmAng_1 = [max(ADAMS_ArmAng_1),max(Simulink_ArmAng_1)];
Min_ArmAng_1 = [min(ADAMS_ArmAng_1),min(Simulink_ArmAng_1)];
Mean_ArmAng_1 = [mean(ADAMS_ArmAng_1),mean(Simulink_ArmAng_1)];
T_ArmAng_1 = table(MSE_ArmAng_1,Max_ArmAng_1,Min_ArmAng_1,Mean_ArmAng_1,
'VariableNames', {'MSE', 'Max', 'Min', 'Mean'});
writetable(T_ArmAng_1, 'C:\Users\user\Desktop\METU\MatLab\Total Vehicle Model\Last
with simscape\Results\LeftSinewave2(1500_1500)\ArmAng_1.csv', 'writevariableNames',
true)

MSE_ArmAng_2 = immse(ADAMS_ArmAng_2,Simulink_ArmAng_2);
Max_ArmAng_2 = [max(ADAMS_ArmAng_2),max(Simulink_ArmAng_2)];
Min_ArmAng_2 = [min(ADAMS_ArmAng_2),min(Simulink_ArmAng_2)];
Mean_ArmAng_2 = [mean(ADAMS_ArmAng_2),mean(Simulink_ArmAng_2)];
T_ArmAng_2 = table(MSE_ArmAng_2,Max_ArmAng_2,Min_ArmAng_2,Mean_ArmAng_2,
'VariableNames', {'MSE', 'Max', 'Min', 'Mean'});
writetable(T_ArmAng_2, 'C:\Users\user\Desktop\METU\MatLab\Total Vehicle Model\Last
with simscape\Results\LeftSinewave2(1500_1500)\ArmAng_2.csv', 'writevariableNames',
true)

MSE_ArmAng_3 = immse(ADAMS_ArmAng_3,Simulink_ArmAng_3);
Max_ArmAng_3 = [max(ADAMS_ArmAng_3),max(Simulink_ArmAng_3)];
Min_ArmAng_3 = [min(ADAMS_ArmAng_3),min(Simulink_ArmAng_3)];
Mean_ArmAng_3 = [mean(ADAMS_ArmAng_3),mean(Simulink_ArmAng_3)];
T_ArmAng_3 = table(MSE_ArmAng_3,Max_ArmAng_3,Min_ArmAng_3,Mean_ArmAng_3,
'VariableNames', {'MSE', 'Max', 'Min', 'Mean'});
writetable(T_ArmAng_3, 'C:\Users\user\Desktop\METU\MatLab\Total Vehicle Model\Last
with simscape\Results\LeftSinewave2(1500_1500)\ArmAng_3.csv', 'writevariableNames',
true)

MSE_ArmAng_4 = immse(ADAMS_ArmAng_4,Simulink_ArmAng_4);
Max_ArmAng_4 = [max(ADAMS_ArmAng_4),max(Simulink_ArmAng_4)];
Min_ArmAng_4 = [min(ADAMS_ArmAng_4),min(Simulink_ArmAng_4)];
Mean_ArmAng_4 = [mean(ADAMS_ArmAng_4),mean(Simulink_ArmAng_4)];
T_ArmAng_4 = table(MSE_ArmAng_4,Max_ArmAng_4,Min_ArmAng_4,Mean_ArmAng_4,

```

```

'VariableNames', {'MSE', 'Max', 'Min', 'Mean'});
writetable(T_ArmAng_4, 'C:\Users\user\Desktop\METU\MatLab\Total Vehicle Model\Last
with Simscape\Results\LeftSinewave2(1500_1500)\ArmAng_4.csv', 'writevariableNames',
true)

MSE_ArmAng_5 = immse(ADAMS_ArmAng_5, Simulink_ArmAng_5);
Max_ArmAng_5 = [max(ADAMS_ArmAng_5), max(Simulink_ArmAng_5)];
Min_ArmAng_5 = [min(ADAMS_ArmAng_5), min(Simulink_ArmAng_5)];
Mean_ArmAng_5 = [mean(ADAMS_ArmAng_5), mean(Simulink_ArmAng_5)];
T_ArmAng_5 = table(MSE_ArmAng_5, Max_ArmAng_5, Min_ArmAng_5, Mean_ArmAng_5,
'VariableNames', {'MSE', 'Max', 'Min', 'Mean'});
writetable(T_ArmAng_5, 'C:\Users\user\Desktop\METU\MatLab\Total Vehicle Model\Last
with Simscape\Results\LeftSinewave2(1500_1500)\ArmAng_5.csv', 'writevariableNames',
true)

MSE_ArmAng_6 = immse(ADAMS_ArmAng_6, Simulink_ArmAng_6);
Max_ArmAng_6 = [max(ADAMS_ArmAng_6), max(Simulink_ArmAng_6)];
Min_ArmAng_6 = [min(ADAMS_ArmAng_6), min(Simulink_ArmAng_6)];
Mean_ArmAng_6 = [mean(ADAMS_ArmAng_6), mean(Simulink_ArmAng_6)];
T_ArmAng_6 = table(MSE_ArmAng_6, Max_ArmAng_6, Min_ArmAng_6, Mean_ArmAng_6,
'VariableNames', {'MSE', 'Max', 'Min', 'Mean'});
writetable(T_ArmAng_6, 'C:\Users\user\Desktop\METU\MatLab\Total Vehicle Model\Last
with Simscape\Results\LeftSinewave2(1500_1500)\ArmAng_6.csv', 'writevariableNames',
true)

```

Load Distribution

```

fig21 = figure(21);
plot(t, table2array(ADAMS_LoadDist), 'Linewidth', 1.5)
xlabel('Time [s]')
ylabel('Force [N]')
title('ADAMS Load Distribution')
ylim([min(min(min(table2array(ADAMS_LoadDist))), -1000))*1.2
max(max(max(table2array(ADAMS_LoadDist)), 1000))*1.2])
legend('ADAMS Ftz 1', 'ADAMS Ftz 2', 'ADAMS Ftz 3', 'ADAMS Ftz 4', 'ADAMS Ftz 5', 'ADAMS
Ftz 6')
grid on

saveas(fig21, 'C:\Users\user\Desktop\METU\MatLab\Total Vehicle Model\Last with
Simscape\Results\LeftSinewave2(1500_1500)\LoadDist_ADAMS.png')

fig22 = figure(22);
plot(t, table2array(Simulink_LoadDist), 'Linewidth', 1.5)
xlabel('Time [s]')
ylabel('Force [N]')
ylim([min(min(min(table2array(Simulink_LoadDist))), -1000))*1.2
max(max(max(table2array(Simulink_LoadDist)), 1000))*1.2])
title('Simulink Load Distribution')
legend('Simulink Ftz 1', 'Simulink Ftz 2', 'Simulink Ftz 3', 'Simulink Ftz

```

```

4', 'Simulink Ftz 5', 'Simulink Ftz 6')
grid on

saveas(fig22, 'C:\Users\user\Desktop\METU\MatLab\Total Vehicle Model\Last with
simscape\Results\LeftSinewave2(1500_1500)\LoadDist_Simulink.png')

MSE_LoadDist_1 = immse(ADAMS_LoadDist_1, Simulink_LoadDist_1);
Max_LoadDist_1 = [max(ADAMS_LoadDist_1), max(Simulink_LoadDist_1)];
Min_LoadDist_1 = [min(ADAMS_LoadDist_1), min(Simulink_LoadDist_1)];
Mean_LoadDist_1 = [mean(ADAMS_LoadDist_1), mean(Simulink_LoadDist_1)];
T_LoadDist_1 = table(MSE_LoadDist_1, Max_LoadDist_1, Min_LoadDist_1, Mean_LoadDist_1,
'VariableNames', {'MSE', 'Max', 'Min', 'Mean'});
writetable(T_LoadDist_1, 'C:\Users\user\Desktop\METU\MatLab\Total Vehicle
Model\Last with simscape\Results\LeftSinewave2(1500_1500)\LoadDist_1.csv',
'WriteVariableNames', true)

MSE_LoadDist_2 = immse(ADAMS_LoadDist_2, Simulink_LoadDist_2);
Max_LoadDist_2 = [max(ADAMS_LoadDist_2), max(Simulink_LoadDist_2)];
Min_LoadDist_2 = [min(ADAMS_LoadDist_2), min(Simulink_LoadDist_2)];
Mean_LoadDist_2 = [mean(ADAMS_LoadDist_2), mean(Simulink_LoadDist_2)];
T_LoadDist_2 = table(MSE_LoadDist_2, Max_LoadDist_2, Min_LoadDist_2, Mean_LoadDist_2,
'VariableNames', {'MSE', 'Max', 'Min', 'Mean'});
writetable(T_LoadDist_2, 'C:\Users\user\Desktop\METU\MatLab\Total Vehicle
Model\Last with simscape\Results\LeftSinewave2(1500_1500)\LoadDist_2.csv',
'WriteVariableNames', true)

MSE_LoadDist_3 = immse(ADAMS_LoadDist_3, Simulink_LoadDist_3);
Max_LoadDist_3 = [max(ADAMS_LoadDist_3), max(Simulink_LoadDist_3)];
Min_LoadDist_3 = [min(ADAMS_LoadDist_3), min(Simulink_LoadDist_3)];
Mean_LoadDist_3 = [mean(ADAMS_LoadDist_3), mean(Simulink_LoadDist_3)];
T_LoadDist_3 = table(MSE_LoadDist_3, Max_LoadDist_3, Min_LoadDist_3, Mean_LoadDist_3,
'VariableNames', {'MSE', 'Max', 'Min', 'Mean'});
writetable(T_LoadDist_3, 'C:\Users\user\Desktop\METU\MatLab\Total Vehicle
Model\Last with simscape\Results\LeftSinewave2(1500_1500)\LoadDist_3.csv',
'WriteVariableNames', true)

MSE_LoadDist_4 = immse(ADAMS_LoadDist_4, Simulink_LoadDist_4);
Max_LoadDist_4 = [max(ADAMS_LoadDist_4), max(Simulink_LoadDist_4)];
Min_LoadDist_4 = [min(ADAMS_LoadDist_4), min(Simulink_LoadDist_4)];
Mean_LoadDist_4 = [mean(ADAMS_LoadDist_4), mean(Simulink_LoadDist_4)];
T_LoadDist_4 = table(MSE_LoadDist_4, Max_LoadDist_4, Min_LoadDist_4, Mean_LoadDist_4,
'VariableNames', {'MSE', 'Max', 'Min', 'Mean'});
writetable(T_LoadDist_4, 'C:\Users\user\Desktop\METU\MatLab\Total Vehicle
Model\Last with simscape\Results\LeftSinewave2(1500_1500)\LoadDist_4.csv',
'WriteVariableNames', true)

MSE_LoadDist_5 = immse(ADAMS_LoadDist_5, Simulink_LoadDist_5);
Max_LoadDist_5 = [max(ADAMS_LoadDist_5), max(Simulink_LoadDist_5)];

```

```

Min_LoadDist_5 = [min(ADAMS_LoadDist_5),min(Simulink_LoadDist_5)];
Mean_LoadDist_5 = [mean(ADAMS_LoadDist_5),mean(Simulink_LoadDist_5)];
T_LoadDist_5 = table(MSE_LoadDist_5,Max_LoadDist_5,Min_LoadDist_5,Mean_LoadDist_5,
'VariableNames', {'MSE', 'Max','Min','Mean'});
writetable(T_LoadDist_5, 'C:\Users\user\Desktop\METU\MatLab\Total Vehicle
Model\Last with Simscape\Results\LeftSinWave2(1500_1500)\LoadDist_5.csv',
'WriteVariableNames', true)

MSE_LoadDist_6 = immse(ADAMS_LoadDist_6,Simulink_LoadDist_6);
Max_LoadDist_6 = [max(ADAMS_LoadDist_6),max(Simulink_LoadDist_6)];
Min_LoadDist_6 = [min(ADAMS_LoadDist_6),min(Simulink_LoadDist_6)];
Mean_LoadDist_6 = [mean(ADAMS_LoadDist_6),mean(Simulink_LoadDist_6)];
T_LoadDist_6 = table(MSE_LoadDist_6,Max_LoadDist_6,Min_LoadDist_6,Mean_LoadDist_6,
'VariableNames', {'MSE', 'Max','Min','Mean'});
writetable(T_LoadDist_6, 'C:\Users\user\Desktop\METU\MatLab\Total Vehicle
Model\Last with Simscape\Results\LeftSinWave2(1500_1500)\LoadDist_6.csv',
'WriteVariableNames', true)

```

Longitudinal Tire Forces

```

fig23 = figure(23);
plot(t,table2array(ADAMS_Ftxi)*-1,'Linewidth',1.5)
xlabel('Time [s]')
ylabel('Force [N]')
title('ADAMS Longitudinal Tire Forces')
ylim([min(min(min(table2array(ADAMS_Ftxi)*-1),-1000))*1.2
max(max(max(table2array(ADAMS_Ftxi)*-1),1000))*1.2])
legend('ADAMS Ftx 1','ADAMS Ftx 2','ADAMS Ftx 3','ADAMS Ftx 4','ADAMS Ftx 5','ADAMS
Ftx 6')
grid on

saveas(fig23,'C:\Users\user\Desktop\METU\MatLab\Total Vehicle Model\Last with
Simscape\Results\LeftSinWave2(1500_1500)\Ftxi_ADAMS.png')

fig24 = figure(24);
plot(t,table2array(Simulink_Ftxi),'Linewidth',1.5)
xlabel('Time [s]')
ylabel('Force [N]')
ylim([min(min(min(table2array(Simulink_Ftxi)),-1000))*1.2
max(max(max(table2array(Simulink_Ftxi)),1000))*1.2])
title('Simulink Longitudinal Tire Forces')
legend('Simulink Ftx 1','Simulink Ftx 2','Simulink Ftx 3','Simulink Ftx
4','Simulink Ftx 5','Simulink Ftx 6')
grid on

saveas(fig24,'C:\Users\user\Desktop\METU\MatLab\Total Vehicle Model\Last with
Simscape\Results\LeftSinWave2(1500_1500)\Ftxi_Simulink.png')

MSE_Ftxi_1 = immse(-1*ADAMS_Ftxi_1,Simulink_Ftxi_1);
Max_Ftxi_1 = [max(-1*ADAMS_Ftxi_1),max(Simulink_Ftxi_1)];
Min_Ftxi_1 = [min(-1*ADAMS_Ftxi_1),min(Simulink_Ftxi_1)];

```



```

Mean_Ftxi_1 = [mean(-1*ADAMS_Ftxi_1),mean(Simulink_Ftxi_1)];
T_Ftxi_1 = table(MSE_Ftxi_1,Max_Ftxi_1,Min_Ftxi_1,Mean_Ftxi_1, 'VariableNames',
{'MSE', 'Max','Min','Mean'});
writetable(T_Ftxi_1, 'C:\Users\user\Desktop\METU\MatLab\Total Vehicle Model\Last
with simscape\Results\LeftSinewave2(1500_1500)\Ftxi_1.csv', 'WriteVariableNames',
true)

MSE_Ftxi_2 = immse(-1*ADAMS_Ftxi_2,Simulink_Ftxi_2);
Max_Ftxi_2 = [max(-1*ADAMS_Ftxi_2),max(Simulink_Ftxi_2)];
Min_Ftxi_2 = [min(-1*ADAMS_Ftxi_2),min(Simulink_Ftxi_2)];
Mean_Ftxi_2 = [mean(-1*ADAMS_Ftxi_2),mean(Simulink_Ftxi_2)];
T_Ftxi_2 = table(MSE_Ftxi_2,Max_Ftxi_2,Min_Ftxi_2,Mean_Ftxi_2, 'VariableNames',
{'MSE', 'Max','Min','Mean'});
writetable(T_Ftxi_2, 'C:\Users\user\Desktop\METU\MatLab\Total Vehicle Model\Last
with simscape\Results\LeftSinewave2(1500_1500)\Ftxi_2.csv', 'WriteVariableNames',
true)

MSE_Ftxi_3 = immse(-1*ADAMS_Ftxi_3,Simulink_Ftxi_3);
Max_Ftxi_3 = [max(-1*ADAMS_Ftxi_3),max(Simulink_Ftxi_3)];
Min_Ftxi_3 = [min(-1*ADAMS_Ftxi_3),min(Simulink_Ftxi_3)];
Mean_Ftxi_3 = [mean(-1*ADAMS_Ftxi_3),mean(Simulink_Ftxi_3)];
T_Ftxi_3 = table(MSE_Ftxi_3,Max_Ftxi_3,Min_Ftxi_3,Mean_Ftxi_3, 'VariableNames',
{'MSE', 'Max','Min','Mean'});
writetable(T_Ftxi_3, 'C:\Users\user\Desktop\METU\MatLab\Total Vehicle Model\Last
with simscape\Results\LeftSinewave2(1500_1500)\Ftxi_3.csv', 'WriteVariableNames',
true)

MSE_Ftxi_4 = immse(-1*ADAMS_Ftxi_4,Simulink_Ftxi_4);
Max_Ftxi_4 = [max(-1*ADAMS_Ftxi_4),max(Simulink_Ftxi_4)];
Min_Ftxi_4 = [min(-1*ADAMS_Ftxi_4),min(Simulink_Ftxi_4)];
Mean_Ftxi_4 = [mean(-1*ADAMS_Ftxi_4),mean(Simulink_Ftxi_4)];
T_Ftxi_4 = table(MSE_Ftxi_4,Max_Ftxi_4,Min_Ftxi_4,Mean_Ftxi_4, 'VariableNames',
{'MSE', 'Max','Min','Mean'});
writetable(T_Ftxi_4, 'C:\Users\user\Desktop\METU\MatLab\Total Vehicle Model\Last
with simscape\Results\LeftSinewave2(1500_1500)\Ftxi_4.csv', 'WriteVariableNames',
true)

MSE_Ftxi_5 = immse(-1*ADAMS_Ftxi_5,Simulink_Ftxi_5);
Max_Ftxi_5 = [max(-1*ADAMS_Ftxi_5),max(Simulink_Ftxi_5)];
Min_Ftxi_5 = [min(-1*ADAMS_Ftxi_5),min(Simulink_Ftxi_5)];
Mean_Ftxi_5 = [mean(-1*ADAMS_Ftxi_5),mean(Simulink_Ftxi_5)];
T_Ftxi_5 = table(MSE_Ftxi_5,Max_Ftxi_5,Min_Ftxi_5,Mean_Ftxi_5, 'VariableNames',
{'MSE', 'Max','Min','Mean'});
writetable(T_Ftxi_5, 'C:\Users\user\Desktop\METU\MatLab\Total Vehicle Model\Last
with simscape\Results\LeftSinewave2(1500_1500)\Ftxi_5.csv', 'WriteVariableNames',
true)

```

```

MSE_Ftxi_6 = immse(-1*ADAMS_Ftxi_6,Simulink_Ftxi_6);
Max_Ftxi_6 = [max(-1*ADAMS_Ftxi_6),max(Simulink_Ftxi_6)];
Min_Ftxi_6 = [min(-1*ADAMS_Ftxi_6),min(Simulink_Ftxi_6)];
Mean_Ftxi_6 = [mean(-1*ADAMS_Ftxi_6),mean(Simulink_Ftxi_6)];
T_Ftxi_6 = table(MSE_Ftxi_6,Max_Ftxi_6,Min_Ftxi_6,Mean_Ftxi_6, 'variableNames',
{'MSE', 'Max', 'Min', 'Mean'});
writetable(T_Ftxi_6, 'C:\Users\user\Desktop\METU\MatLab\Total Vehicle Model\Last
with Simscape\Results\LeftSinewave2(1500_1500)\Ftxi_6.csv', 'writeVariableNames',
true)

```

Lateral Tire Forces

```

fig25 = figure(25);
plot(t,table2array(ADAMS_Ftyi)*-1,'Linewidth',1.5)
xlabel('Time [s]')
ylabel('Force [N]')
title('ADAMS Lateral Tire Forces')
ylim([min(min(min(table2array(ADAMS_Ftyi)*-1),-1000))*1.2
max(max(max(table2array(ADAMS_Ftyi)*-1),1000))*1.2])
legend('ADAMS Fty 1','ADAMS Fty 2','ADAMS Fty 3','ADAMS Fty 4','ADAMS Fty 5','ADAMS
Fty 6')
grid on

```

```

saveas(fig25,'C:\Users\user\Desktop\METU\MatLab\Total Vehicle Model\Last with
Simscape\Results\LeftSinewave2(1500_1500)\Ftyi_ADAMS.png')

```

```

fig26 = figure(26);
plot(t,table2array(Simulink_Ftyi),'Linewidth',1.5)
xlabel('Time [s]')
ylabel('Force [N]')
ylim([min(min(min(table2array(Simulink_Ftyi)),-1000))*1.2
max(max(max(table2array(Simulink_Ftyi)),1000))*1.2])
title('Simulink Lateral Tire Forces')
legend('Simulink Fty 1','Simulink Fty 2','Simulink Fty 3','Simulink Fty
4','Simulink Fty 5','Simulink Fty 6')
grid on

```

```

saveas(fig26,'C:\Users\user\Desktop\METU\MatLab\Total Vehicle Model\Last with
Simscape\Results\LeftSinewave2(1500_1500)\Ftyi_Simulink.png')

```

```

MSE_Ftyi_1 = immse(-1*ADAMS_Ftyi_1,Simulink_Ftyi_1);
Max_Ftyi_1 = [max(-1*ADAMS_Ftyi_1),max(Simulink_Ftyi_1)];
Min_Ftyi_1 = [min(-1*ADAMS_Ftyi_1),min(Simulink_Ftyi_1)];
Mean_Ftyi_1 = [mean(-1*ADAMS_Ftyi_1),mean(Simulink_Ftyi_1)];
T_Ftyi_1 = table(MSE_Ftyi_1,Max_Ftyi_1,Min_Ftyi_1,Mean_Ftyi_1, 'variableNames',
{'MSE', 'Max', 'Min', 'Mean'});
writetable(T_Ftyi_1, 'C:\Users\user\Desktop\METU\MatLab\Total Vehicle Model\Last
with Simscape\Results\LeftSinewave2(1500_1500)\Ftyi_1.csv', 'writeVariableNames',
true)

```

```

MSE_Ftyi_2 = immse(-1*ADAMS_Ftyi_2,Simulink_Ftyi_2);
Max_Ftyi_2 = [max(-1*ADAMS_Ftyi_2),max(Simulink_Ftyi_2)];
Min_Ftyi_2 = [min(-1*ADAMS_Ftyi_2),min(Simulink_Ftyi_2)];
Mean_Ftyi_2 = [mean(-1*ADAMS_Ftyi_2),mean(Simulink_Ftyi_2)];
T_Ftyi_2 = table(MSE_Ftyi_2,Max_Ftyi_2,Min_Ftyi_2,Mean_Ftyi_2, 'VariableNames',
{'MSE', 'Max', 'Min', 'Mean'});
writetable(T_Ftyi_2, 'C:\Users\user\Desktop\METU\MatLab\Total Vehicle Model\Last
with simscape\Results\LeftSinewave2(1500_1500)\Ftyi_2.csv', 'WriteVariableNames',
true)

```

```

MSE_Ftyi_3 = immse(-1*ADAMS_Ftyi_3,Simulink_Ftyi_3);
Max_Ftyi_3 = [max(-1*ADAMS_Ftyi_3),max(Simulink_Ftyi_3)];
Min_Ftyi_3 = [min(-1*ADAMS_Ftyi_3),min(Simulink_Ftyi_3)];
Mean_Ftyi_3 = [mean(-1*ADAMS_Ftyi_3),mean(Simulink_Ftyi_3)];
T_Ftyi_3 = table(MSE_Ftyi_3,Max_Ftyi_3,Min_Ftyi_3,Mean_Ftyi_3, 'VariableNames',
{'MSE', 'Max', 'Min', 'Mean'});
writetable(T_Ftyi_3, 'C:\Users\user\Desktop\METU\MatLab\Total Vehicle Model\Last
with simscape\Results\LeftSinewave2(1500_1500)\Ftyi_3.csv', 'WriteVariableNames',
true)

```

```

MSE_Ftyi_4 = immse(-1*ADAMS_Ftyi_4,Simulink_Ftyi_4);
Max_Ftyi_4 = [max(-1*ADAMS_Ftyi_4),max(Simulink_Ftyi_4)];
Min_Ftyi_4 = [min(-1*ADAMS_Ftyi_4),min(Simulink_Ftyi_4)];
Mean_Ftyi_4 = [mean(-1*ADAMS_Ftyi_4),mean(Simulink_Ftyi_4)];
T_Ftyi_4 = table(MSE_Ftyi_4,Max_Ftyi_4,Min_Ftyi_4,Mean_Ftyi_4, 'VariableNames',
{'MSE', 'Max', 'Min', 'Mean'});
writetable(T_Ftyi_4, 'C:\Users\user\Desktop\METU\MatLab\Total Vehicle Model\Last
with simscape\Results\LeftSinewave2(1500_1500)\Ftyi_4.csv', 'WriteVariableNames',
true)

```

```

MSE_Ftyi_5 = immse(-1*ADAMS_Ftyi_5,Simulink_Ftyi_5);
Max_Ftyi_5 = [max(-1*ADAMS_Ftyi_5),max(Simulink_Ftyi_5)];
Min_Ftyi_5 = [min(-1*ADAMS_Ftyi_5),min(Simulink_Ftyi_5)];
Mean_Ftyi_5 = [mean(-1*ADAMS_Ftyi_5),mean(Simulink_Ftyi_5)];
T_Ftyi_5 = table(MSE_Ftyi_5,Max_Ftyi_5,Min_Ftyi_5,Mean_Ftyi_5, 'VariableNames',
{'MSE', 'Max', 'Min', 'Mean'});
writetable(T_Ftyi_5, 'C:\Users\user\Desktop\METU\MatLab\Total Vehicle Model\Last
with simscape\Results\LeftSinewave2(1500_1500)\Ftyi_5.csv', 'WriteVariableNames',
true)

```

```

MSE_Ftyi_6 = immse(-1*ADAMS_Ftyi_6,Simulink_Ftyi_6);
Max_Ftyi_6 = [max(-1*ADAMS_Ftyi_6),max(Simulink_Ftyi_6)];
Min_Ftyi_6 = [min(-1*ADAMS_Ftyi_6),min(Simulink_Ftyi_6)];
Mean_Ftyi_6 = [mean(-1*ADAMS_Ftyi_6),mean(Simulink_Ftyi_6)];
T_Ftyi_6 = table(MSE_Ftyi_6,Max_Ftyi_6,Min_Ftyi_6,Mean_Ftyi_6, 'VariableNames',
{'MSE', 'Max', 'Min', 'Mean'});
writetable(T_Ftyi_6, 'C:\Users\user\Desktop\METU\MatLab\Total Vehicle Model\Last

```

```
with simscape\Results\LeftSinewave2(1500_1500)\Ftyi_6.csv', 'writeVariableNames',
true)
```

Suspension Torque

```
fig27 = figure(27);
plot(t,table2array(ADAMS_Tsdi),'Linewidth',1.5)
xlabel('Time [s]')
ylabel('Torque [Nm]')
title('ADAMS Suspension Torques')
ylim([min(min(table2array(ADAMS_Tsdi)))*1.2 max(max(table2array(ADAMS_Tsdi)))*1.2])
legend('ADAMS Tsd 1','ADAMS Tsd 2','ADAMS Tsd 3','ADAMS Tsd 4','ADAMS Tsd 5','ADAMS
Tsd 6')
grid on
```

```
saveas(fig27,'C:\Users\user\Desktop\METU\MatLab\Total Vehicle Model\Last with
simscape\Results\LeftSinewave2(1500_1500)\Tsd_i_ADAMS.png')
```

```
fig28 = figure(28);
plot(t,table2array(Simulink_Tsdi),'Linewidth',1.5)
xlabel('Time [s]')
ylabel('Torque [Nm]')
ylim([min(min(table2array(Simulink_Tsdi)))*1.2
max(max(table2array(Simulink_Tsdi)))*1.2])
title('Simulink Suspension Torques')
legend('Simulink Tsd 1','Simulink Tsd 2','Simulink Tsd 3','Simulink Tsd
4','Simulink Tsd 5','Simulink Tsd 6')
grid on
```

```
saveas(fig28,'C:\Users\user\Desktop\METU\MatLab\Total Vehicle Model\Last with
simscape\Results\LeftSinewave2(1500_1500)\Tsd_i_Simulink.png')
```

```
MSE_Tsdi_1 = immse(-1*ADAMS_Tsdi_1,Simulink_Tsdi_1);
Max_Tsdi_1 = [max(-1*ADAMS_Tsdi_1),max(Simulink_Tsdi_1)];
Min_Tsdi_1 = [min(-1*ADAMS_Tsdi_1),min(Simulink_Tsdi_1)];
Mean_Tsdi_1 = [mean(-1*ADAMS_Tsdi_1),mean(Simulink_Tsdi_1)];
T_Tsdi_1 = table(MSE_Tsdi_1,Max_Tsdi_1,Min_Tsdi_1,Mean_Tsdi_1, 'variableNames',
{'MSE', 'Max', 'Min', 'Mean'});
writetable(T_Tsdi_1, 'C:\Users\user\Desktop\METU\MatLab\Total Vehicle Model\Last
with simscape\Results\LeftSinewave2(1500_1500)\Tsd_i_1.csv', 'writeVariableNames',
true)
```

```
MSE_Tsdi_2 = immse(-1*ADAMS_Tsdi_2,Simulink_Tsdi_2);
Max_Tsdi_2 = [max(-1*ADAMS_Tsdi_2),max(Simulink_Tsdi_2)];
Min_Tsdi_2 = [min(-1*ADAMS_Tsdi_2),min(Simulink_Tsdi_2)];
Mean_Tsdi_2 = [mean(-1*ADAMS_Tsdi_2),mean(Simulink_Tsdi_2)];
T_Tsdi_2 = table(MSE_Tsdi_2,Max_Tsdi_2,Min_Tsdi_2,Mean_Tsdi_2, 'variableNames',
{'MSE', 'Max', 'Min', 'Mean'});
writetable(T_Tsdi_2, 'C:\Users\user\Desktop\METU\MatLab\Total Vehicle Model\Last
with simscape\Results\LeftSinewave2(1500_1500)\Tsd_i_2.csv', 'writeVariableNames',
```

```

true)

MSE_Tsdi_3 = immse(-1*ADAMS_Tsdi_3,Simulink_Tsdi_3);
Max_Tsdi_3 = [max(-1*ADAMS_Tsdi_3),max(Simulink_Tsdi_3)];
Min_Tsdi_3 = [min(-1*ADAMS_Tsdi_3),min(Simulink_Tsdi_3)];
Mean_Tsdi_3 = [mean(-1*ADAMS_Tsdi_3),mean(Simulink_Tsdi_3)];
T_Tsdi_3 = table(MSE_Tsdi_3,Max_Tsdi_3,Min_Tsdi_3,Mean_Tsdi_3, 'VariableNames',
{'MSE', 'Max','Min','Mean'});
writetable(T_Tsdi_3, 'C:\Users\user\Desktop\METU\MatLab\Total Vehicle Model\Last
with simscape\Results\LeftSinewave2(1500_1500)\Tsdi_3.csv', 'writeVariableNames',
true)

MSE_Tsdi_4 = immse(-1*ADAMS_Tsdi_4,Simulink_Tsdi_4);
Max_Tsdi_4 = [max(-1*ADAMS_Tsdi_4),max(Simulink_Tsdi_4)];
Min_Tsdi_4 = [min(-1*ADAMS_Tsdi_4),min(Simulink_Tsdi_4)];
Mean_Tsdi_4 = [mean(-1*ADAMS_Tsdi_4),mean(Simulink_Tsdi_4)];
T_Tsdi_4 = table(MSE_Tsdi_4,Max_Tsdi_4,Min_Tsdi_4,Mean_Tsdi_4, 'VariableNames',
{'MSE', 'Max','Min','Mean'});
writetable(T_Tsdi_4, 'C:\Users\user\Desktop\METU\MatLab\Total Vehicle Model\Last
with simscape\Results\LeftSinewave2(1500_1500)\Tsdi_4.csv', 'writeVariableNames',
true)

MSE_Tsdi_5 = immse(-1*ADAMS_Tsdi_5,Simulink_Tsdi_5);
Max_Tsdi_5 = [max(-1*ADAMS_Tsdi_5),max(Simulink_Tsdi_5)];
Min_Tsdi_5 = [min(-1*ADAMS_Tsdi_5),min(Simulink_Tsdi_5)];
Mean_Tsdi_5 = [mean(-1*ADAMS_Tsdi_5),mean(Simulink_Tsdi_5)];
T_Tsdi_5 = table(MSE_Tsdi_5,Max_Tsdi_5,Min_Tsdi_5,Mean_Tsdi_5, 'VariableNames',
{'MSE', 'Max','Min','Mean'});
writetable(T_Tsdi_5, 'C:\Users\user\Desktop\METU\MatLab\Total Vehicle Model\Last
with simscape\Results\LeftSinewave2(1500_1500)\Tsdi_5.csv', 'writeVariableNames',
true)

MSE_Tsdi_6 = immse(-1*ADAMS_Tsdi_6,Simulink_Tsdi_6);
Max_Tsdi_6 = [max(-1*ADAMS_Tsdi_6),max(Simulink_Tsdi_6)];
Min_Tsdi_6 = [min(-1*ADAMS_Tsdi_6),min(Simulink_Tsdi_6)];
Mean_Tsdi_6 = [mean(-1*ADAMS_Tsdi_6),mean(Simulink_Tsdi_6)];
T_Tsdi_6 = table(MSE_Tsdi_6,Max_Tsdi_6,Min_Tsdi_6,Mean_Tsdi_6, 'VariableNames',
{'MSE', 'Max','Min','Mean'});
writetable(T_Tsdi_6, 'C:\Users\user\Desktop\METU\MatLab\Total Vehicle Model\Last
with simscape\Results\LeftSinewave2(1500_1500)\Tsdi_6.csv', 'writeVariableNames',
true)

```